NASA CR 114275
(Available to the public)

APOLLO WINDOW DEFORMATION AND RAY TRACE ANALYSES

By David M Kelley

NOVEMBER 1970

Prepared under Contract No NAS2-5044 by
PHILCO-FORD CORPORATION
WDL DIVISION
For
NATIONAL AERONAUTICS AND SPACE ADMINISTRATION
AMES RESEARCH CENTER
MOFFETT FIELD, CALIFORNIA

NASA CR 114275
(Available to the public)

APOLLO WINDOW DEFORMATION

AND

RAY TRACE ANALYSES

By David M. Kelley

NOVEMBER 1970

Prepared under Contract No. NAS2-5044 by
PHILCO-FORD CORPORATION
WESTERN DEVELOPMENT LABORATORIES DIVISION

For

NATIONAL AERONAUTICS AND SPACE ADMINISTRATION
AMES RESEARCH CENTER
MOFFETT FIELD, CALIFORNIA

FOREWARD

This report was prepared by Philco-Ford, Western Development Laboratories' personnel, under NASA Contract No. NAS2-5044. Work was administered under the direction of the Manned Systems Research Branch, Ames Research Center, Moffett Field, California. The Technical Monitor for the contract was Mr. Kenneth C. White.

This report covers work conducted between June 1968 and August 1970. The manuscript was released by the author for publication as a NASA technical report in November 1970.

ABSTRACT

This document describes results of deformation and ray trace analyses of the Apollo spacecraft side window. The window is studied in three configurations: isolated with simply supported edges, isolated with clamped edges, and in its Apollo structural environment. Data are appropriate for correcting scientific observations and evaluating the effect of window support on optical performance.

It reports deformations based on a finite element analysis. It defines the errors associated with the analyses. They are within the one second of arc accuracy required for ray tracing. It presents contours of equal deflection for the configurations analyzed.

It cites deviations of light rays entering the window on a one-inch grid for in-flight loading conditions. It gives deviation data for single rays entering the isolated window. It reports deviations for both single and two ray sextant observations for the window in its structural environment. It identifies areas of the window in the Apollo structure through which observations can be made without interference from the supporting structure. For single line-of-sight observations, this area is centered on the window. For sextant observations, the area is skewed toward the edge of the window.

TABLE OF CONTENTS

Section		Page
	FOREWARD	ii
	ABSTRACT	iii
	LIST OF ILLUSTRATIONS	vi
	LIST OF TABLES	xi
1	INTRODUCTION	1
2	TECHNICAL APPROACH	3
3	VALIDATION ANALYSES	8
	Selection of Mesh Size	8
	Evaluation of Analysis Accuracy	15
4	APOLLO WINDOW DEFORMATIONS	19
	Isolated Window Analyses	19
	The Window in its Structural Environment	30
	First-Phase Analysis Procedure	32
	Second-Phase Analysis Procedure	34
	Phase I - Analyses and Results	35
	Phase II - Analyses and Results	42
5	APOLLO WINDOW RAY TRACE ANALYSES	51
	Single Ray Trace Analysis	51
	Two Ray Trace Analysis	113
6	REVIEW OF RESULTS	137
	REFERENCES	140

TABLE OF CONTENTS (CONT'D)

Section | Page

APPENDIX A - RECTANGULAR PLATE ANALYSES 141

APPENDIX B - FORMULATION OF EXTRAPOLATION CURVES 152

APPENDIX C - ISOLATED WINDOW ANALYSES 159

APPENDIX D - APOLLO WINDOW STRUCTURAL ANALYSES . 165

APPENDIX E - DEFINITION OF APOLLO WINDOW DEFORMATIONS AT THE WINDOW FRAME 199

APPENDIX F - APOLLO WINDOW FINAL DEFORMATION ANALYSES 208

LIST OF ILLUSTRATIONS

Figure		Page
1	Square Plate Model Articulation	12
2	Extrapolation Curve for Deflections	16
3	Extrapolation Curve for Rotations	17
4	Isolated Window Model Articulation	20
5	Deflections of Isolated Window - Simply Supported	22
6	Deflections of Isolated Window - Clamped	23
7	Deflections along x-axis of Simply Supported Window	24
8	Deflections along y-axis of Simply Supported Window	25
9	Deflections along x-axis of Clamped Window	26
10	Deflections along y-axis of Clamped Window	27
11	Apollo Structure Model Articulation	36
12	Contours of Equal Deflection for Inner Pane	44
13	Contours of Equal Deflection for Outer Pane	45
14	Deflections along x-axis of Apollo Window	47
15	Deflections along y-axis of Apollo Window	48
16	Single Ray Trace Angles	53
17	Mean of Ray Deviations - Edge Variation	57
18	RMS of Ray Deviations - Edge Variation	58
19	Mean of Ray Deviations - Interstitial Pressure Variation	60
20	RMS of Ray Deviations - Interstitial Pressure Variation	61
21	Mean of Ray Deviations - Cabin Pressure Variation	62

LIST OF ILLUSTRATIONS (CONT'D)

Figure		Page
22	RMS of Ray Deviations - Cabin Pressure Variation .	63
23	Mean of Ray Deviations - Incidence Angle Variation (Clamped Edge Condition)	64
24	RMS of Ray Deviations - Incidence Angle Variation (Clamped Edge Condition)	65
25	Mean of Ray Deviations - Incidence Angle Variation (Simply Supported Edge Condition)	66
26	RMS of Ray Deviations - Incidence Angle Variation (Simply Supported Edge Condition)	67
27	Mean of Ray Deviations - Incidence Angle Variation (Actual Edge Condition)	68
28	RMS of Ray Deviations - Incidence Angle Variation (Actual Edge Condition)	69
29	Points of Interest - Single Ray Trace	71
30	Total Deviation - Point 1	72
31	Total Deviation - Point 2	73
32	Total Deviation - Point 3	74
33	Total Deviation - Point 4	75
34	Total Deviation - Point 5	76
35	Total Deviation - Point 6	77
36	Total Deviation - Point 7	78
37	Total Deviation - Point 8	79
38	Total Deviation - Point 9	80
39	Total Deviation - Point 10	81
40	Total Deviation - Point 11	82

LIST OF ILLUSTRATIONS (CONT'D)

Figure		Page
41	Total Deviation - Point 12	83
42	Total Deviation - Point 13	84
43	Plane Angle Deviation - Point 1	86
44	Plane Angle Deviation - Point 2	87
45	Plane Angle Deviation - Point 3	88
46	Plane Angle Deviation - Point 4	89
47	Plane Angle Deviation - Point 5	90
48	Plane Angle Deviation - Point 6	91
49	Plane Angle Deviation - Point 7	92
50	Plane Angle Deviation - Point 8	93
51	Plane Angle Deviation - Point 9	94
52	Plane Angle Deviation - Point 10	95
53	Plane Angle Deviation - Point 11	96
54	Plane Angle Deviation - Point 12	97
55	Plane Angle Deviation - Point 13	98
56	Incidence Angle Deviation - Point 1	99
57	Incidence Angle Deviation - Point 2	100
58	Incidence Angle Deviation - Point 3	101
59	Incidence Angle Deviation - Point 4	102
60	Incidence Angle Deviation - Point 5	103
61	Incidence Angle Deviation - Point 6	104
62	Incidence Angle Deviation - Point 7	105

LIST OF ILLUSTRATIONS (CONT'D)

Figure		Page
63	Incidence Angle Deviation - Point 8	106
64	Incidence Angle Deviation - Point 9	107
65	Incidence Angle Deviation - Point 10	108
66	Incidence Angle Deviation - Point 11	109
67	Incidence Angle Deviation - Point 12	110
68	Incidence Angle Deviation - Point 13	111
69	Best Observation Area - Single Ray Trace	112
70	Two Ray Trace Angles	114
71	Points of Interest - Two Ray Trace	115
72	Sextant Angle Changes - Point 1	117
73	Sextant Angle Changes - Point 2	118
74	Sextant Angle Changes - Point 3	119
75	Sextant Angle Changes - Point 4	120
76	Sextant Angle Changes - Point 5	121
77	Sextant Angle Changes - Point 6	122
78	Sextant Angle Changes - Point 7	123
79	Sextant Angle Changes - Point 8	124
80	Sextant Angle Changes - Point 9	125
81	Sextant Angle Changes - Point 10	126
82	Sextant Angle Changes - Point 11	127
83	Sextant Angle Changes - Point 12	128
84	Sextant Angle Changes - Point 13	129

LIST OF ILLUSTRATIONS (CONT'D)

Figure		Page
85	Sextant Angle Changes - Point 14	130
86	Sextant Angle Changes - Point 15	131
87	Best Observation Area - Two Ray Trace	132
88	Sextant Angle Change vs. X-Coordinate	134
89	Mean and RMS of Sextant Angle Changes	135

LIST OF TABLES

Table		Page
1	Deformations of Square Plate (clamped)	9
2a	Rotations of Square Plate (simply supported) . . .	13
2b	Rotations of Square Plate (clamped)	13
2c	Deflections of Square Plate	14
3	Comparison of Window Deformations	29
4	Analysis Accuracy Comparison	31
5	Deformations of Window Frame (Normal Facet Element)	38
6	Apollo Window System Analysis (Deflections for 4.1 psia Cabin Pressure)	40
7	Apollo Window System Analysis (Rotations for 4.1 psia Cabin Pressure)	41
8	Apollo Window Load Conditions	43
9	Mean of Error Measure	50
10	Load Conditions for Ray Tracing	52
11	Mean of Light Ray Deviations	55
12	RMS of Light Ray Deviations	56
13	Number of Values in Mean and RMS Calculations . . .	136

Section 1

INTRODUCTION

Several optical experiments have been planned for the Apollo Space Program. These experiments involve scientific observations made through one of the spacecraft windows. Thus, the window is one part of the optical system. Distortions of the window surfaces alter the direction of lines of sight passing through the window. Consequently, a prediction of the deformations of the window under various flight conditions is useful to correct scientific observations.

The principal errors in optical observations through the window are induced by refraction of the light rays at the window surfaces. The deviation of a ray path from a straight line depends on the geometry and density of the window components. The deformed window geometry can be determined by a numerical simulation of the system. With geometric data and indices of light refraction, the path of any ray can be accurately traced.

White and Gadeberg(1)* have described analyses of line-of-sight deviations associated with isolated Gemini windows with idealized boundary conditions. Warner and Walsh(2) presented Gemini isolated window deformation contours developed by careful experimentation. These reports provide a useful background, basis, and checkpoints for the present study.

* Numbers in brackets refer to references listed at the end of the report.

The purpose of this report is to evaluate, to one second of arc accuracy, light ray (line-of-sight) deviations for the Apollo window for a variety of flight conditions. Deformations are calculated for the window supported in the Apollo structural environment and for the window when isolated and assigned two sets of idealized edge conditions. Deviations of light rays entering at points on a one-inch grid and with six different incident angles are cited for nine different flight-pressure conditions.

In order to obtain the one second of arc accuracy in ray tracing, the deformations of the window must be accurately known and the slopes of the deformed window must be accurate to one second of arc. The window deformation data given here were developed by numerical analyses of the structures. A set of validation analyses were performed to insure adequate mesh refinement and sufficient structure were included to obtain ray deviations accurate to one second of arc.

The next section of the document describes the technical approach used for the analyses. The third section deals with the supporting validation analyses. The fourth and fifth sections describe the Apollo window deformation and ray trace analyses. The sixth section is a review of the results of the study. References are given and detailed plots and tabulations of the deformations and ray trace data are included.

Calculations made during the course of this study were performed using the Ames Computer Laboratory's 7094/DCS Computer Configuration. The assistance and cooperation rendered by the Computer Laboratory are gratefully acknowledged.

Section 2

TECHNICAL APPROACH

Determination of the errors in optical observations caused by the Apollo Scientific Side Window requires developing and validating a numerical simulation of the structure, particularizing the numerical model, obtaining the deformations, and then tracing rays through the deformed window.

Validating the numerical simulation is accomplished by performing a set of analyses to insure adequacy of the model refinement. Any analysis will produce estimates of the deformations. These estimates will improve monotonically as the mesh is refined. Then, an estimate of the accuracy of the analyses can be made by determining the changes in the deformation predictions for two analyses with different mesh refinements and correlating with comparable analyses of a control problem for which an exact solution is known. The estimate of analysis accuracy is based on the assumption that modeling of the structural geometry and material properties is precise.

A square plate analysis was chosen as the control problem. Analyses were performed with various mesh refinements. In order to compare the accuracy of the real problem with that of the square plate, analyses were also performed using an alternate facet element (a planar finite element). These alternate analyses, along with those using the normal facet element, were used to give estimates of the accuracy of the deformation predictions.

Deformation data were developed for three types of boundary conditions for the Apollo window. Two of these consisted of the isolated window. one with simply supported and one with clamped edge conditions. These window models were loaded with unit uniform pressures. The third was the window in its actual structural environment. This last model was loaded with nine different pressure conditions.

The structures were modeled as linear, elastic systems undergoing small strains and small deformations. The materials of the structures were represented as homogeneous, isotropic, and Hookean. Realism was provided in modeling by representing line element eccentricities and honey-comb facets geometric orthotropy. Core shear deformations were included in the model.

Predictions of deformations were made using the Structural Analysis and Matrix Interpretive System (SAMIS)[3,4] computer program developed by Philco-Ford Corporation under Jet Propulsion Laboratory contract. The technical basis for the program has been described by Melosh and Christiansen[5].

The basis used to define the mathematical model of the structure is referred to in the literature as the Direct Stiffness Method. The method involves two essential ideas. The first is to replace the continuous structure by an assemblage of elements. The continuous structural system is cut into pieces by fictitious cuts. Intersections of cutting lines are called grid-points or joints. From this viewpoint, load-deflection relations are defined independently for each element of the structure.

The second idea is to formulate the problem from the stiffness viewpoint to facilitate forming the mathematical model for the complete stiffness of the structural system. The load-deflection relations are written in stiffness form as

$$\left[K\right] \left\{u\right\} = \left\{P\right\} \tag{1}$$

where $\left[K\right]$ is the stiffness matrix of the element, $\left\{u\right\}$ is a column vector of joint deformations, and $\left\{P\right\}$ is a column matrix of the loads applied at the joints. A given column of the stiffness matrix $\left[K\right]$ consists of a list of forces at each grid-point of the element for unit deformation in a given direction. Then, forming the load-deformation relations for the system involves summing the stiffness grid-point forces from the pieces. Where two or more members have a common grid-point, forces are simply added. These data form a stiffness matrix for the complete structural system. Boundary conditions can be formulated in terms of grid-point loads and deformations. Deformations are found by solving simultaneous equations of the form of Eq. (1), but for the complete structural system.

The simplicity of the approach is a principal advantage for automation. The procedure for assembling the simultaneous equations is a clerical one. The process is independent of the geometric or topological complexity of the structure, the material characteristics, the boundary conditions, the choice of coordinates, or the identity or number of the force redundants of the system.

The ray trace analyses were performed for a variety of rays entering the window at various points. The ray tracing was performed on the isolated window for simply supported and clamped edge condition for single rays passing through the window. Both single and double ray tracing were done on the window in its structural environment. The basis for the ray trace analyses is presented by White and Gadeberg[1,6]. Details of the ray trace computer code are given by Kelley and Diether[7].

"Ray tracing" consists of determining the path of an observed ray as seen from the interior of the spacecraft. Since the mathematical description of the optical phenomenon is reversible, the ray can be considered as emerging from the observer's eye, extending to the window surface, refracting through the window, and then continuing on to the object under observation.

The process by which the ray is traced is to first assume the direction of a ray from the eye of the observer toward the window. The point of intersection of the ray with the deformed window surface is determined by successive improvement of estimates. (This process is used because the deformed surface is defined by tabular data rather than by formulas.) At the intersection point, the normal to the surface is determined. The refraction of the ray in the medium is determined from Snell's Law using the measured value of the index of refraction. The index of refraction of the air is calculated as a function of the air pressure.

The ray is traced through each medium and its refraction calculated at each interface. The position and orientation of the exiting ray is then compared with the position and orientation of the assumed ray. The differences in position and angle define the deviation of the light ray and are a measure of the optical performance of the window system.

The equations necessary to determine the path of the refracted light ray are functions of the geometry of the systems and the indices of refraction of the components of the system. Details of these equations are given by White and Gadeberg[1,6].

Section 3

VALIDATION ANALYSES

To insure errors of less than one second of arc in angular deformation predictions, several validation analyses were performed. One set of analyses was made to determine the mesh refinement required. An alternate set of analyses was made to predict the accuracy of the analyses of the Apollo window deformations by comparison of analyses within the set.

Selection of Mesh Size

Identification of the mesh refinement was based upon the analyses of a square plate. Since, in true view, the Apollo Scientific Side Window is almost square, this geometry should yield excellent estimates of analysis accuracy.

The exact solutions for the square plate were developed using equations formulated by Timoshenko[8]. These equations are summarized in Appendix A. The solutions take the form of infinite series for both the simply supported and clamped edge conditions and are thus approximate solutions unless an infinite number of terms are taken. The clamped edge condition involves the additional complexity of requiring solution of an infinite set of simultaneous equations to determine the redundant moments along the edge.

Table 1 shows predicted central deflections of the clamped square plate for several exact solution approximations using various numbers of terms in the infinite series. The plate is loaded with a unit uniform pressure. These results show that sixteen terms in the series result in predictions with an error of less than two parts in the sixth decimal figure.

Table 1

Deformations of Square Plate (clamped)

No. of Terms[a]	w^{b}	dw/dy^{c}	$\Delta(dw/dy)^{b}$
10	.00109116	0801095	
			.0000235
12	.00109120	.0801330	
			.0000147
14	.00109115	.0801477	
			.0000069
16	.00109115	.0801546	
			.0000018
18	.00109115	.0801564	
			.0000012
20	.00109115	.0801552	

a. Number of terms of infinite series taken in the solution.

b. Deflections at center of plate, measured in inches.

c. Slopes at one inch from edge of plate, measured in radians.

d. Changes in slopes at one inch from edge of plate, measured in radians.

(Four parts in the sixth decimal figure is less than one second of arc.) This conclusion is deduced by the extrapolated data in Column 4. This column cites the change in predicted angular deformations. To insure that the measurements described in Table 1 were not affected by round-off error, the calculations were made in double precision. Details of the code used to generate the exact solution are discussed by Kelley and Diether[7].

Several finite element analyses were made for the square plate using different mesh sizes. Two of these were made using the triangular (1/1) facet element of Melosh[9]. Two were made with an alternate (3/1) facet element model. This alternate facet element model takes the input data for the normal facet element and replaces that element with three sub-elements. The extra nodes are then eliminated by reduction of the equations. The resulting stiffness matrix is of the same order as that of the normal facet. Since this model involves facets with obtuse angles, an additional approximation is introduced into the analysis[10] so that the accuracy of the predictions of the deformations may be less than that for the normal facet element. This alternate model, however, gives another numerical representation which will theoretically become exact as the mesh size approaches zero.

To establish the accuracy of the deformations of a structure for which the exact solution is not available, it is necessary to have two analyses of the structure and to know the relationship between the errors associated with these analyses. For the Apollo window, the two analyses will be those using the normal and alternate facet elements. The relationship between the errors associated with each of these analyses will be established by performing analyses of a square plate for which an "exact" solution is available.

Figure 1 shows the model articulation used for a one-inch mesh analysis of the square plate. The model for the one-half inch mesh is basically the same except that the one-inch dimensions become one-half-inch dimensions. Exploiting the symmetry about one of the axes, only one-half the plate is modeled in each analysis.

Table 2 lists the deformations predicted for three points on the plate under simply supported and clamped edge conditions. One of these points is that at which the maximum rotation occurs, another is a point midway between the points of maximum and minimum rotation (denoted as "average rotation"), and the third is the point exhibiting maximum deflection. The errors associated with each rotation are given in terms of seconds of arc. The error cited for the point with maximum deflection is the relative error in deflection using the exact solution approximation as a basis. Table 2a shows the rotation data for the simply supported plate for the exact solution approximation and for both the one-inch and one-half-inch models using the normal (1/1) and alternate (3/1) facet elements. The same data for the clamped plate is shown in Table 2b. Table 2c gives the deflection data for the simply supported and clamped plate for the same set of analyses.

Considering, for the moment, only the normal element analyses results, it is concluded from the data in Table 2 that the one-inch grid network is not fine enough to obtain the one second of arc accuracy which is required. Consequently, a one-half-inch network will be used. For this mesh, the accuracy criterion is met with the exception of the maximum rotation of the simply supported plate. The rotation is within one-tenth of one second of arc of meeting the criterion. Since the point in question

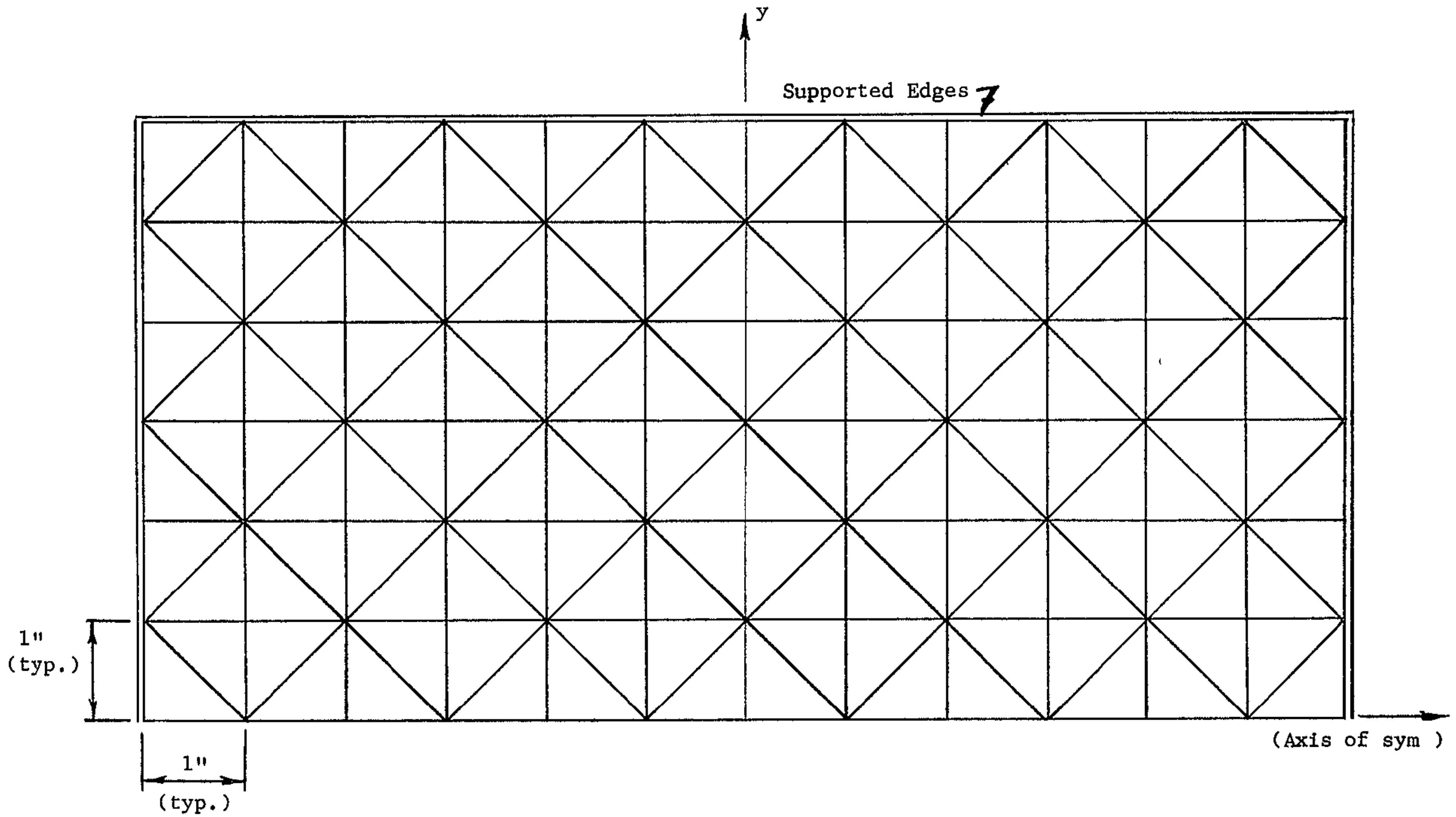

Figure 1. Square Plate Model Articulation

Table 2a

Rotations of Square Plate (simply supported)

Analysis	Maximum Rotation	Error[a]	Average Rotation[b]	Error[a]
Exact	.0009758	0.206[e]	.0006340	0.206[e]
1"-1/1[c]	0009763	0.309	.0006287	1.298
1"-3/1[d]	.0009500	5.526	.0006273	1.588
1/2"-1/1[c]	.0009801	1.094	.0006378	0.989
1/2"-3/1[d]	.0009651	2.411	.0006280	1.444

Table 2b

Rotations of Square Plate (clamped)

Analysis	Maximum Rotation	Error[a]	Average Rotation[b]	Error[a]
Exact	.0002830	0.206[e]	.0001981	0.206[e]
1"-1/1[c]	.0002902	1.689	.0002032	1.258
1"-3/1[d]	.0002750	1.856	.0001940	1.051
1/2"-1/1[c]	.0002852	0.659	.0001997	0.536
1/2"-3/1[d]	.0002806	0.701	.0001968	0.474

a. Measured in seconds of arc.

b. Rotation midway between maximum and minimum rotations

c. Normal facet element.

d. Alternate facet element.

e. Errors associated with "exact" solution are due to truncation of the infinite series solution.

Table 2c

Deflections of Square Plate

Analysis	Simply Supported		Clamped	
	Center Deflection	% Error	Center Deflection	% Error
Exact	.003528	--	.001099	--
1"-1/1[c]	.003508	.57	.001090	.82
1"-3/1[d]	.003460	1.93	.001072	2 46
1/2"-1/1[c]	.003539	-.31	.001098	.09
1/2"-3/1[d]	.003495	.93	.001091	.73

a. Measured in seconds of arc.

b. Rotation midway between maximum and minimum rotations.

c. Normal facet element.

d. Alternate facet element.

e. Errors associated with "exact" solution are due to truncation of the infinite series solution.

is on the edge of the plate, a region disregarded in the ray tracing, it was deemed acceptable. All the interior points were within the accuracy requirement. A tabulation of the deformations of the square plate for the various analyses is included in Appendix A.

Evaluation of Analysis Accuracy

The criterion for estimating the accuracy of the Apollo window analyses, by comparison with the results of the validation analyses, was established by using analyses of the square plate performed with the alternate facet element, as well as those using the normal facet element. The results of the analyses using the alternate facet element model are designated by 3/1 in Table 2.

To establish the criterion, a study was made of the results of the various analyses for ten arbitrary points on the square plate. Since both the one-inch and one-half-inch models for each of the simply supported and clamped edge conditions were studied, the resulting sample included about forty points. Using these data, plots (one for deflection and one for rotation) were made showing the ratio of the alternate element solutions to the normal element solutions plotted against the ratio of the exact solutions to the normal element solutions. These ratios were plotted to eliminate the possibility that geometric or dimensional considerations would bias the data. Through these plotted points, smooth curves were faired. Figures 2 and 3 show the resulting deflection and rotation extrapolation curves. The maximum errors in these curves are 2.2 percent for the rotation curve and 4.5 percent for the deflection curve. The errors in the extrapolation curves are based on the maximum distance of

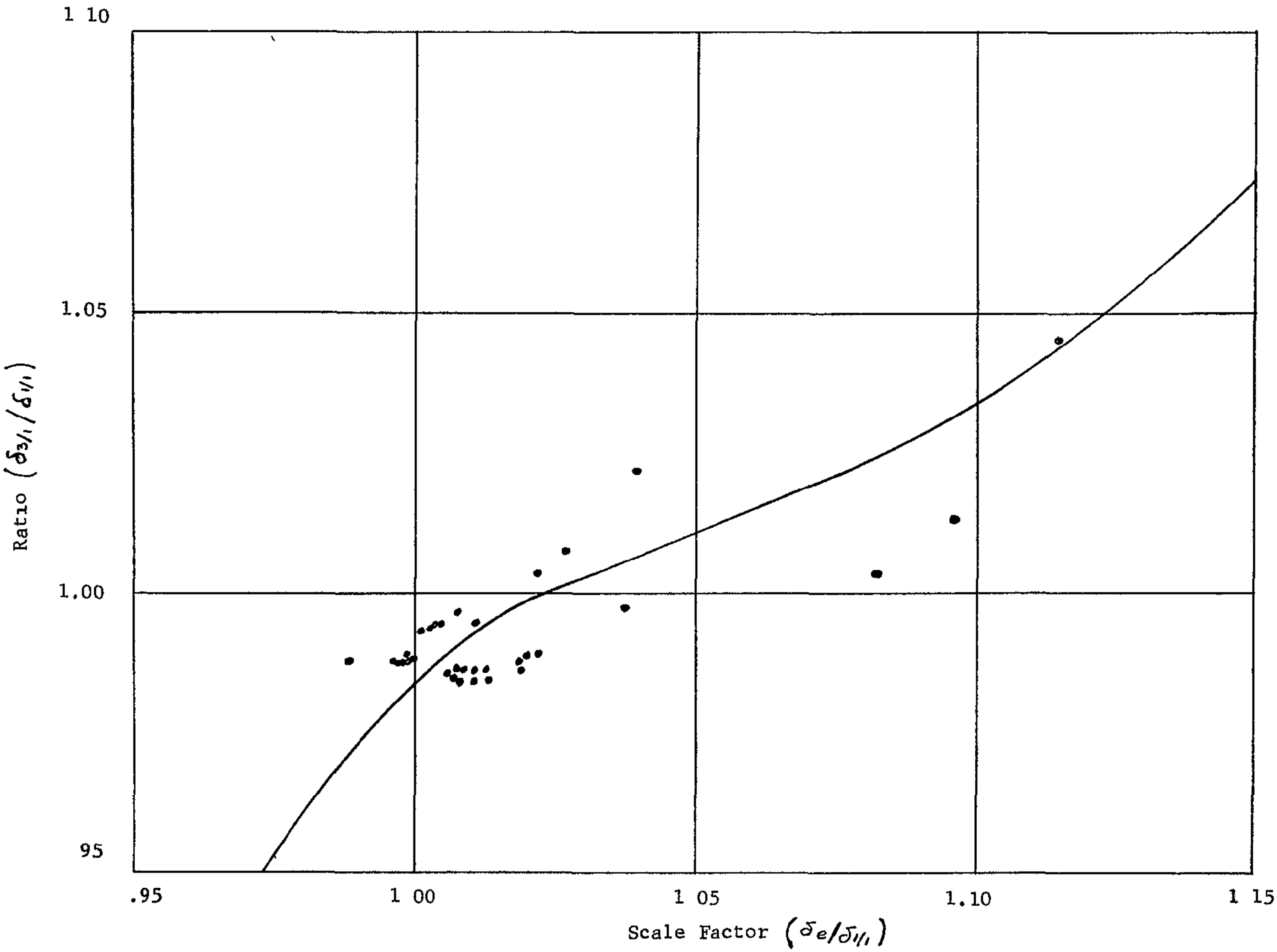

Figure 2. Extrapolation Curve for Deflections

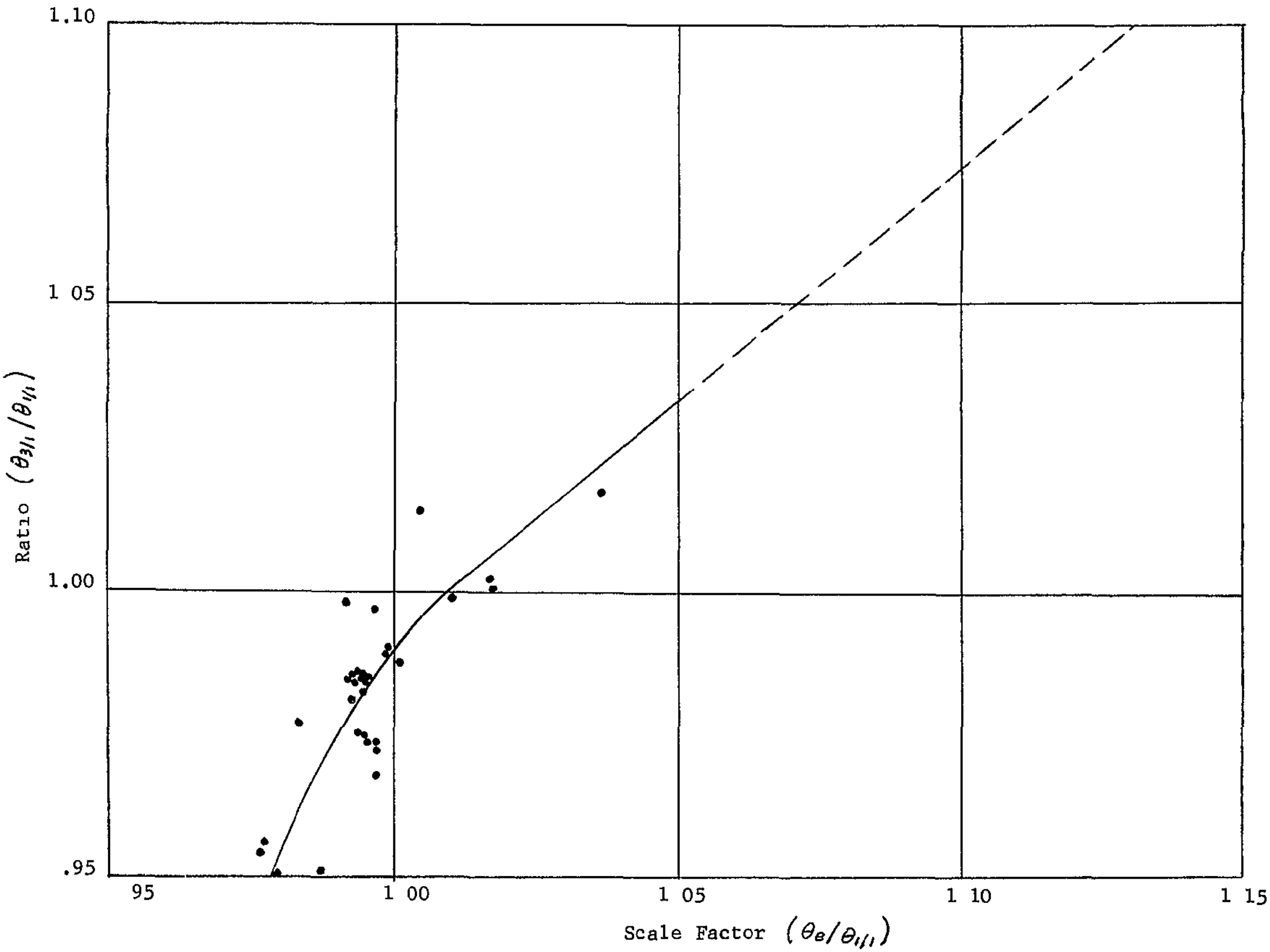

Figure 3. Extrapolation Curve for Rotations

any data point from the curve under consideration. Tabulations of the deformations of the points on the square plates used in the sample, calculation of the various ratios needed, and plots of these ratios are given in Appendix B.

The approach to determination of the accuracy of the solutions obtained is to enter the curve with the value of the ratio of the alternate element solution to the normal element solution and arrive at a value for the ratio of the exact solution to the normal element solution. Using this ratio and the normal element solution, a prediction of the exact solution is made. The error in the analysis is then determined to be the difference between the normal element solution and the predicted exact solution plus or minus the appropriate error of the extrapolation curve.

This approach provides a procedure whereby the accuracy of any analysis can be determined regardless of the nature or magnitude of the loading, the geometry of the structure, or the degree of mesh refinement. All that is required for the determination of the accuracy are the analyses using the normal and alternate facet elements. Checks were made using this procedure to predict the errors for the square plate analyses for points not included in curve development. The results showed that the error predictions were correct to within the accuracy of the extrapolation curves.

Validation analyses for the ray trace calculations of this study are not required. The equations upon which the ray tracing is based are relationships between geometry and indices of refraction of various media. The only approximation involved in these equations is associated with accuracy of the measured indices of refraction. These are available to eight digits of accuracy. Thus, the resulting ray trace analyses require no special validation.

Section 4

APOLLO WINDOW DEFORMATIONS

The Apollo Scientific Side Window was analyzed for three sets of boundary conditions. For two of these, the window was isolated: one with simply supported and one with clamped edge conditions. In the third analysis, the window was supported in its actual structural configuration.

Isolated Window Analyses

Figure 4 shows the finite element model articulation of the window. The x-axis is an axis of symmetry. The remaining boundary of the window is defined by the window's supporting frame. Only one-half of the window was modeled. Symmetry boundary conditions imply the other half. To obtain the required accuracy, a one-half inch mesh was used. The material mechanical properties used were those of fused silica glass (Corning Glass Works, Glass 7940). Young's modulus of elasticity for this glass is $10.5 \cdot 10^6$ psi and Poisson's ratio is 0.16 [11]. Appendix C contains the joint and element numbering for the finite element model of the window, along with a tabulation of joint coordinates.

The SAMIS computer program was used to obtain the deformations of the window. To impose the boundary condition for the simply supported case, it was necessary to solve a set of 54 simultaneous equations. The simultaneous equations were needed because the window was curved along portions of the boundary. This meant the boundary was not orthogonal to either of the axes of the coordinate system. To impose the boundary conditions, unit moments were applied to those boundary points on edges

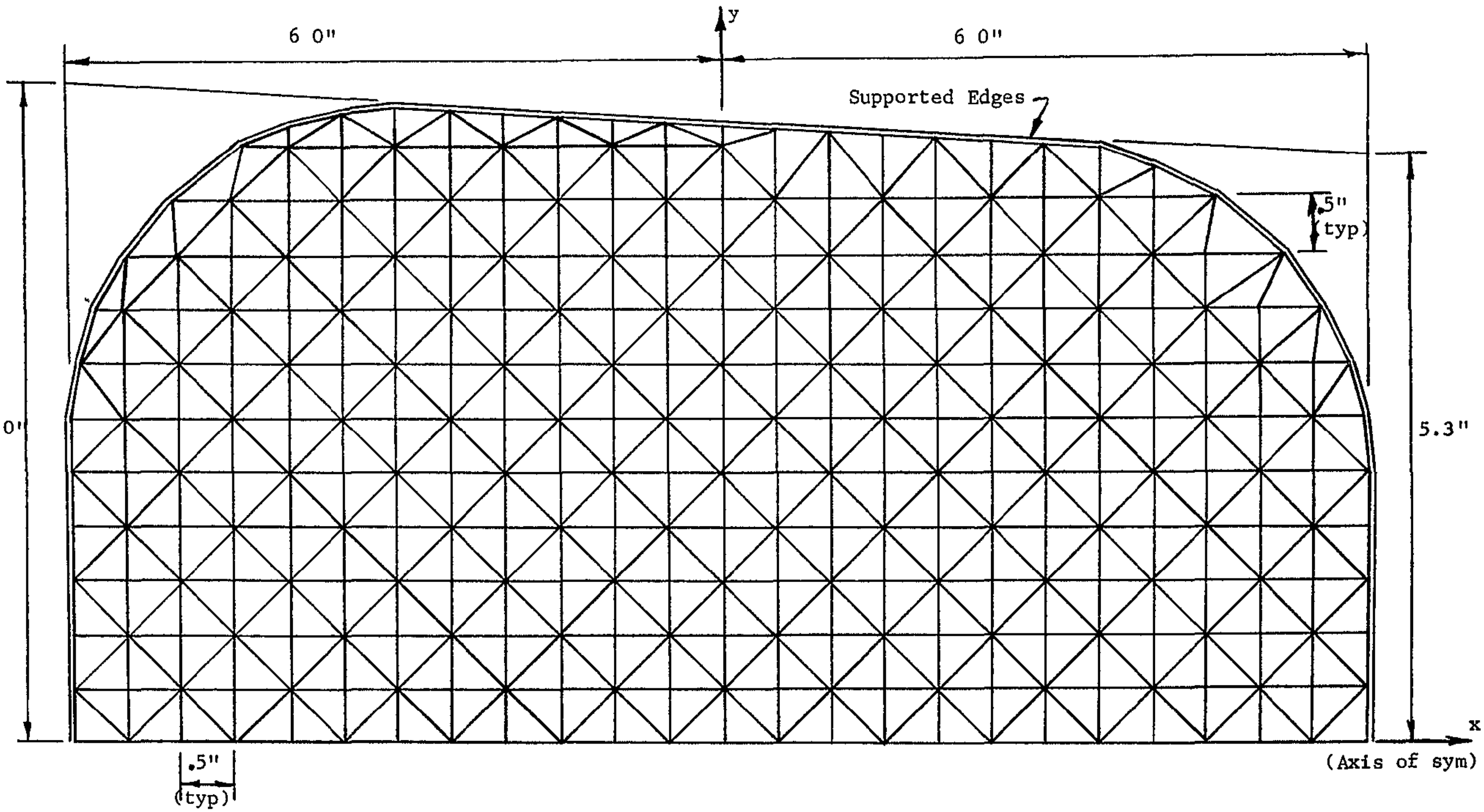

Figure 4. Isolated Window Model Articulation

not orthogonal to either of the coordinate axes. Deformations were then calculated for these moments and the pressure loading on the window. From the superposition of these sets of deformations and the condition that the slopes orthogonal to the boundary must be unconstrained, the set of simultaneous equations was generated. The solution to these equations results in the values of the moments that must be applied at the boundary points to secure the correct slopes at these points. The final deformations were obtained by applying these moments and the pressure loading to the window structure. For the clamped edge condition, on the other hand, boundary conditions could be imposed directly by requiring that slopes about the two coordinate axes, at the edge, be zero.

Figures 5 and 6 show the contours of equal deflection for a window of thickness 0.563 inches loaded with a unit pressure for the simply supported and clamped edge conditions, respectively. These contours show that the isolated window deforms in much the same way as does a square plate similarly loaded and supported, i.e., the deformed window is almost spherical near the center and gradually takes the shape of the boundaries as they are approached.

Cross-sectional plots of deflections along the coordinate axes of Fig. 5 are given in Figs. 7 and 8. Figures 9 and 10 show the cross-sectional plots of deflections along the coordinate axes of Fig. 6. These curves again exhibit the expected behavior, i.e., very similar to a square plate of like dimensions similarly loaded and supported.

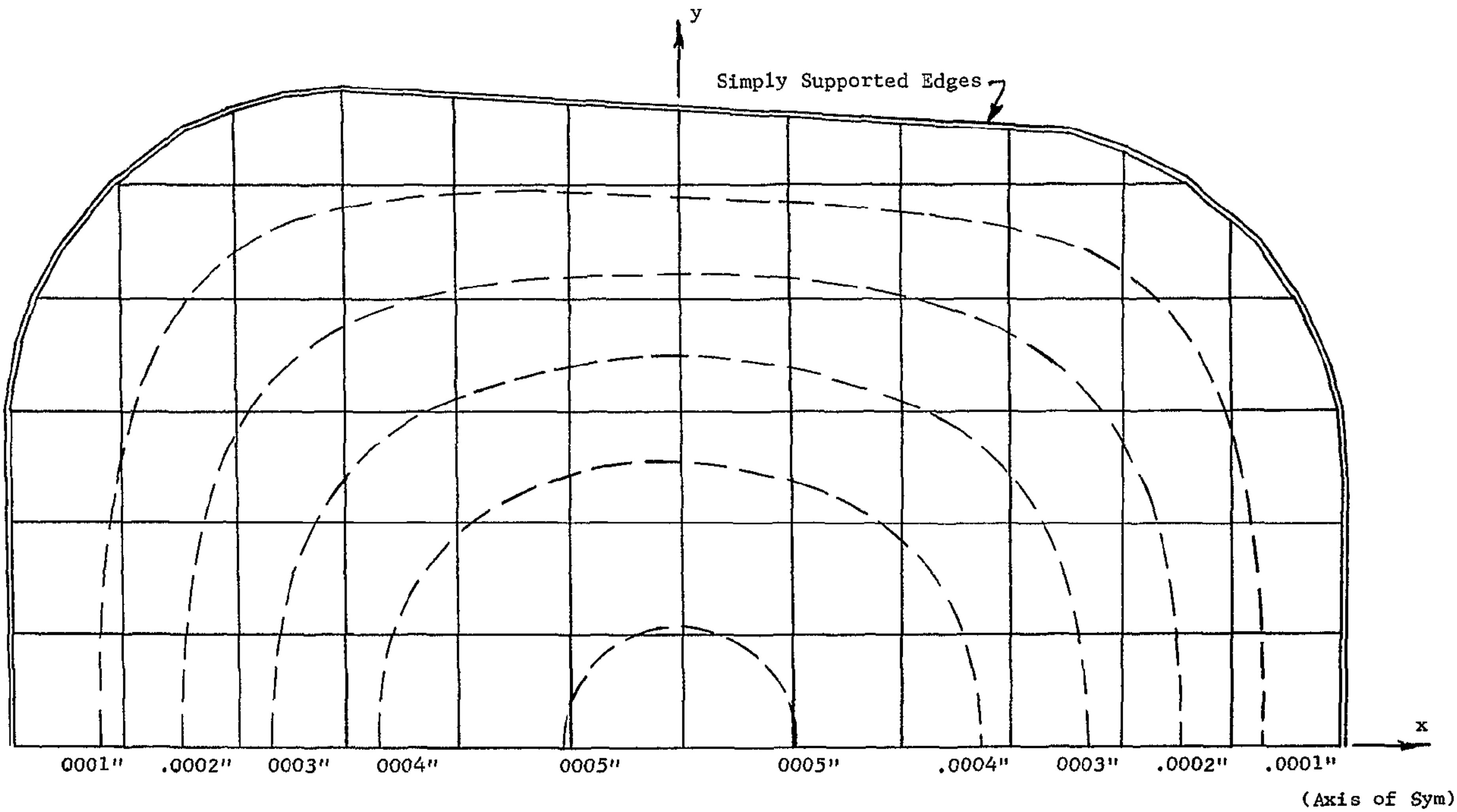

Figure 5 Deflections of Isolated Window-Simply Supported

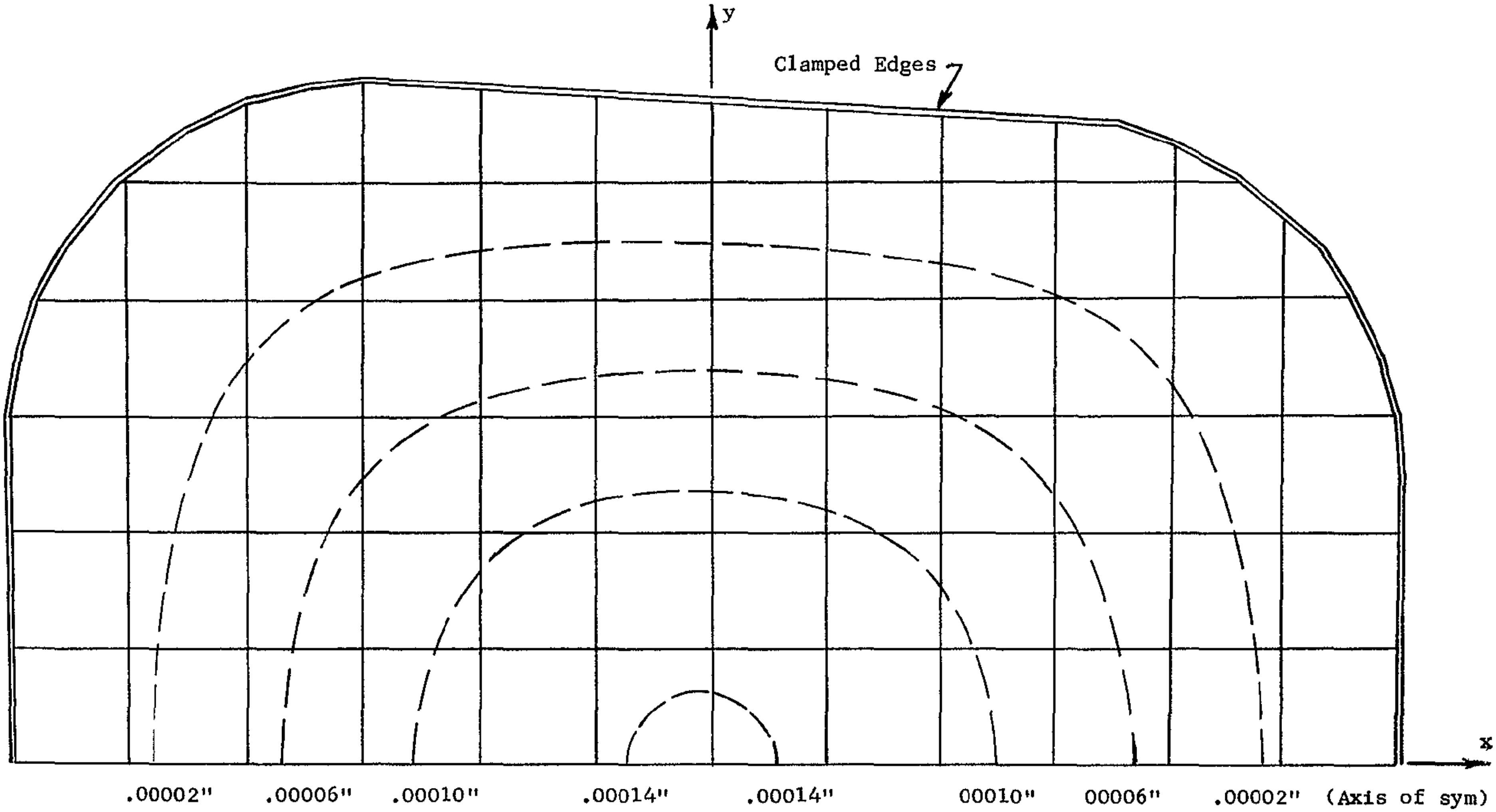

Figure 6 Deflections of Isolated Window-Clamped

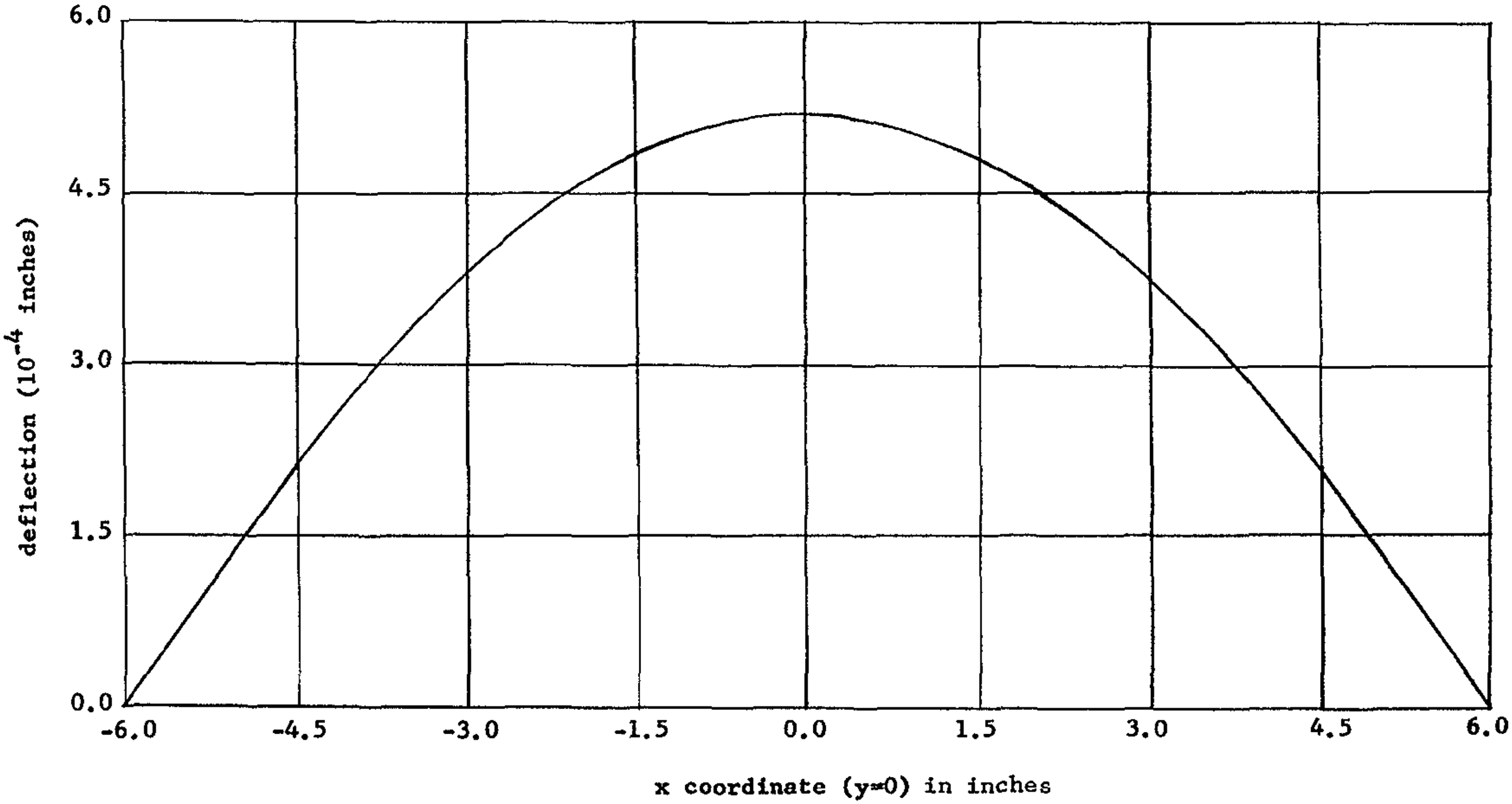

Figure 7. **Deflections** along x-axis of Simply Supported Window

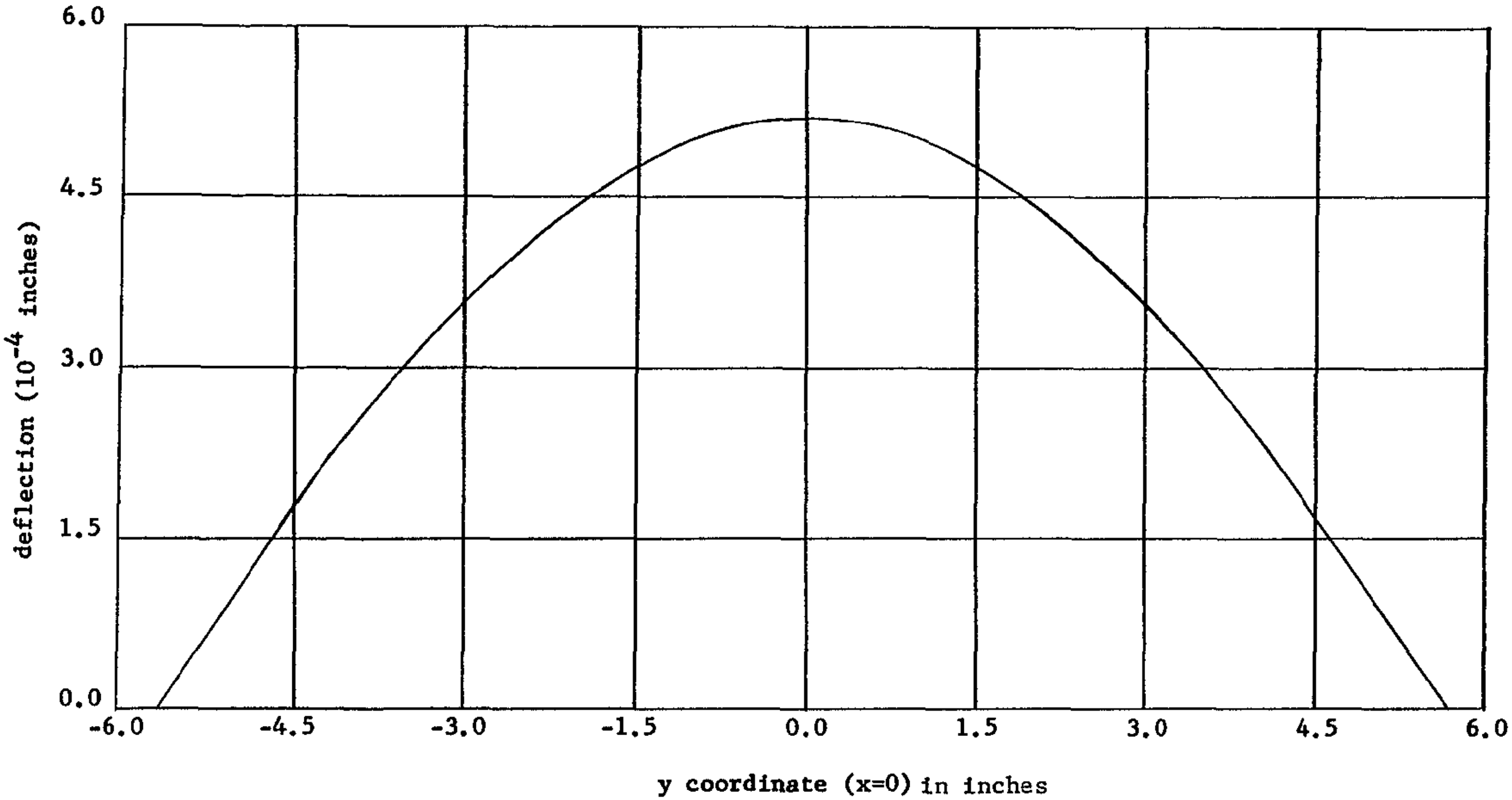

Figure 8. Deflections along y-axis of Simply Supported Window

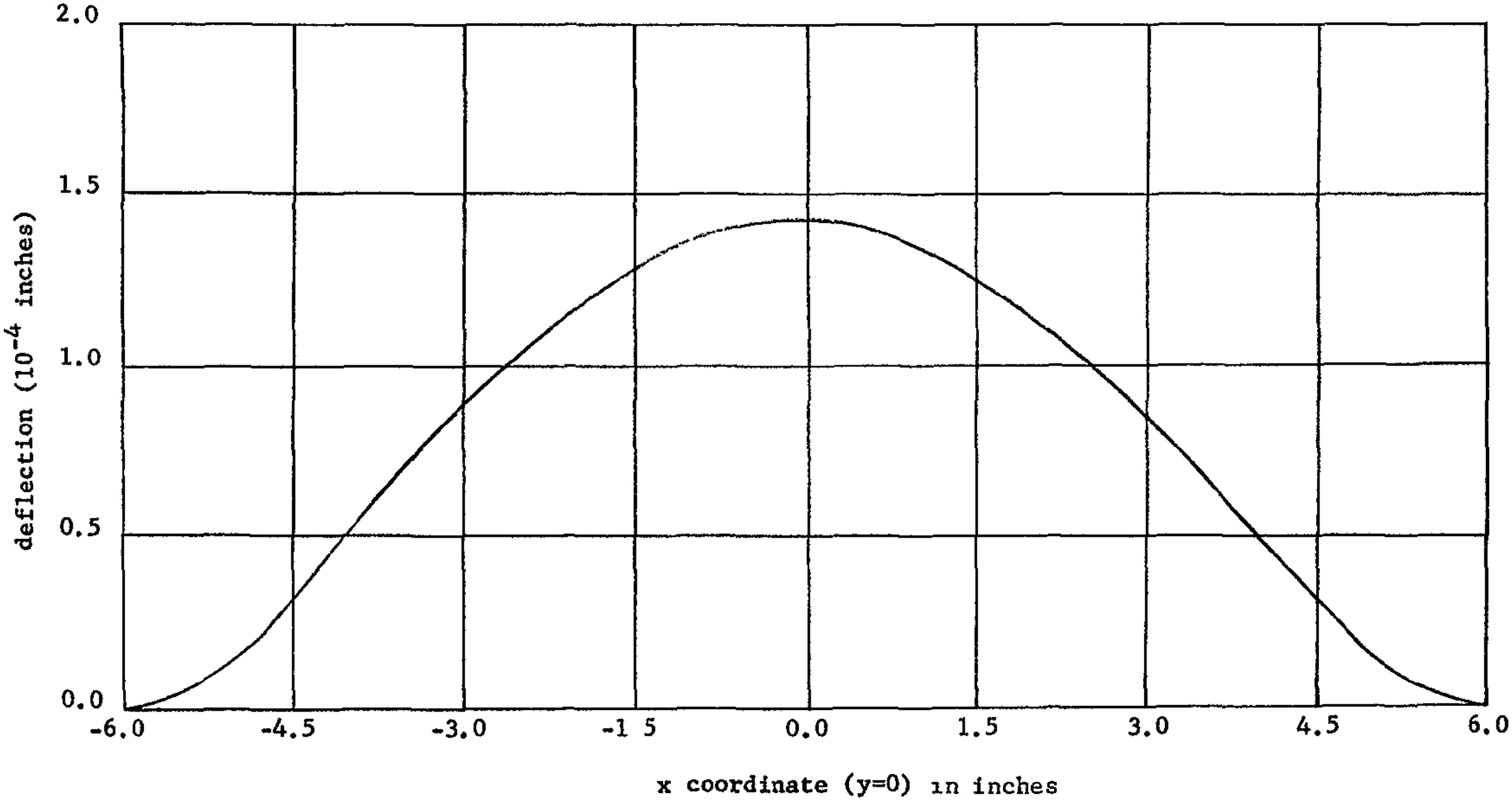

Figure 9 Deflections along x-axıs of Clamped Window

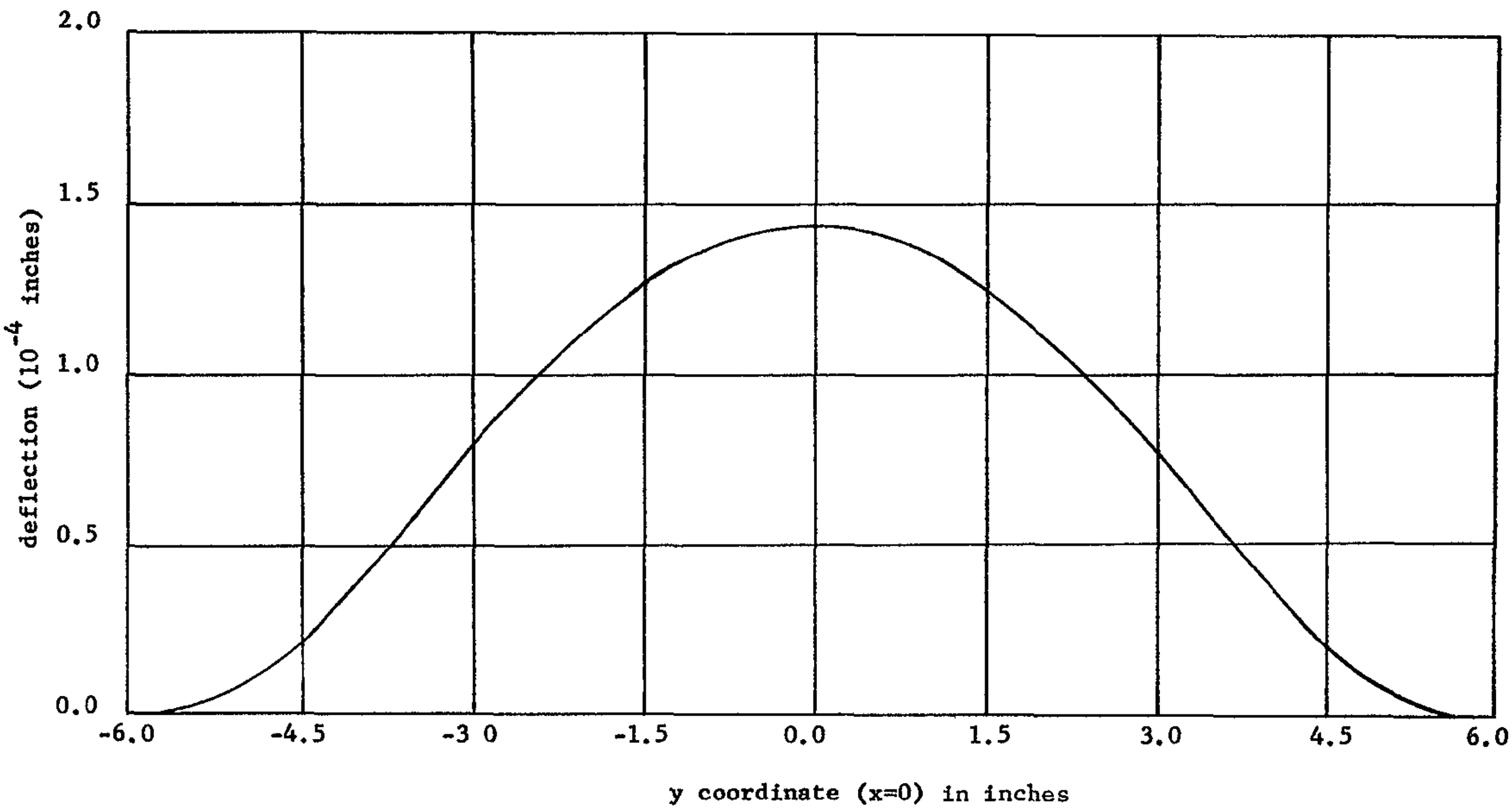

Figure 10 Deflections along y-axis of Clamped Window

To use the data for other pressure loadings and different window thicknesses, the principle of linear superposition may be applied. Thus, to find the magnitude of the deflection for a pressure loading other than unity, simply multiply the deflections for the unit pressure loading case by the desired pressure. To determine the deflections for windows of other thicknesses, multiply the given deflections by the cube of the ratio 0.563 to the new thickness, measured in inches. To determine the deformations of the window when the glass has elastic properties different from those cited above, simply multiply the deformation by the ratio $10.776 \cdot 10^6$ to $E/(1-\nu^2)$ where E is Young's modulus of elasticity measured in psi and ν is Poisson's ratio of the new material.

To validate the results obtained for the isolated window, the deformations were compared with the deformations of square plates which circumscribe and inscribe the boundaries of the isolated window. The deformations obtained for the isolated window must be bounded by the deformations obtained for the two square plates. The circumscribed plate was 12 inches by 12 inches and the inscribed plate was 10 inches by 10 inches. The maximum deflections and rotations for both the simply supported and clamped edge conditions were compared. Deformations for the 10-inch square plate were obtained by scaling those of the 12-inch plate.

The deformations obtained using the normal facet element with a one-half-inch grid network for these two simulations and for the isolated window are shown in Table 3. As required, deformations of the isolated window lie between those of the circumscribed and inscribed square plates.

Table 3

Comparison of Window Deformations

Edge Condition	Type of Deformation	Circumscribed Square Plate	Isolated Window	Inscribed Square Plate
Simply Supported	Deflection[a]	0.00053549	0.00051963	0.00025824
Simply Supported	Rotation[b]	0.00014830	0.00014787	0.00008582
Clamped	Deflection[a]	0.00016618	0.00014321	0.00008014
Clamped	Rotation[b]	0.00004315	0.00003921	0.00002497

a. Measured in inches.

b. Measured in radians.

Maximum deflections and rotations are within about 15 percent of those of the 12-inch square plate. These results substantiate the validity of the results obtained for the isolated window.

To establish the accuracy of the deformations of the isolated window, using the normal facet element on a one-half-inch grid, a comparison was made with the deformations obtained using the alternate facet element. The window analyzed was 0.563 inches thick, clamped around the edges, and loaded with a uniform unit pressure. Table 4 shows the results of these analyses for the maximum deflections and rotations occurrring in the window. The extrapolation curves, developed in Section 3, were used to predict the errors associated with the normal element solution. The predicted total error is less than 0.3 seconds of arc. Based upon the similarity of the analyses for the clamped and simply supported edge conditions, the same error can be associated with the solution obtained for the isolated window with simply supported edge conditions.

The Window in its Structural Environment

Predictions of the deformations of the Apollo Scientific Side Window in its structural environment were made in two phases. The objective of the first phase was to determine the amount of the structure surrounding the window which must be modeled in finer detail to predict the deformations of the window surfaces to the desired accuracy. These analyses include predictions of the structural deformations of the Apollo spacecraft under environmental conditions and determination of the errors associated with these deformations. The objective of the second phase analyses was to predict the deformations (and associated errors) of the refined model of the window.

Table 4

Analysis Accuracy Comparison

	Type of Deformation	
	Deflection	Rotation
Normal Element Solution	.000143210"	.0000392141 rad.
Alternate Element Solution	.000142526"	.0000392504 rad.
Ratio of Normal Element Solution to Alternate Element Solution	.995225	1.000927
Predicted Ratio of Exact Solution to Normal Element Solution Using Extrapolation Curves	1.0135	1.0105
Predicted Error in Normal Element Solution	1.25%	1.05%
Error in Extrapolation Curves	4.50%	2.20%
Total Error on Normal Element Solution	5.85%	3.25% (0.26 sec.)

First-Phase Analysis Procedure.- The first-phase objective is consistent with an extension of Saint Venant's Principle[12]. This principle states that the stresses (and, consequently, elongations) due to locally applied self-equilibrating loads become increasingly smaller as the distance from the point of application of the load increases. In the spacecraft window analysis, boundary conditions suppress rigid body motions. Thus, deformations, for loads applied at the window, must exhibit a decay as well as the stresses and elongations.

A relative measure of the magnitude of the deformations is needed to determine their significance. This measure is obtained by comparing the deformations due to a self-equilibrating load with those due to a cabin pressure load. In accord with the principle, there will be some boundary contour at which the self-equilibrating load deformations become negligible compared to the cabin pressure deformations. Beyond this "Saint Venant boundary," the self-equilibrating load has no significant effect. Thus, by imposing the appropriate deformations on the boundary of the refined model, the effect of the rest of the structure on the refined model can be represented.

Saint Venant boundary deformations will be predicted approximately. An estimate of the prediction error can be obtained using the normal and alternate finite analyses of the structure, along with the extrapolation curves developed in Section 3. The deformations resulting from the normal element analyses then can be extrapolated to a set of deformations with smaller errors, using the extrapolation curves. These extrapolated deformations will be imposed on the boundary of the refined model.

The Saint Venant boundary deformations consist of rigid body and elastic deformations. The rigid body deformations are those which incur translation and/or rotation of the undeformed window system. The elastic deformations occur due to the development of strains in the window system. To determine an approximation of the amount of rigid body deformations in the extrapolated deformations, the following procedure is used

1) The extrapolated deformations are transformed to the coordinate system of the isolated window model described previously in this section.
2) A least-square plane is fit through these deformations.
3) The deviations of the extrapolated deformations from the least-square plane are determined.
4) An estimate of the amount of rigid rotations is obtained by comparing the deviations of the extrapolated deformations from the least-square plane with the rotations of the least-square plane.

Assuming that the error in the extrapolated deformations is more than allowed, two questions arise.

1) How much do the errors in the elastic deformations at the window frame decay in the interior of the window due to the flexibilities of the gasket material and the window panes?
2) What effect does the rigid body rotation and its associated error have on the deviations of rays passing through the window panes?

The first question is answered by studying the deformations resulting from the deviations of the extrapolated deformations from the least-square plane applied to the edge of the unloaded refined model. The second question is examined by performing ray trace studies on the window undergoing only rigid body rotations.

Second-Phase Analysis Procedure.- In the second phase of the analysis, the extrapolated deformations from the first-phase analysis are imposed on a refined model of the window and its surrounding structure to arrive at the final sets of deformations for the window surfaces. Included in the refined model are the window frame and gasket material. A study is made to determine the extent to which these components must be modeled.

It should be noted that while the structure and pressure loadings are symmetric, the imposed deformations, in general, are not. Consequently, superposition of deformations resulting from symmetric and asymmetric analyses are used to develop the final deformations. This method of analysis reduces data processing time. By appropriately scaling the imposed deformations and loadings, all nine flight-loading conditions, along with the deviations from the least-square plane, are applied to the model for both the symmetric and asymmetric cases. Appropriate combinations of the deformations obtained from these analyses result in the prediction of final deformations over the window panes.

To determine how much the error in the elastic deformations at the boundary contour decays on the interior of the window, the deflections resulting from the imposition of the least-square deviations at the boundary contour were compared to the deflections resulting from a representative loading. A mean of the ratio of deflections for these two cases is calculated for points on the boundary contour and for points within the refined region A comparison of these means gives an estimate of the amount of decay of the error.

Phase I - Analyses and Results.- In the first phase of the analysis, the Apollo spacecraft between the forward and aft bulkheads is modeled using a coarse grid network. Exploiting the symmetry of the structure, only the left half is modeled. Figure 11 shows the finite element model articulation which is used in the analyses. Appendix D lists the coordinates of the control points and the kinematic restraints. In addition to the symmetry boundary conditions, the model is fixed in space at three other points to prevent rigid body translations.

The forward and aft bulkheads are modeled with radial beams with stiffnesses equivalent to those of the bulkheads. The details of the derivation of the section properties of these beams are given in Appendix D. Appendix D also includes calculations of the section properties of other structural components of the spacecraft. The eccentricities of the stiffeners are modeled for both circumferential and longitudinal stiffeners.

The honeycomb panels, of which the shell of the spacecraft is composed, are modeled with flat triangular shell elements (facets) of equivalent stiffnesses. These equivalent facets are developed using the procedure outlined by Lang[4]. The development of the equivalent facets is included in Appendix D.

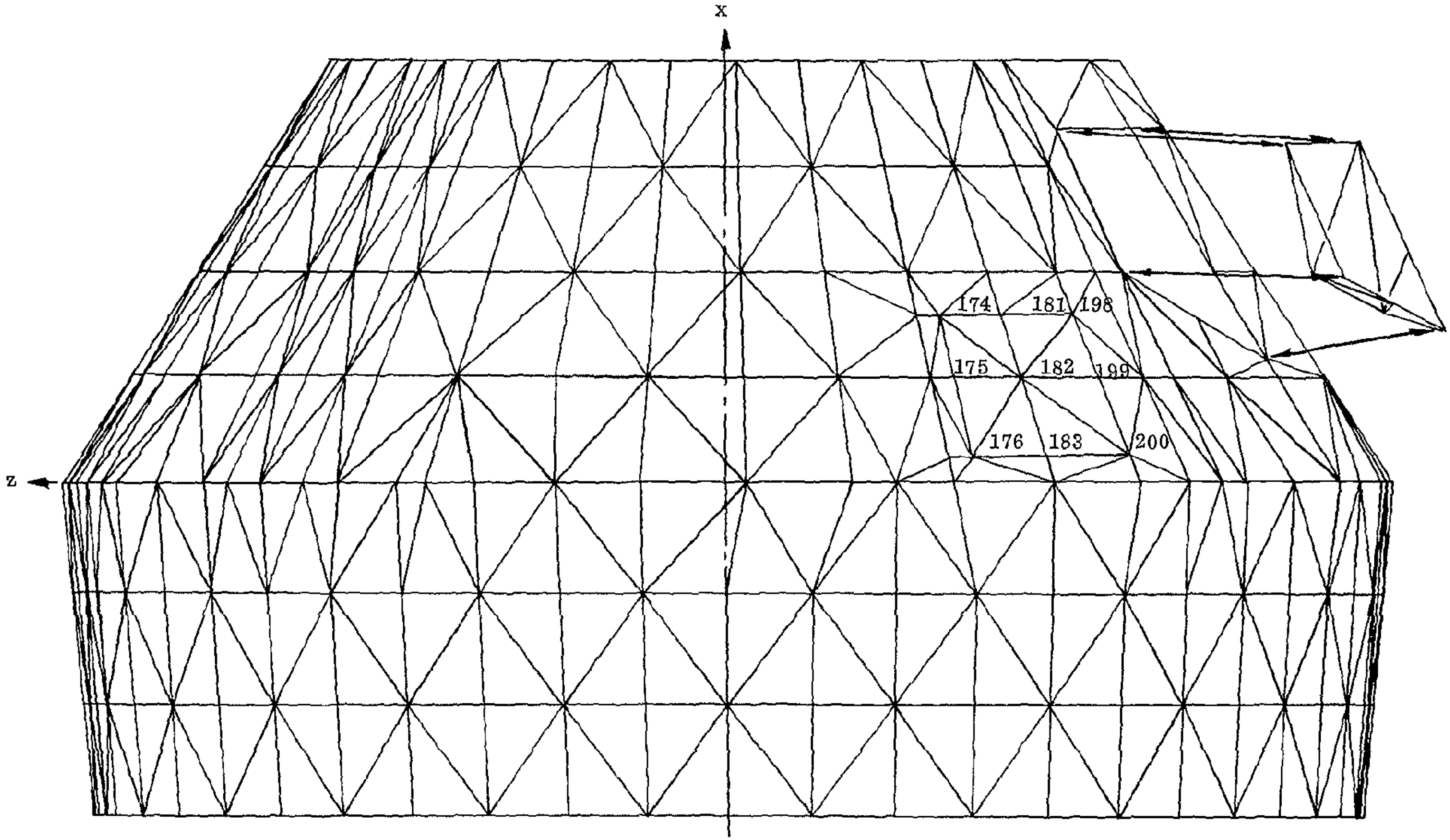

Figure 11 Apollo Structure Model Articulation

The material model is described in Section 2. The materials are those designated on the assembly drawings supplied by the NASA Ames Research Center. These are 2014-T6 and 7075-T6 aluminum for the rings and stiffeners, 5052 Hexcel honeycomb for the shell structure and fused silica glass for the window panes. Material elastic constants are given in Appendix D. A partial cross-section of the window is shown below.

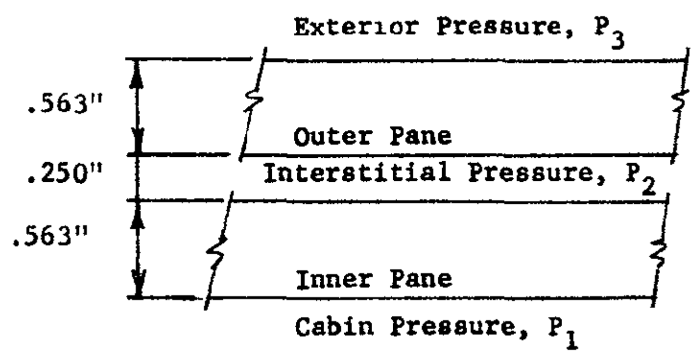

Apollo Window Cross-Section

The self-equilibrating loads which applied in the Phase I analysis are in-plane loads on the window frame resulting from the largest interstitial pressure (8.5 psia). The cabin pressure applied to the structure (4.1 psia) for the comparison gives the greatest pressure differential with the interstitial pressure.

Table 5 shows the deformations at points on the window frame resulting from the above analysis. These deformations have been transformed to a coordinate system which has its x-y plane lying in the plane of the window. A comparison of these deformations shows that the maximum effect of the self-equilibrating loads is a rotation of $0.279 \cdot 10^{-6}$ radians (less than one-tenth of one second of arc) occurring at the center of one edge of the

Table 5

Deformations of Window Frame
(Normal Facet Element)

Joint	Cabin Pressure Load*			Interstitial Pressure Load		
	w (inches)	Θ_x (rad)	Θ_y (rad)	w (inches)	Θ_x (rad)	Θ_y (rad)
174	$.303.10^{-1}$	$.359.10^{-3}$	$-.221.10^{-3}$	$.800.10^{-8}$	$.193.10^{-6}$	$-.147.10^{-7}$
175	$.279.10^{-1}$	$.122.10^{-3}$	$-.427.10^{-3}$	$.960.10^{-7}$	$.279.10^{-6}$	$.135.10^{-7}$
176	$.250.10^{-1}$	$-.895.10^{-4}$	$-.305.10^{-3}$	$.365.10^{-6}$	$.104.10^{-6}$	$.266.10^{-7}$
181	$.291.10^{-1}$	$.261.10^{-3}$	$-.152.10^{-3}$	$-.619.10^{-6}$	$.118.10^{-6}$	$-.632.10^{-7}$
185	$.250.10^{-1}$	$.750.10^{-4}$	$-.252.10^{-3}$	$-.116.10^{-6}$	$.108.10^{-6}$	$.111.10^{-6}$
198	$.274.10^{-1}$	$.201.10^{-3}$	$-.202.10^{-4}$	$-.782.10^{-7}$	$-.246.10^{-6}$	$-.388.10^{-7}$
199	$.260.10^{-1}$	$.174.10^{-3}$	$-.299.10^{-3}$	$-.126.10^{-6}$	$-.235.10^{-6}$	$.397.10^{-8}$
200	$.241.10^{-1}$	$.134.10^{-3}$	$-.175.10^{-3}$	$.204.10^{-6}$	$-.172.10^{-6}$	$.519.10^{-7}$

* Joint numbers correspond to those of the Apollo structural model articulation.

window. Since this effect is negligible, compared with the deformations due to the cabin pressure load, the window frame itself is the Saint Venant boundary contour.

Results of the study of the normal and alternate facet element analyses of the Apollo structure are given in Tables 6 and 7. (Each of these analyses required the solution of 1,524 equations.) The data show that the maximum extrapolation from the normal element solution is 25.6 seconds of arc for a cabin pressure of 6.1 psia. Based on the error established for the extrapolation curves developed in Section 3, the maximum error in the extrapolated deformations is 2.6 seconds of arc under a cabin pressure loading of 6.1 psia. Thus, the maximum error in the normal element solutions could be as much as 28 2 seconds.

Rigid rotation in the boundary deformations of the least-square plane about the x and y axes of the window for a cabin pressure of 4.1 psia are 10.3 and 16.7 seconds, respectively. The deviations of the extrapolated deformations from the least-square plane are 8.6 and 8.7 seconds, respectively, for the two rotations. Thus, roughly speaking, fifty percent of the deformations is rigid body and fifty percent is elastic deformation. Applying this same ratio to the error in the extrapolated deformations, about 1.3 seconds of the error is in the rigid body deformations and 1.3 seconds in the elastic deformations.

Appendix E contains further data of the Phase I analysis, including tabulations of the deformations at the window frame resulting from the analysis of the window in its structural environment and the extrapolation of these deformations using the curves develped in Section 3. Also included in Appendix E are the transformations of the deformations to the

Table 6

Apollo Window System Analysis
(Deflections for 4.1 psia Cabin Pressure)

Node[a]	$\delta_{1/1}$ [b]	$\delta_{3/1}$ [b]	$\delta_{3/1}/\delta_{1/1}$	$\delta_e/\delta_{1/1}$ [c]	δ [d]	Error[e]
1741	-.063739	-.059253	.929619	.955	-.060871	4.5
1742	.123450	.116015	.939773	.965	.119129	3.5
1743	.341409	.343477	1.006057	1.040	.354895	4.0
1751	-.054042	-.051076	.945117	.970	-.052421	3.0
1752	.105778	.101509	.959642	.980	.103662	2.0
1753	.327821	.332315	1.013709	1.058	.346671	5.8
1761	-.040907	-.037401	.914293	.945	-.038657	5.5
1762	.085472	.080457	.941326	.967	.082651	3.3
1763	.312461	.316428	1.012969	1.055	.329646	5.5
1811	-.060387	-.056353	.933198	.960	-.057972	4.0
1812	.114315	.107805	.943052	.968	.110657	3.2
1813	.334386	.337104	1.008128	1.044	.349099	4.4
1831	-.041571	-.037558	.903466	.935	-.038869	6.5
1832	.085843	.079928	.931095	.957	.082152	4.3
1833	.311300	.314438	1.010080	1.049	.326554	4.9
1981	-.054263	-.048560	.894901	.925	-.050193	7.5
1982	.100944	.092098	.912367	.943	.095190	5.7
1983	.324439	.325018	1.001785	1.029	.333686	2.9
1991	-.047353	-.042804	.903934	.936	-.044322	6.4
1992	.092088	.085123	.924366	.952	.087668	4.8
1993	.316526	.318633	1.006657	1.040	.329187	4.0
2001	-.038052	-.033581	.882503	.915	-.034818	8.5
2002	.078956	.072469	.917840	.948	.074850	5.2
2003	.305957	.308396	1.007972	1.044	.319266	4.4

a. Node numbers correspond to those of the Apollo structural model articulation.

b. Measured in 10^{-1} inches.

c. Taken from extrapolation curve developed previously.

d. Extrapolated solution measured in 10^{-1} inches.

e. Amount of extrapolation from normal element solutions (%).

Table 7

Apollo Window System Analysis
(Rotations for 4.1 psia Cabin Pressure)

Node[a]	$\Theta_{1/1}$[b]	$\Theta_{3/1}$[b]	$\Theta_{3/1}/\Theta_{1/1}$	$\Theta_e/\Theta_{1/1}$[c]	Θ[d]	Error[e]
1744	-.083582	-.066022	.789907	.885	-.073970	2.0
1745	-.280496	-.242762	.865474	.925	-.259459	4.3
1746	.302862	.257209	.849261	.920	.278633	5.0
1754	-.327846	-.247327	.754400	.870	-.285226	8.8
1755	-.278382	-.270582	.971981	1.000	-.278382	0
1756	.106889	.141171	1.320775	1.390	.148576	8.6
1764	-.294221	-.351293	1.193977	1.235	-.363363	14.3
1765	-.104860	-.171701	1.637431	1.770	-.185602	16.7
1766	-.061917	.006788	-.109631	.450	-.027863	7.0
1814	-.044957	-.065119	1.448473	1.545	-.069459	5.1
1815	-.213907	-.226586	1.059273	1.075	-.229950	3.3
1816	.209284	.216426	1.034126	1.050	.219748	2.2
1834	-.186916	-.230624	1.233838	1.285	-.240187	11.0
1835	-.175998	-.205988	1.170400	1.205	-.212078	7.4
1836	.057631	.043278	.750950	.870	.050139	1.5
1984	.043624	.031285	.717151	.850	.037080	1.3
1985	-.106676	-.175636	1.646443	1.780	-.189883	17.2
1986	..165635	.230153	1.389486	1.475	.244312	16.2
1994	-.189331	-.103956	.549070	.770	-.145785	9.0
1995	-.260618	-.209677	.804538	.895	-.233253	5.6
1996	.130287	.151886	1.165780	1.200	.156344	5.4
2004	-.115282	-.164963	1.430952	1.520	-.175229	12.4
2005	-.144931	-.208746	1.440313	1.535	-.222469	16.0
2006	.120137	.129140	1.074939	1.090	.130949	2.2

a. Node numbers correspond to those of the Apollo structural model articula

b. Measured in 10^{-3} radians.

c. Taken from extrapolation curve developed previously.

d. Extrapolated solution measured in 10^{-3} radians.

e. Amount of extrapolation from normal element solutions (sec.).

coordinate system of the isolated window and the interpolation between these deformations to determine the deformations to be imposed at each point on the window frame. Appendix E also contains data supporting the above discussion of rigid rotation and elastic deformation errors.

Phase II - Analyses and Results.- For the second phase of the analysis, the refined model consists of two window panes, modeled with the isolated window models, and the window frame system. The study of the window frame structure determined that it is essentially rigid except for the gasket material and the projecting ribs which support the edge of the window panes. The model of the frame system consists of equivalent beams interconnecting the edges of the two window panes and the points at which deformations are imposed. The refined model then consists of two one-half window models joined with the model of the frame and gasket material. It is loaded with the flight pressures and has imposed edge deformations along with the symmetric and asymmetric boundary conditions on the x-axis. (See Fig. 4.)

Details of the study of the window system and the development of the model for the window frame and gasket material are given in Appendix F. Also included in Appendix F are the joint numbering for the refined model and details of the equations relating the symmetric and asymmetric loadings and deformations.

Table 8 gives the loading conditions for which the above analyses are performed. Both the symmetric and asymmetric analyses require the solution of 2,318 equations.

Figures 12 and 13 show the deformation contours of the above analyses for a cabin pressure of 5.1 psia and an interstitial pressure of 7.5 psia

Table 8

Apollo Window Load Conditions

Load Number	Cabin Pressure*	Interstitial Pressure*	Exterior Pressure*
1	4.1	6.5	0
2	5.1	6.5	0
3	6.1	6.5	0
4	4.1	7.5	0
5	5.1	7.5	0
6	6.1	7.5	0
7	4.1	8.5	0
8	5.1	8.5	0
9	6.1	8.5	0

* Measured in psia.

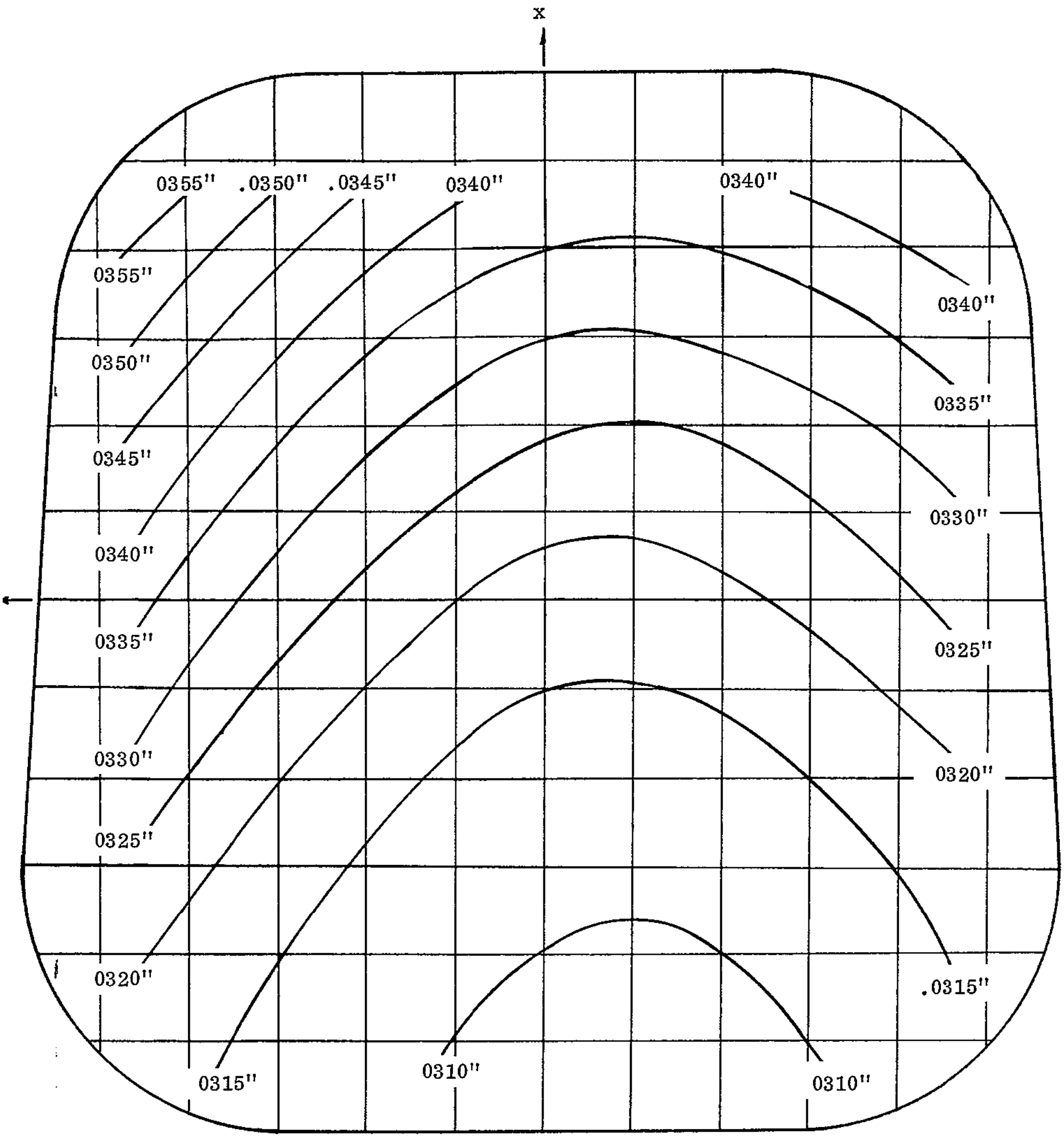

Figure 12 Contours of Equal Deflection for Inner Pane

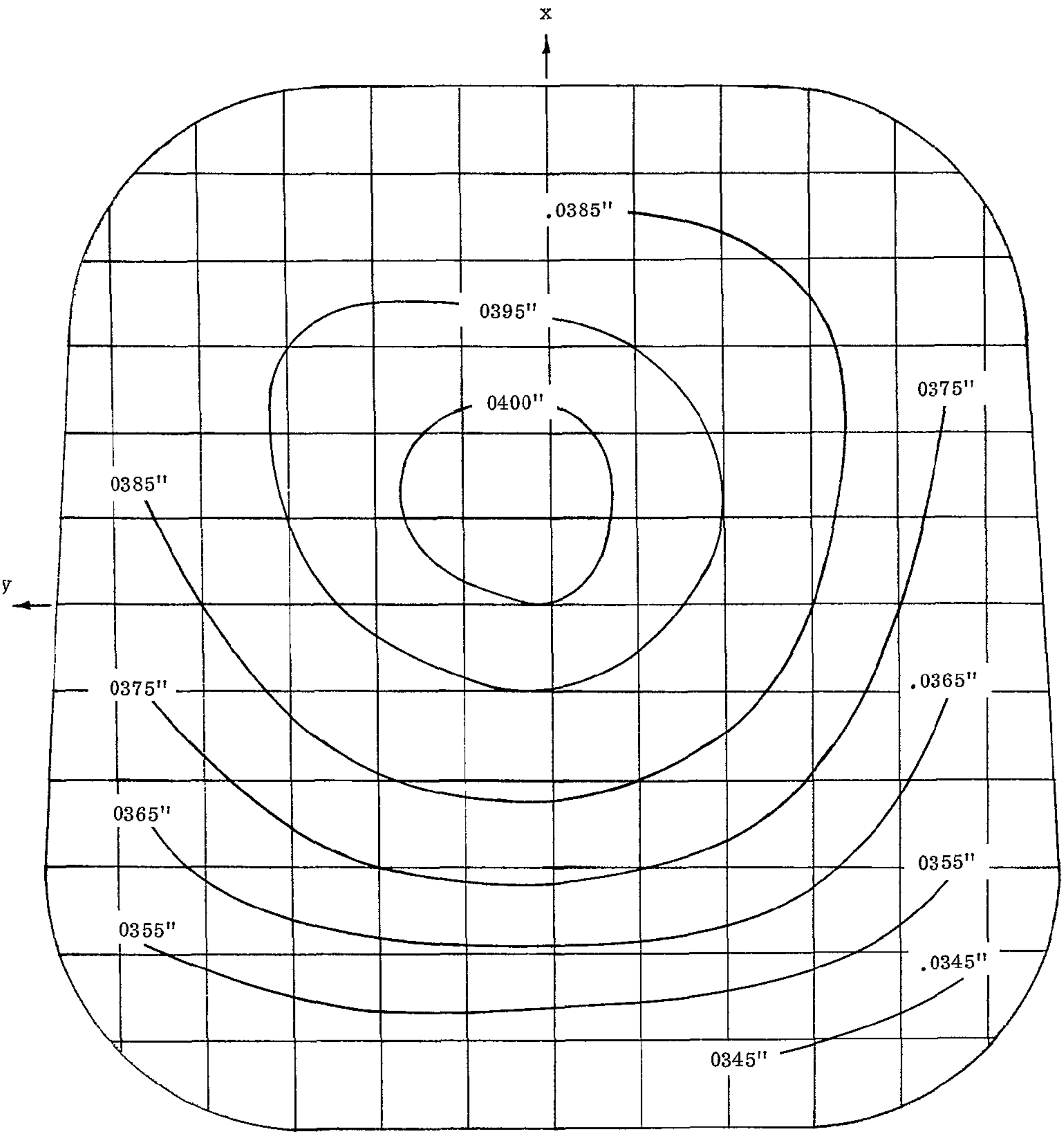

Figure 13 Contours of Equal Deflection for Outer Pane

(load number 5). Figure 12 shows the contours for the inner pane (relative to the undeformed surface) and Fig. 13 those for the outer pane. Both sets of contours show the effect of a rigid body rotation. The contours are not centered on the window. If the rigid body rotations are removed, the contours would show the spherical deformation pattern exhibited by the isolated window. The fact that some of the contours are closed for the outer pane (see Fig. 13) is due to the larger pressure loading on it. This yields deflections which are larger than those resulting from the rigid body rotations.

Cross-sectional plots of deflections along the coordinate axes of Figs. 12 and 13 are given in Figs. 14 and 15. The actual window spacing is not shown to make deflection pattern clear. The difference in deflection magnitudes of the inner and outer panes is shown by these plots. The amount of rigid rotation of the window about each of the axes is obtained by drawing a line connecting the edge points of each pane and measuring the inclination of the lines with the coordinate axes. The resulting rotations about the x and y axes are 26 seconds and 64 seconds, respectively. These differ from the rotations of the least-square plane through the window frame deformations due to the flexibilities of the gasket material and the supporting ribs of the window frame.

The deflections resulting from application of load number one are used to determine the decay of the error associated with the elastic deformations at the window frame. The mean of the deflection ratios is calculated for each of three sets of points on the window points on the window frame, points on the window panes at the window frame, and points on the window panes near the area of maximum deflection. The resulting

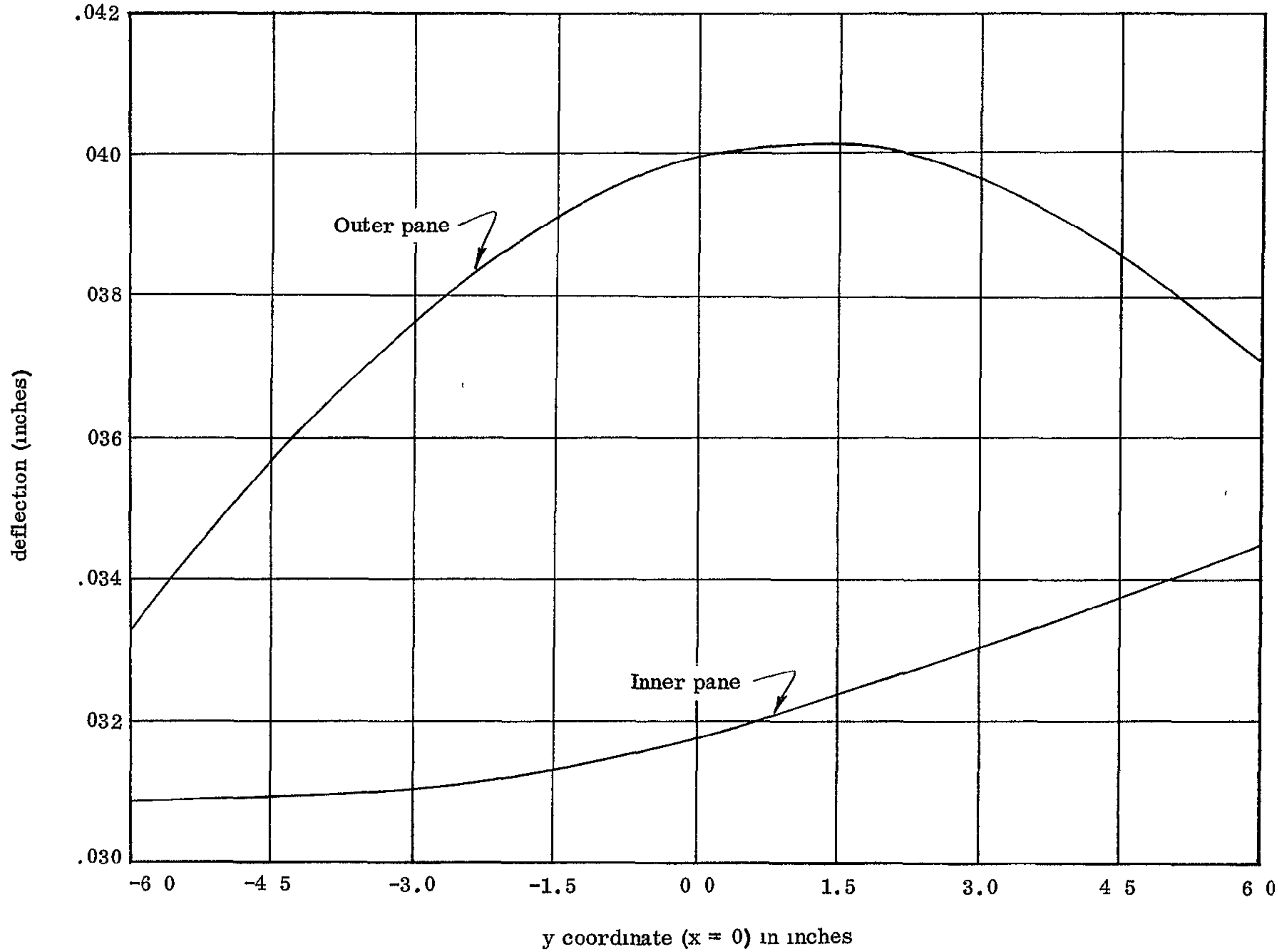

Figure 14 Deflections along x-axis of Apollo Window

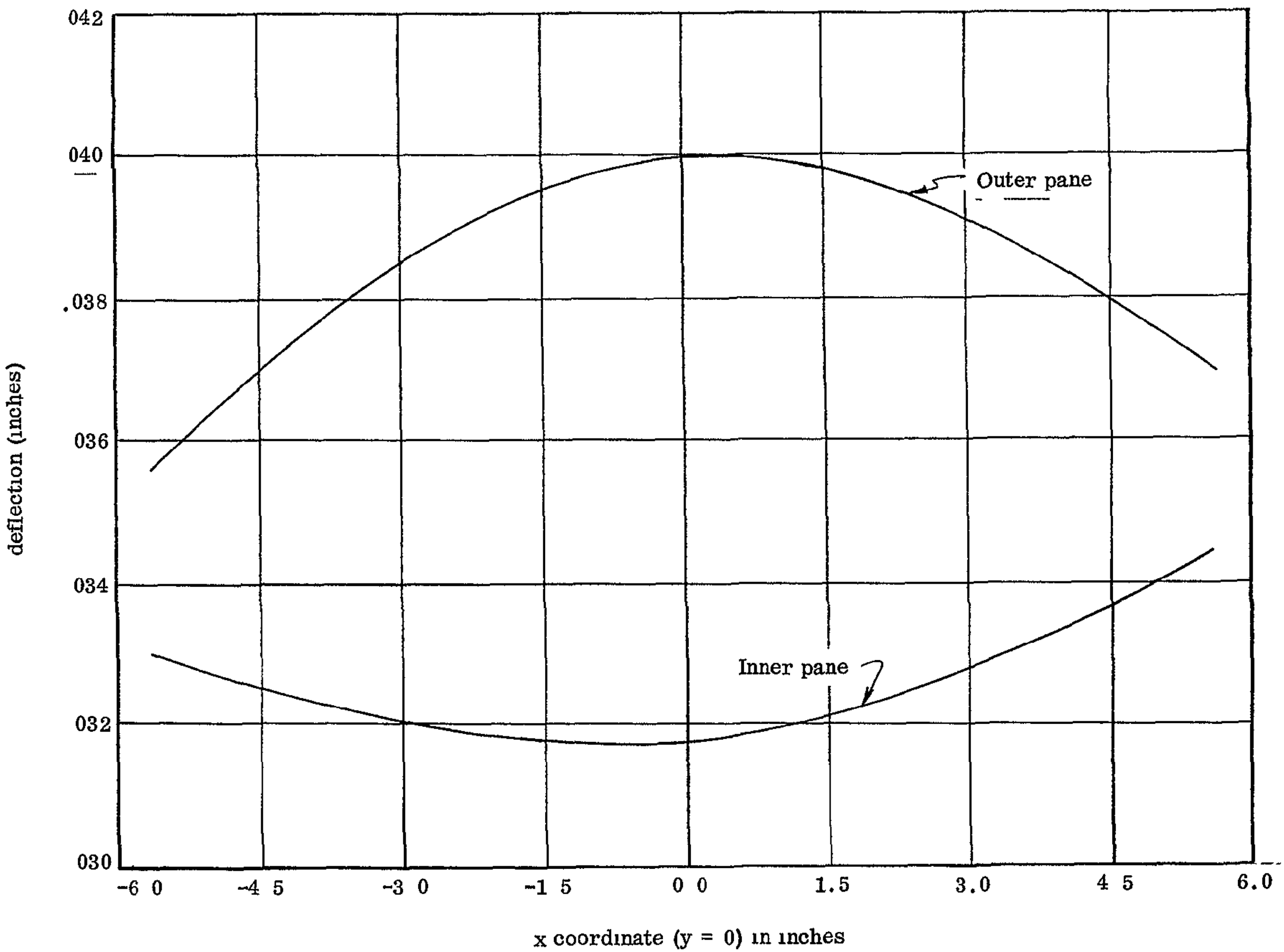

Figure 15 Deflections along y-axis of Apollo Window

means are given in Table 9. From these data, it is concluded that the error in the deflections at the window frame are reduced by 59 percent due to the flexibility of the gasket material and by another 7 percent due to the flexibility of the window panes. Using these percentage reductions, the error in elastic deformations of 1.3 seconds at the window frame is reduced to 0.5 seconds on the window pane at the window frame and to 0.4 seconds near the point of maximum deflection.

Consequently, neglecting the rigid rotations, predictions of deformations over the interior of the window have less than one second of arc error.

In Section 5, small rigid rotations are shown to have a negligible effect on deviations of light rays.

Table 9

Mean of Error Measure

Location of Points	Mean Error	Error Reduction
On Window Frame	0.88%	---
On Window Panes at Window Frame	0.36%	59%
On Window Panes Near Maximum Deflection	0.30%	66%

Section 5

APOLLO WINDOW RAY TRACE ANALYSES

This section describes the ray trace analyses which were performed on the Apollo Scientific Side Window. Single ray trace analyses were performed on the isolated window and on the window in its structural environment. Two ray trace analyses were performed only on the latter. Deformation analyses, upon which the ray trace analyses are based, are described in Section 4. The computer program used for the ray trace analyses is described in Ref. 7. A complete set of results is available for review at NASA Ames Research Center, Moffett Field, California.

Single Ray Trace Analysis

Single ray trace analyses are performed on the Apollo window for three sets of boundary conditions. For the first two of these, the window is isolated. For the third, the window is supported in its actual structural environment. Table 10 shows the loading conditions used in each analysis. Figure 16 defines the angles associated with the single ray trace analyses. (The plane angle is measured positive from the x-axis to the y-axis.)

Prior to performing the ray trace analyses, it is necessary to determine the effects of a rigid rotation on the deviations of light rays passing through the window. This analysis is performed on a square window with dimensions 12 4 inches by 12.4 inches. The window consists of two simply supported panes each 0.563 inches thick and separated by a distance of one-quarter of an inch. The cabin pressure is 5.1 psia and the interstitial pressure is 7.5 psia. There is no external pressure. The material properties used are those of the actual window.

Table 10

Load Conditions for Ray Tracing

Planform	Edge Condition	Cabin Pressure*	Interstitial Pressure*	Exterior Pressure*	No. of Cases
Isolated	Clamped	5.1	7.5	0	1
Isolated	Simply Supported	5.1	7.5	0	1
Actual	Actual	4.1,5.1,6.1	6.5,7.5,8.5	0	9

* Measured in psia.

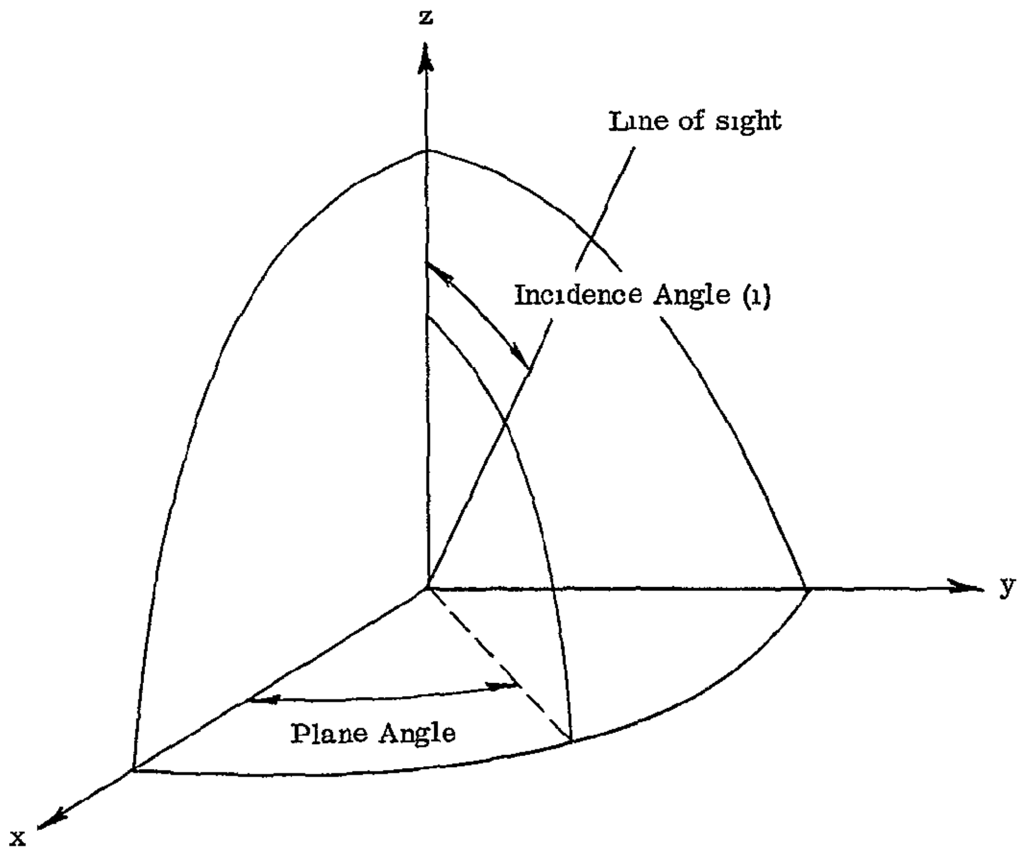

Figure 16 Single Ray Trace Angles

Tables 11 and 12 give the results of the ray trace analyses for this window configuration for various incidence angles. Table 11 shows the mean of light ray deviations for all points on a one-inch grid on the window surface. Table 12 gives the root mean square of these deviations.

Data in these tables indicate that for rigid rotations of the order of one minute, the maximum change in the mean of the deviations is 0.04 seconds. In the root mean square of the deviations, the maximum change is 0.05 seconds. Therefore, for small rigid rotations, the change in the light ray deviations is negligible. Thus, rigid rotations of the order which occur in the Apollo window system can be neglected. The error estimates given in Section 4 for elastic deformations indicate the deformations are effectively predicted with less than one second of arc error.

Figures 17 and 18 are plots of the mean deviations and root mean square (rms) deviations of light rays passing through the window system for the three edge conditions: clamped, simply supported (hinged), and actual. The deviations are plotted as functions of the plane angle for two incidence angles ($i = 30^{\circ}$ and $i = 60^{\circ}$). These analyses are performed for a cabin pressure of 5.1 psia, an interstitial pressure of 7.5 psia, and no external pressure.

These plots indicate that the mean and rms deviations for the simply supported and actual edge conditions are approximately the same. The mean deviation for the clamped edge condition is higher than either of the other two, while the rms deviations is smaller. The rms deviation for the actual edge condition shows more variation than either of the other two cases.

Table 11

Mean of Light Ray Deviations*

Incidence Angle	Plane Angle 0°	45°	90°	135°	180°	225°	270°	315°
$14^{\circ}59'$	4.158	4.141	4.157	4.141	4.158	4.141	4.158	4.141
$15^{\circ}00'$	4.162	4.146	4.162	4.146	4.163	4.146	4.163	4.146
$15^{\circ}01'$	4.167	4.151	4.166	4.151	4.167	4.151	4.167	4.151
$74^{\circ}59'$	35.84	28.79	35.71	28.74	35.88	28.91	35.99	28.83
$75^{\circ}00'$	35.87	28.82	35.74	28.77	35.91	28.94	36.03	28.87
$75^{\circ}01'$	35.91	28.84	35.78	28.79	35.95	28.96	36.07	28.89

* Measured in seconds.

Table 12

RMS of Light Ray Deviations*

Incidence Angle	Plane Angle 0°	45°	90°	135°	180°	225°	270°	315°
$14^{\circ}59'$	.4898	.9799	.4899	.9799	.4896	.9797	.4891	.9798
$15^{\circ}00'$	.4906	.9816	.4908	.9817	.4904	.9815	.4897	.9816
$15^{\circ}01'$	.4910	.9823	.4913	.9823	.4908	.9821	.4905	.9822
$74^{\circ}59'$	15.35	26.64	15.39	26.71	15.30	26.60	15.26	26.66
$75^{\circ}00'$	15.37	26.69	15.42	26.76	15.33	26.64	15.28	26.71
$75^{\circ}01'$	15.40	26.74	15.44	26.81	15.35	26.69	15.31	26.76

* Measured in seconds.

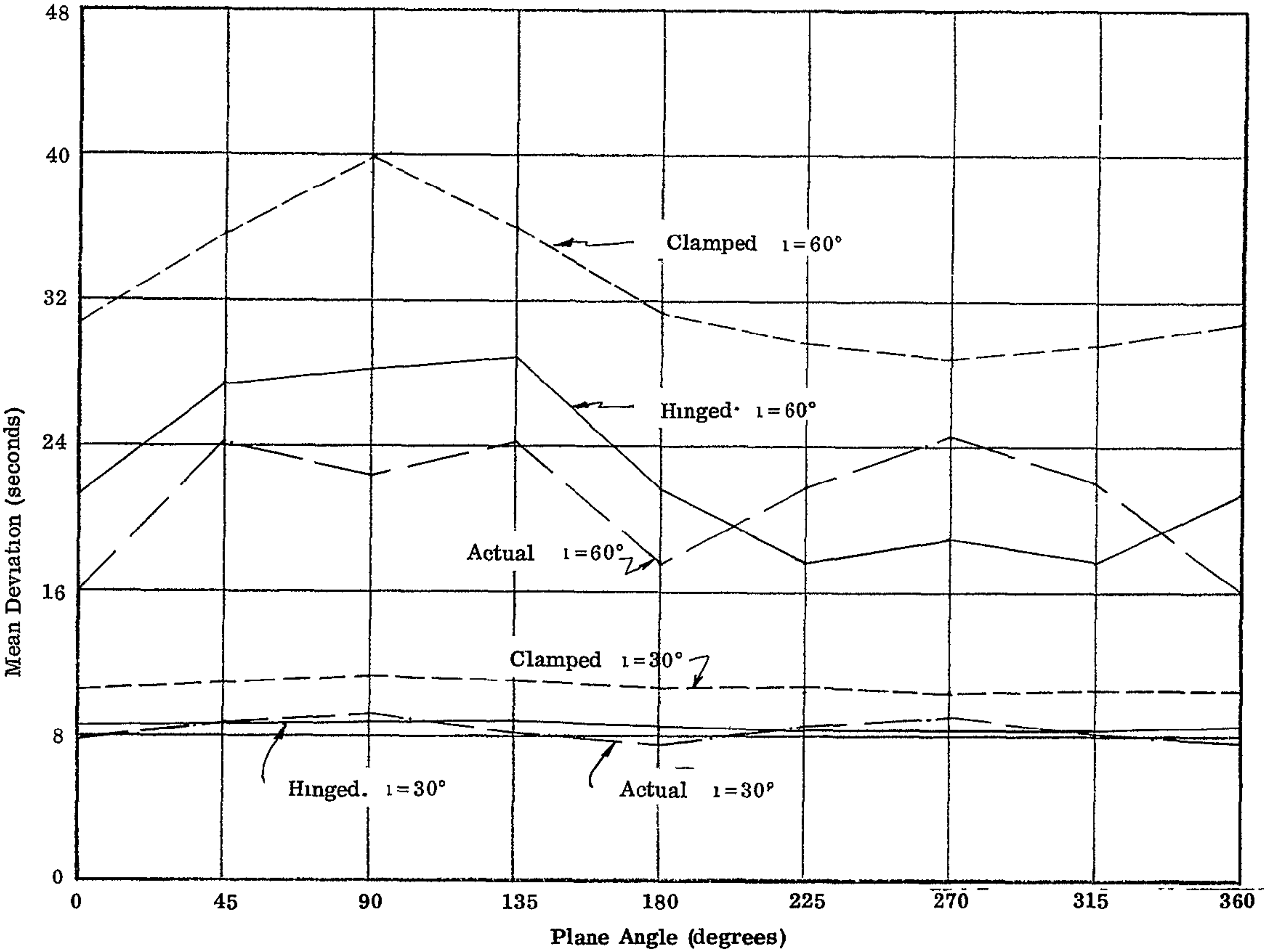

Figure 17. Mean of Ray Deviations - Edge Variation

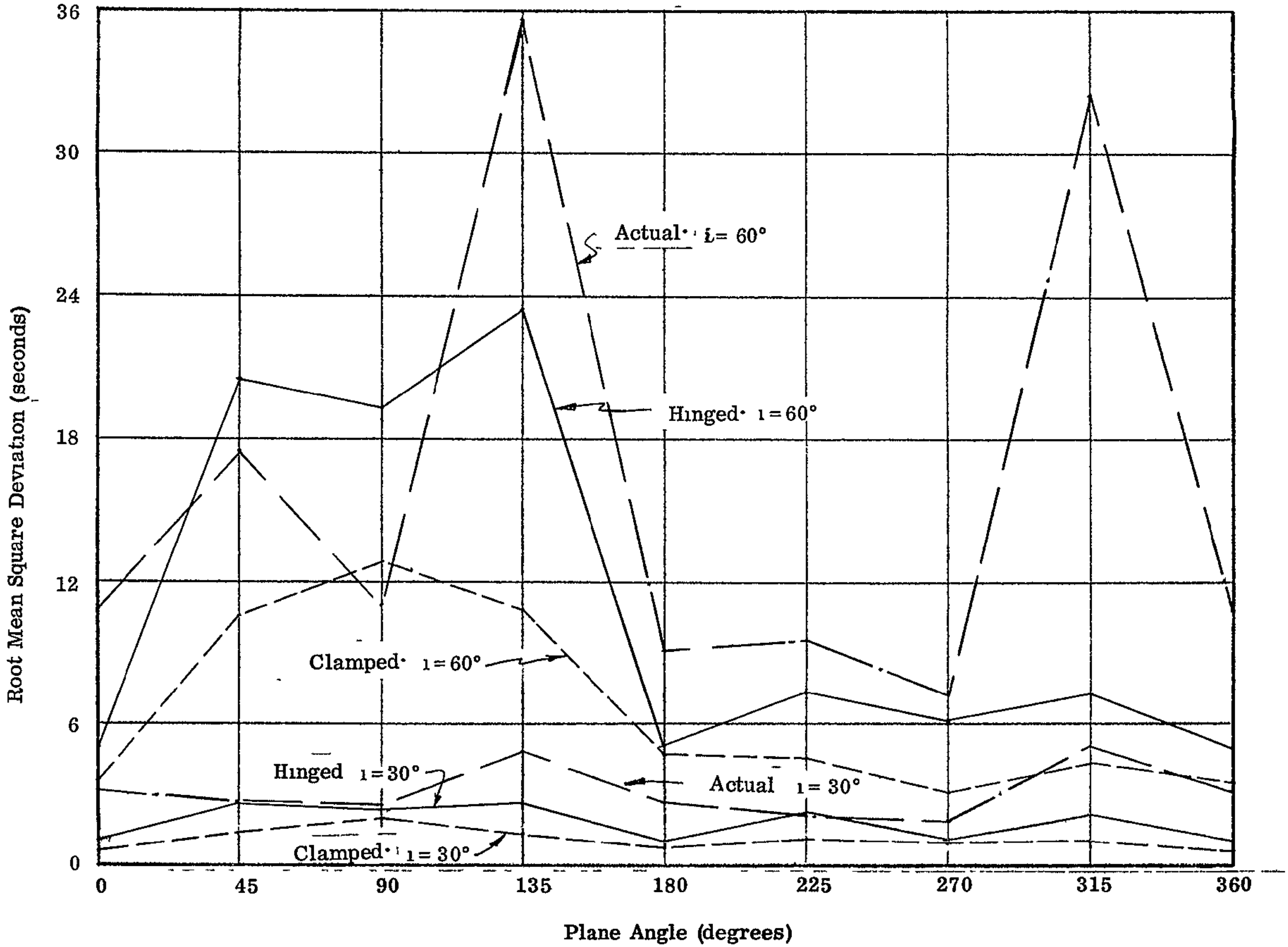

Figure 18. RMS of Ray Deviations - Edge Variation

Figures 19 through 22 show the plots of the mean and rms deviations of light rays passing through the window system supported with the actual edge condition. The deviations are plotted as functions of the plane angle for two incidence angles ($i = 30^{o}$ and $i = 60^{o}$). The curves of Figs. 19 and 20 are drawn from data generated by analyses performed with a cabin pressure of 5.1 psia, interstitial pressures (P_2) of 6.5, 7.5, and 8.5 psia, and no external pressure. These curves show that variations in the interstitial pressure have no significant effect on the mean or rms deviations of light rays passing through the window for any value of the plane angle or incidence angle.

Figures 21 and 22 show the results of analyses performed with cabin pressures (P_1) of 4.1, 5.1, and 6.1 psia, an interstitial pressure of 7.5 psia, and no external pressure. These curves show a definite increase in the mean and rms deviations as the magnitude of the cabin pressure is increased for all values of the plane and incidence angles.

The mean and rms deviations for analyses performed to study the effects of variations in the incidence angle are shown in Figs. 23 through 28. The analyses are performed for the three edge conditions and with a cabin pressure of 5.1 psia, an interstitial pressure of 7.5 psia, and no external pressure. The deviations are plotted as a function of the plane angle. Figures 23 and 24 show the results for the clamped edge condition, Figs. 25 and 26 for the simply supported edge condition, and Figs. 27 and 28 for the actual edge condition. Each set of curves exhibits the same tendencies. For $i = 0^{o}$, the deviations are negligible. As the incidence angle increases, the magnitudes of the mean and rms deviations increase for all values of the plane angle.

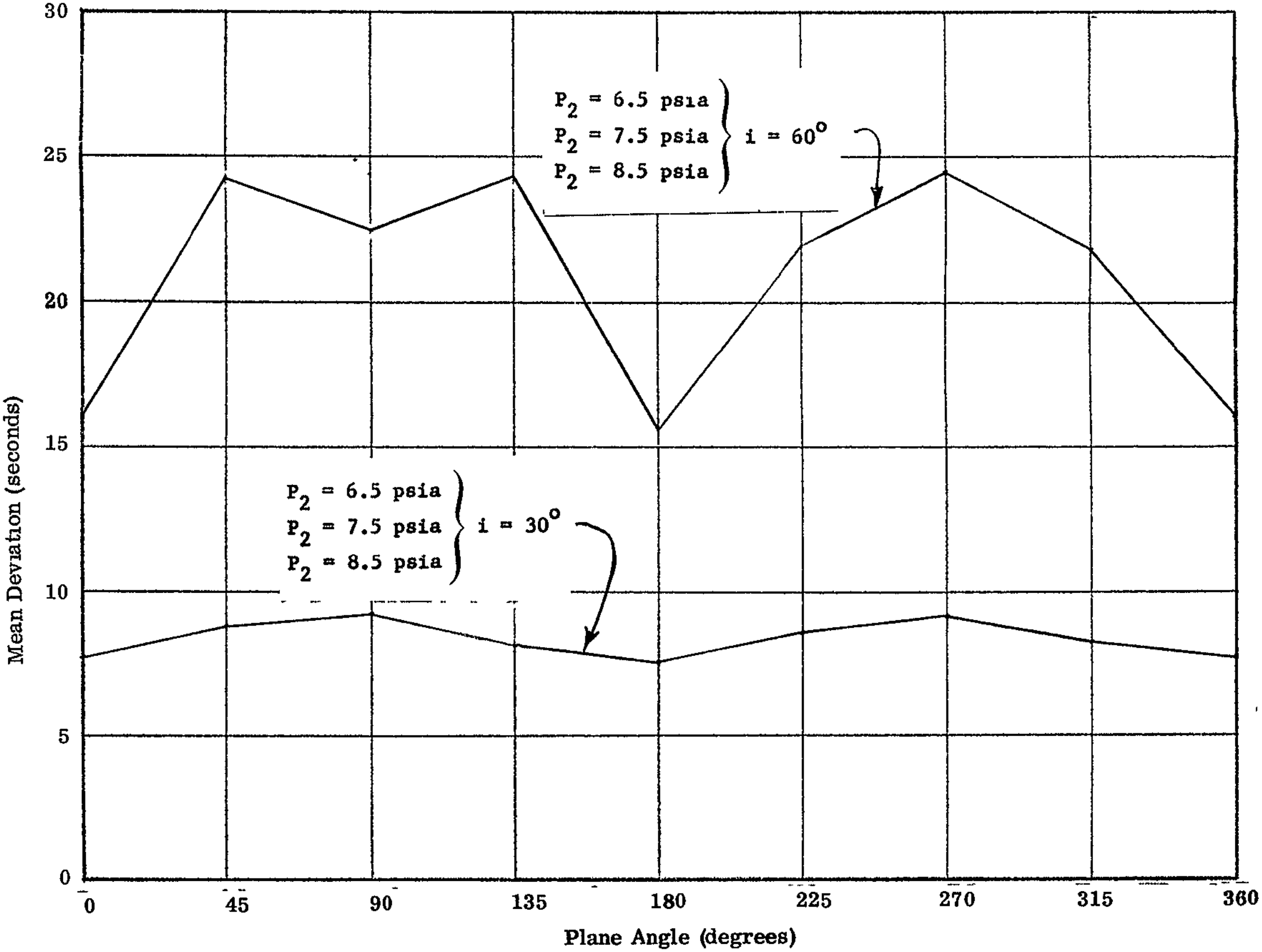

Figure 19 Mean of Ray Deviations - Interstitial Pressure Variation

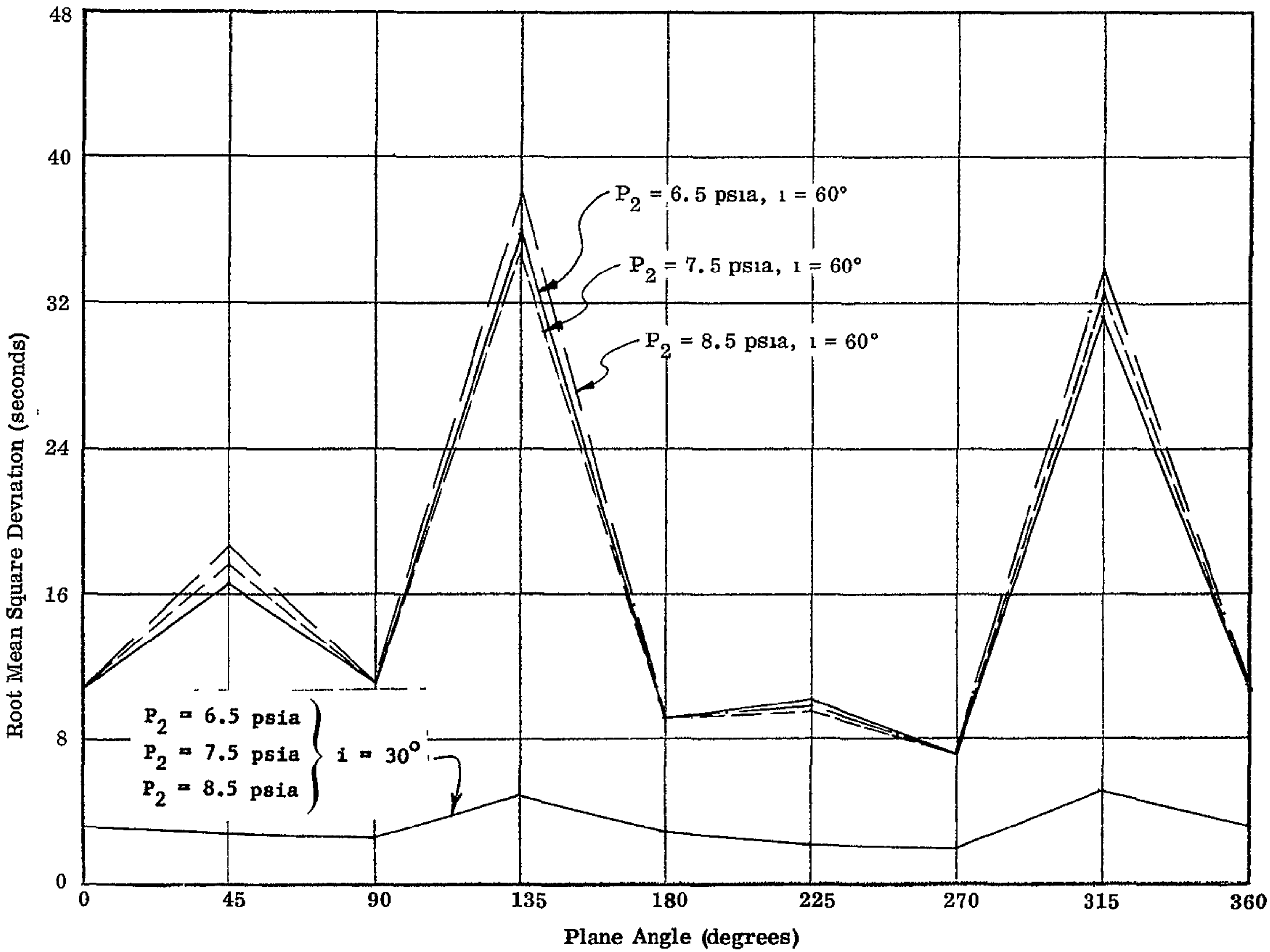

Figure 20. RMS of Ray Deviations - Interstitial Pressure Variation

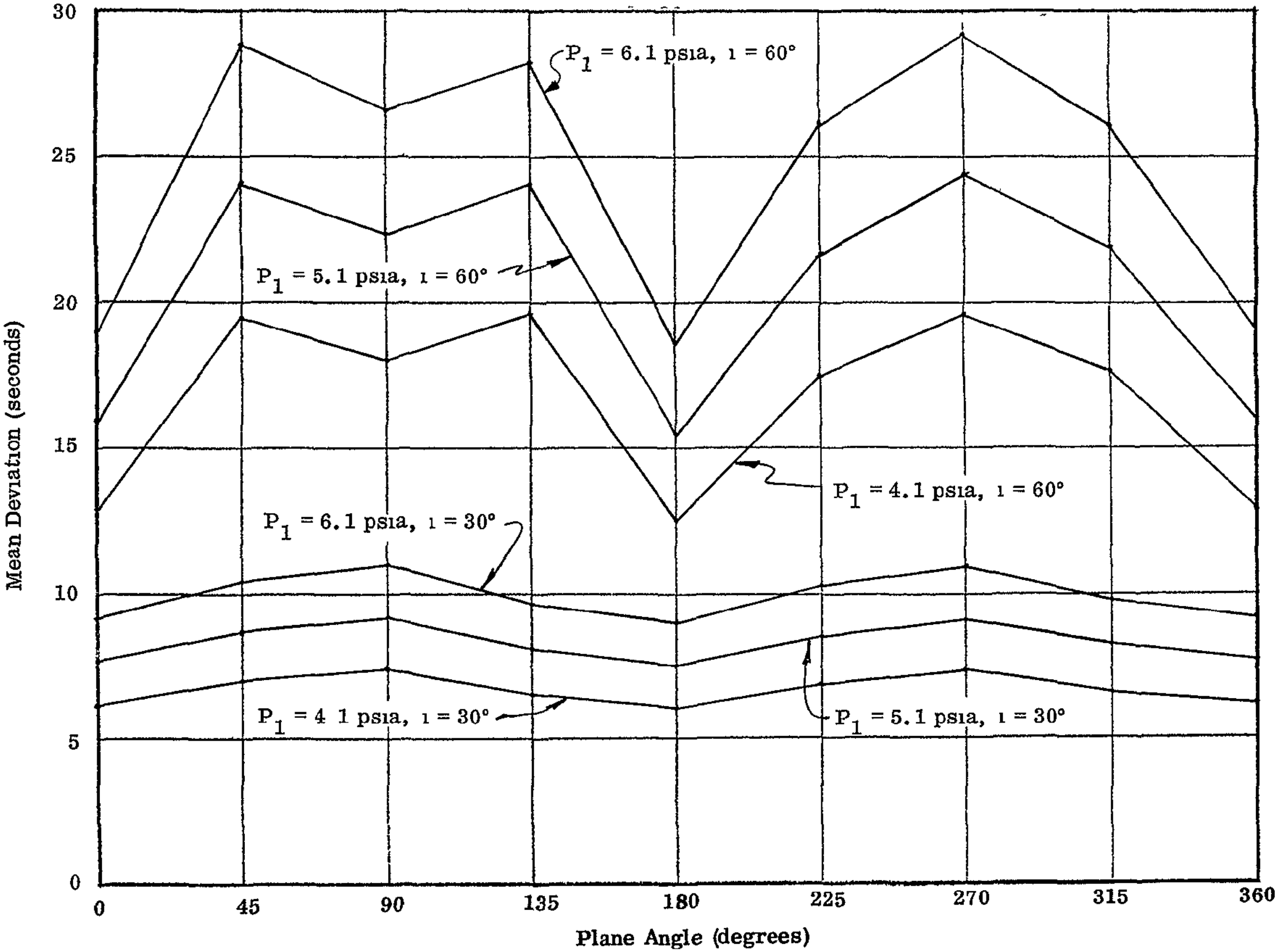

Figure 21. Mean of Ray Deviations - Cabin Pressure Variation

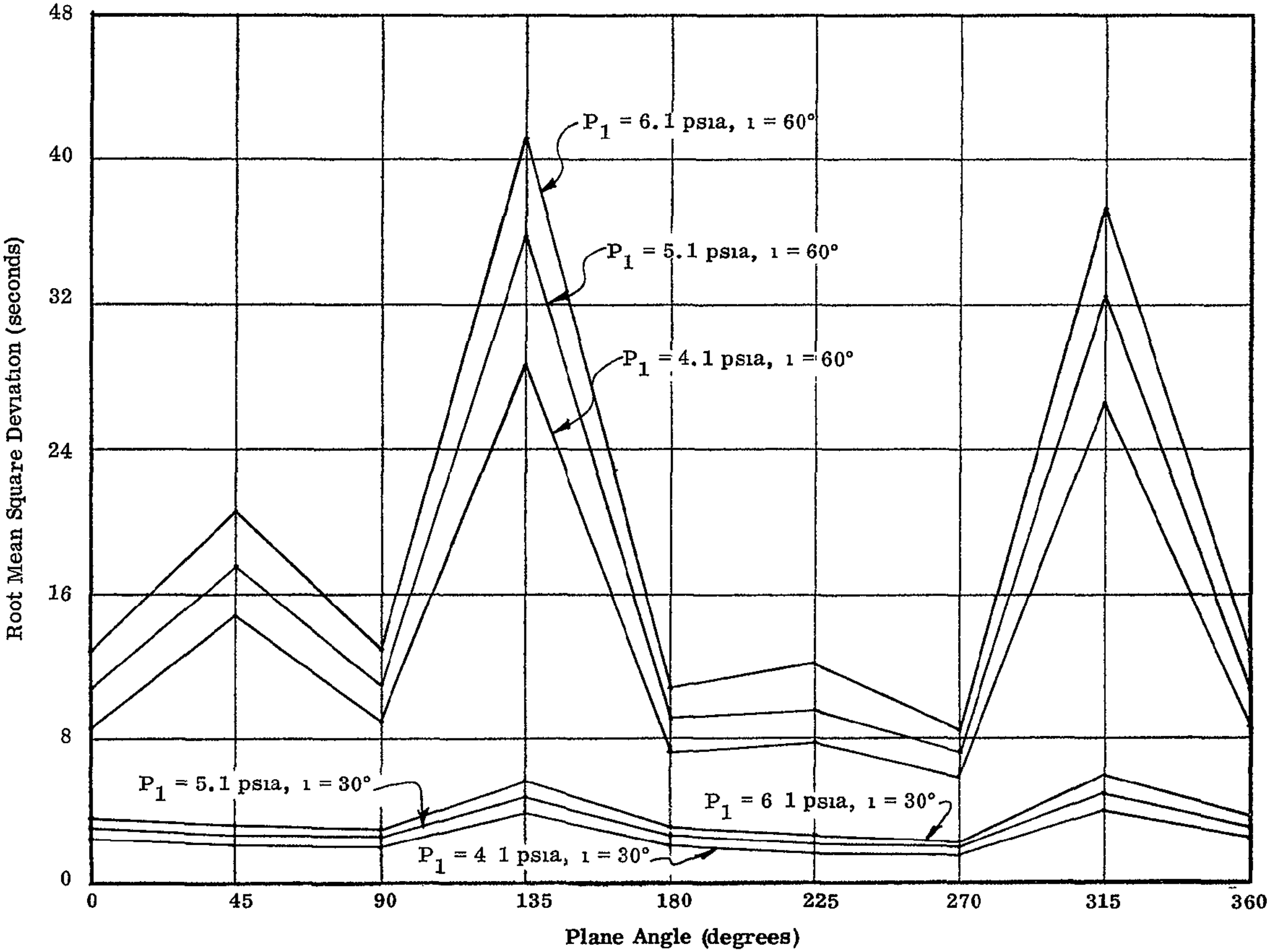

Figure 22 RMS of Ray Deviations - Cabin Pressure Variation

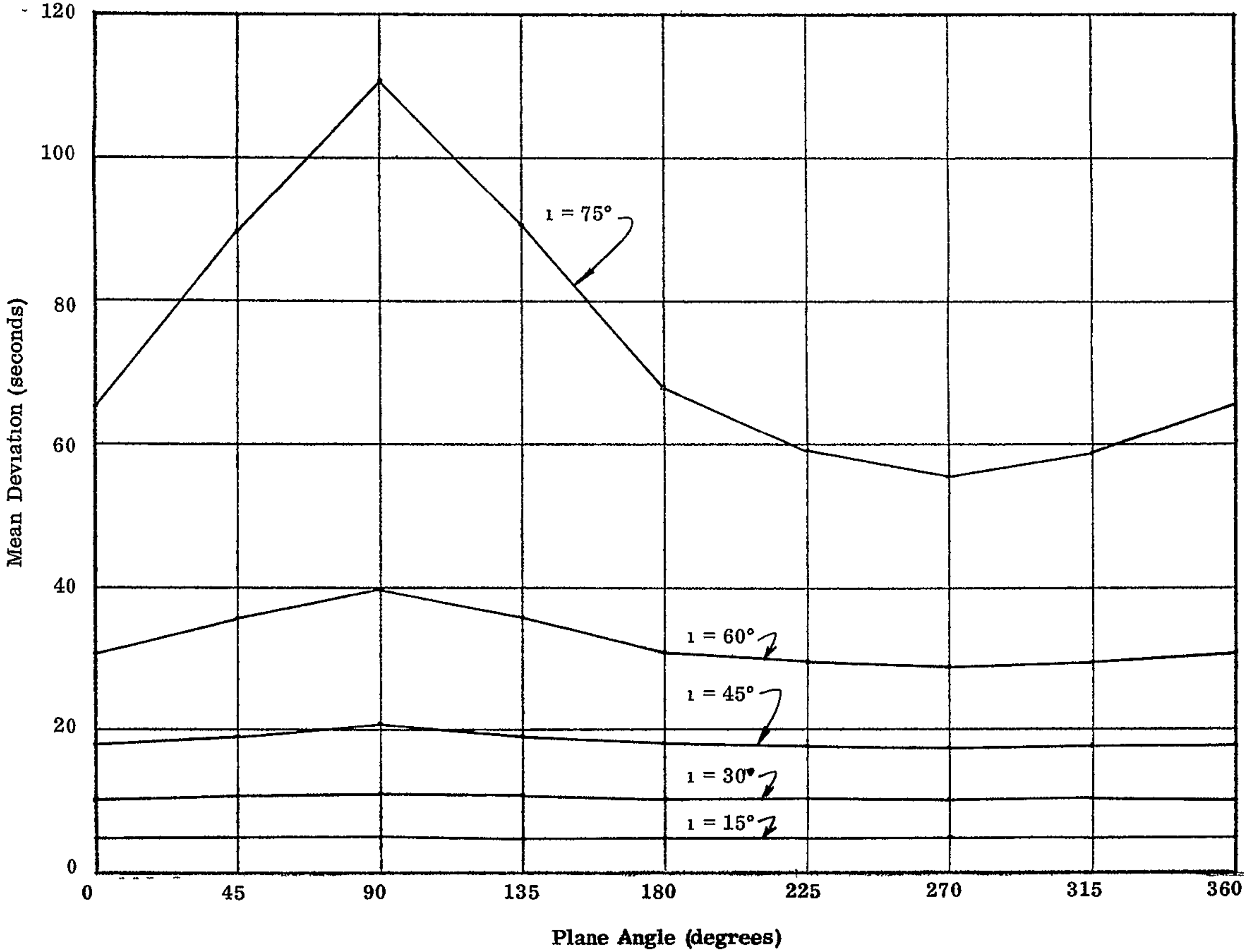

Figure 23. Mean of Ray Deviations - Incidence Angle Variation (Clamped Edge Condition)

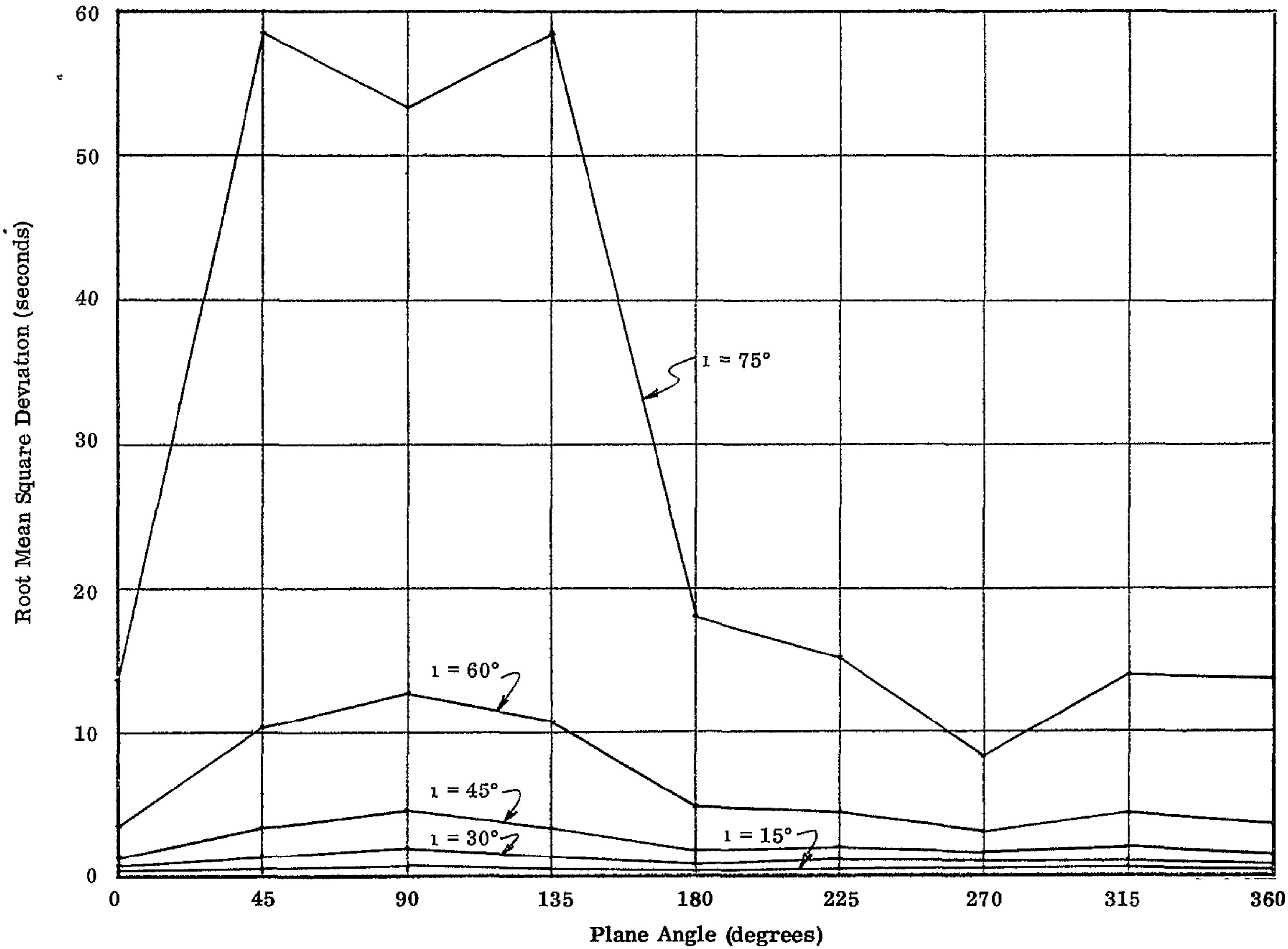

Figure 24. RMS of Ray Deviations - Incidence Angle Variation
(Clamped Edge Condition)

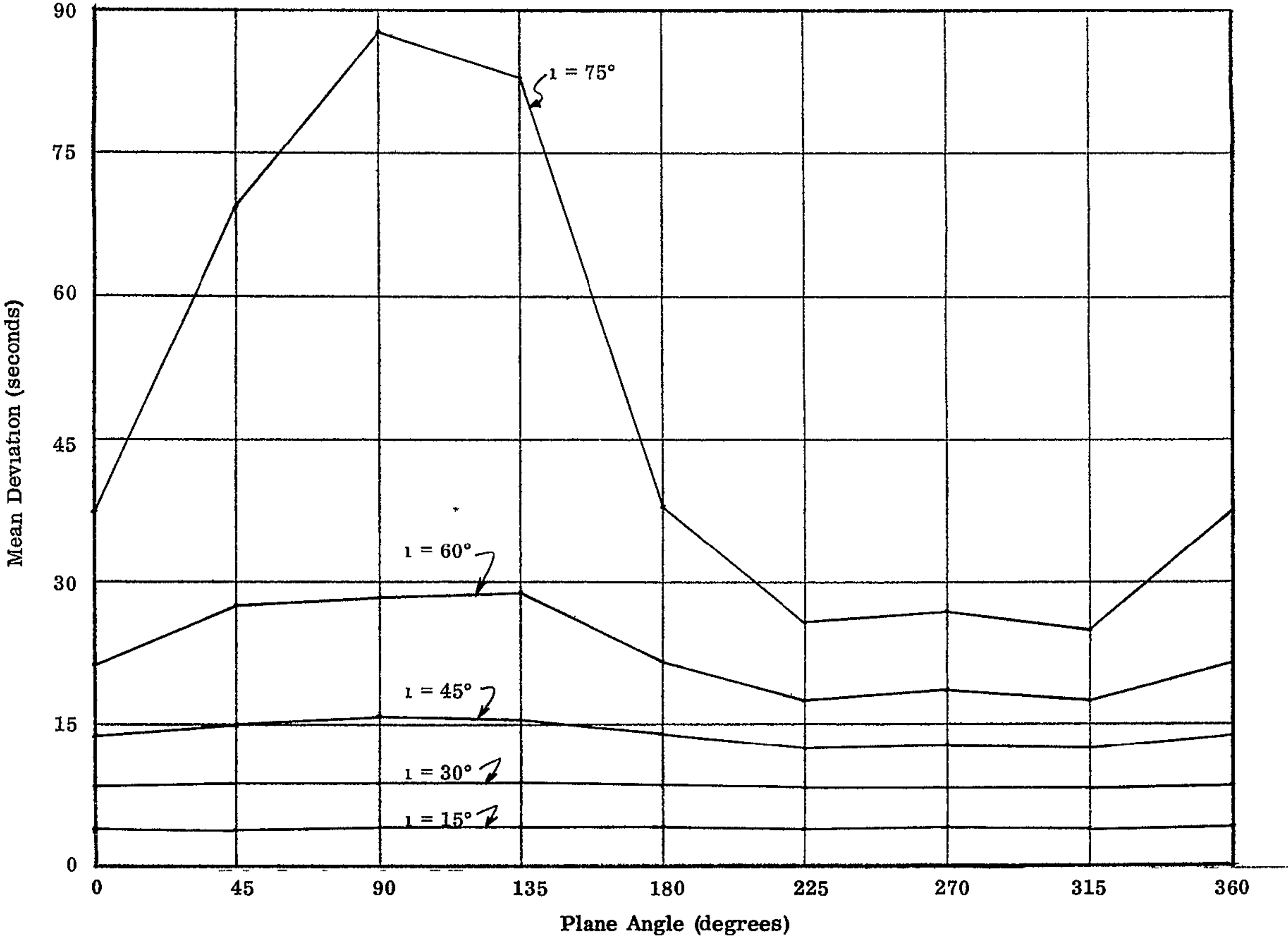

Figure 25 Mean of Ray Deviations - Incidence Angle Variation
(Simply Supported Edge Condition)

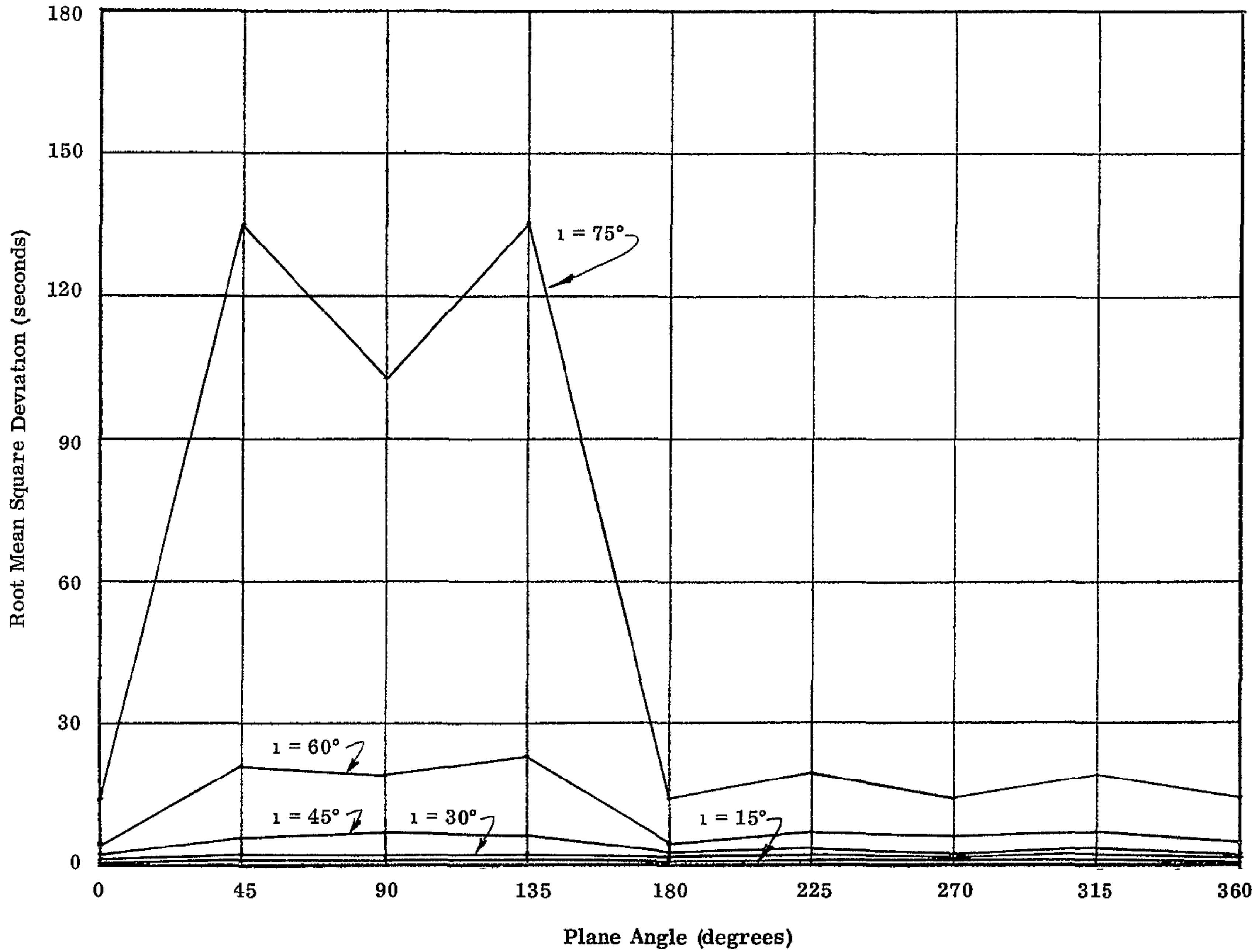

Figure 26. RMS of Ray Deviations - Incidence Angle Variation (Simply Supported Edge Condition)

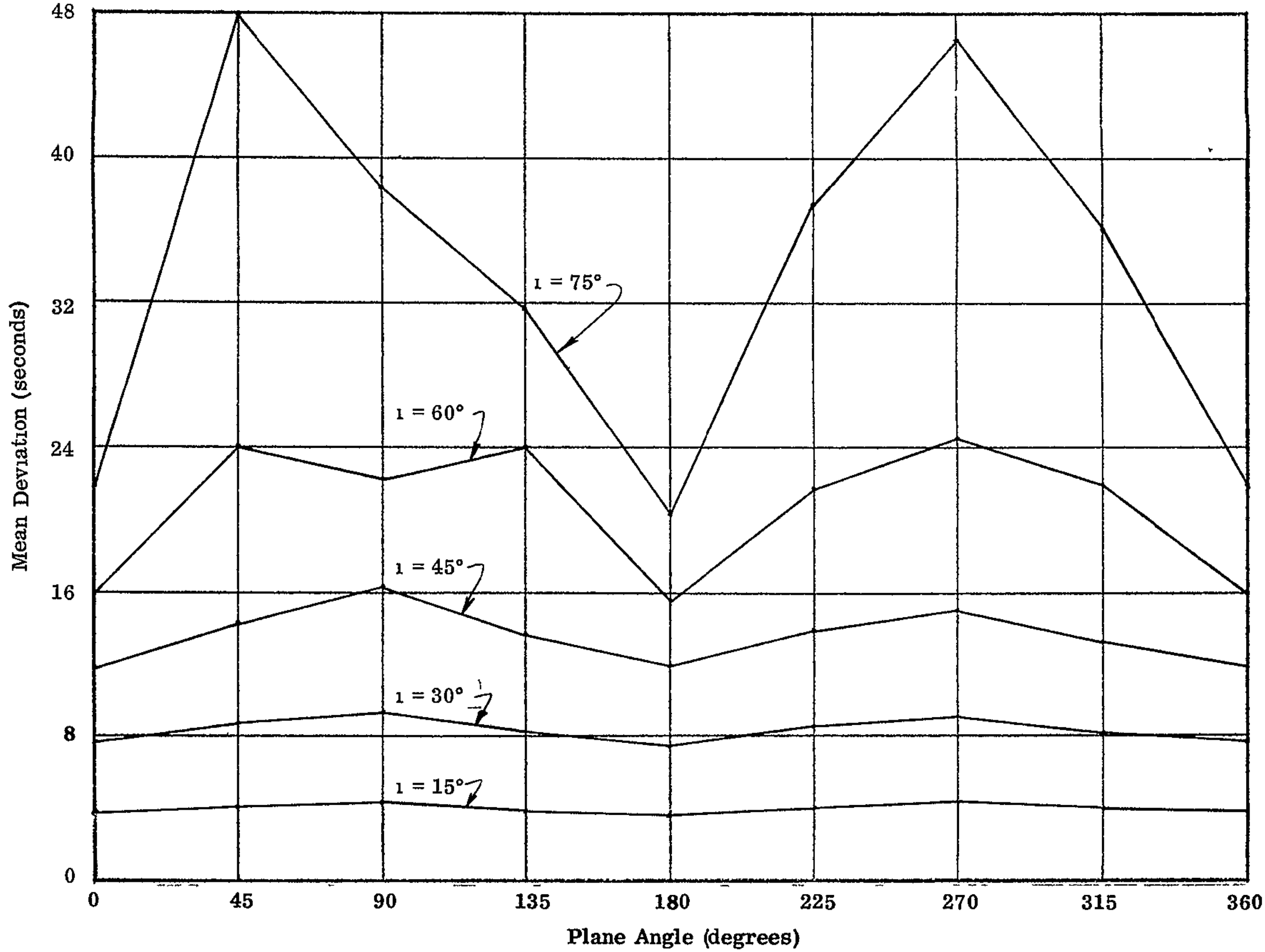

Figure 27. Mean of Ray Deviations - Incidence Angle Variation (Actual Edge Condition)

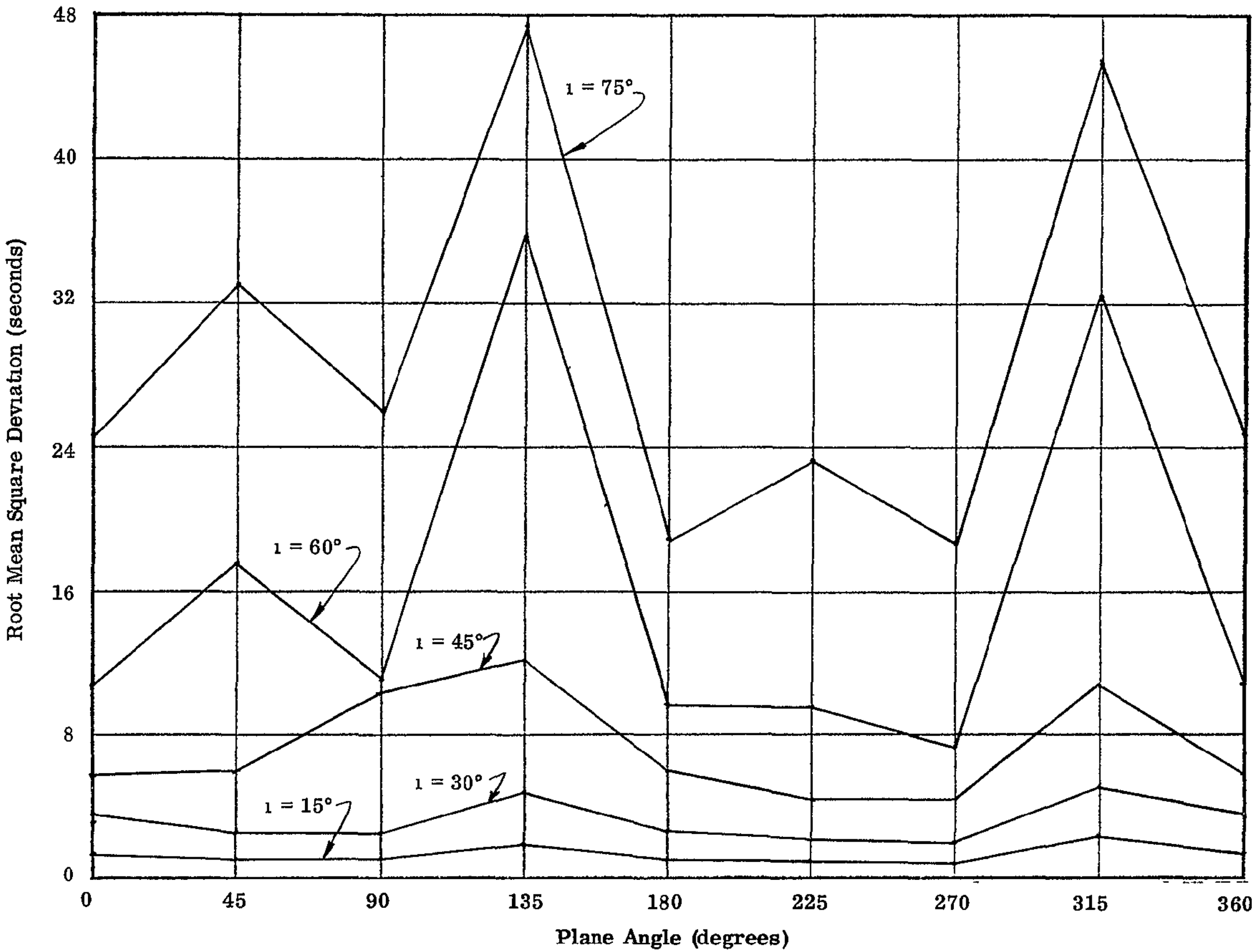

Figure 28 RMS of Ray Deviations - Incidence Angle Variation
(Actual Edge Condition)

The mean and rms deviation curves for the clamped and simply supported edge conditions show a marked growth in the maximum deviation at a plane angle of 90°. The curves for the actual edge condition show the same trend but at plane angles of 90° and 270°.

Figure 29 gives designation numbers for the individual points on the window surface which are studied in detail in the following analysis. This analysis is performed on the window with actual edge conditions and loaded with a cabin pressure of 5.1 psia, interstitial pressures (P_2) of 7.5 and 8.5 psia, and no external pressure. For each point, three sets of curves are presented: total deviation, plane angle deviation, and incidence angle deviation. The plane angle deviation is that portion of the total deviation parallel to the plane of the window surface. The incidence angle deviation is that portion of the total deviation normal to the plane of the window surface. The deviations are plotted as functions of the plane angle for four incidence angles ($i = 15°$, $i = 30°$, $i = 45°$, and $i = 60°$).

Figures 30 through 42 show the plots of the total deviation for the thirteen points designated in Fig. 29. For an incidence angle of 60°, there is a very small difference in the total deviation for interstitial pressures of 7.5 psia and 8.5 psia. For the other incidence angles, the difference is so small that it can't be seen on the plots.

With the exceptions of Points 1, 3, and 11, the maximum total deviation for any plane angle is less than 60 seconds. Except for certain plane angles, these three points also have maximum total deviations of less than 60 seconds. For Point 1 this angle is 45°, for Point 3 the angle is 135°, and for Point 11 the angles are 270° and 315°.

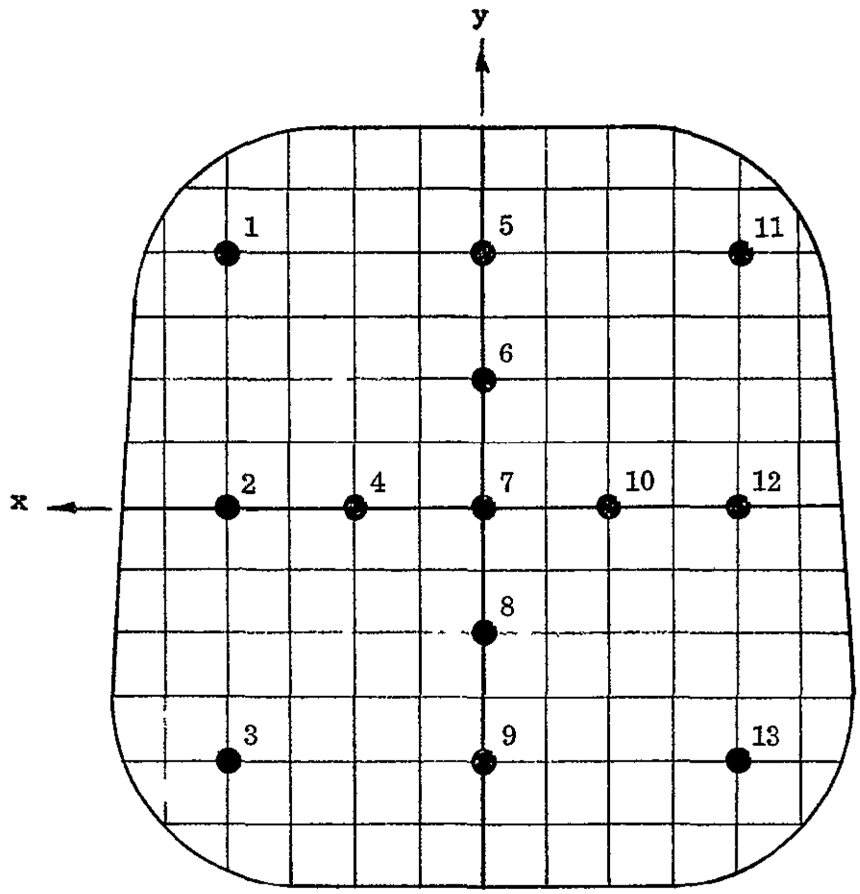

Figure 29 Points of Interest - Single Ray Trace

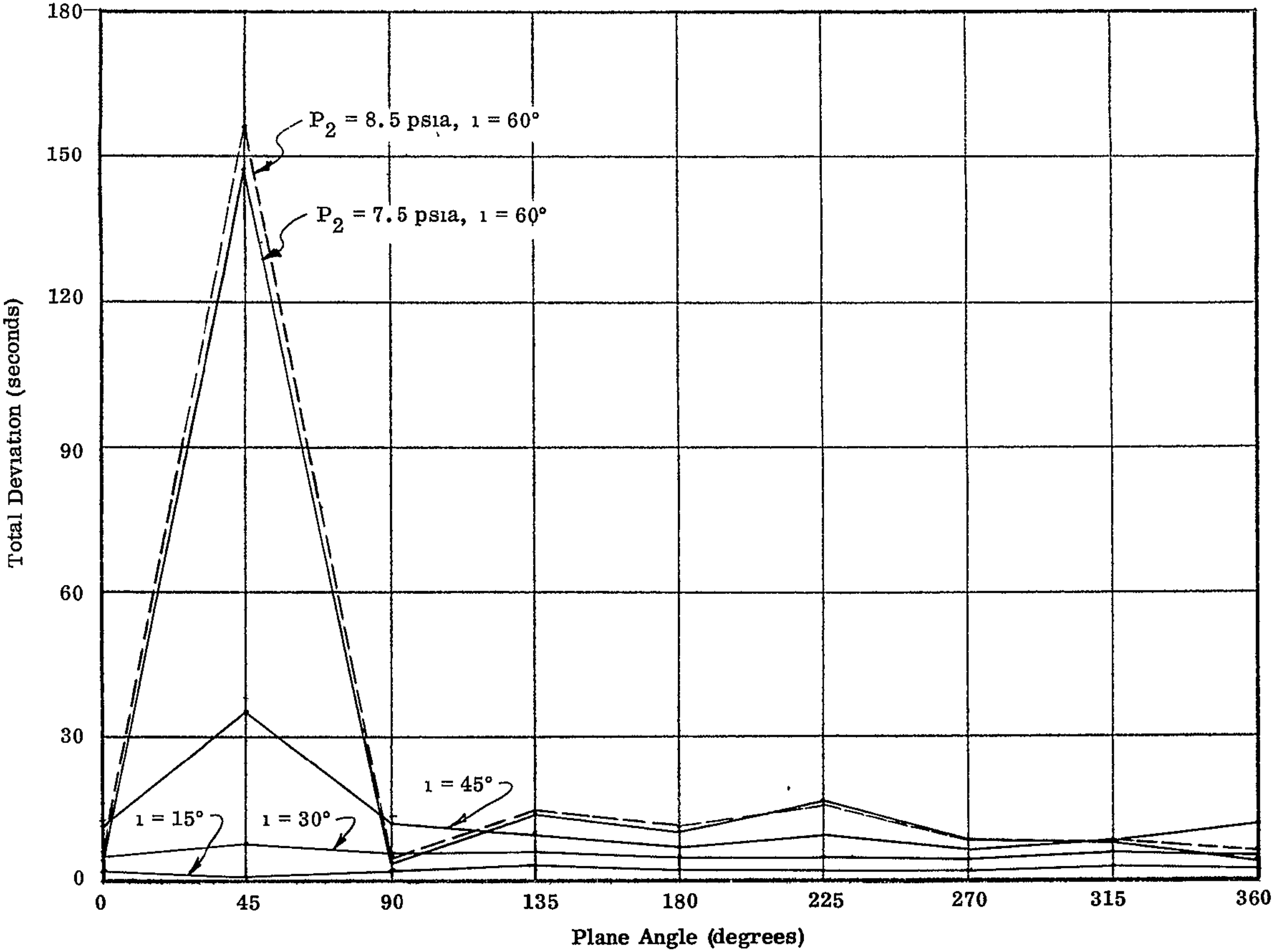

Figure 30. Total Deviation - Point 1

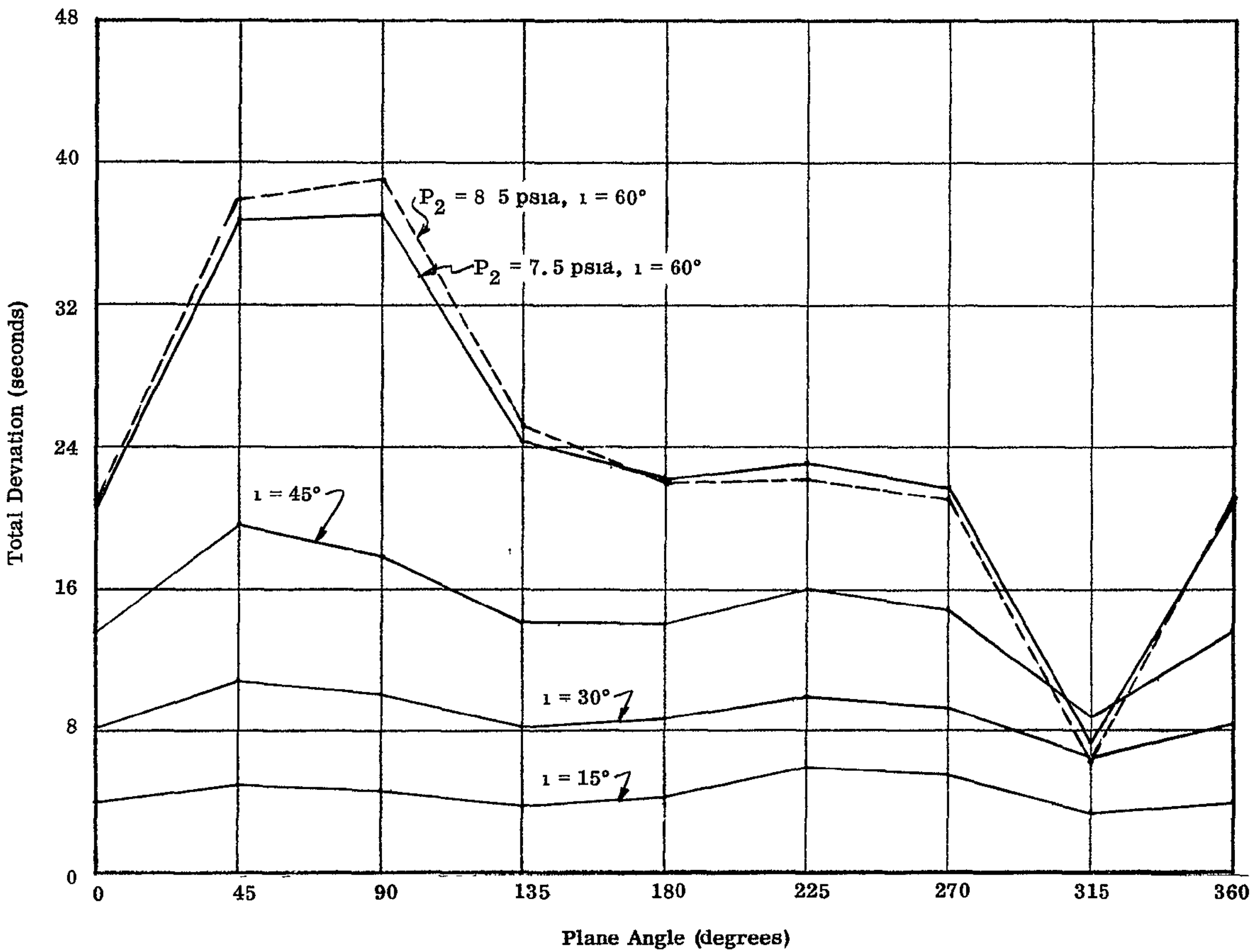

Figure 31 Total Deviation - Point 2

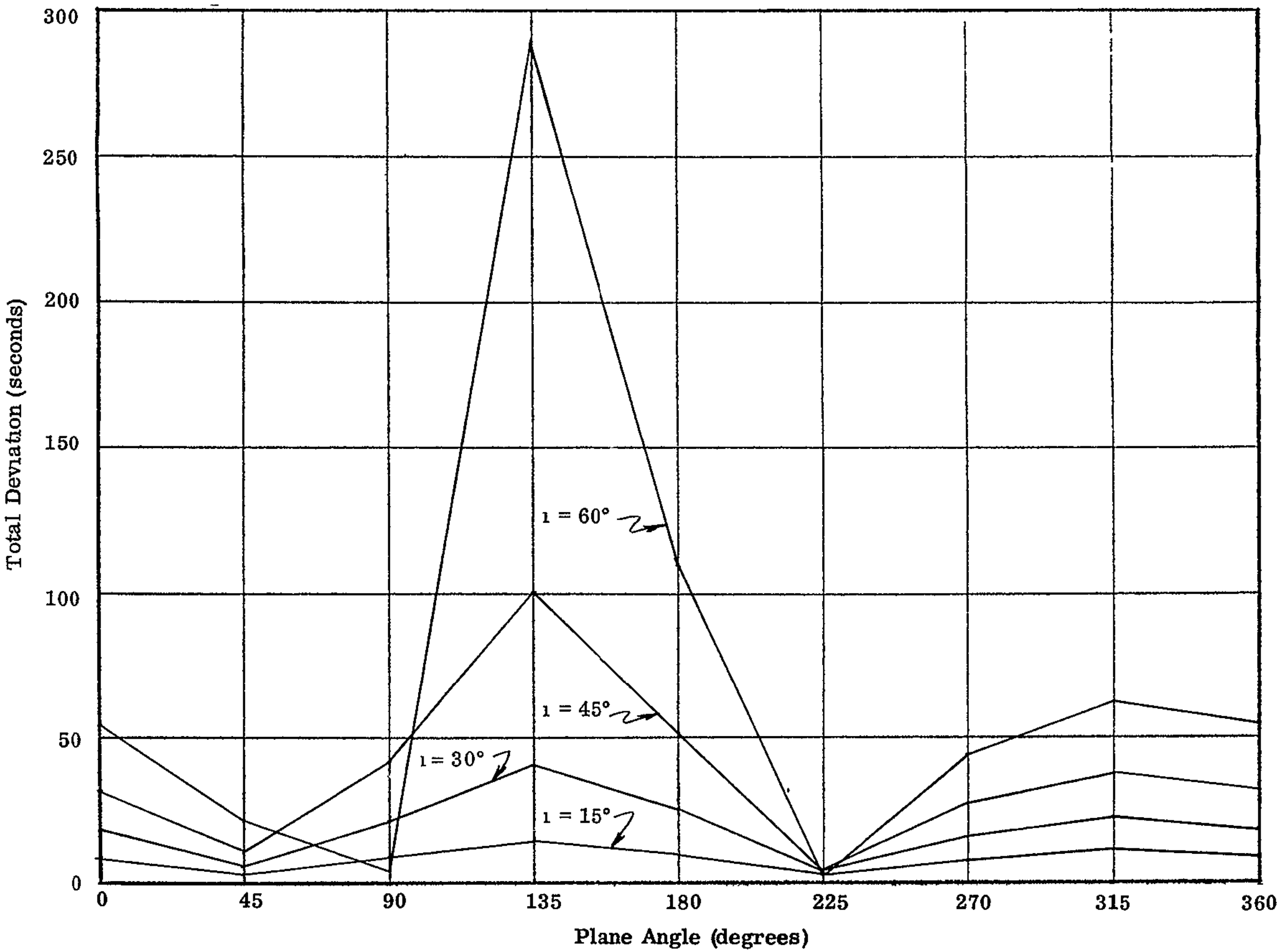

Figure 32 Total Deviation - Point 3

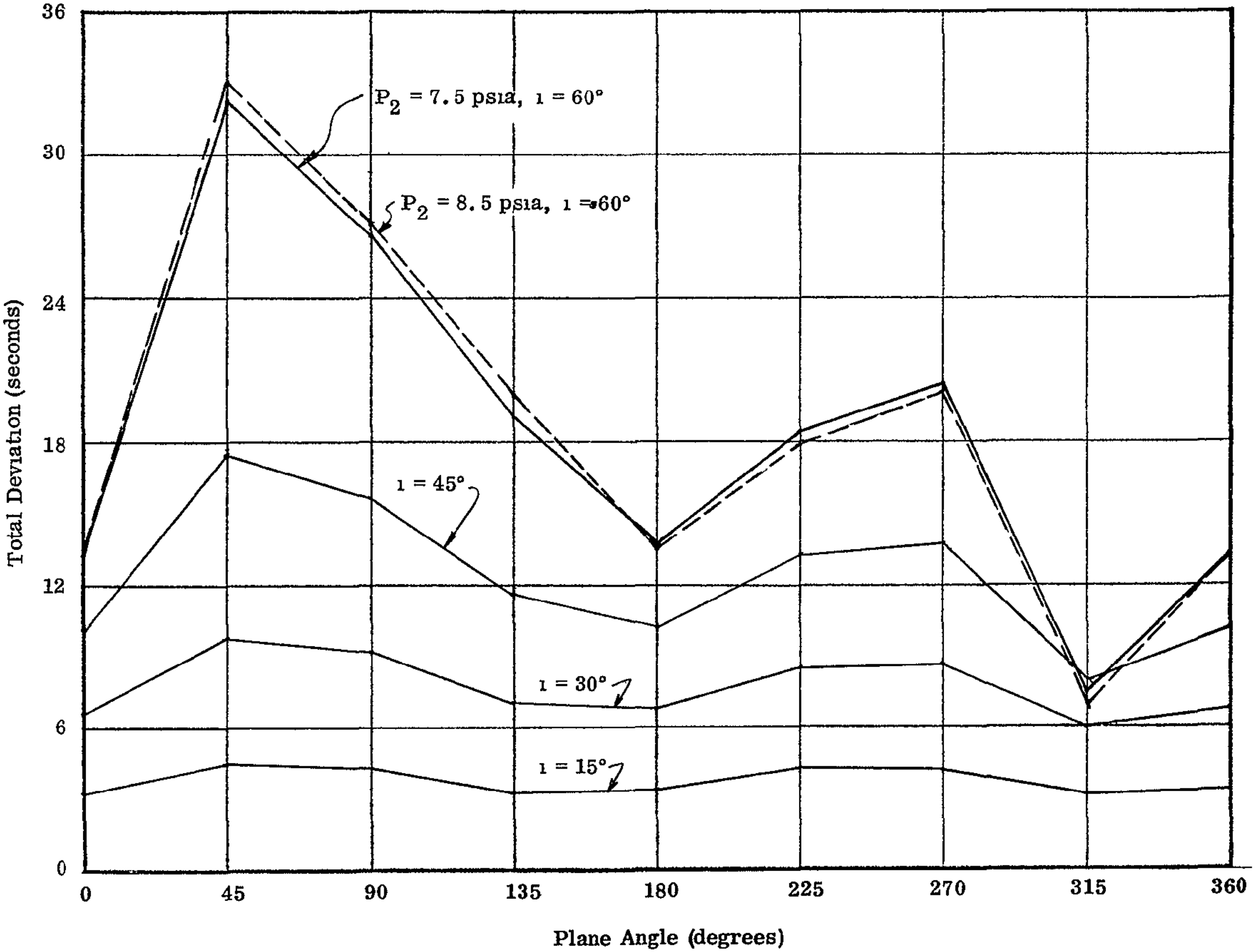

Figure 33. Total Deviation - Point 4

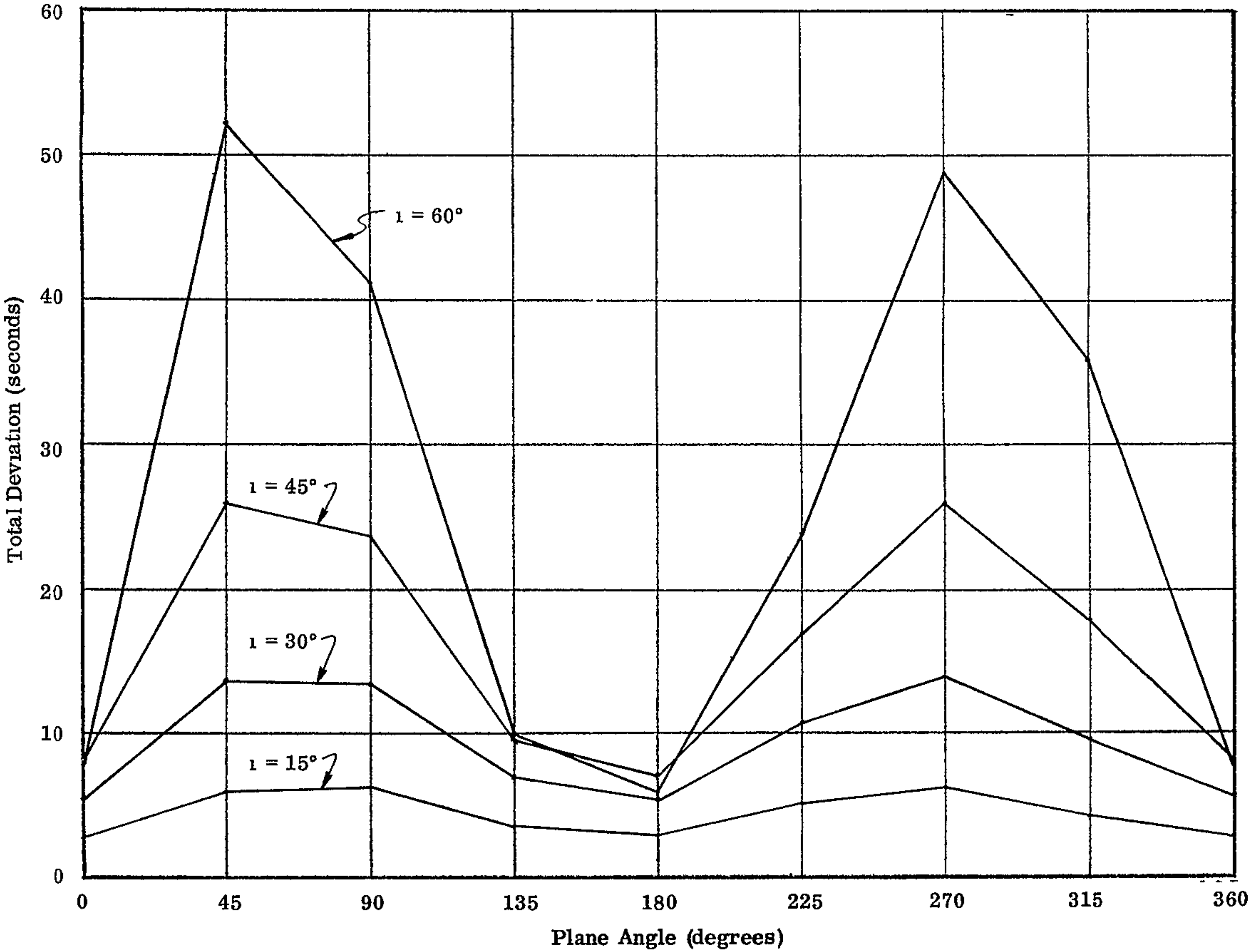

Figure 34 Total Deviation - Point 5

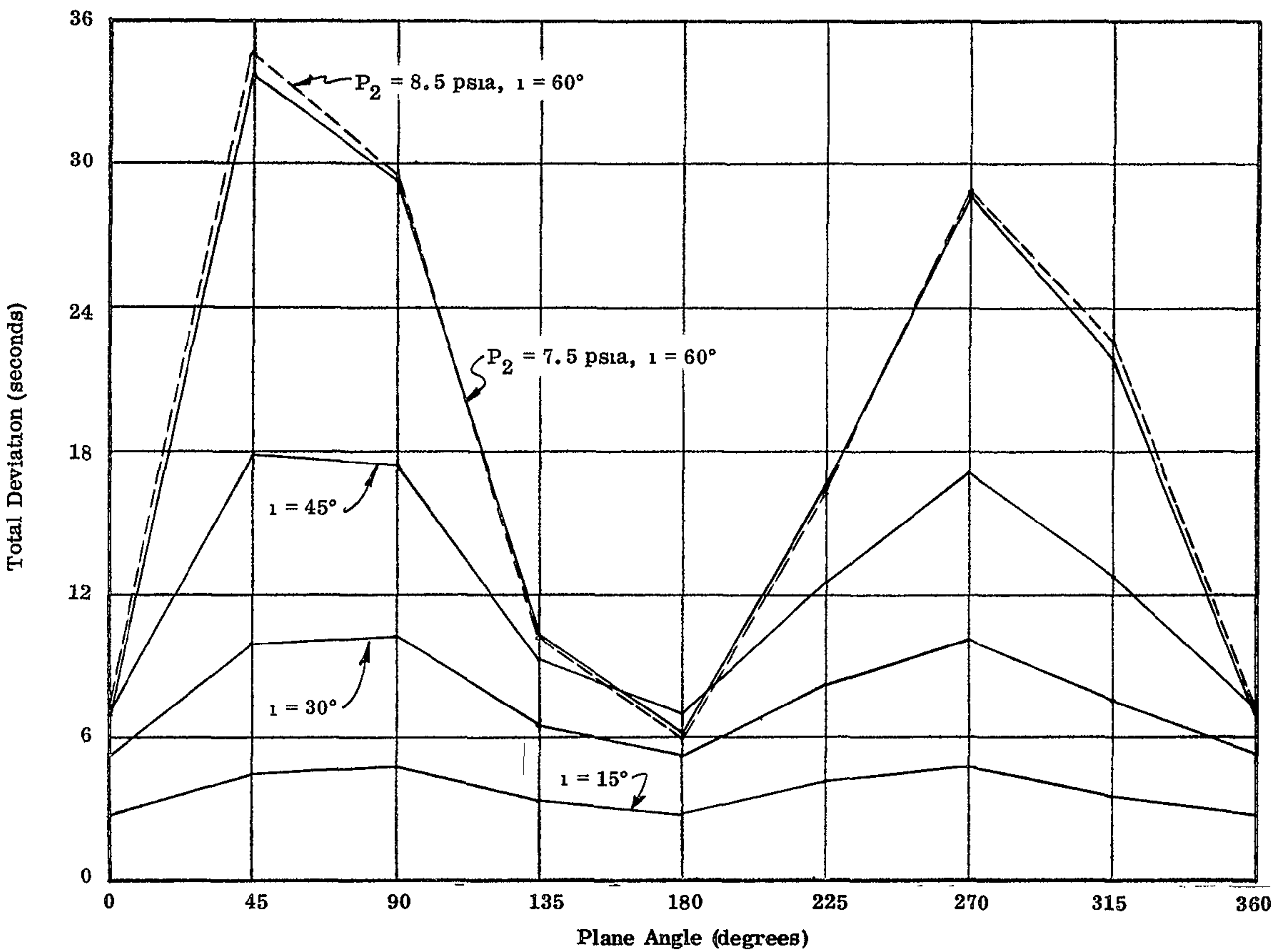

Figure 35. Total Deviation - Point 6

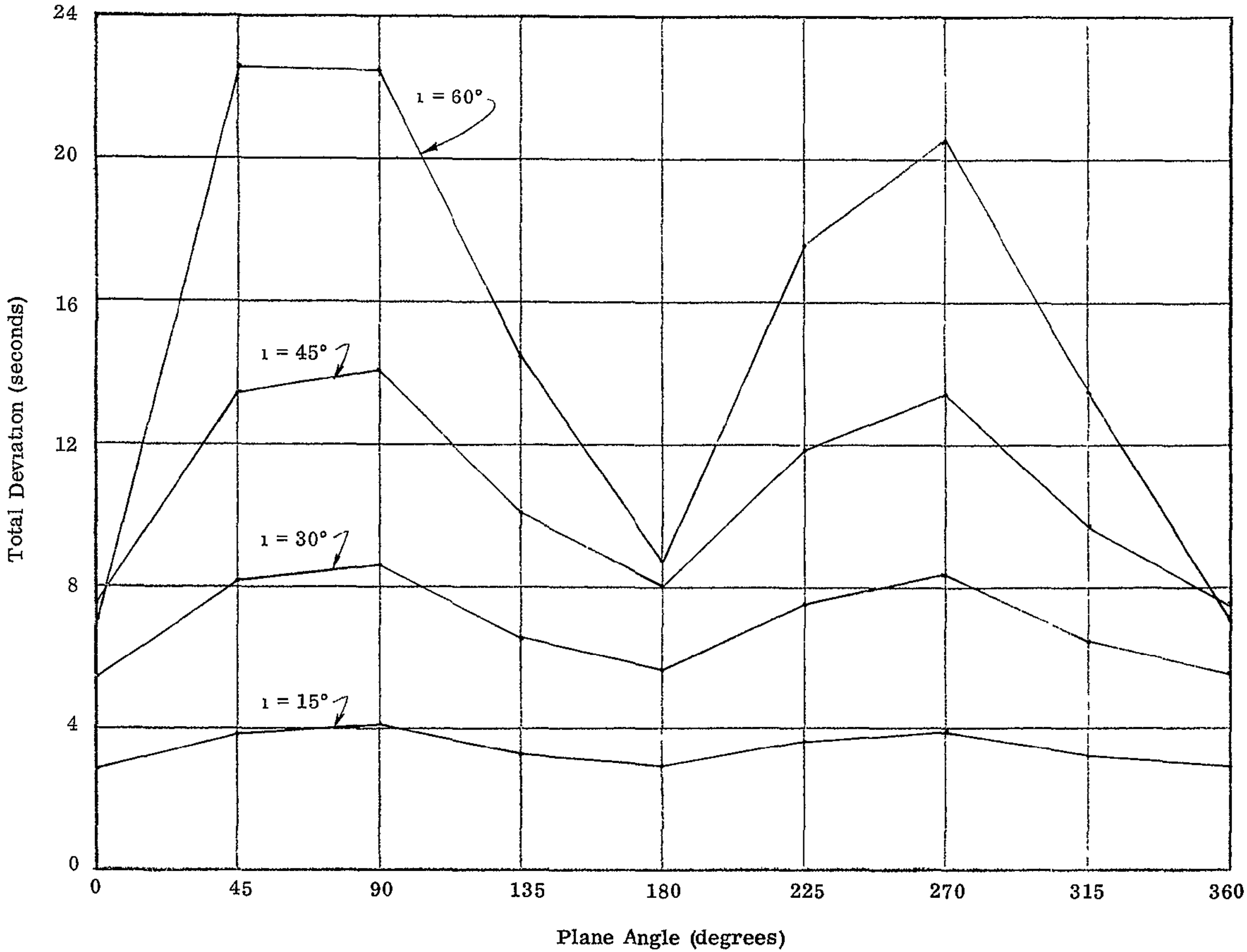

Figure 36 Total Deviation - Point 7

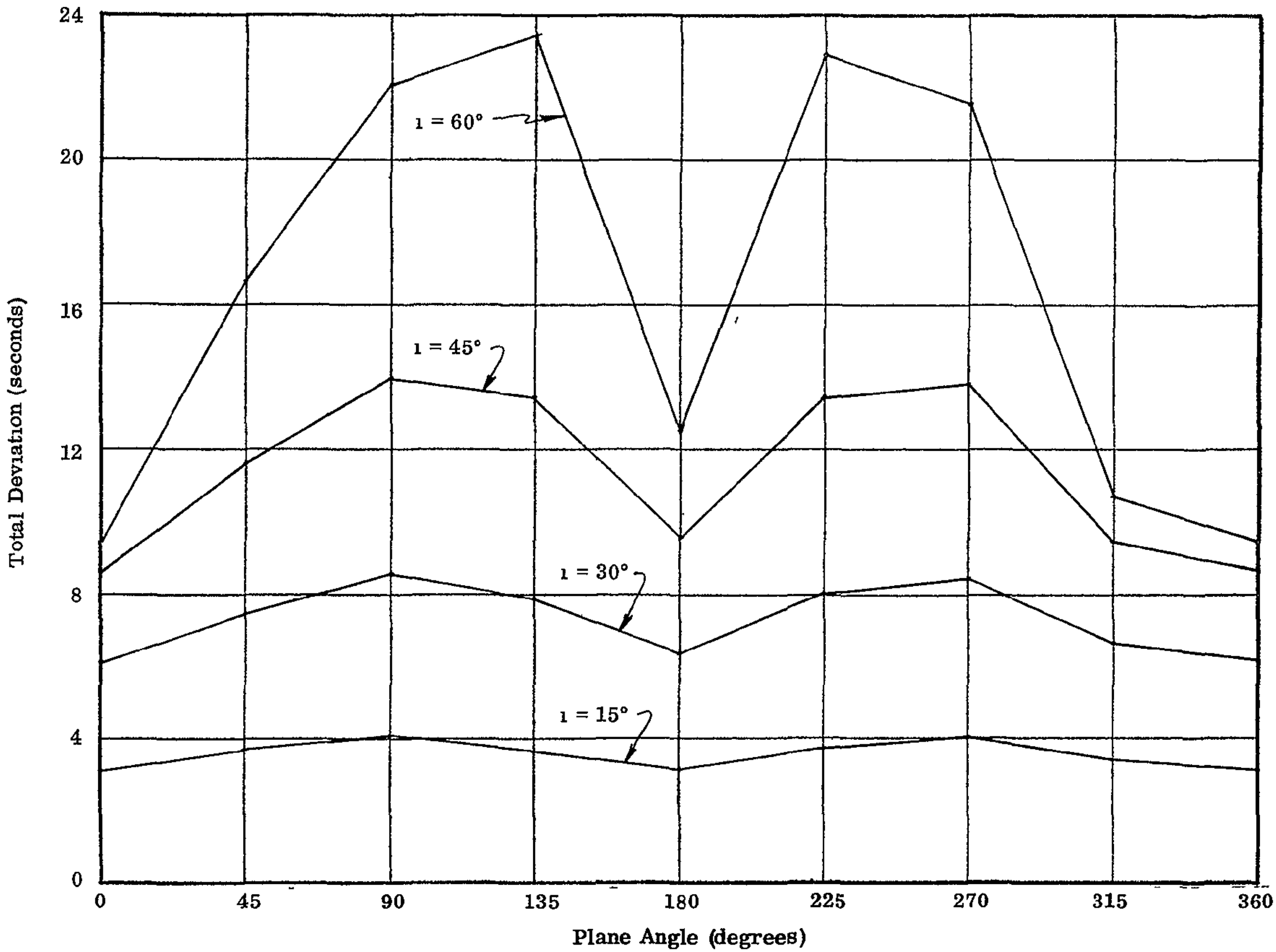

Figure 37 Total Deviation - Point 8

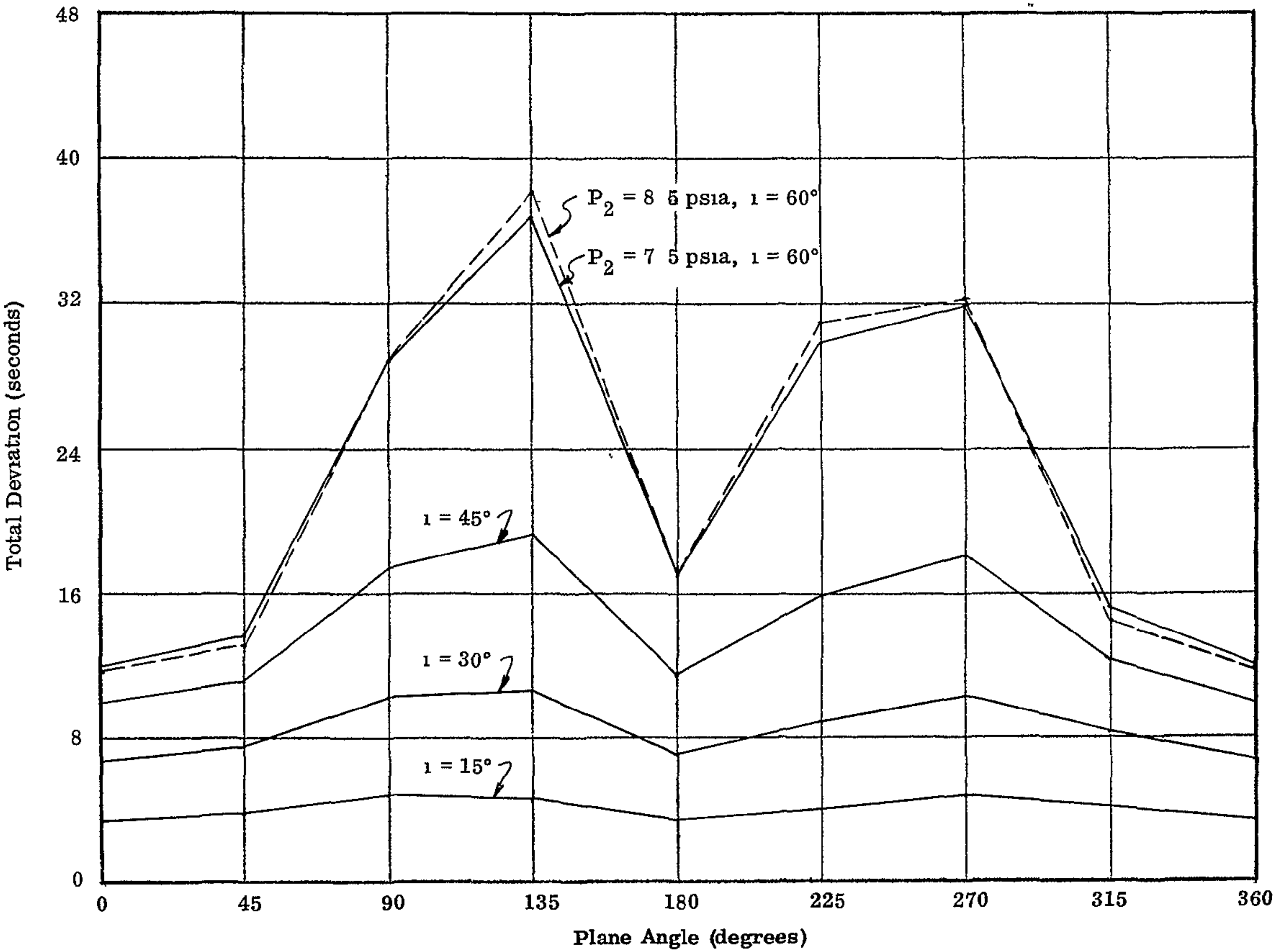

Figure 38. Total Deviation - Point 9

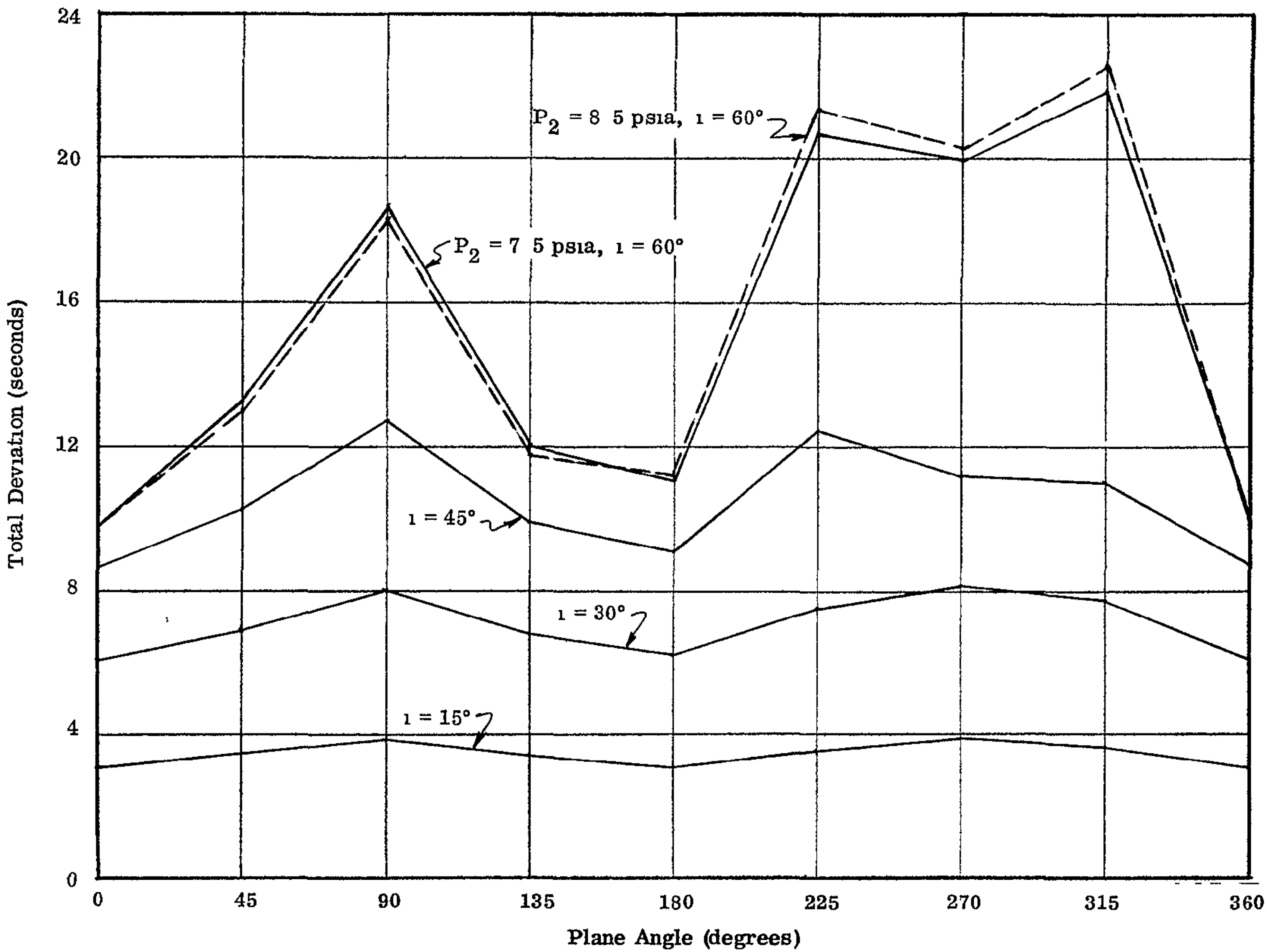

Figure 39. Total Deviation - Point 10

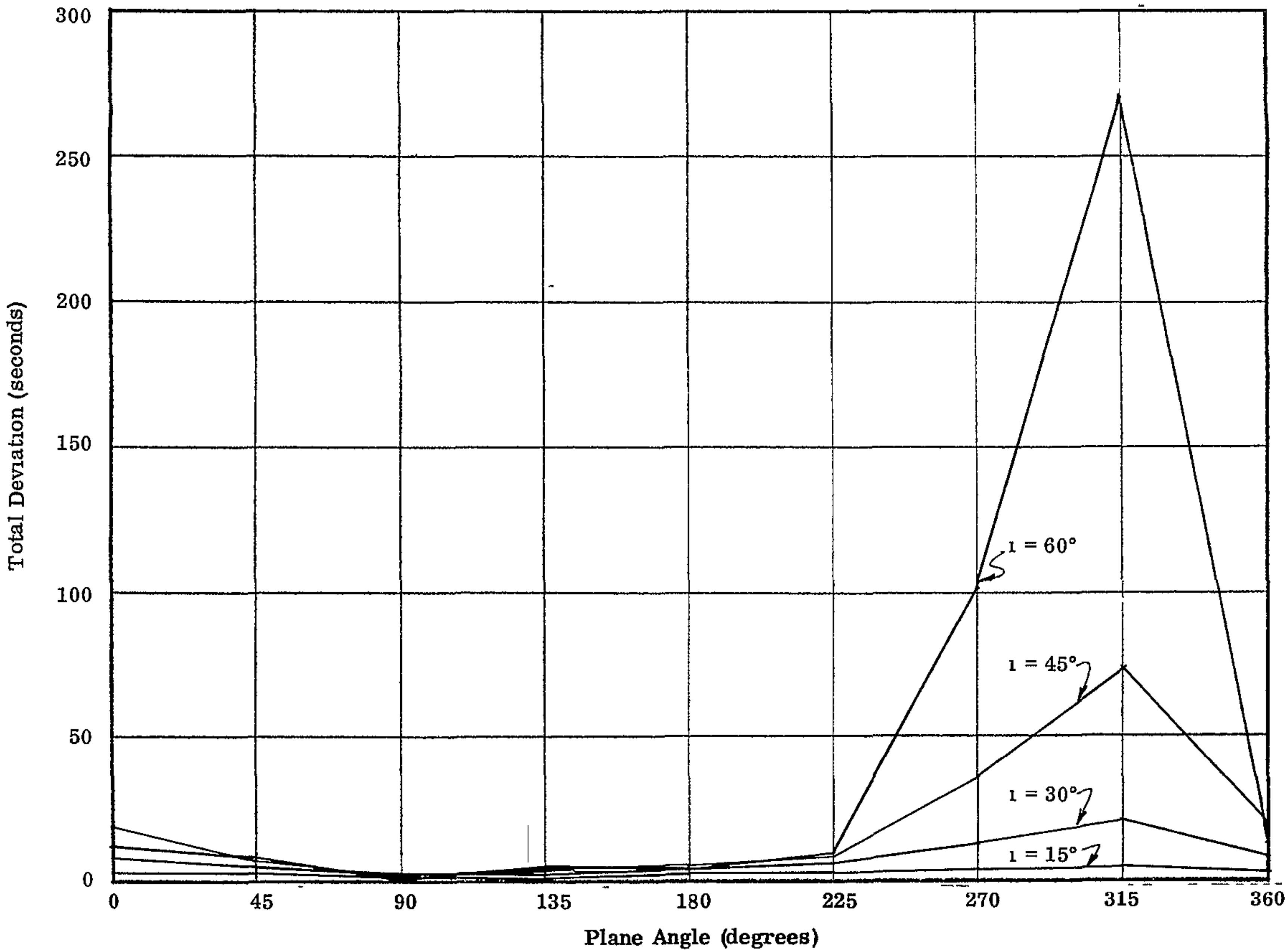

Figure 40. Total Deviation - Point 11

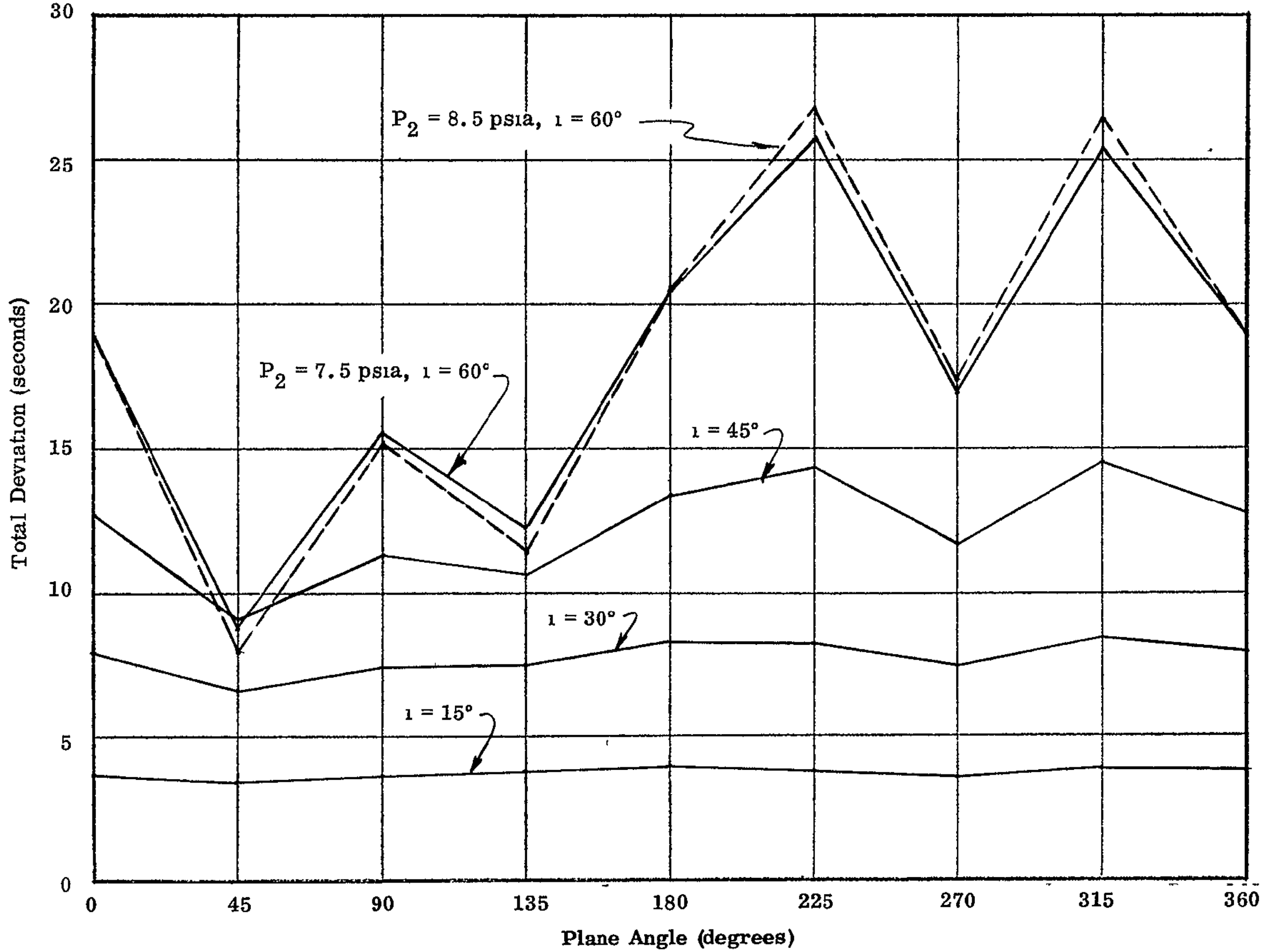

Figure 41. Total Deviation – Point 12

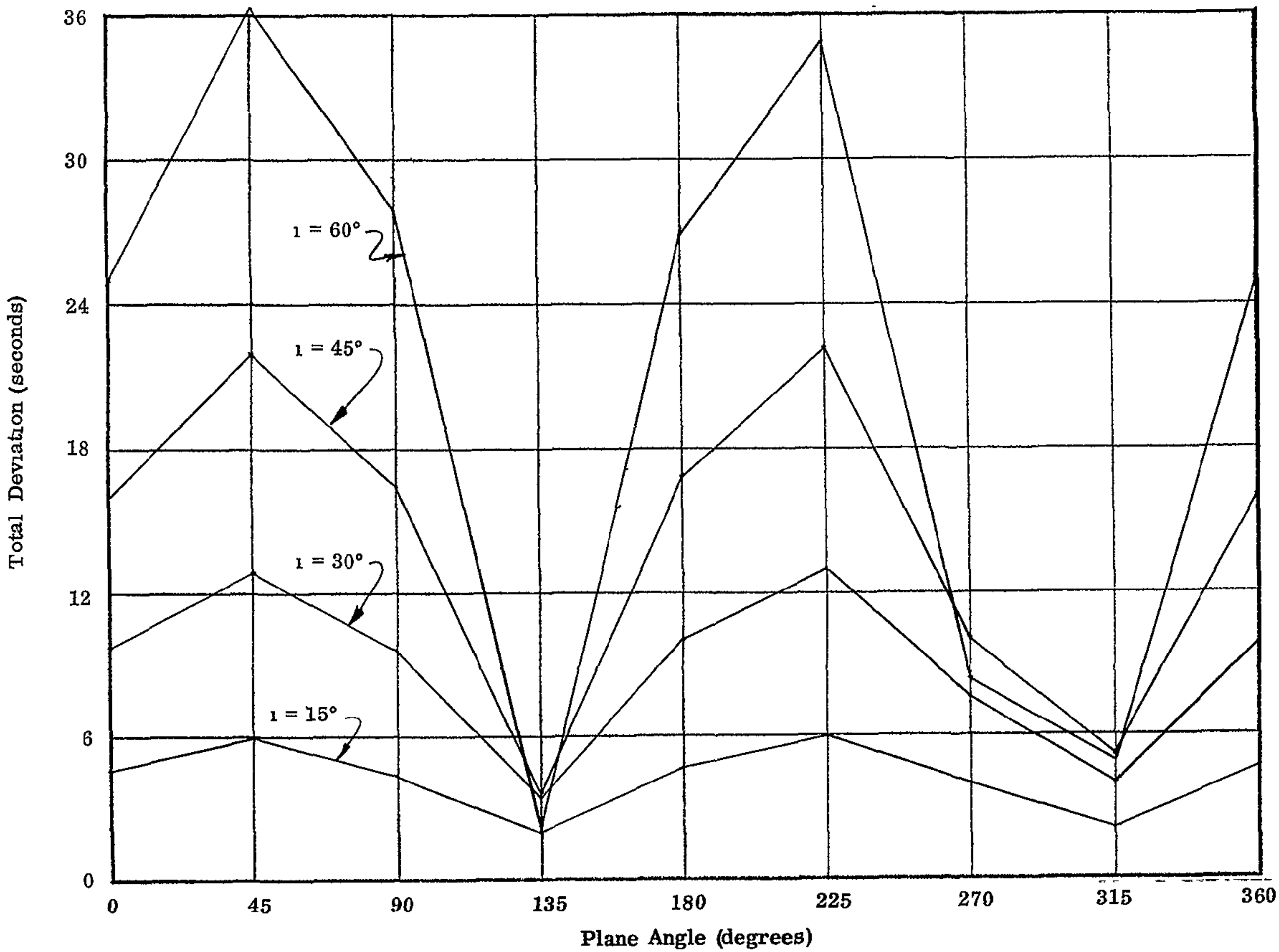

Figure 42 Total Deviation - Point 13

Figures 43 through 55 show the plots of the plane angle deviations for the thirteen points. The differences in the deviations for the interstitial pressures of 7.5 psia and 8.5 psia are so small that they do not show up on the plots.

With the exceptions of Points 3 and 11, the maximum plane angle deviation is less than 20 seconds for all plane angles. For these two points, the maximum plane angle deviation is less than 20 seconds, except for the angles of 90° and 180° for Point 3 and for the angles of 0° and 270° for Point 11.

Generally, the direction of the plane angle deviation changes, i.e., the sign of the deviation changes from plus to minus or vice versa. These changes occur for approximately every 90° change in the plane angle.

Figures 56 through 68 show the plots of the incidence angle deviations for the thirteen points being investigated. Again, the differences in the deviations for the interstitial pressures (P_2) of 7.5 psia and 8.5 psia are not significant. With only minor exceptions, the plots of incidence angle deviations are the same as those for total deviations. Thus, it appears that the total deviations consist mainly of deviations in the incidence angle rather than in the plane angle.

Based on the observations made concerning the three plots of deviations for each point, the area of the window through which single ray observations can be made with deviations less than 60 seconds is the shaded area shown in Fig. 69. In addition, making observations with low incidence angles (i.e., almost normal to the window surface) will result in smaller deviations of the light rays regardless of the direction of sighting (plane angle).

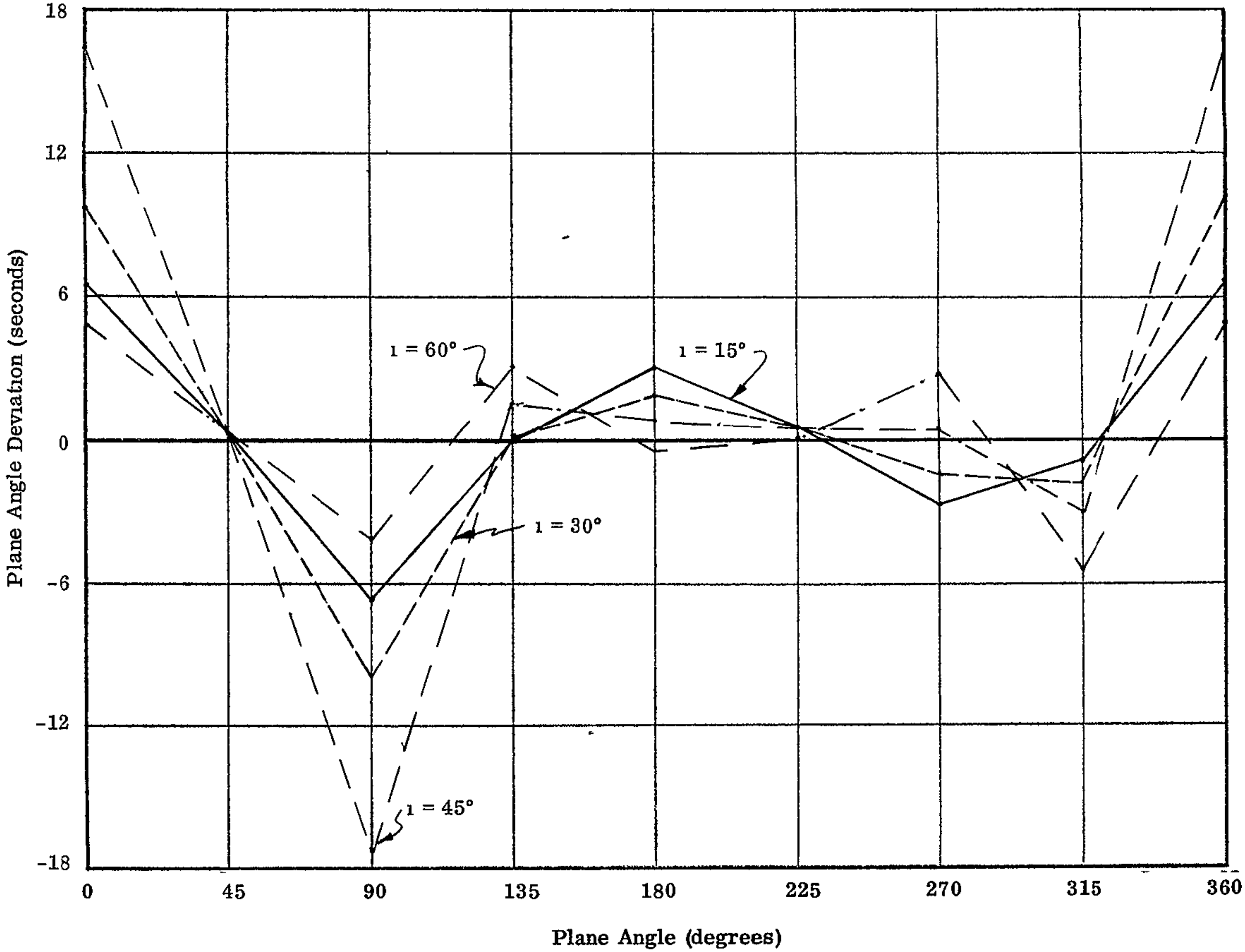

Figure 43 Plane Angle Deviation – Point 1

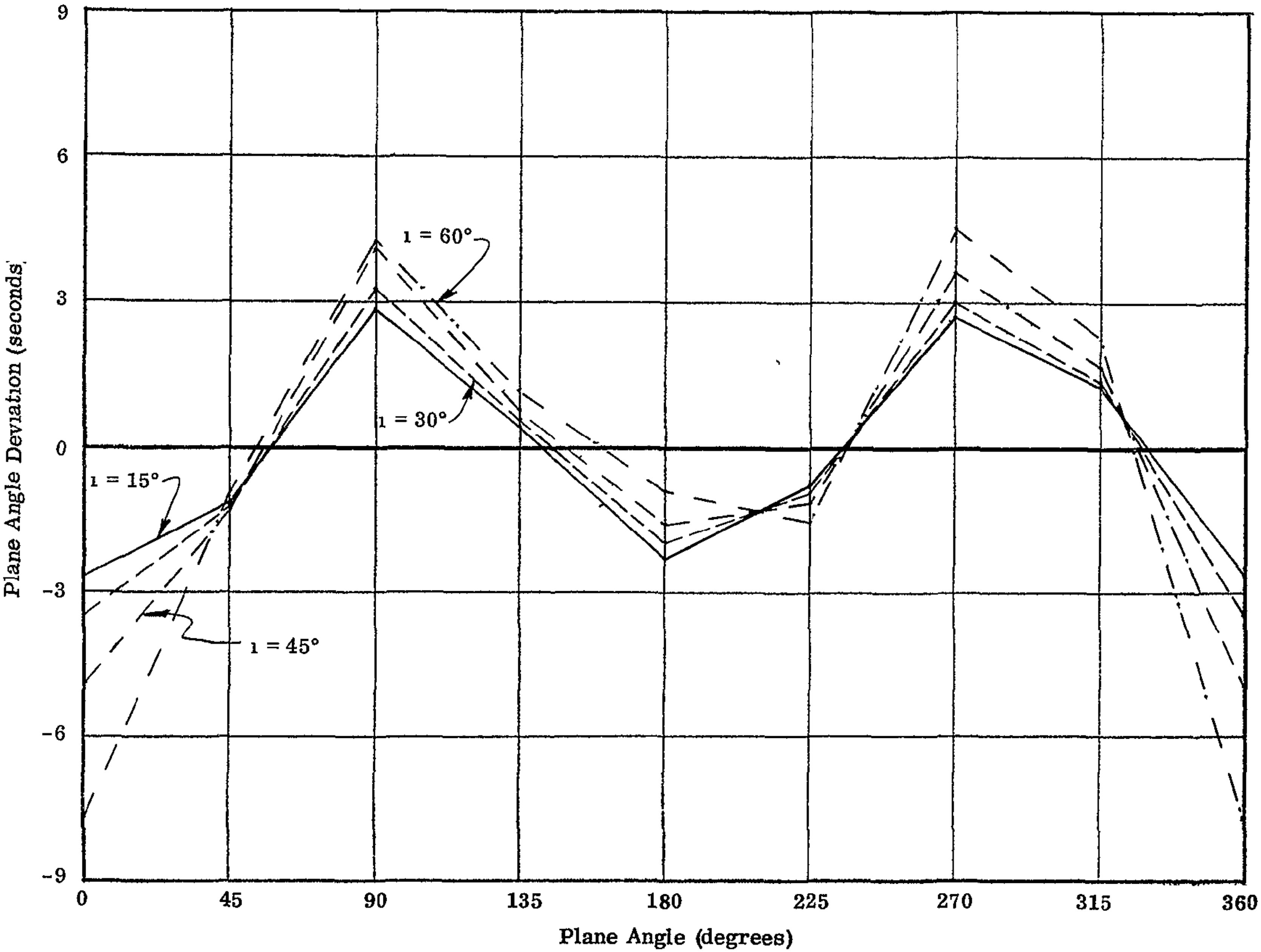

Figure 44 Plane Angle Deviation - Point 2

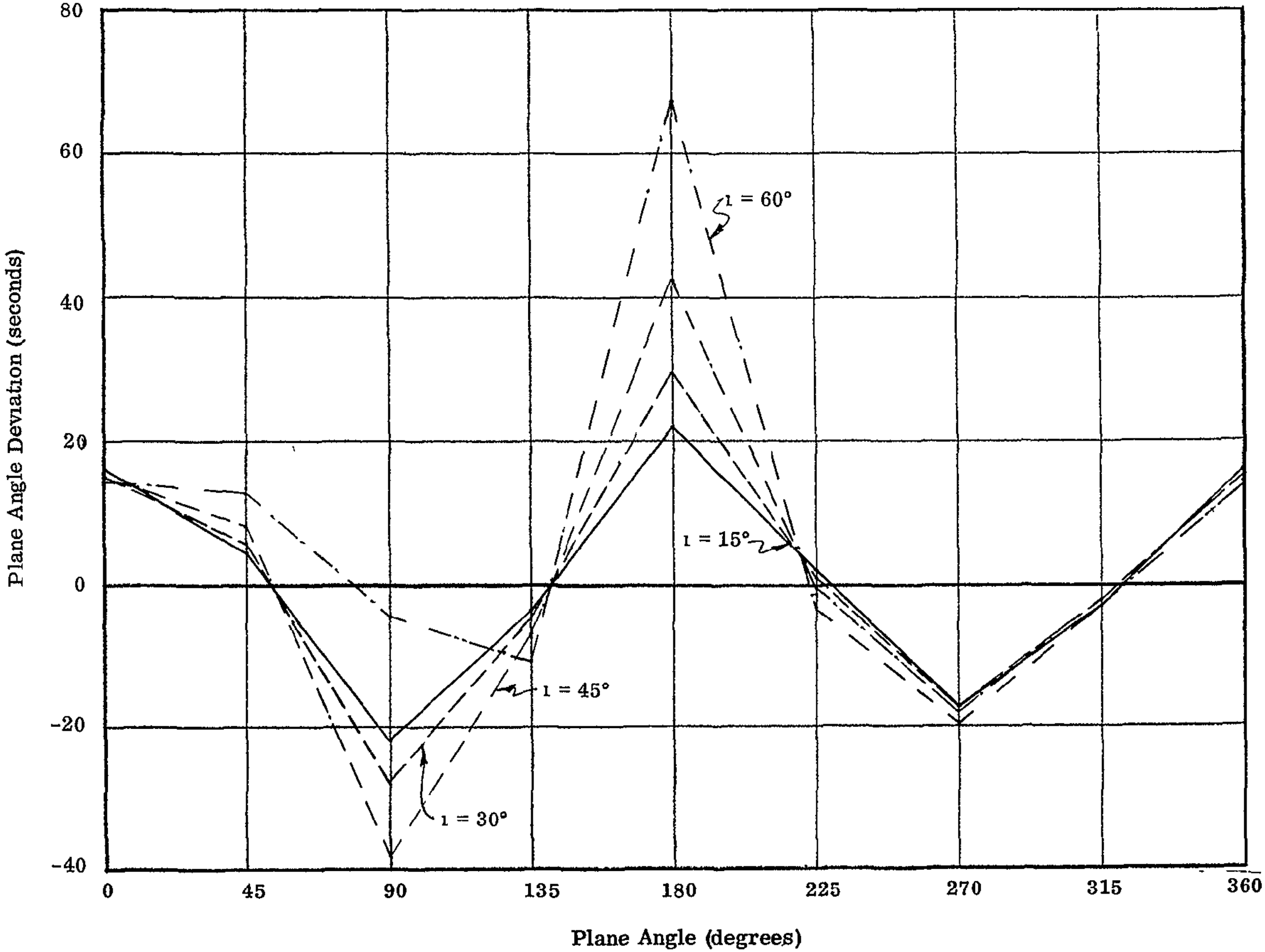

Figure 45 Plane Angle Deviation - Point 3

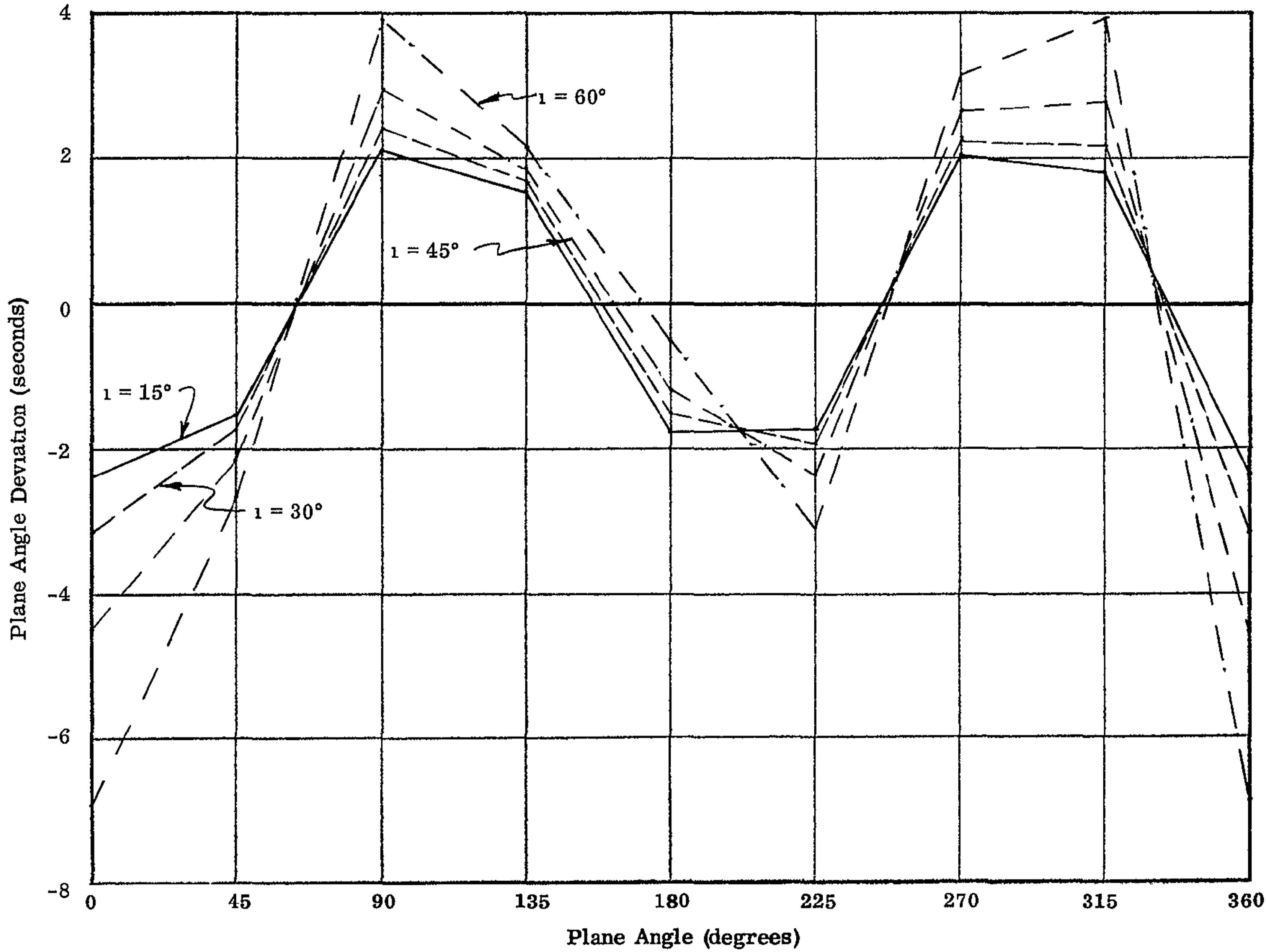

Figure 46 Plane Angle Deviation – Point 4

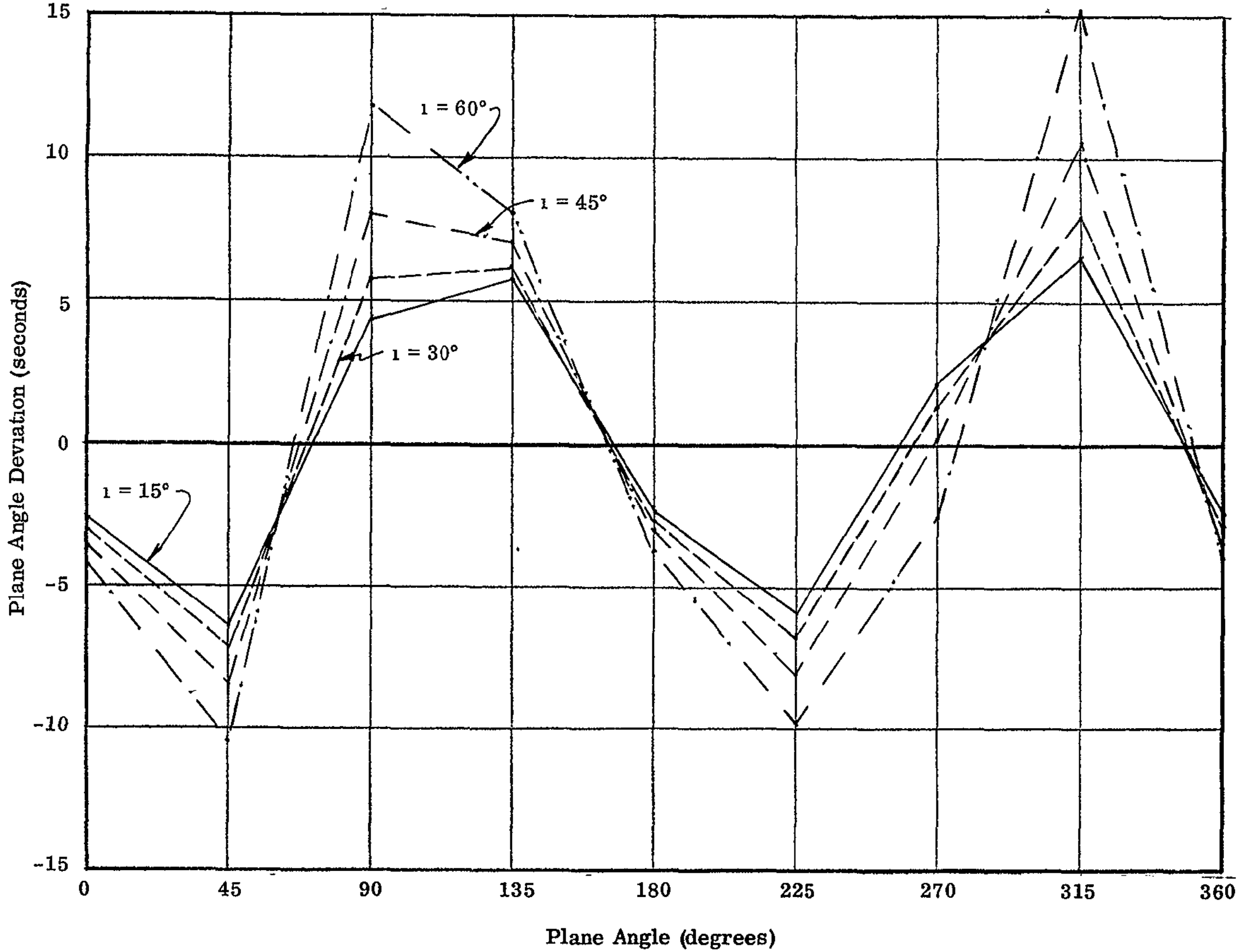

Figure 47. Plane Angle Deviation - Point 5

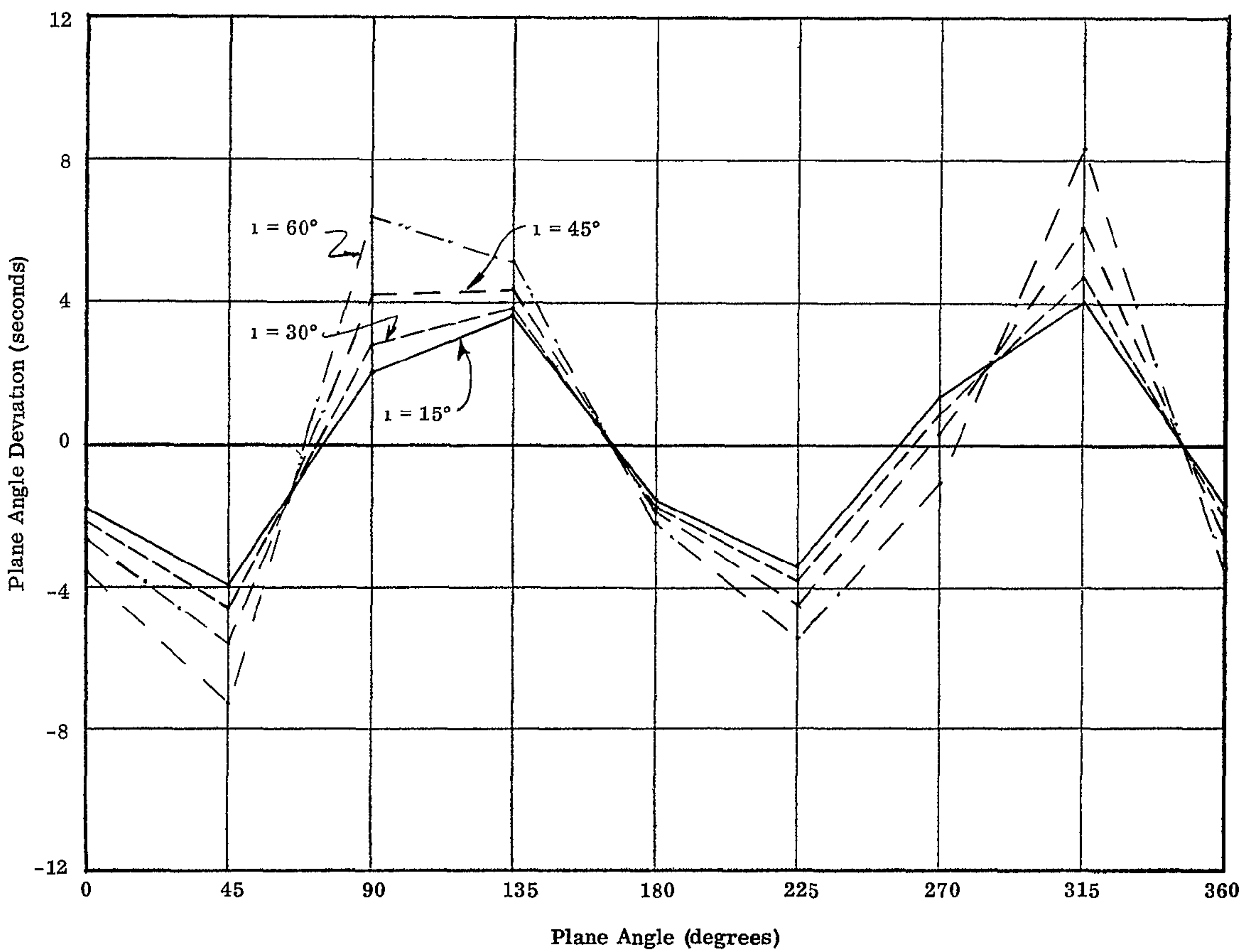

Figure 48 Plane Angle Deviation - Point 6

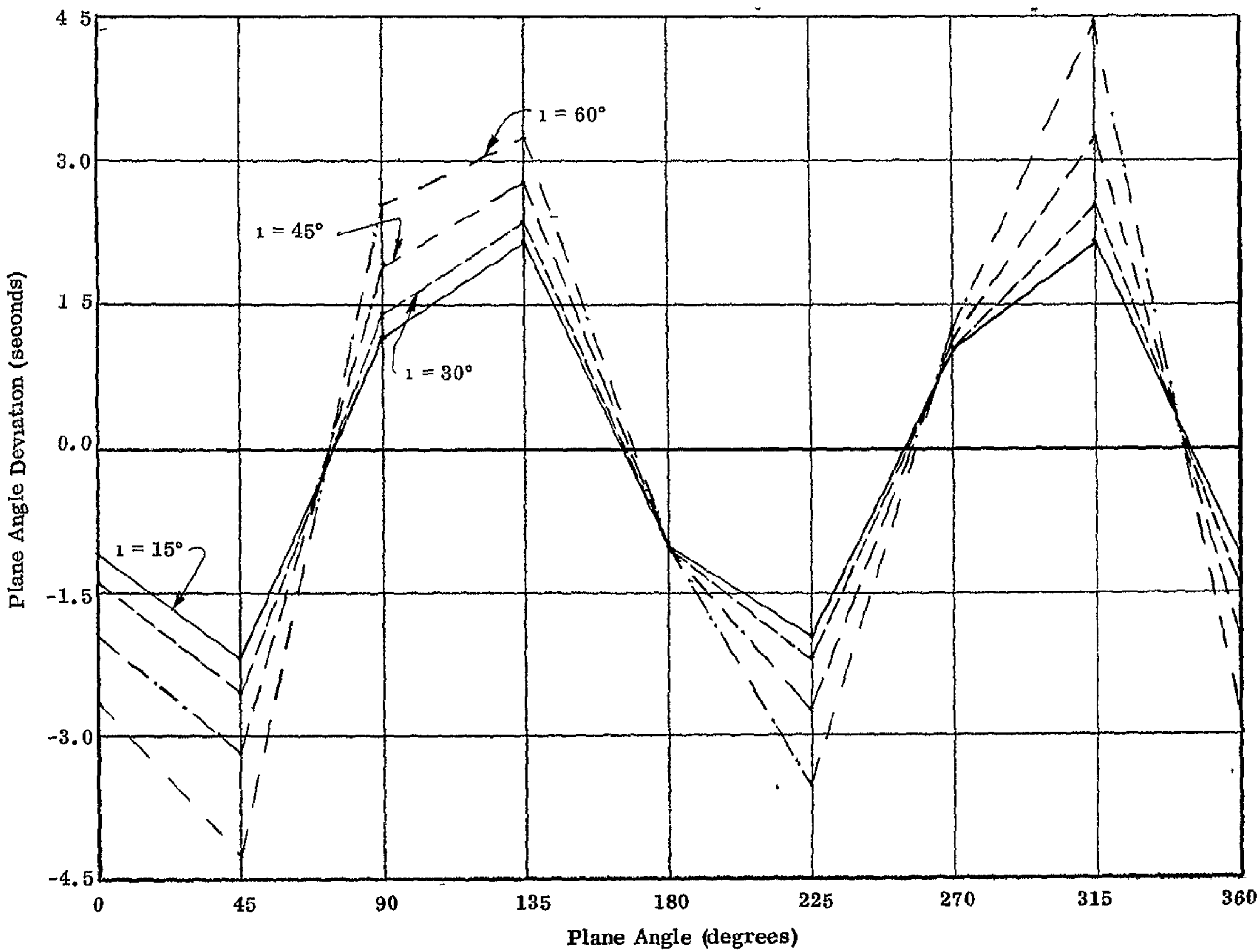

Figure 49. Plane Angle Deviation - Point 7

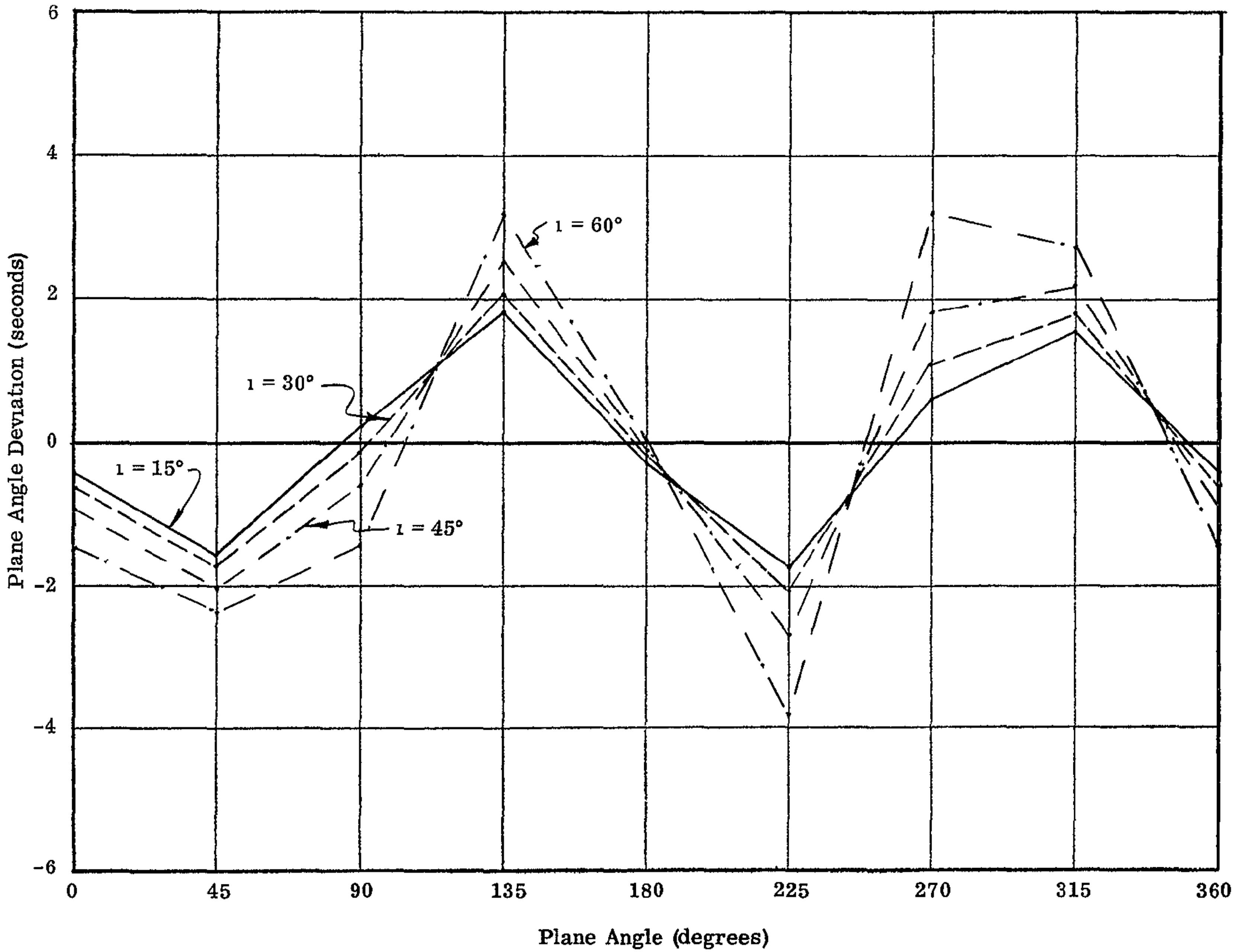

Figure 50. Plane Angle Deviation - Point 8

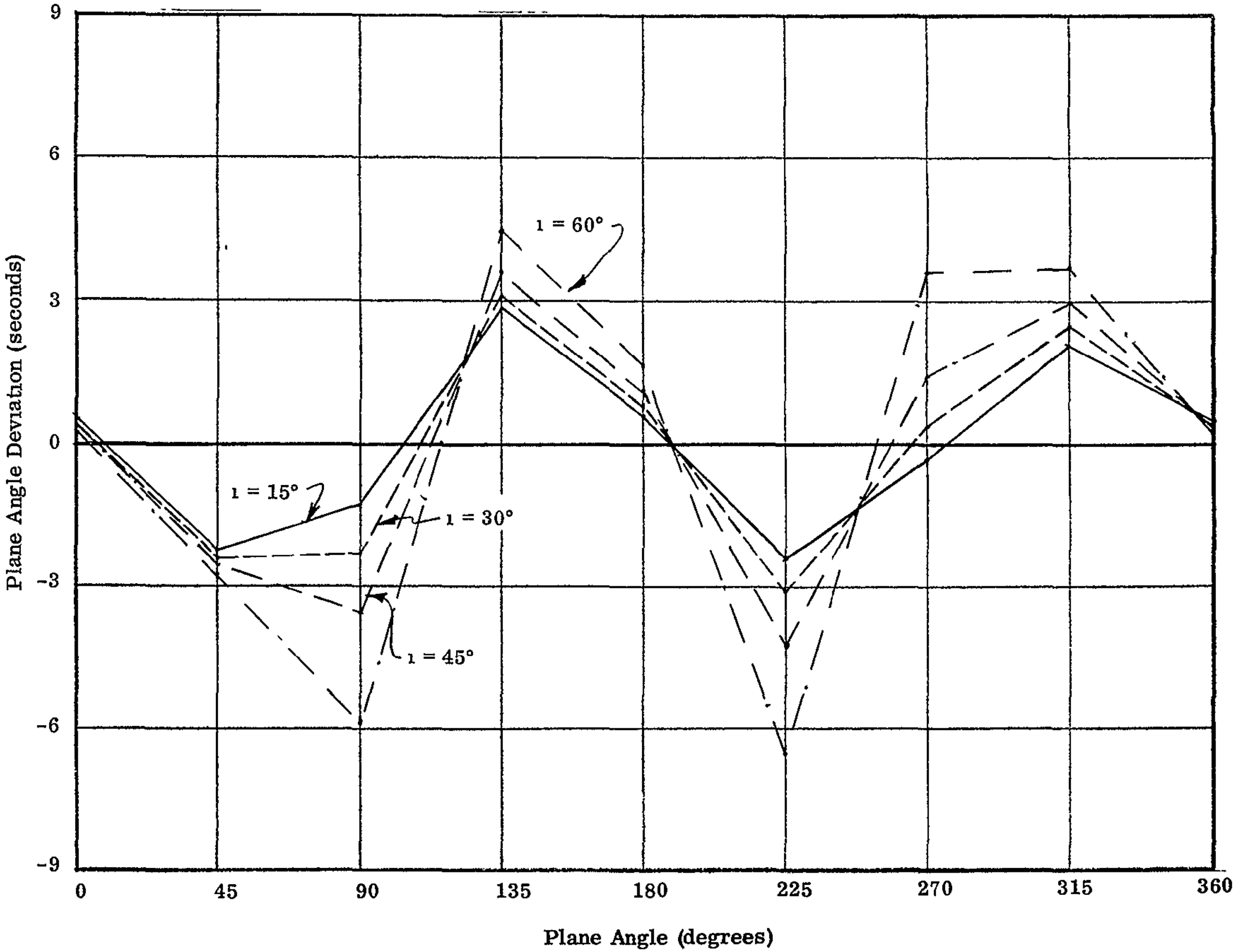

Figure 51 Plane Angle Deviation - Point 9

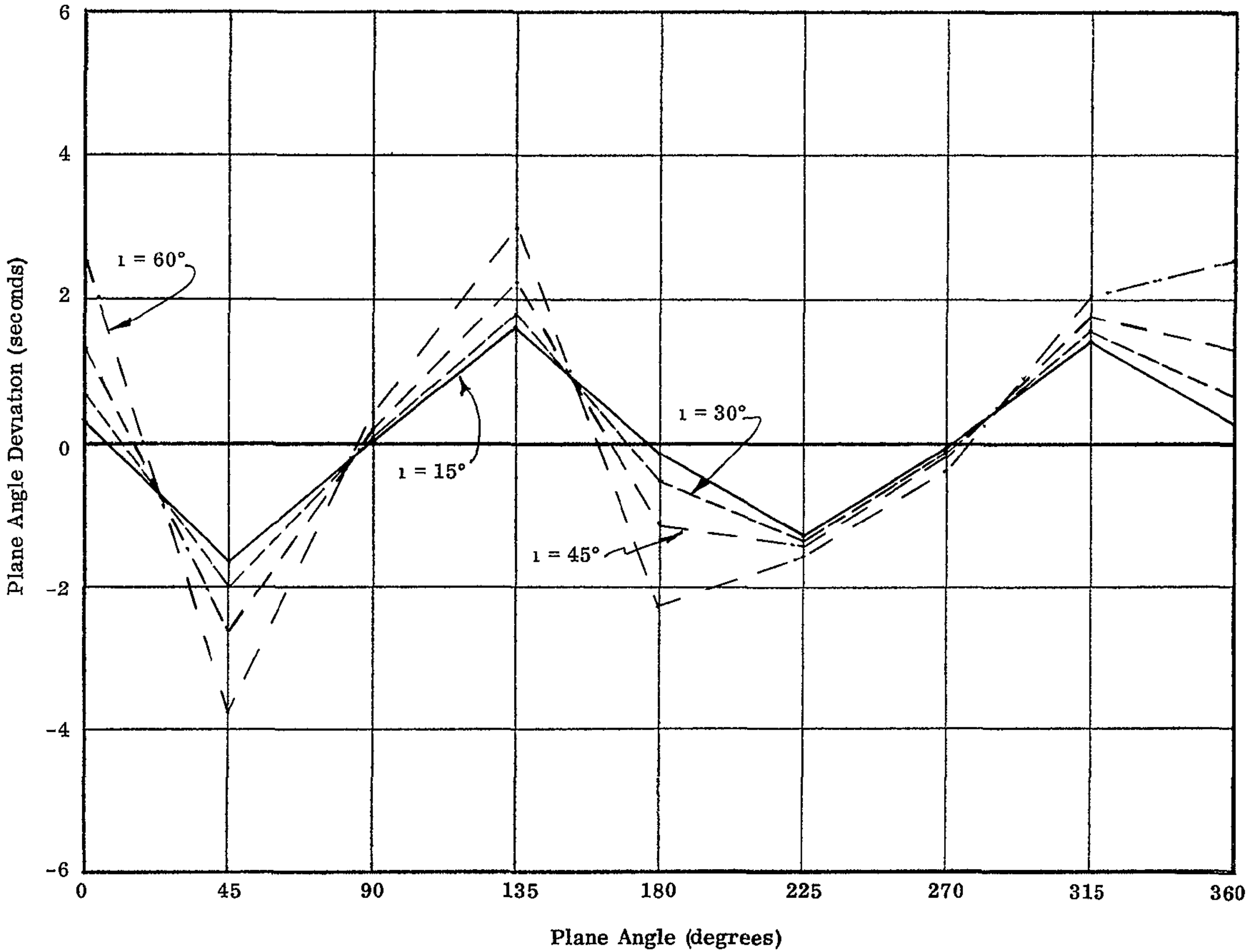

Figure 52 Plane Angle Deviation - Point 10

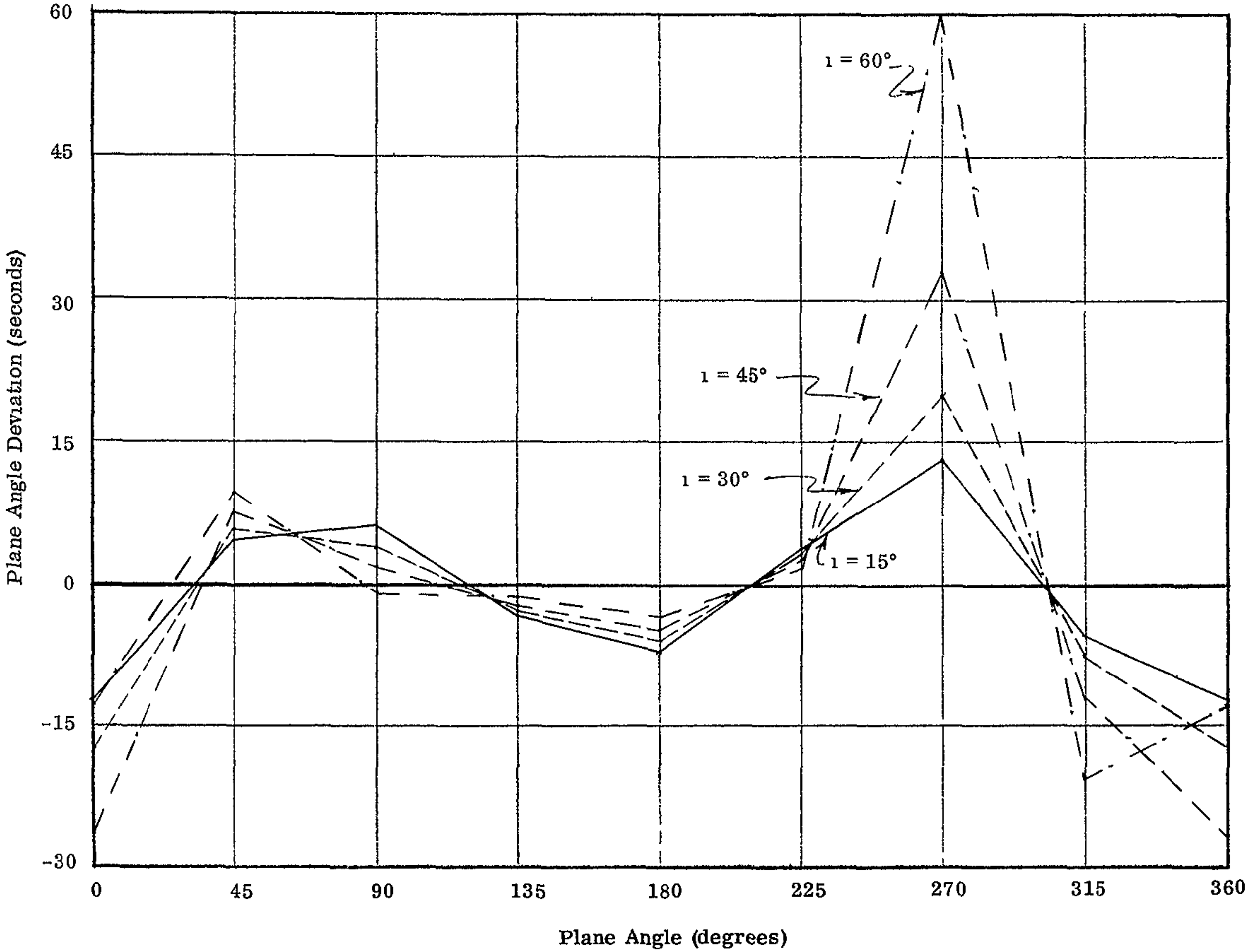

Figure 53 Plane Angle Deviation - Point 11

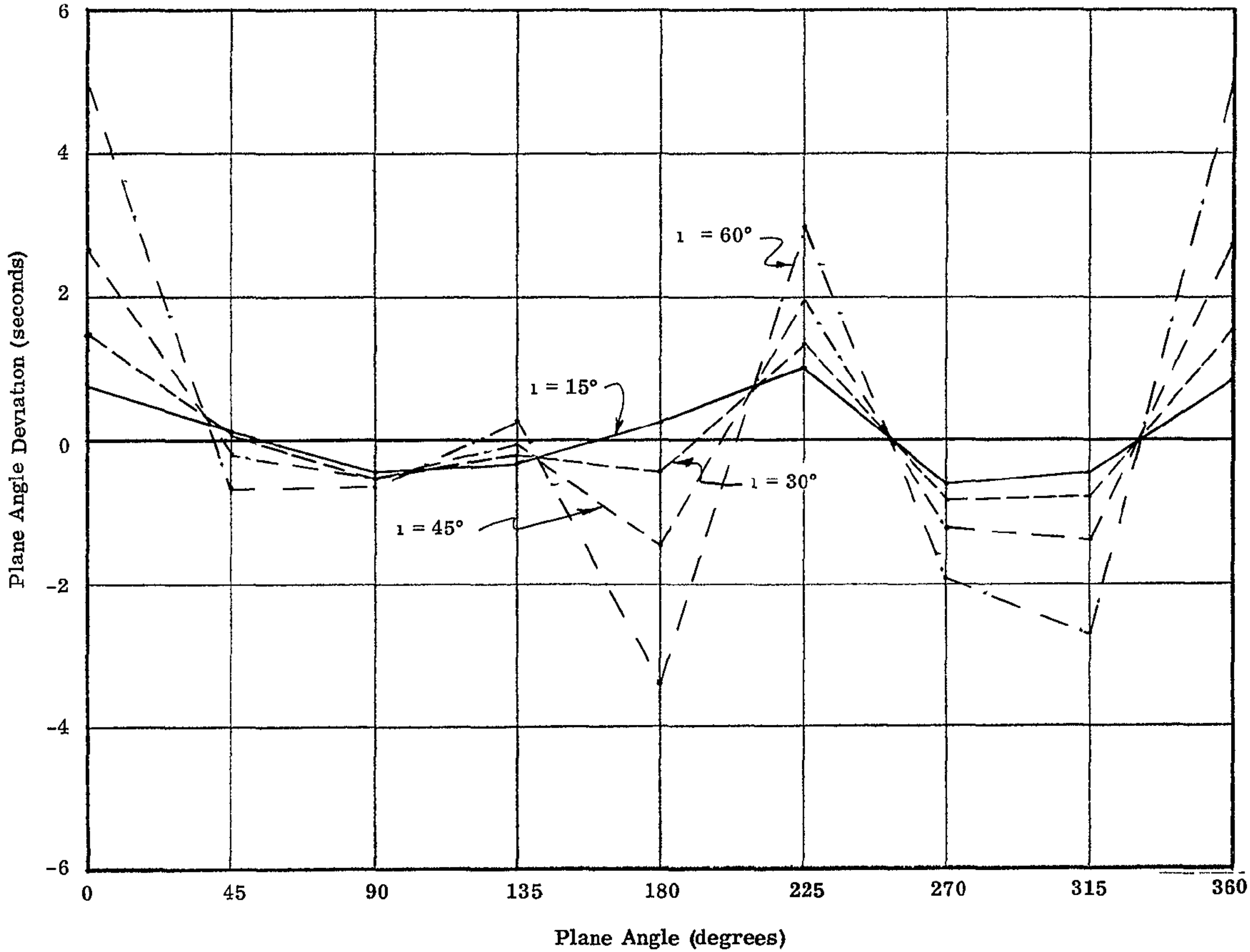

Figure 54. Plane Angle Deviation - Point 12

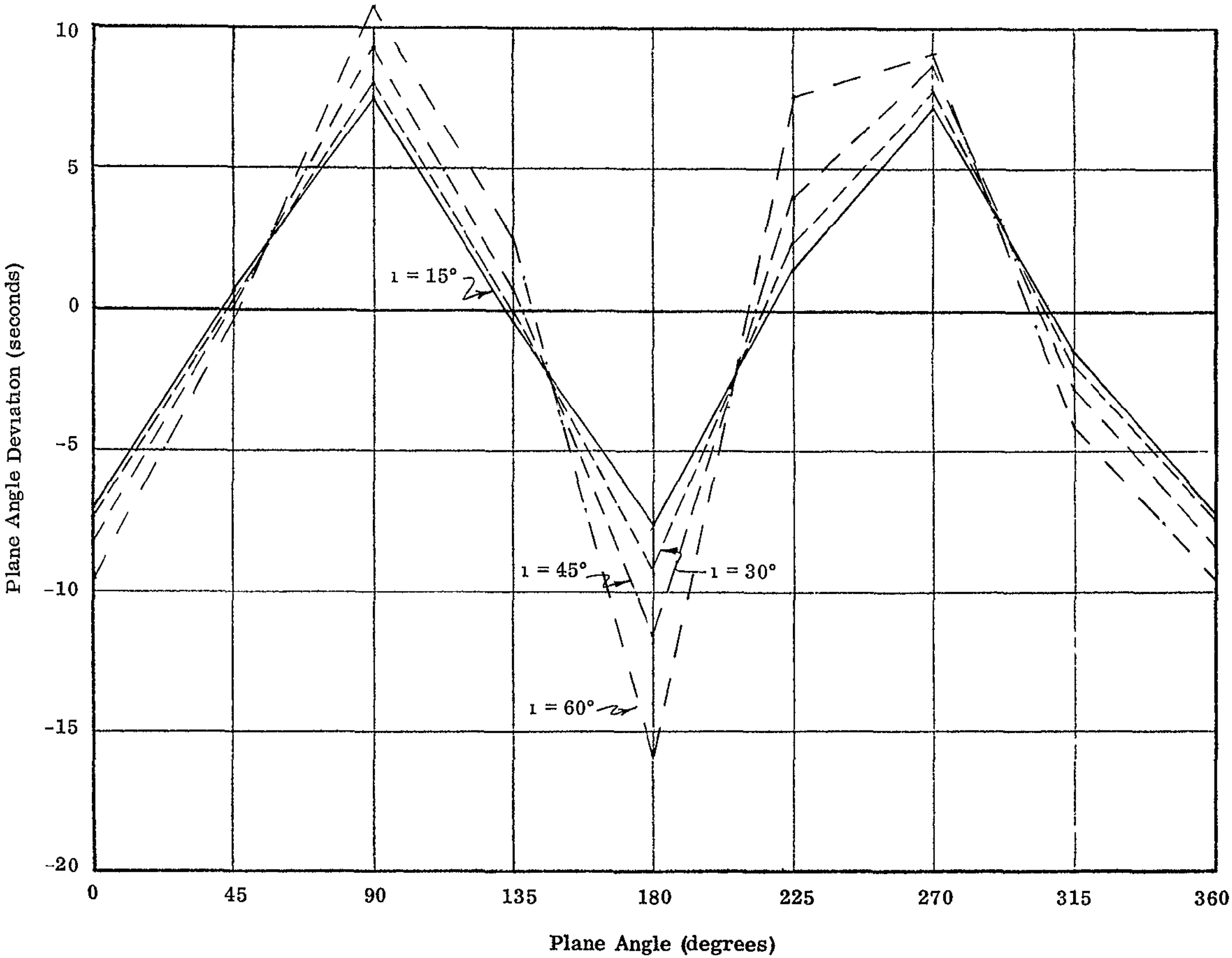

Figure 55 Plane Angle Deviation - Point 13

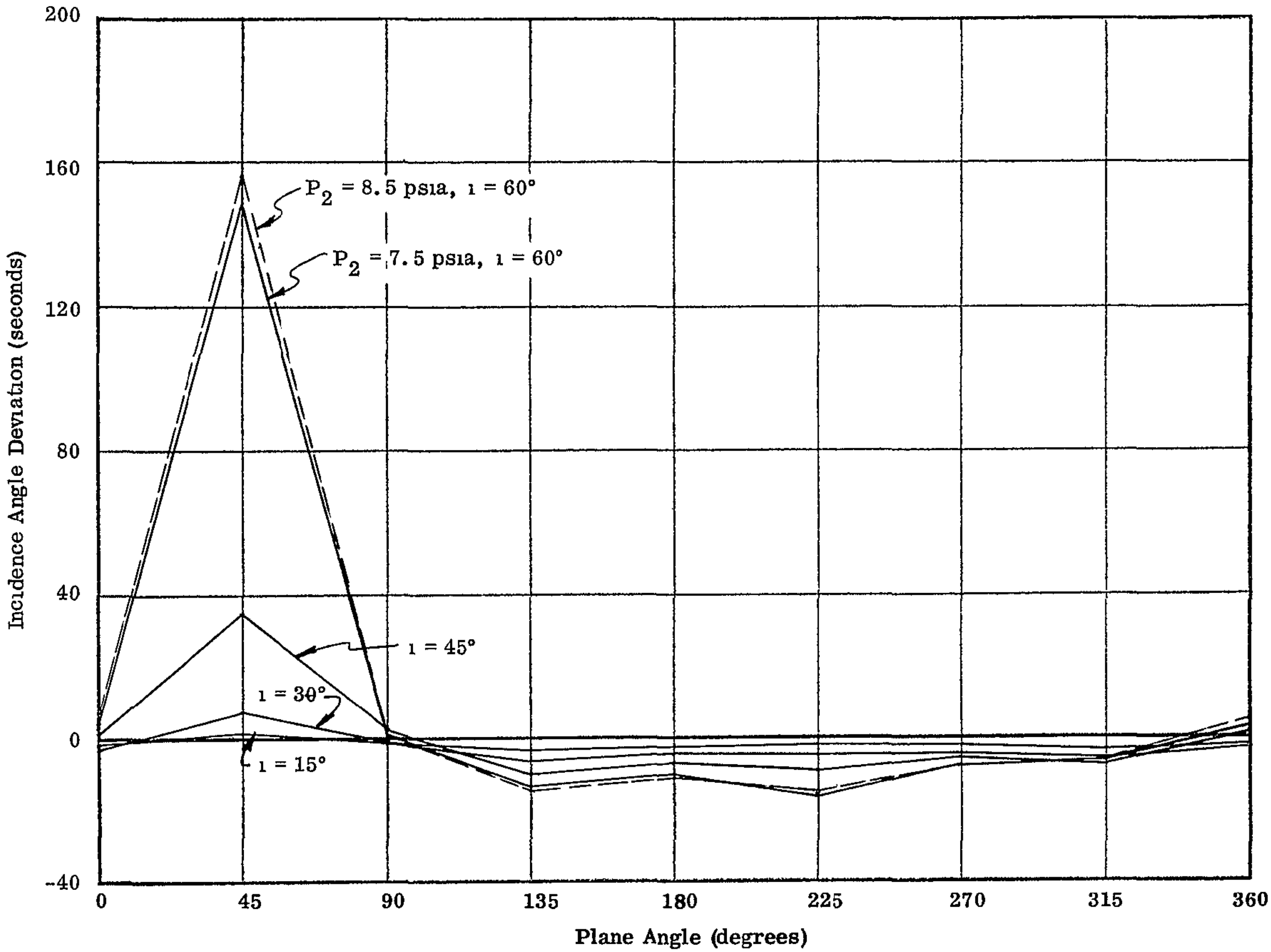

Figure 56 Incidence Angle Deviation - Point 1

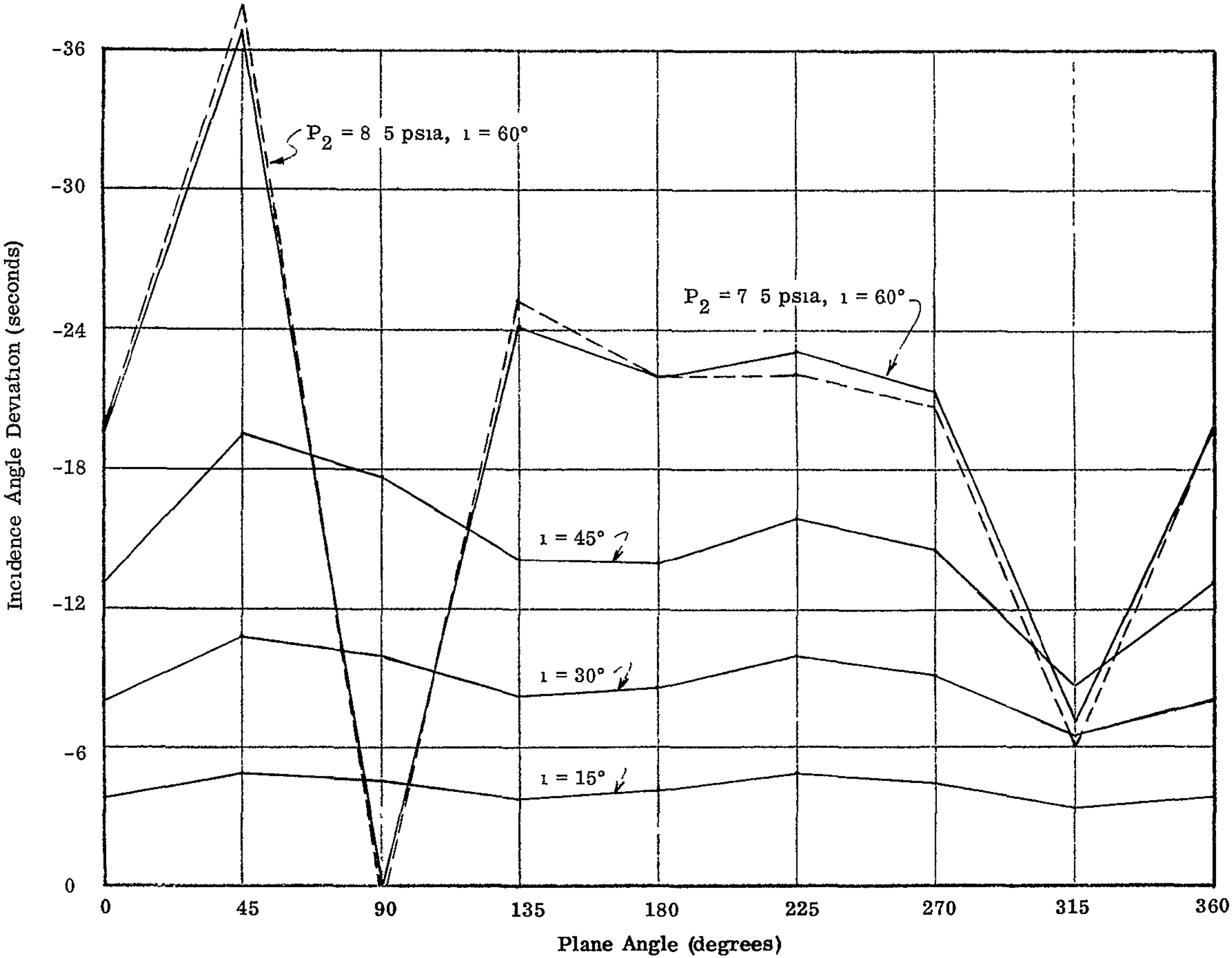

Figure 57. Incidence Angle Deviation - Point 2

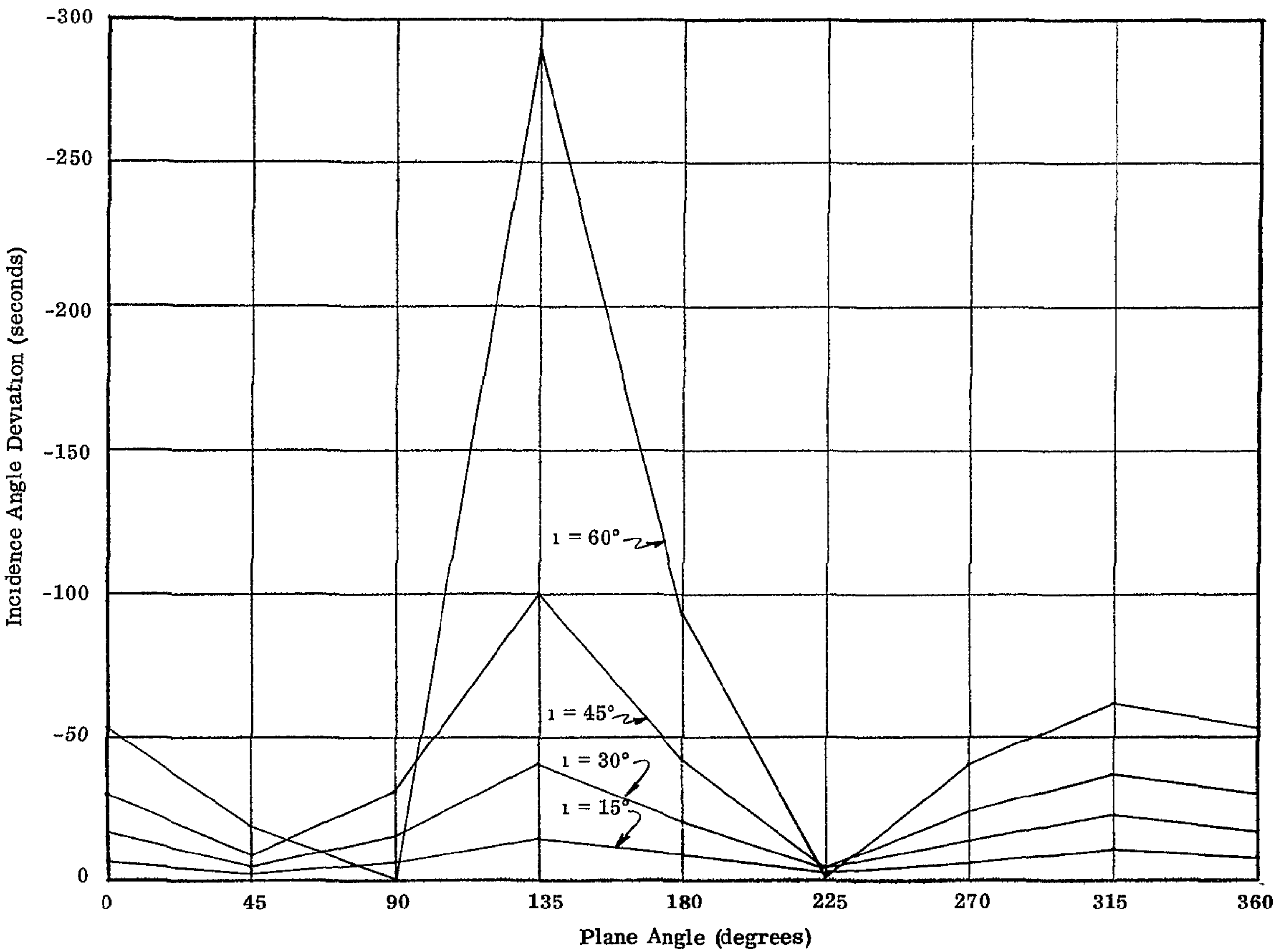

Figure 58 Incidence Angle Deviation - Point 3

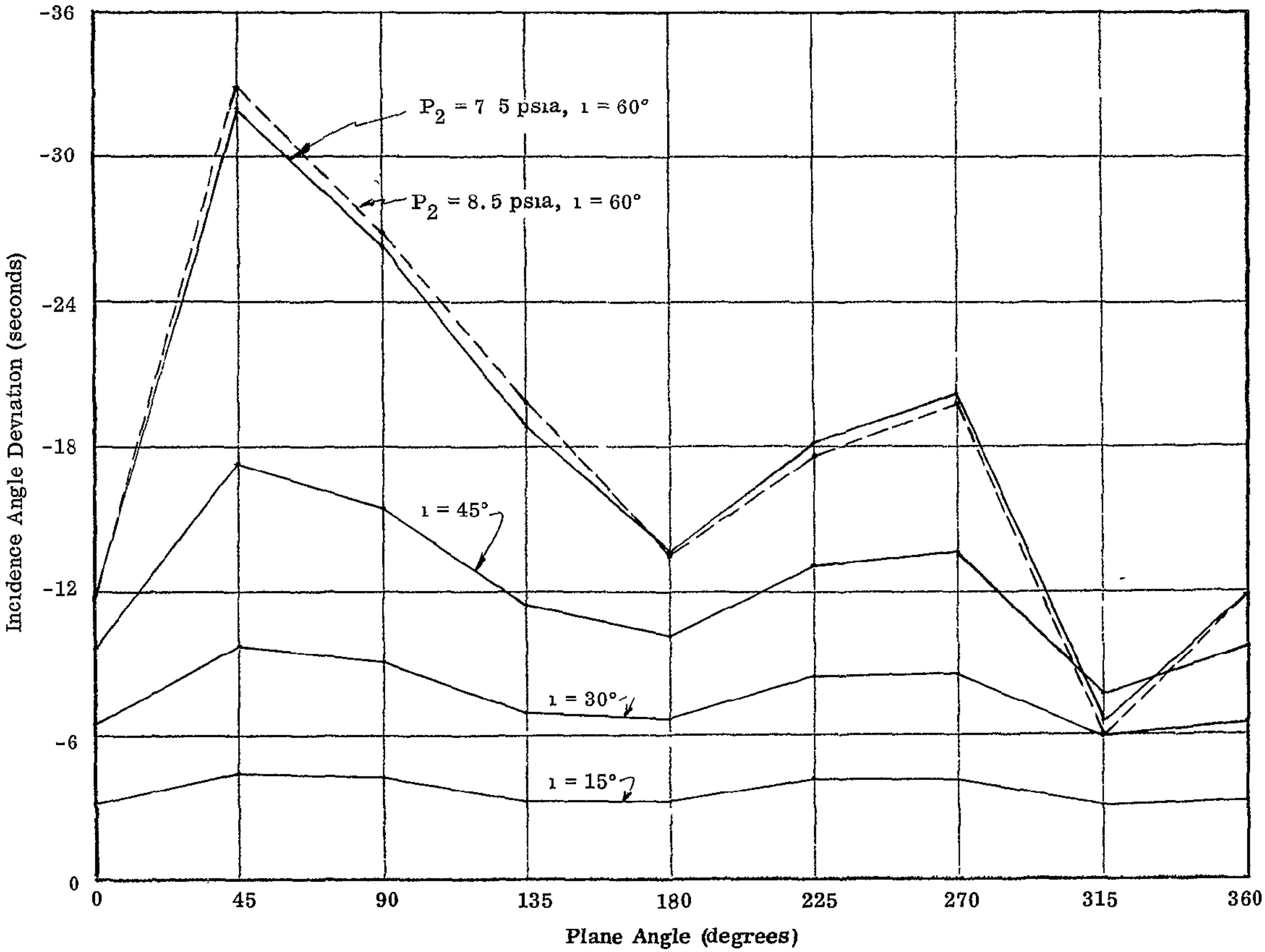

Figure 59. Incidence Angle Deviation - Point 4

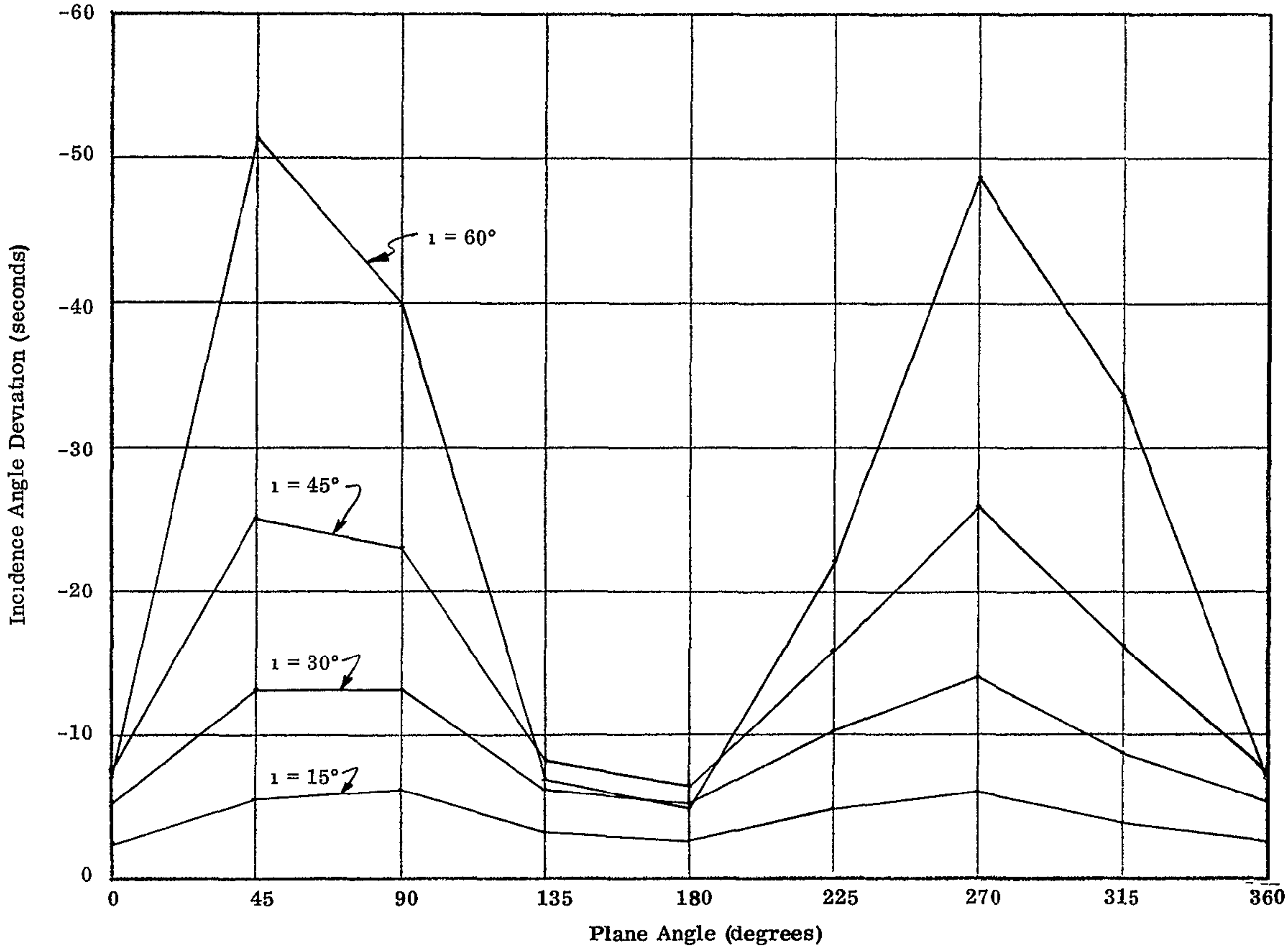

Figure 60 Incidence Angle Deviation - Point 5

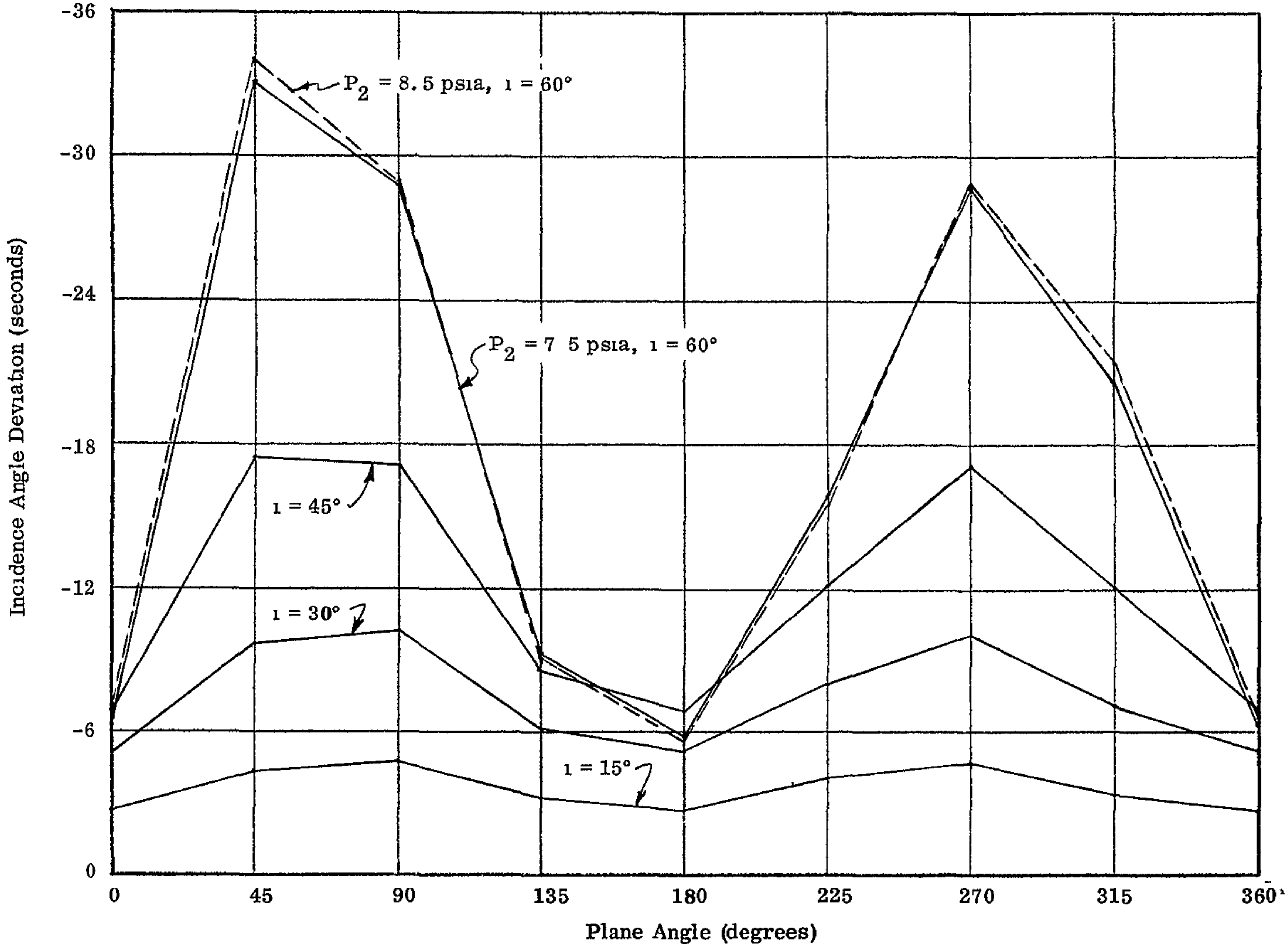

Figure 61. Incidence Angle Deviation - Point 6

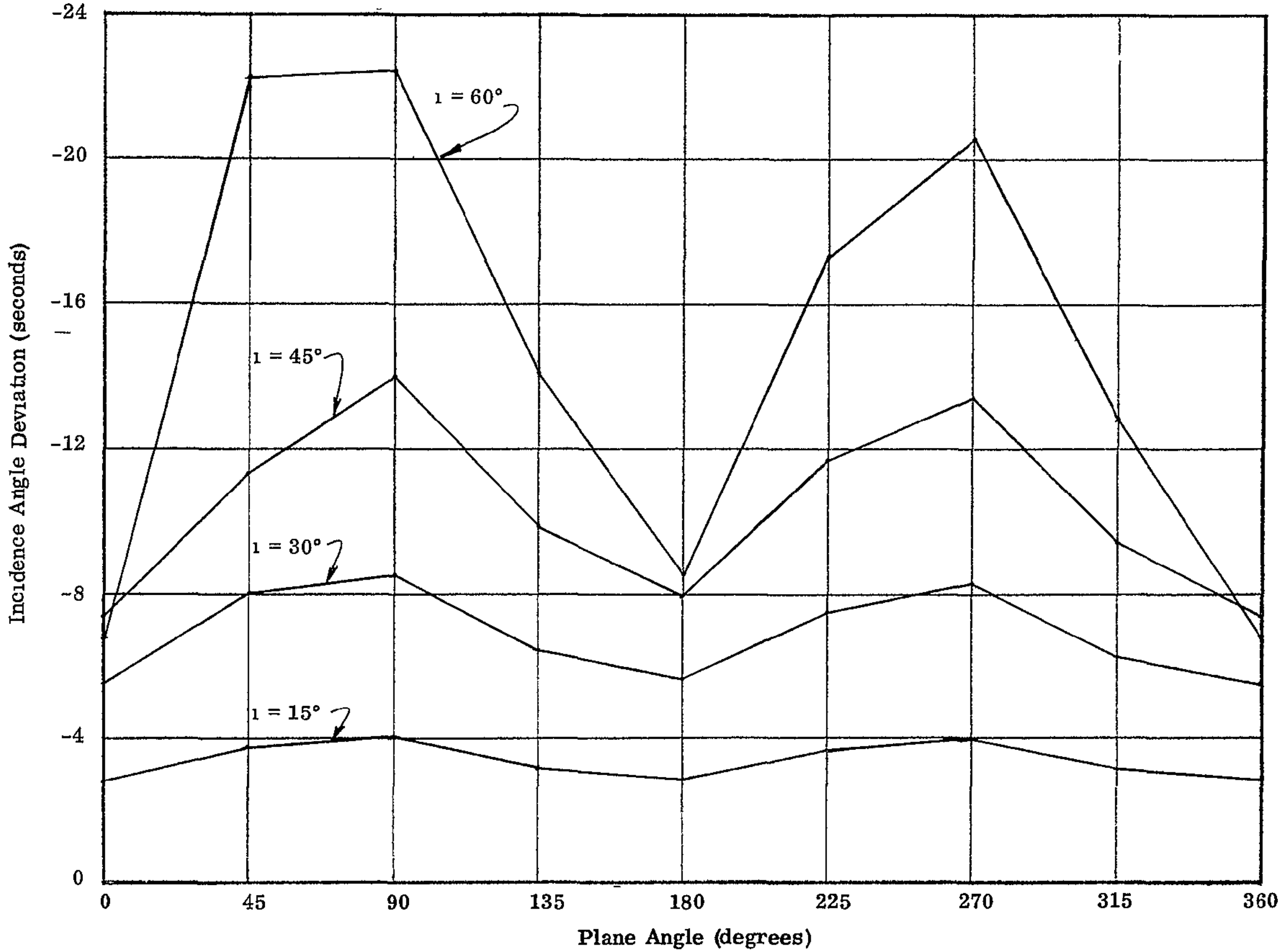

Figure 62 Incidence Angle Deviation - Point 7

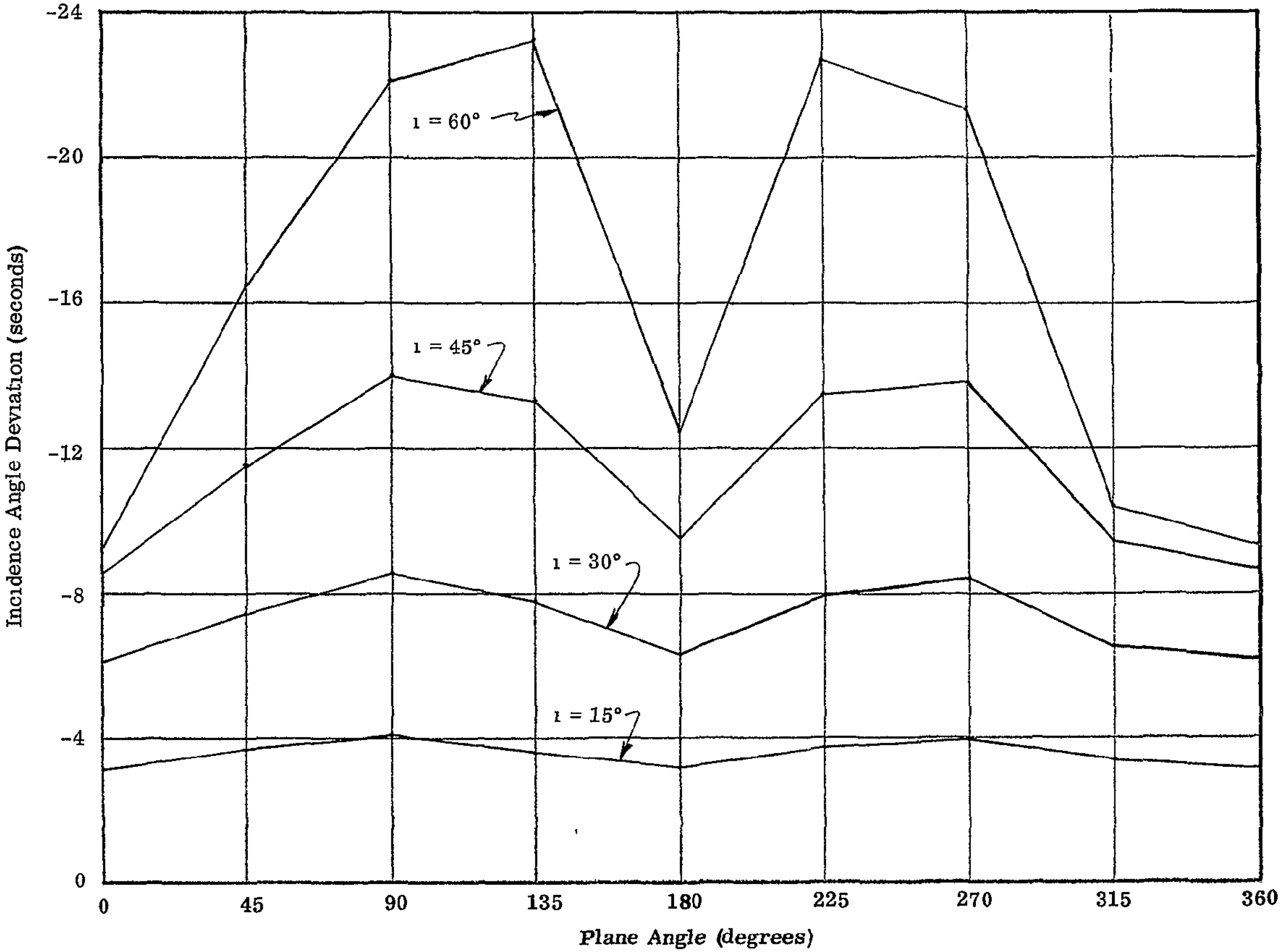

Figure 63 Incidence Angle Deviation - Point 8

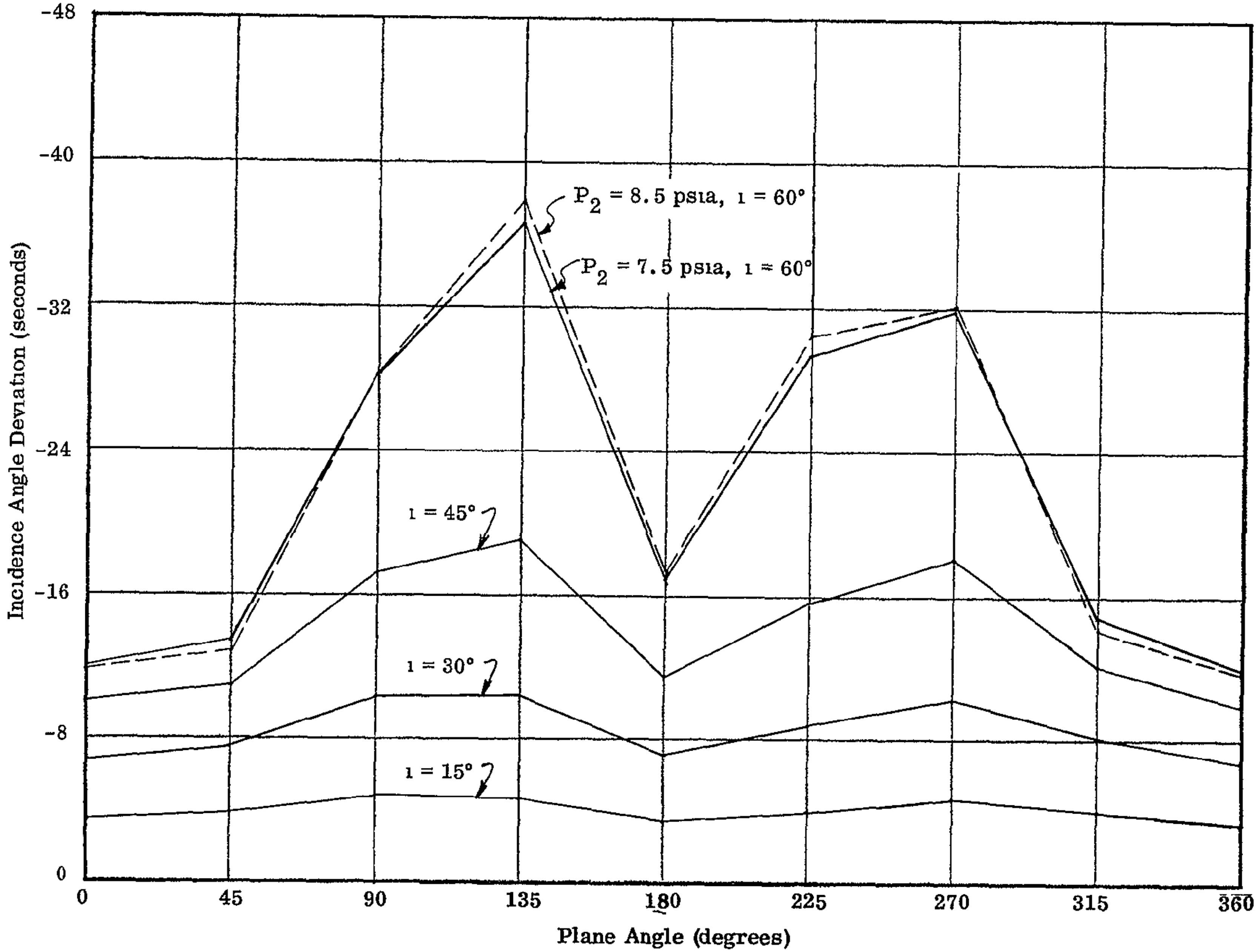

Figure 64 Incidence Angle Deviation - Point 9

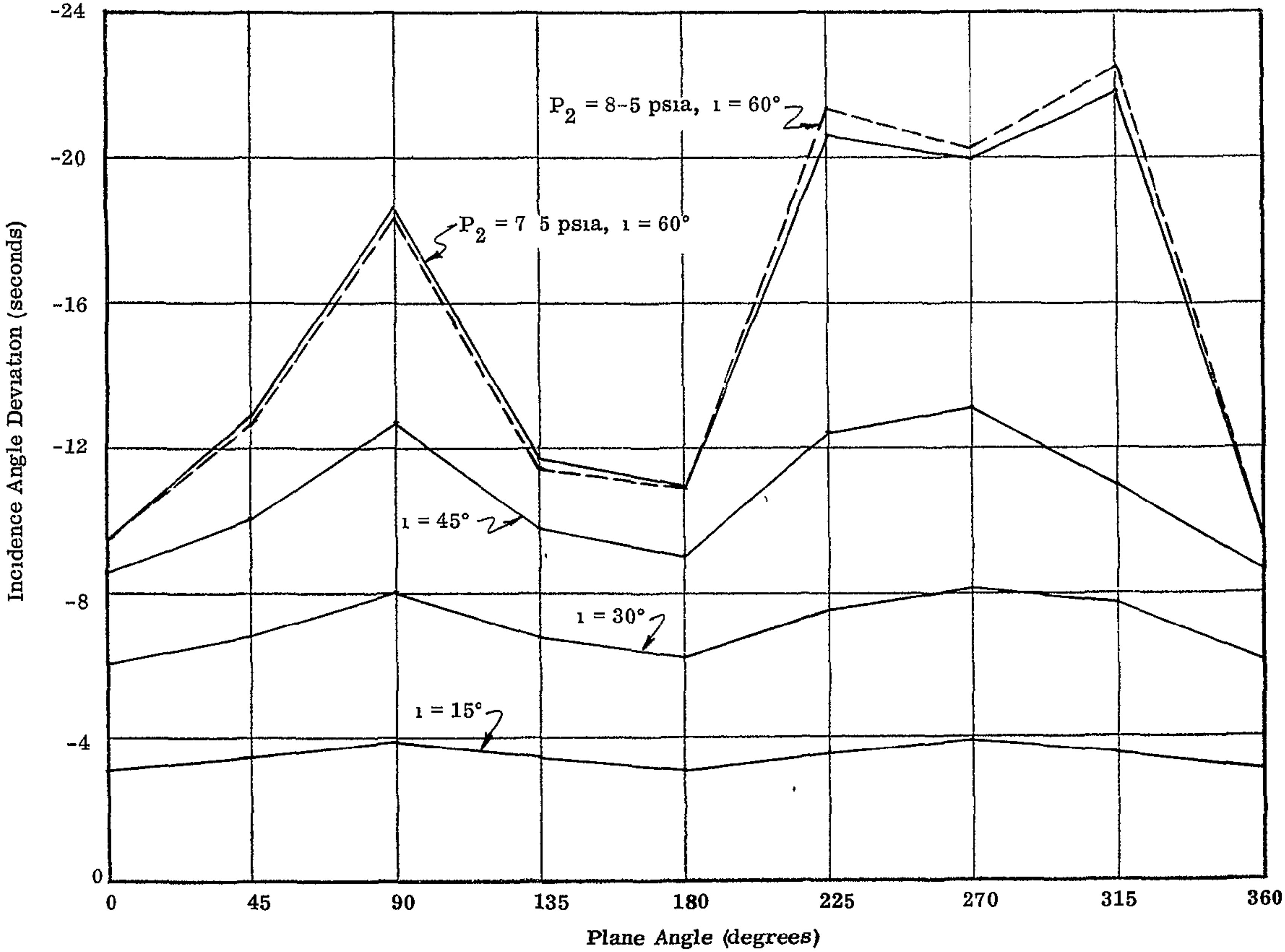

Figure 65 Incidence Angle Deviation - Point 10

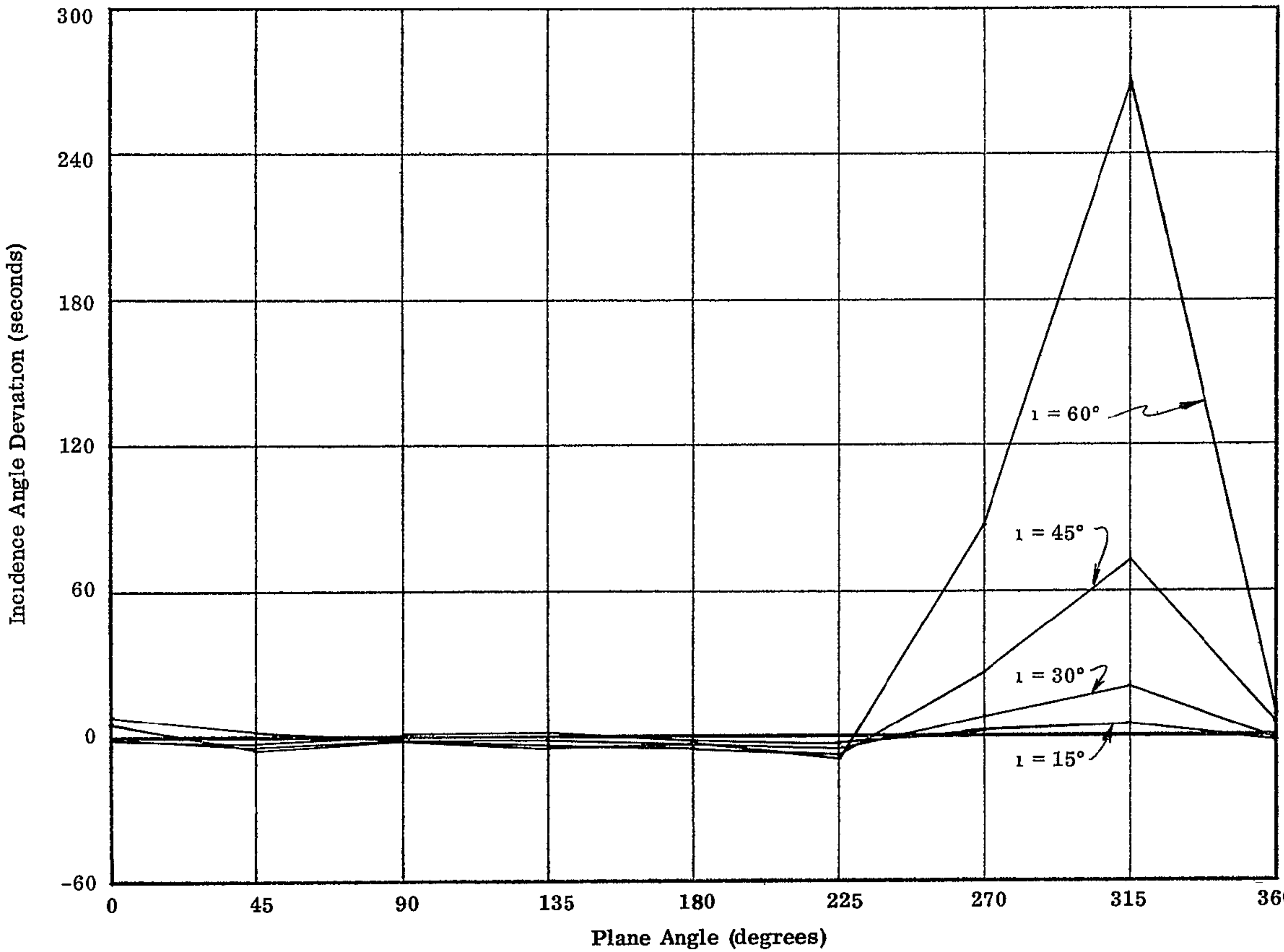

Figure 66 Incidence Angle Deviation - Point 11

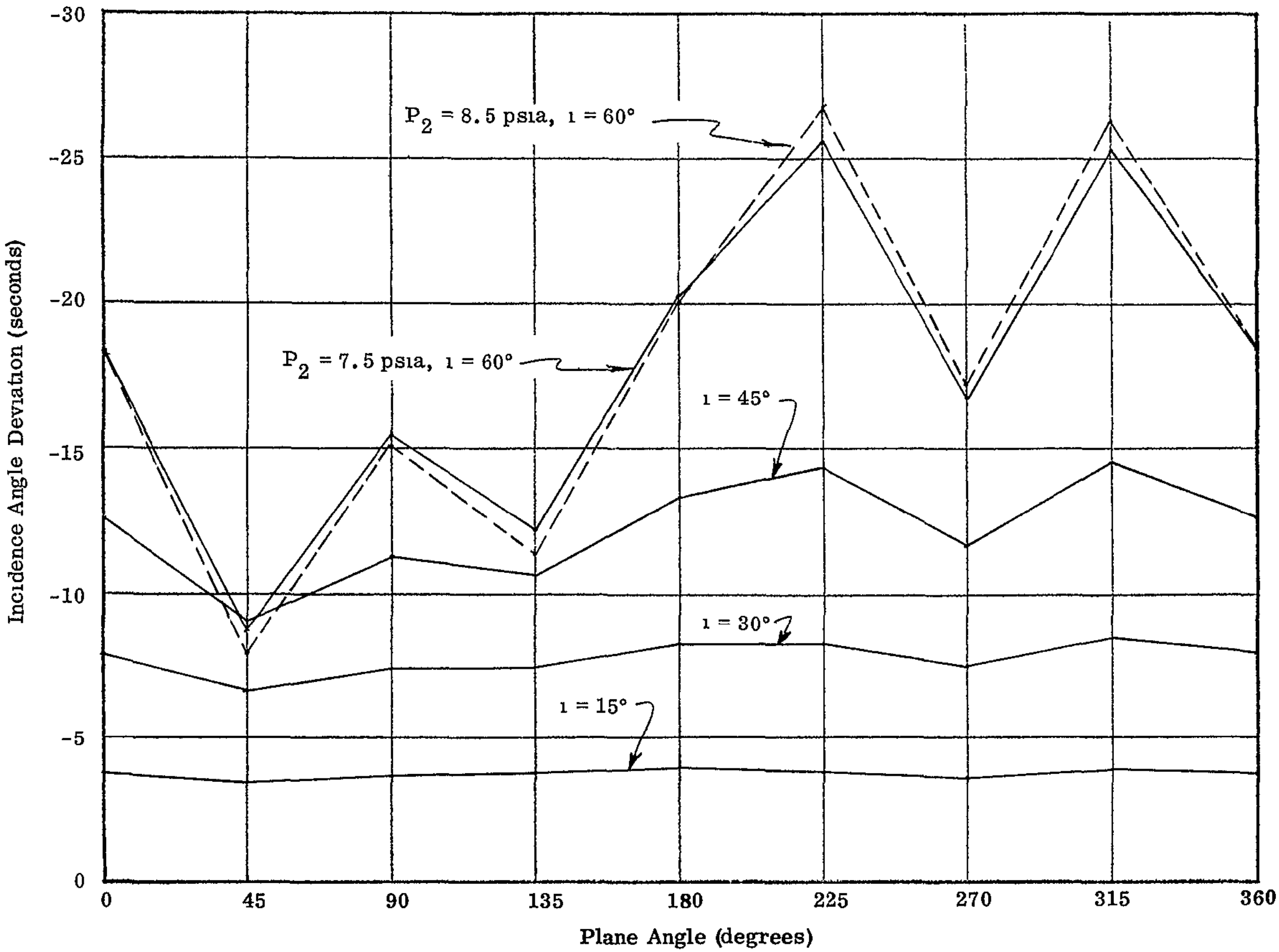

Figure 67 Incidence Angle Deviation - Point 12

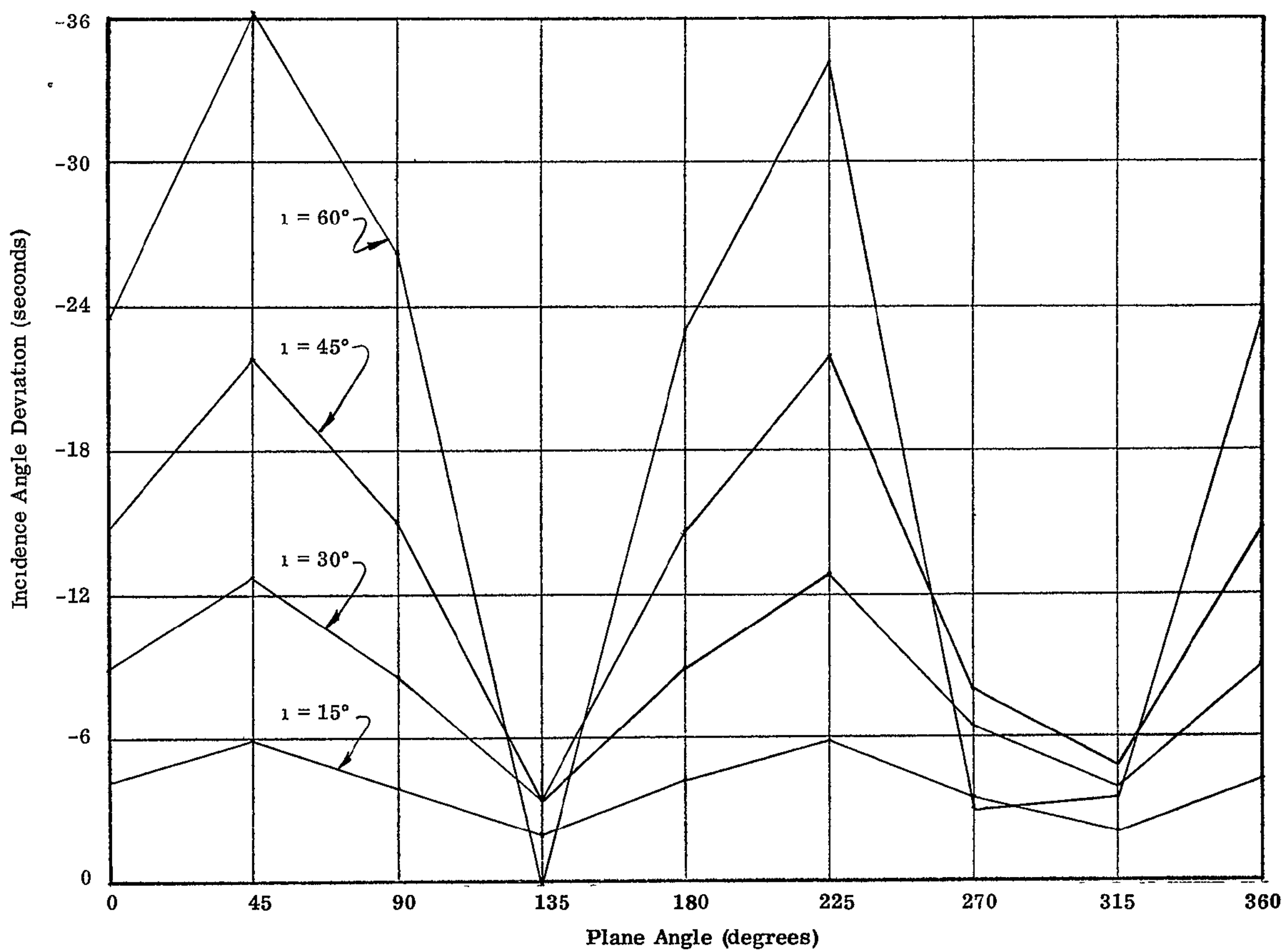

Figure 68. Incidence Angle Deviation - Point 13

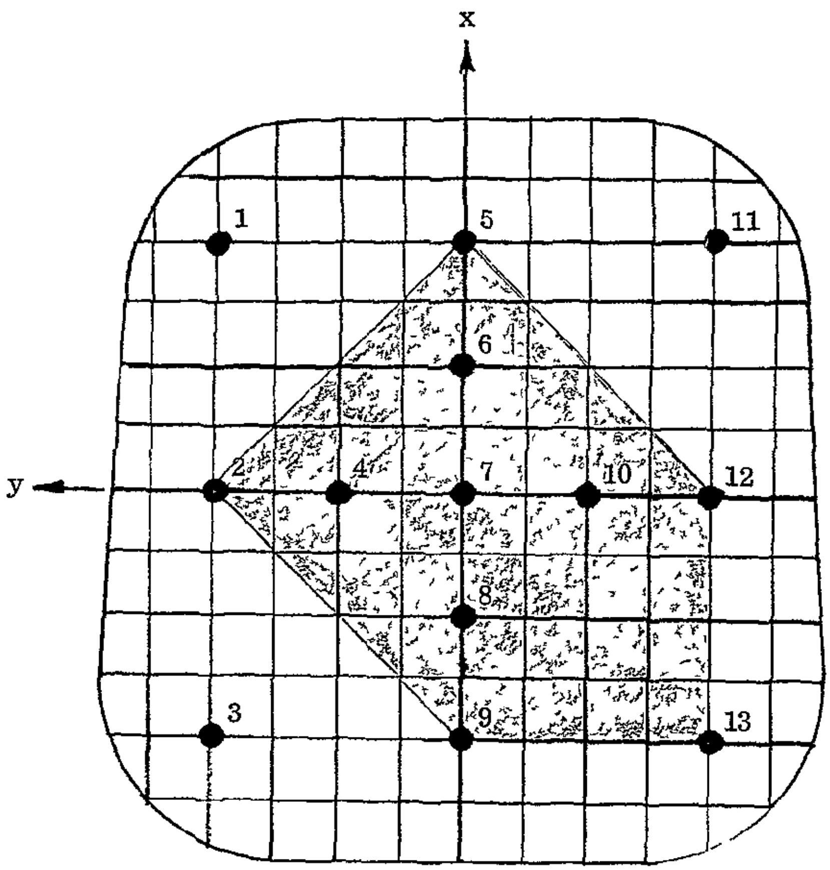

Figure 69 Best Observation Area - Single Ray Trace

Two Ray Trace Analysis

Two ray trace analyses are performed on the Apollo Scientific Side Window for the window supported in its actual structural configuration. Figure 70 defines the angles associated with the two ray trace analyses.

Figure 71 gives designation numbers for the individual points on the window surface which are studied in detail in the following analysis. These points are located on the left-hand window and correspond to the points through which observations are made on the right-hand window. The analysis is performed on the window with actual edge conditions and loaded with a cabin pressure of 5.1 psia, an interstitial pressure of 7.5 psia, and no external pressure. For each point, four sets of curves are presented. Each set of curves is a plot of the sextant angle change as a function of three plane angles (135°, 180°, and 225°). It should be noted that the coordinate system used for the finite element model generation of the deformations was rotated 90° from the coordinate system used in the two ray trace analyses. Therefore, to make a study of the plane angles above, angles of 225°, 270°, and 315° were actually input into the ray trace program. Further references will be made to these angles as though they were measured in the coordinate system used in the two ray trace analyses.

The first set of curves shows the results for a variation in the primary incidence angle of $i = 70^\circ$, $i = 90^\circ$, and $i = 110^\circ$. The second set gives the results of a variation in the z-plane inclination angle for $\psi = -15^\circ$, $\psi = 0^\circ$, and $\psi = 15^\circ$. The third set shows the results for a variation in the sextant distance from the inner window surface for z = 2", z = 4", and z = 6". The fourth set of curves indicates the results for a variation in the sextant angle of $\theta = 0^\circ$, $\theta = 20^\circ$, and $\theta = 40^\circ$.

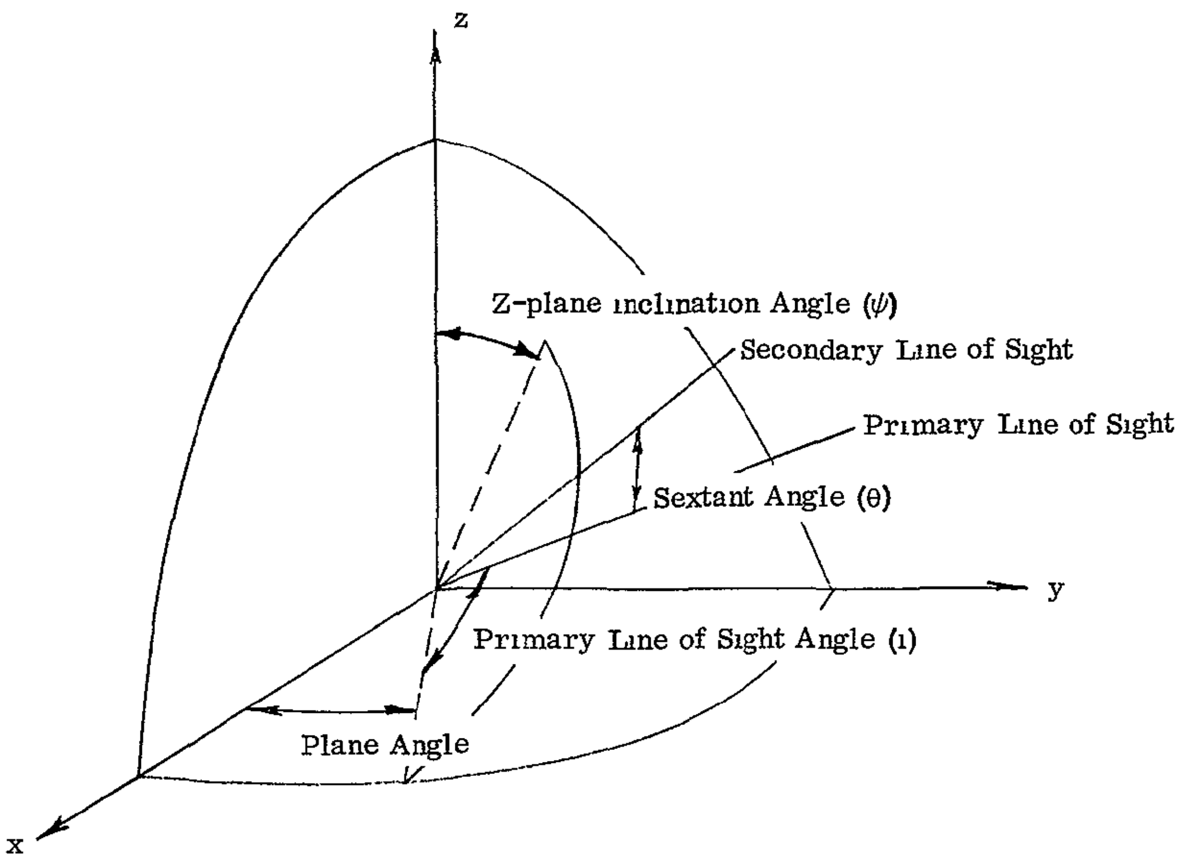

Figure 70 Two Ray Trace Angles

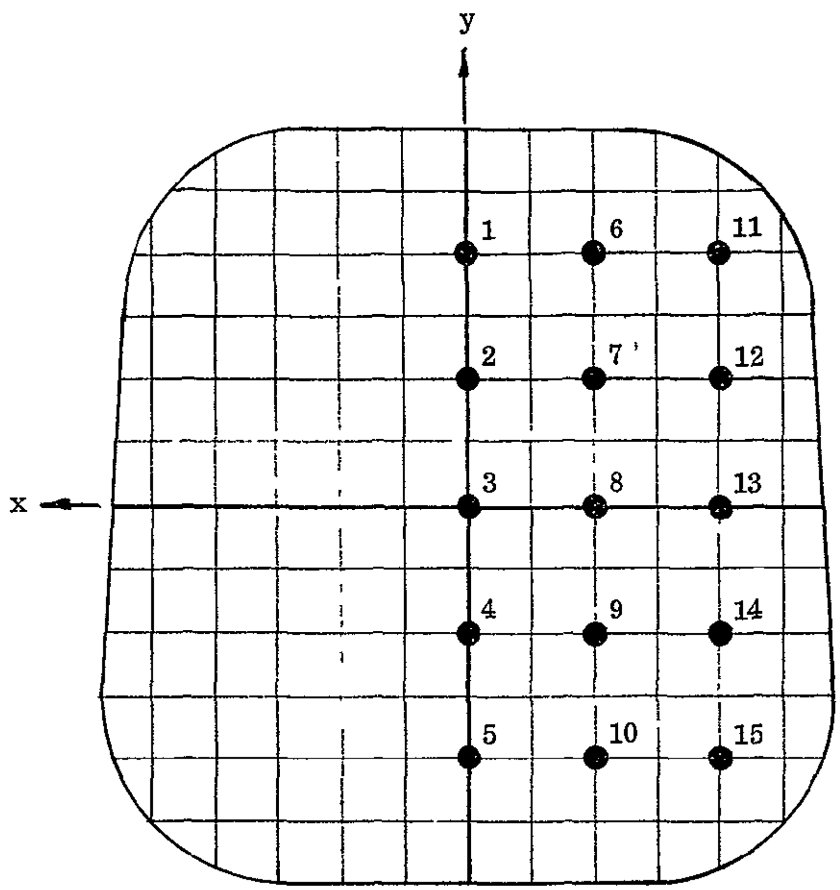

Figure 71   Points of Interest - Two Ray Trace

The basic set of parameters for each set of curves is $i = 90^{\circ}$, $\psi = 0^{\circ}$, $z = 2''$, and $\theta = 20^{\circ}$. These parameters are constant for any set of curves with the exception of the variation studied for that particular set.

The sextant distance, z, is measured from the undeformed inner surface of the inner pane to a point on the sextant. This point and the geometry of the particular sextant which will be used in making observations through the Apollo Window have been incorporated into the computer code used to perform the two ray trace analyses.

Figures 72 through 86 show the plots for the four sets of curves for each of the fifteen points studied. For these curves, no value of the sextant angle change is plotted if either of the exiting primary or secondary rays fall outside the window planform.

These plots indicate most of the rays exit outside the window planform for Points 1 through 5. This is true for all variable parameters. For Points 6 and 7, sightings can be made for all values of the parameters and for plane angles of 135° and 180°, except when the sextant angle is 40°. The same holds for Points 9 and 10, except the plane angles must be 180° and 225°. Observations can be made from Points 8 and 13 for all parameter values, except a sextant angle of 40°. Sightings can be made from Points 11 and 12, except at plane angles of 225° and from Points 14 and 15, except at plane angles of 180°.

Figure 87 indicates the areas of the window from which observations can be made with the sextant. The 60° cross-hatched area indicates that area from which sightings can be made with the exception of a plane angle of 225° and a sextant angle of 40°. The shaded portion of this area indicates areas from which sightings can be made with a sextant angle of

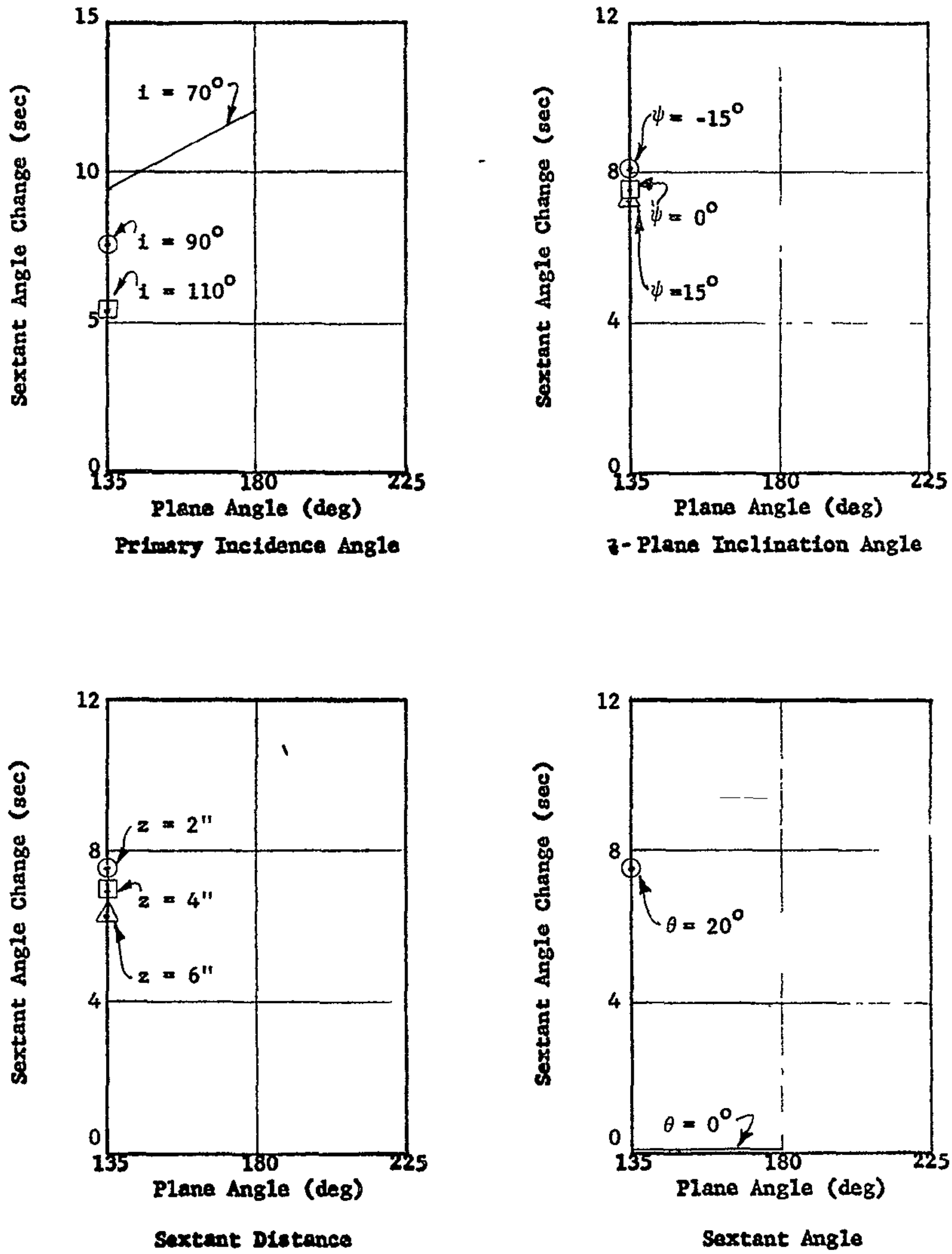

Figure 72. Sextant Angle Changes - Point 1

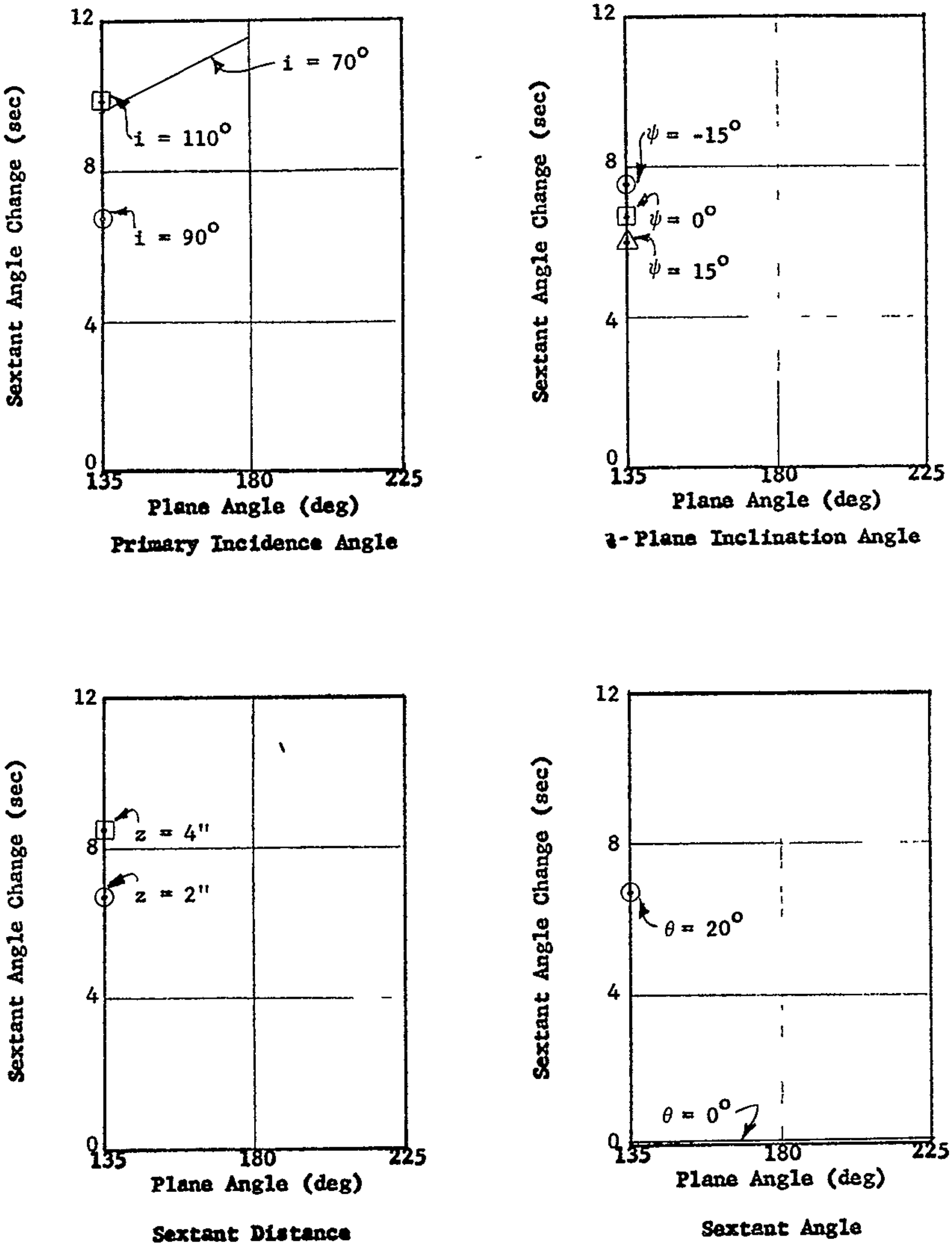

Figure 73 Sextant Angle Changes - Point 2

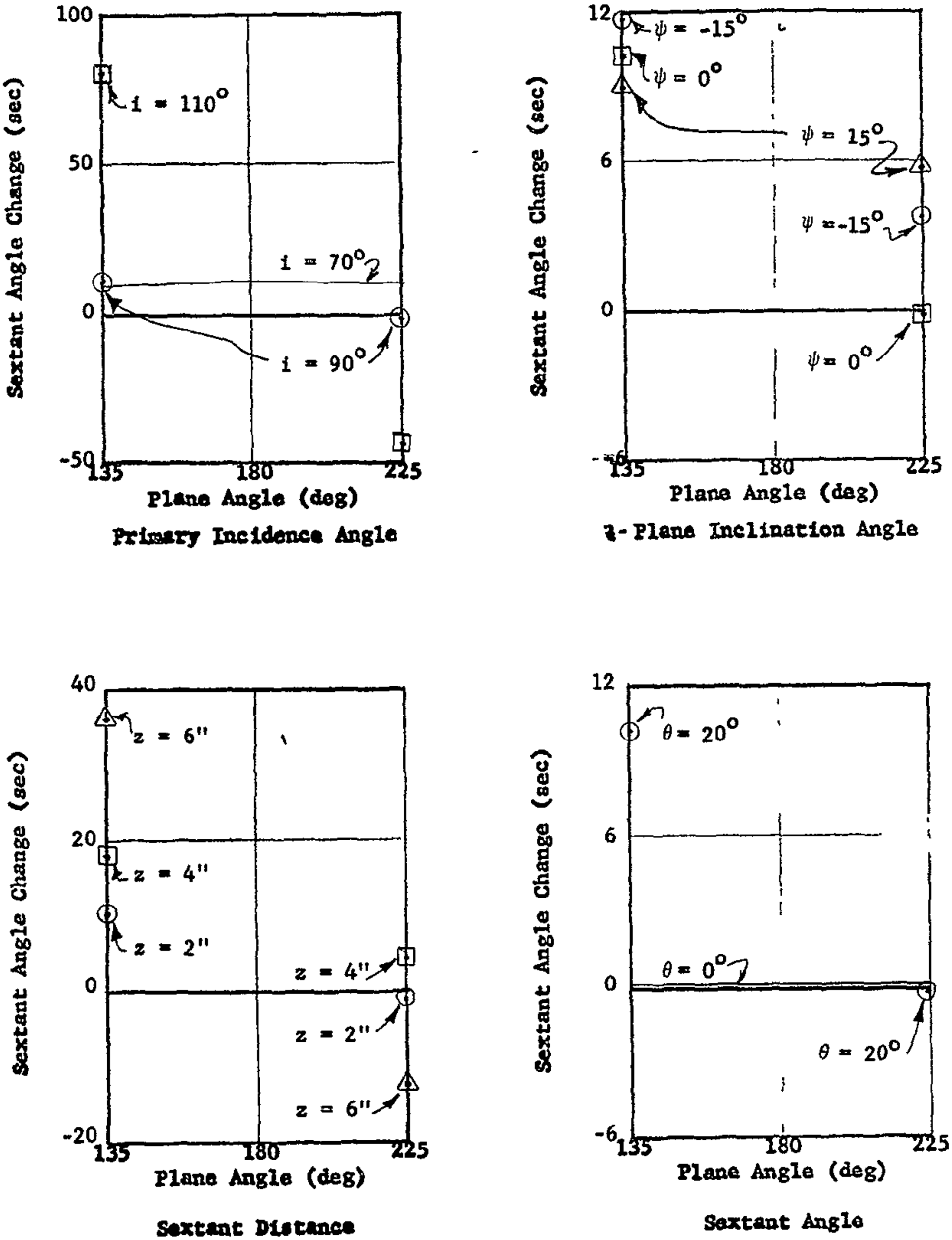

Figure 74 Sextant Angle Changes – Point 3

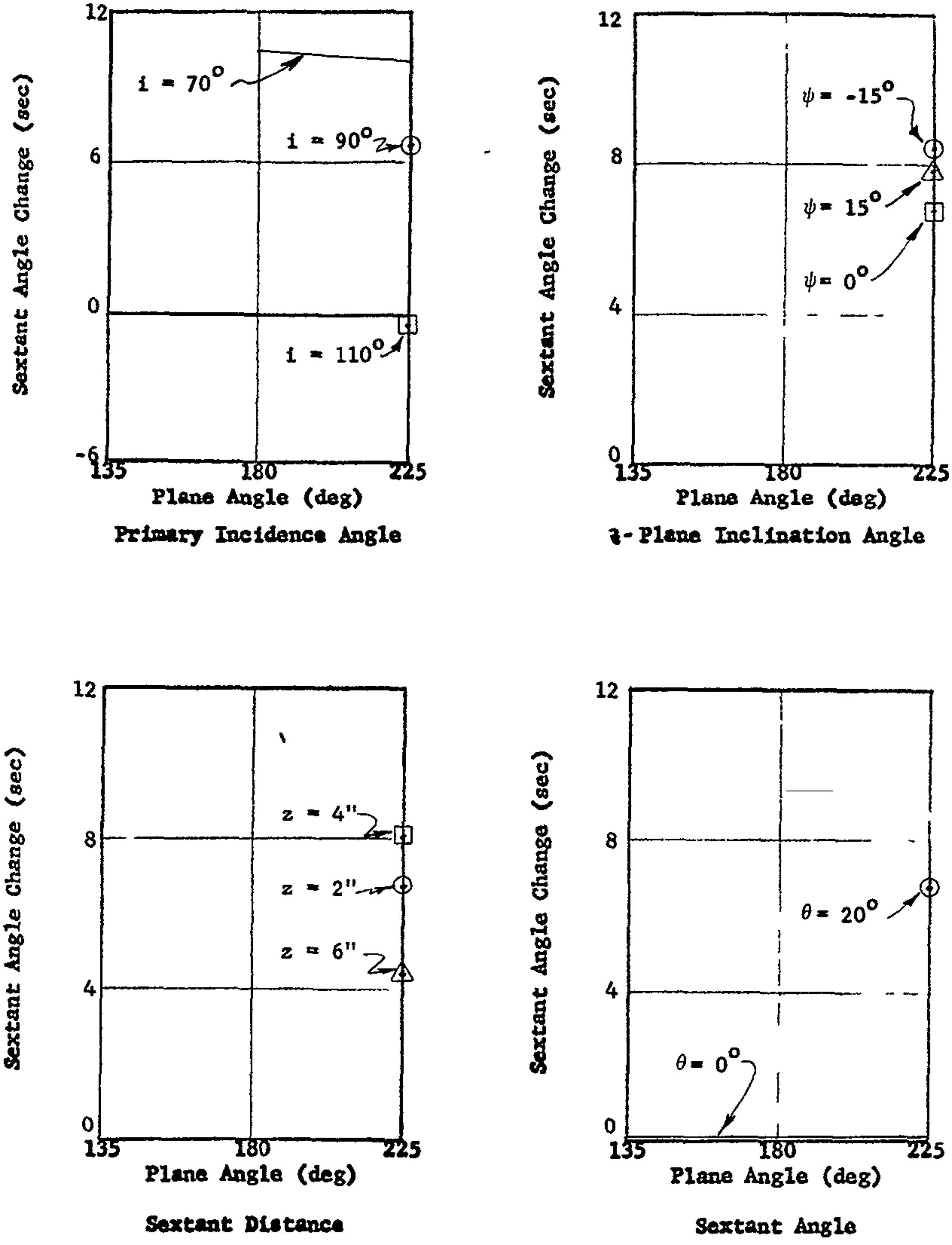

Figure 75 Sextant Angle Changes - Point 4

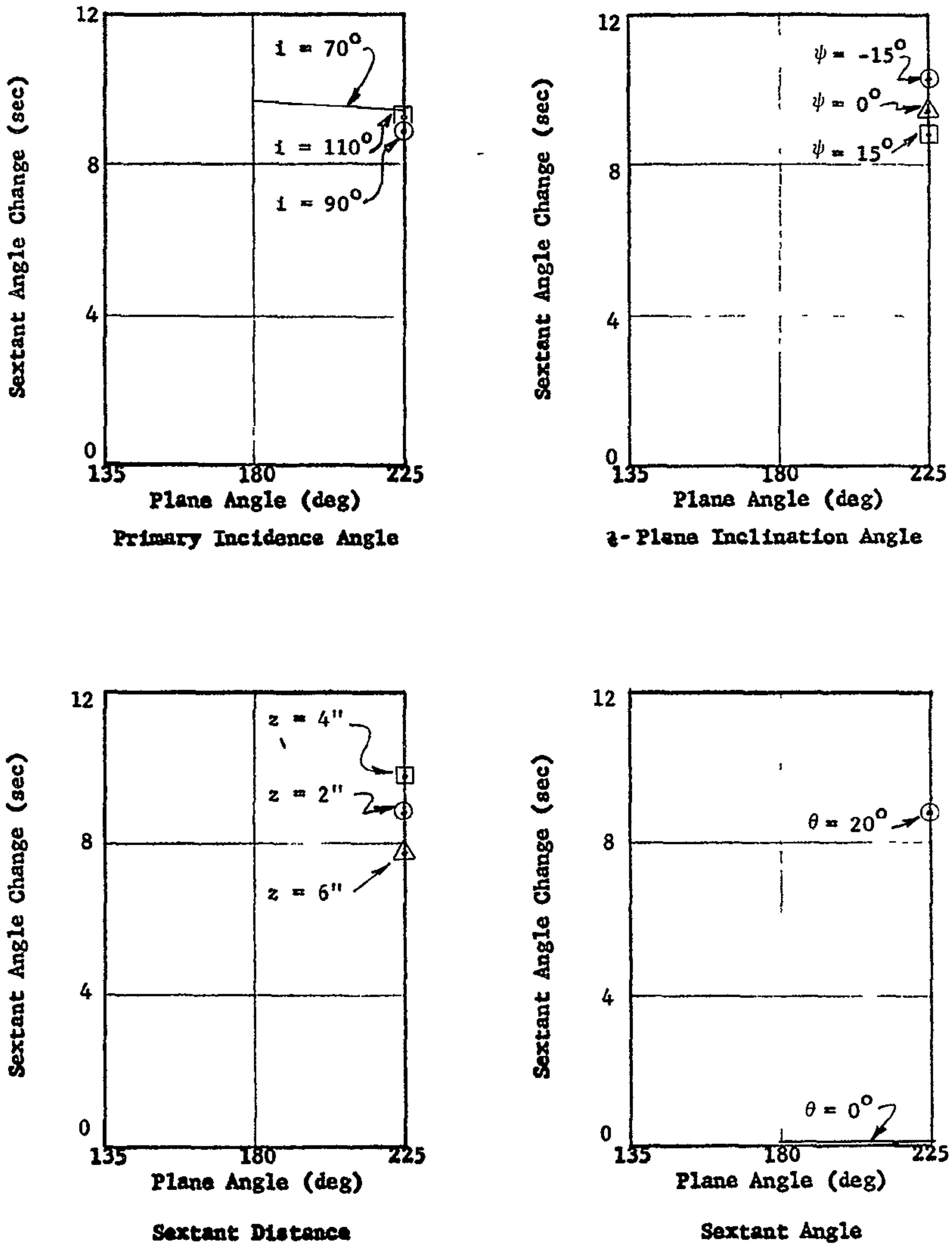

Figure 76 Sextant Angle Changes - Point 5

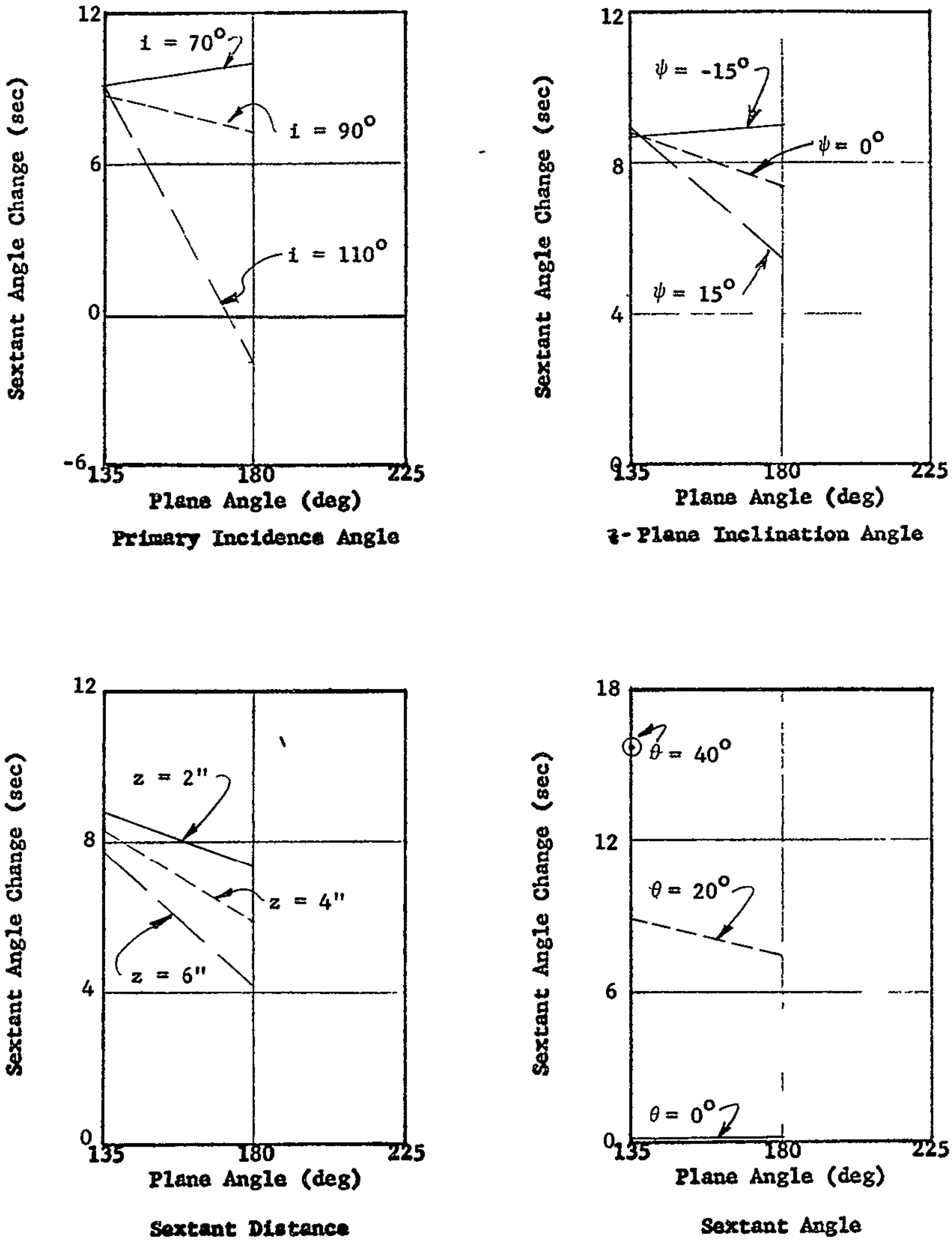

Figure 77 Sextant Angle Changes - Point 6

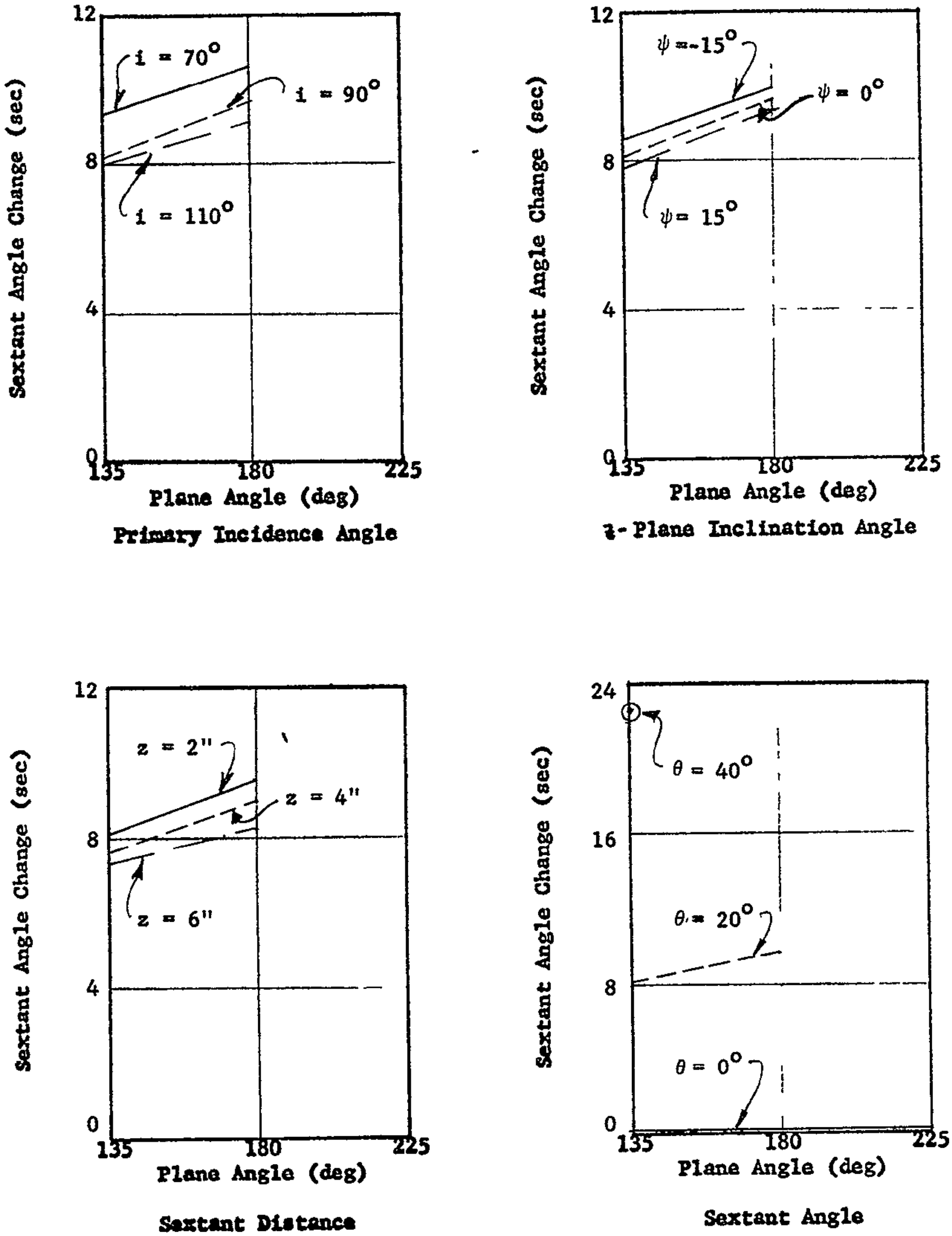

Figure 78 Sextant Angle Changes - Point 7

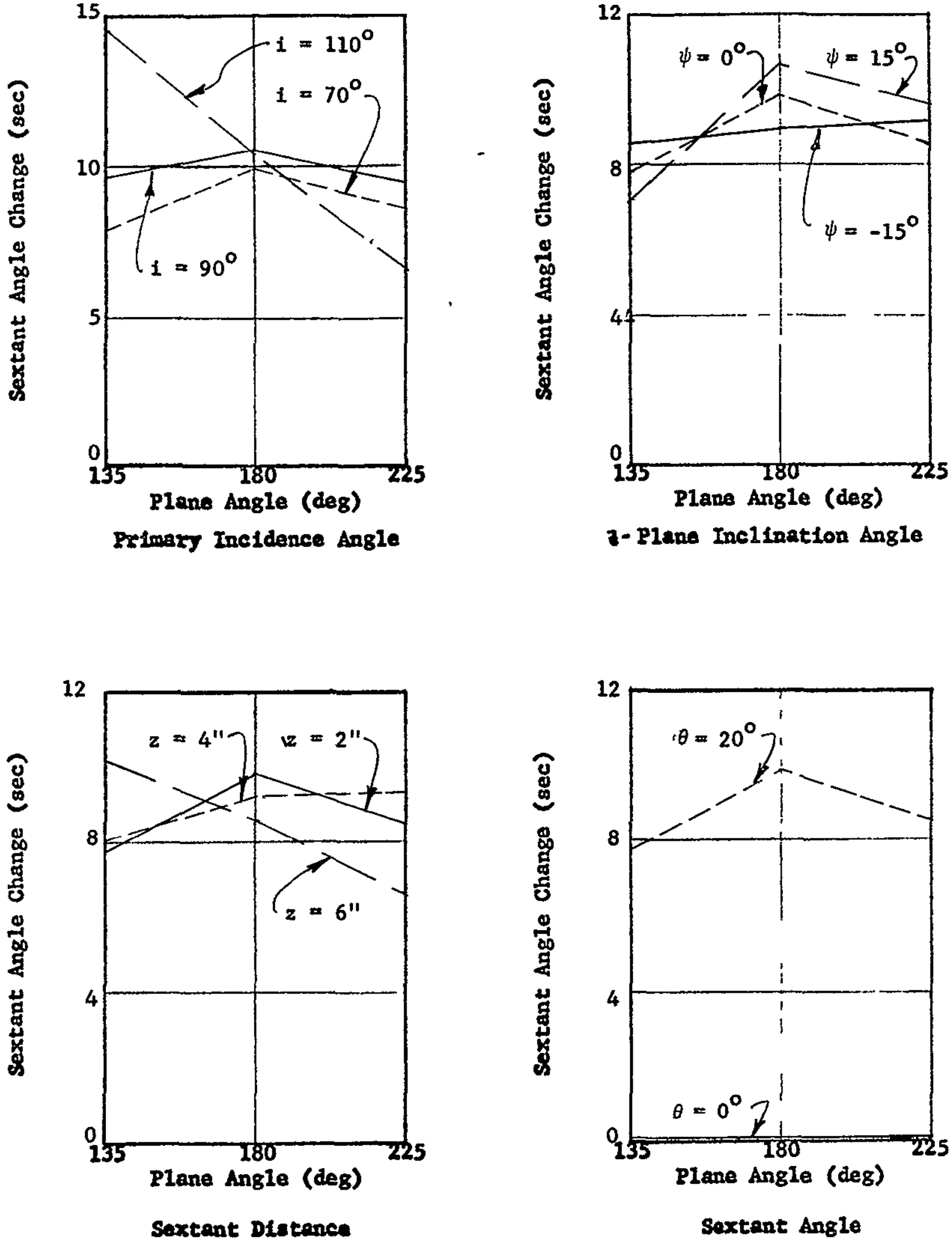

Figure 79 Sextant Angle Changes - Point 8

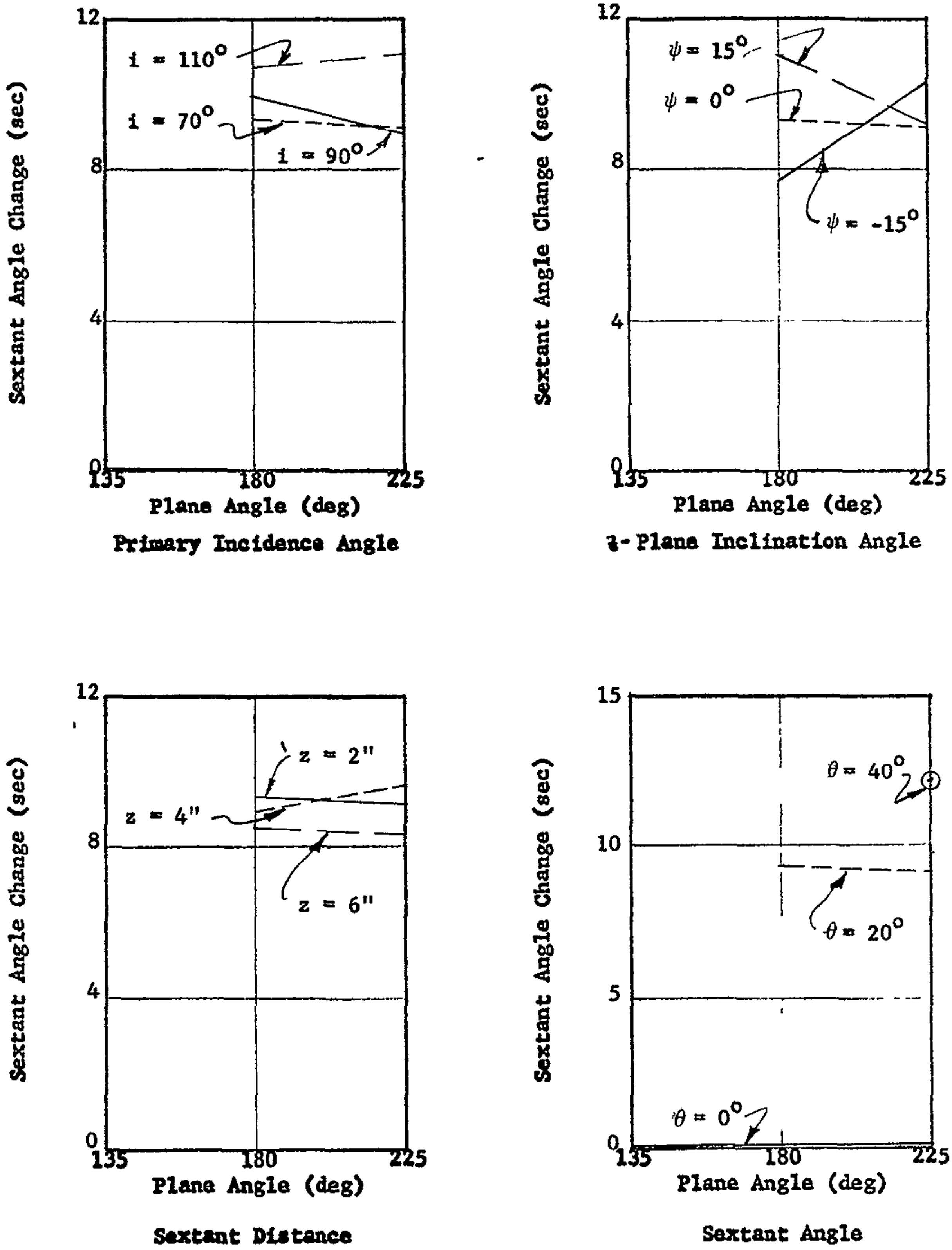

Figure 80 Sextant Angle Changes - Point 9

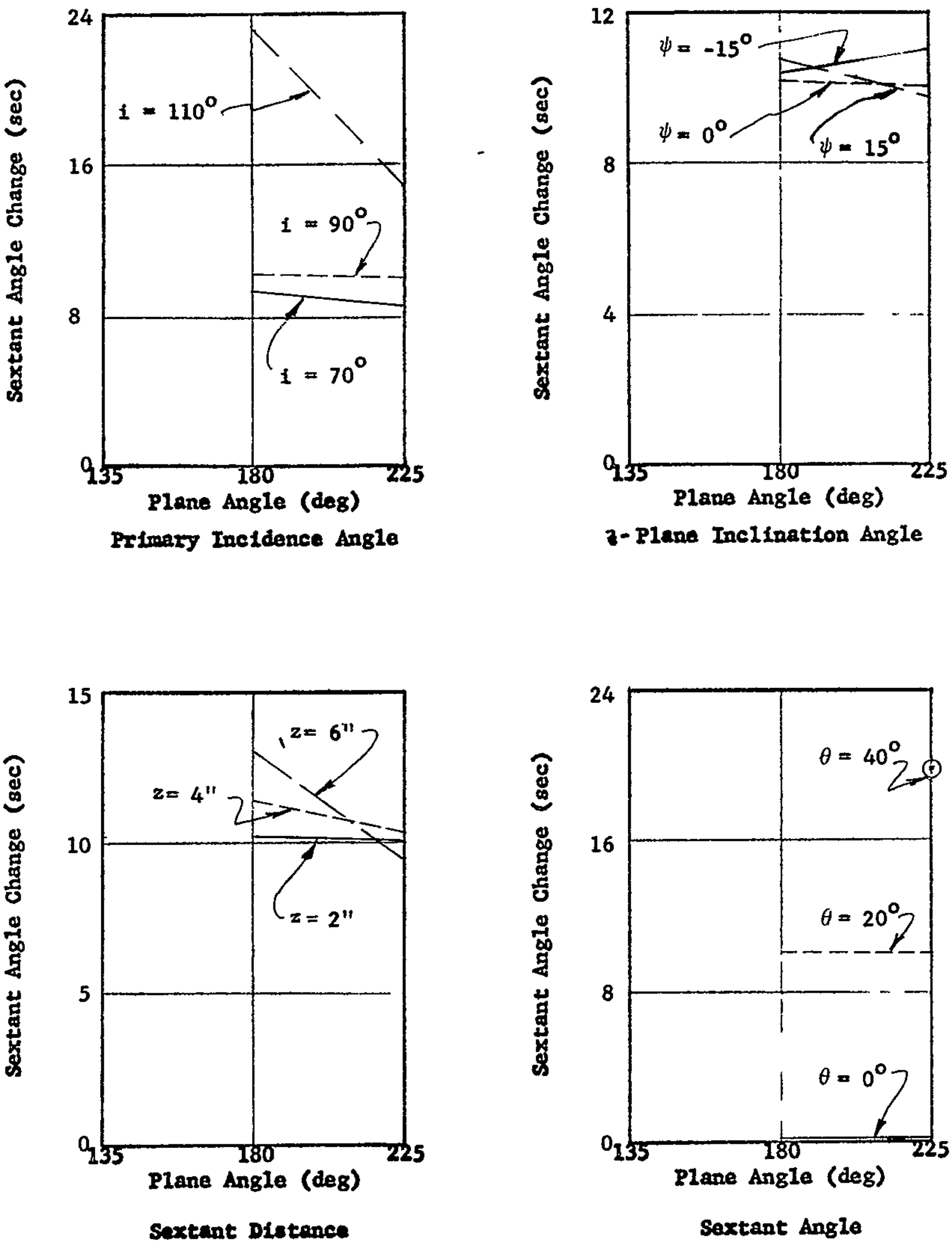

Figure 81 Sextant Angle Changes - Point 10

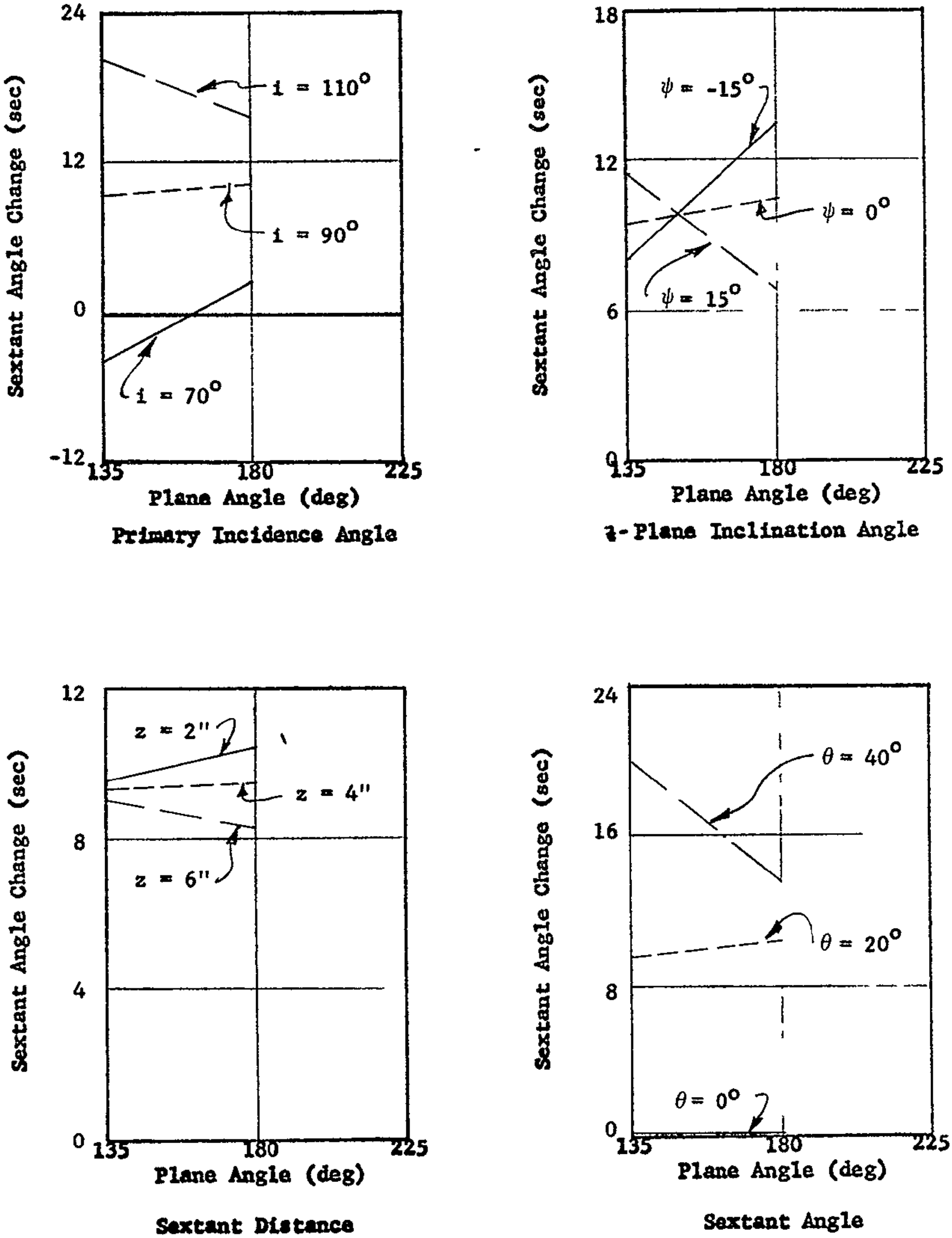

Figure 82 Sextant Angle Changes - Point 11

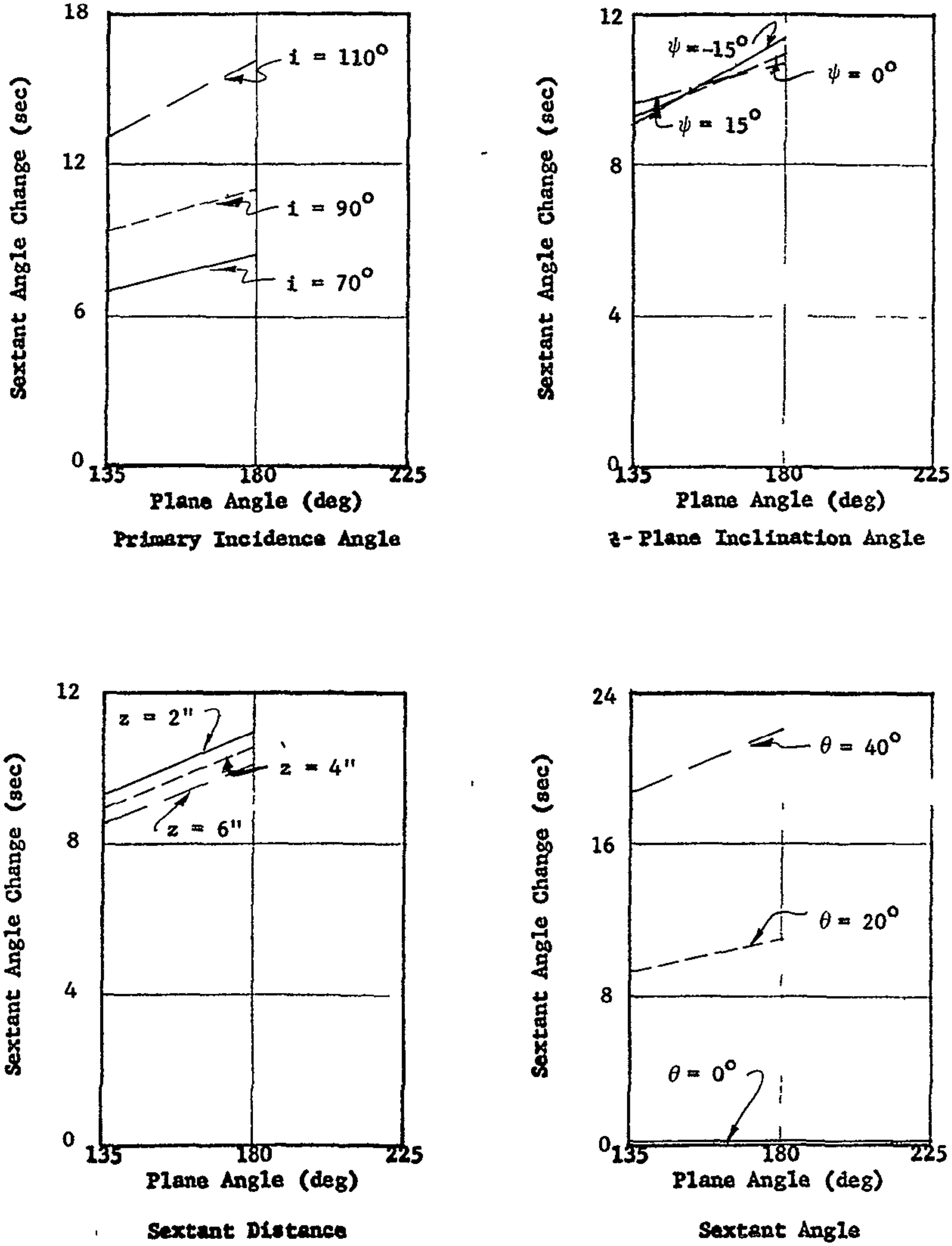

Figure 83 Sextant Angle Changes - Point 12

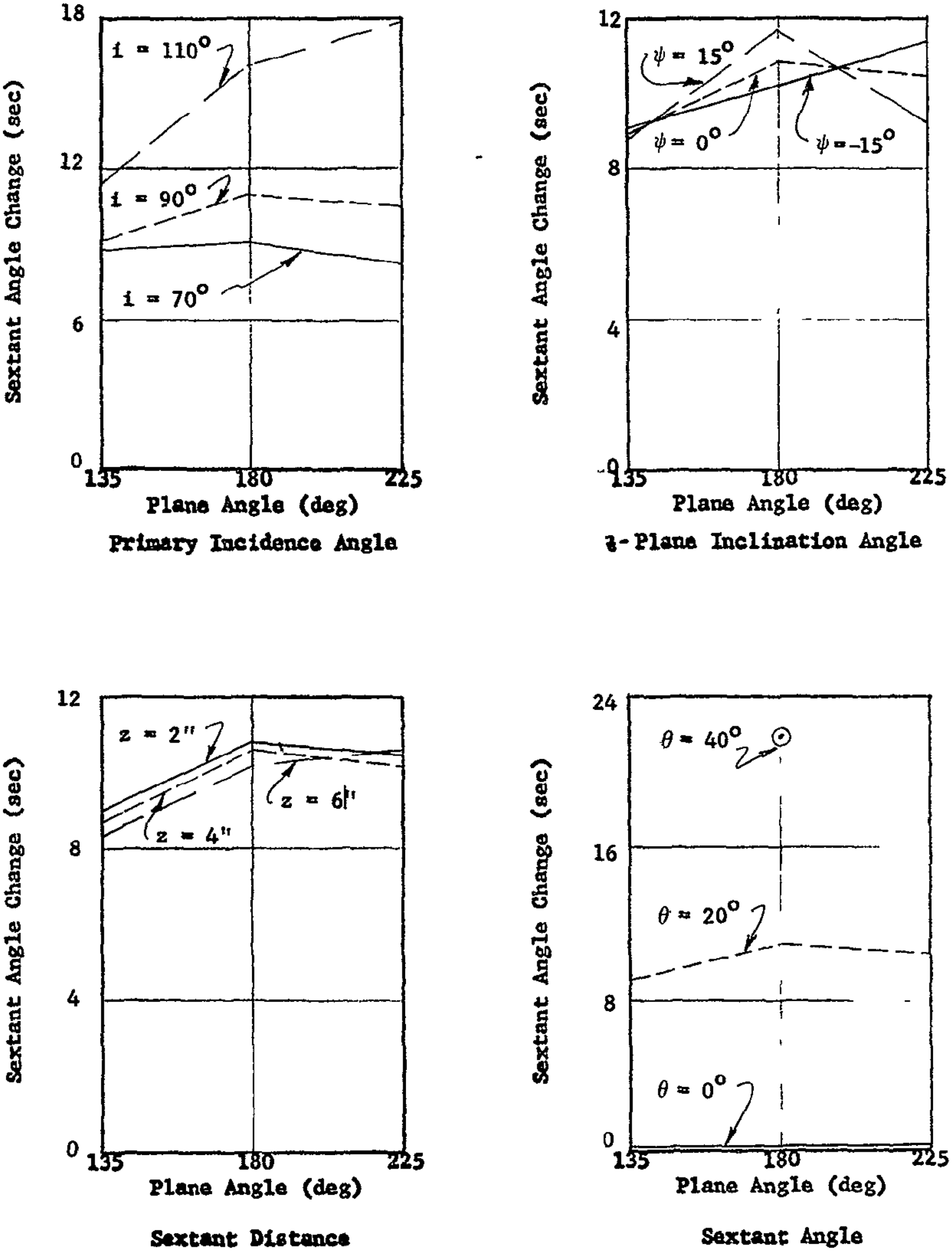

Figure 84 Sextant Angle Changes - Point 13

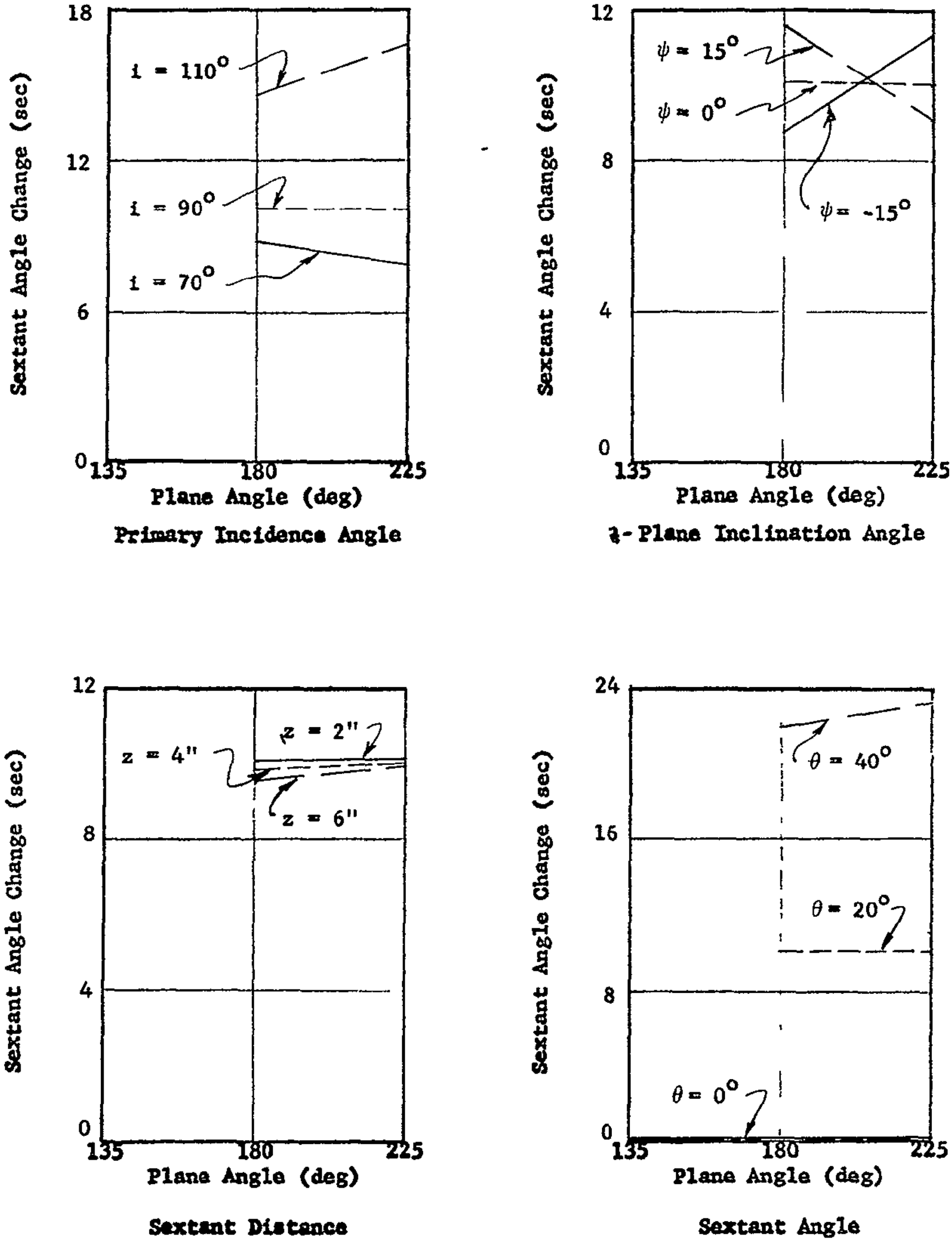

Figure 85. Sextant Angle Changes - Point 14

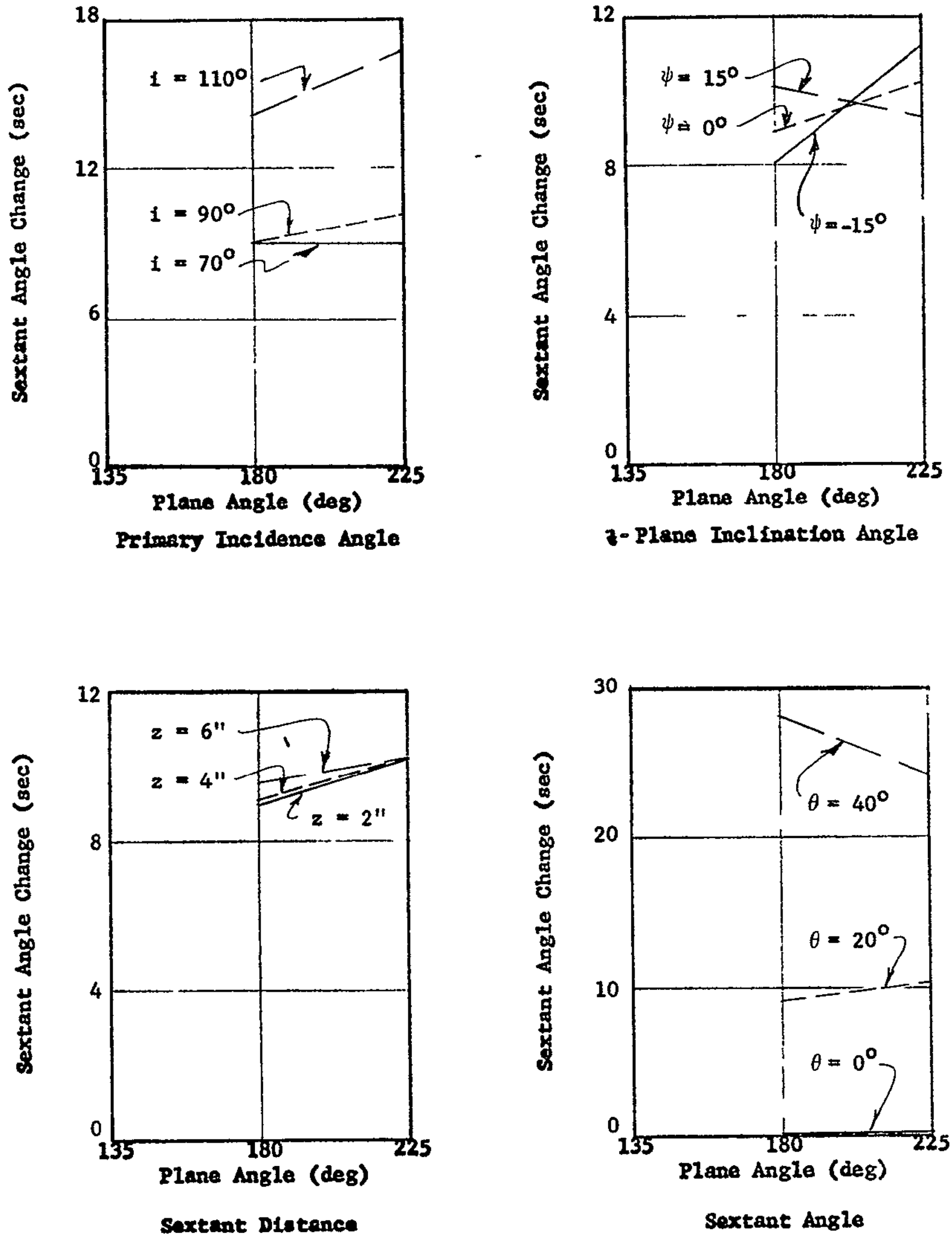

Figure 86 Sextant Angle Changes - Point 15

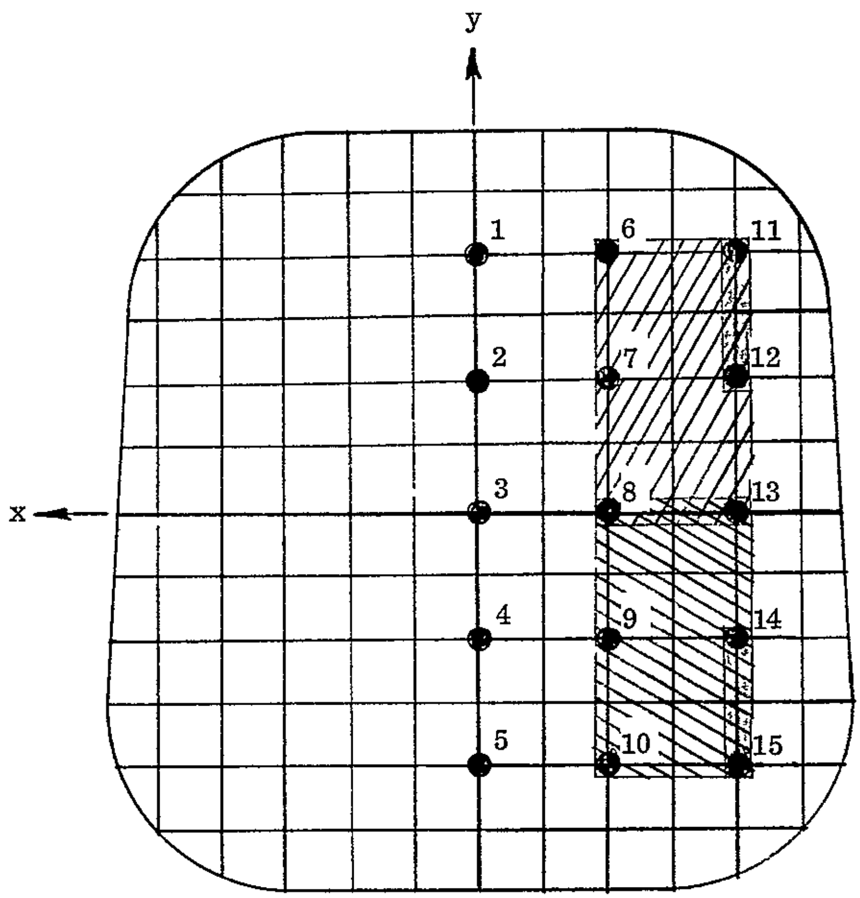

Figure 87 Best Observation Area - Two Ray Trace

40° under the same plane angle restriction. The 30° cross-hatched area indicates that area from which sightings can be made with the exception of a plane angle of 135° and a sextant angle of 40°. The shaded portion of this area indicates areas from which sightings can be made with a sextant angle of 40° under the same plane angle restriction.

Figure 88 shows the plots of the sextant angle change as a function of the x-coordinate for various values of the y-coordinate. The analysis was performed for a plane angle of 180°, a z-plane inclination angle of 0°, a primary incidence angle of 90°, a sextant distance of 2", and a sextant angle of 20°. For an x-coordinate of 0", all exiting rays were outside the window planform. With the exception of the y = 4" coordinate curve, the value of the sextant angle change was smaller for the x-coordinate of -2" than for the x-coordinate of -4".

Figure 89 shows the plots of the mean and root mean square sextant angle changes for three sextant angles as a function of plane angle for the 15 points shown in Fig. 71. The analysis was performed for a primary incidence angle of 90°, a z-plane inclination angle of 0°, and a sextant distance of 2". Table 13 gives the number of values used to compute the mean and rms for each value of the sextant angle and plane angle. This number varies because some of the rays exited outside the window planform. Both the mean and rms sextant changes increase with an increase in the sextant angle.

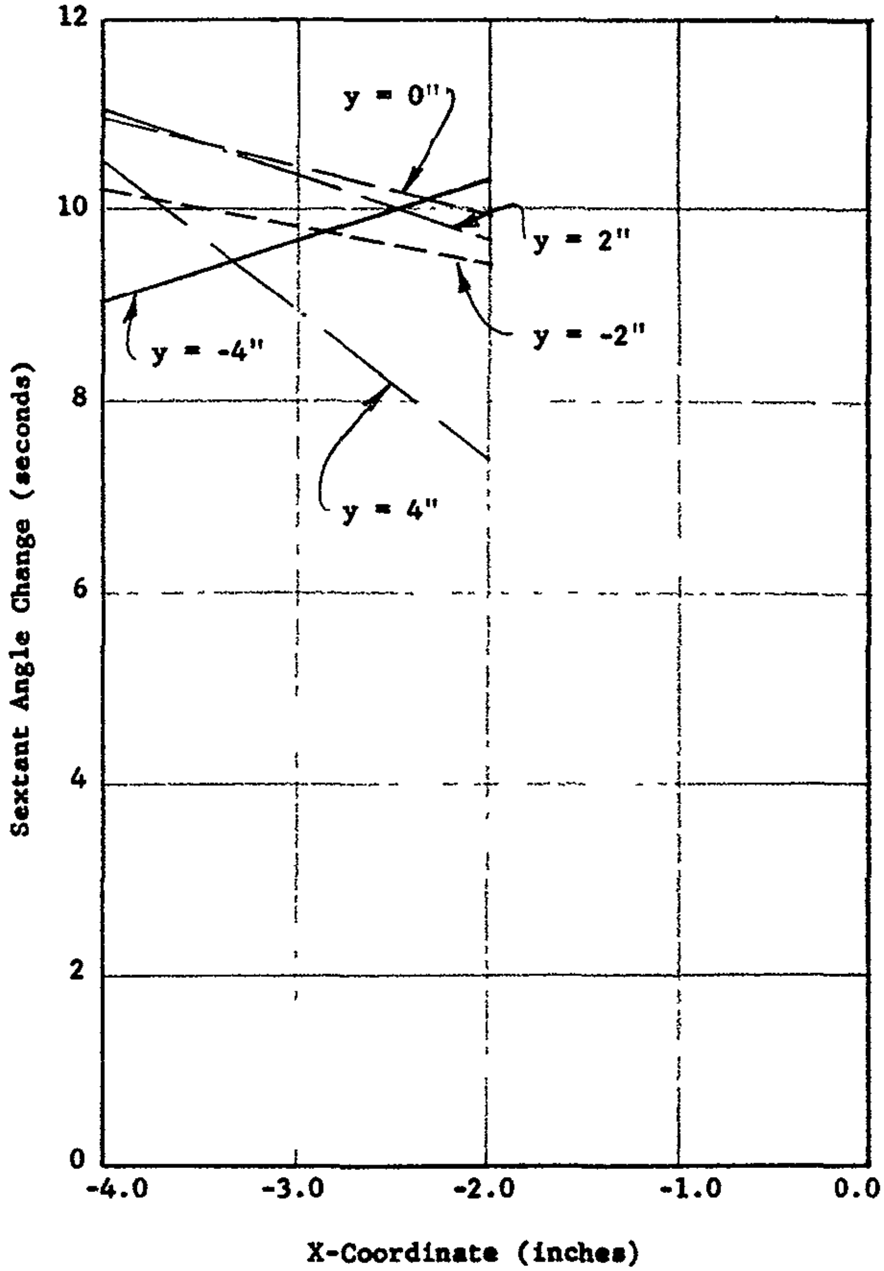

Figure 88 Sextant Angle Change vs X-Coordinate

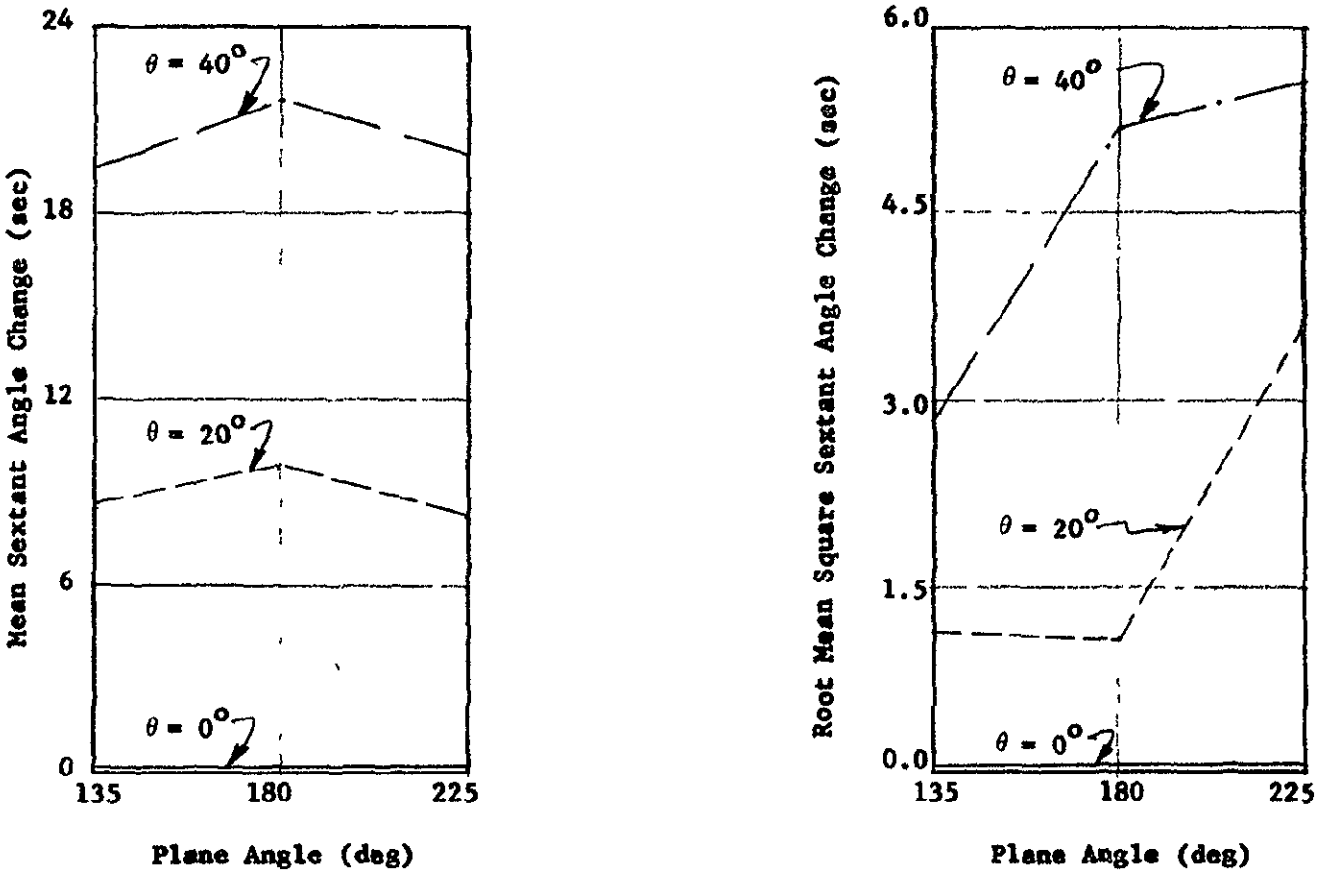

Figure 89. Mean and RMS of Sextant Angle Changes

Table 13

Number of Values in Mean and RMS Calculations

Sextant Angle	Plane Angle 135°	180°	225°
0	12	15	12
20°	9	10	9
40°	4	5	4

Section 6

REVIEW OF RESULTS

The magnitude of light-ray deviations for the Apollo window under various flight loading conditions has been reported. Validation studies indicate predictions involve less than one second of error. Deformations are given for the window supported in the Apollo structural environment and isolated. Two independent sets of idealized edge conditions are represented for the isolated system. Deviations of light rays entering at points on a one-inch grid and with six different incident angles are given for nine different flight-pressure conditions.

The window deformation data were developed by numerical analyses of the structure. The results were validated to insure adequate mesh refinement and sufficient structure were included to obtain the ray deviations to the required accuracy. The rotations of the isolated window were predicted with an accuracy of less than 0.3 seconds of arc. Those of the window in its structural environment have an error of less than 0.5 seconds of arc.

Predictions of the deformations of the Apollo window in its structural environment were made in two phases. The first phase involved a study of the Apollo structure to determine the amount of the structure which should be included in a refined model and a prediction of the deformations on the boundary of this refined model. In the second phase, the deformations from the first phase were imposed on a refined model of the window region to arrive at the final sets of window deformations.

In the first phase study, it was determined that the window frame itself could be chosen as the boundary of the surrounding structure which should be included in the refined model. The deformations at the window frame were decomposed into rigid body and elastic deformations. These deformations, when extrapolated using curves developed within the report, had associated errors of 1.3 seconds of arc for each type of deformation. The effects of the rigid rotation on the ray trace analyses were studied and determined to be negligible. It was also determined that the error in the elastic deformations decayed in the interior of the window due to the flexibilities of the gasket material and the window panes themselves. This decay results in a decrease in the error in deformation prediction from 1.3 seconds at the window frame to 0.5 seconds over the interior of the window   the desirable region for scientific observations.

Single ray trace analyses were performed on the isolated window and on the window in its structural environment. Results indicate that the isolated window with simply supported edges and the window with actual edge conditions have similar mean and rms deviations of light rays. In all cases, the mean and rms deviations increase with an increase in the incidence angle or an increase in the cabin pressure loading, but remain unchanged for an increase in the interstitial pressure.

The area of the window in its structural environment through which observations can be made without interference from the supporting structure was determined. This area comprises approximately 30% of the window area and is centered on the window.

Two ray trace analyses were performed on the window in its actual structural environment. These analyses evaluate deviations for observations with a hand-held sextant. The window area through which observations can be made without interference from the surrounding structure was determined. This area is skewed toward one edge of the window. Approximately 12% of the window is available for making observations for at least one line-of-sight direction. Only 1.5% of the window is available for making observations in all the line-of-sight directions studied in this analysis. However, the allowable viewing area increases as the sextant angle decreases.

This report cited deviations of light rays passing through the Apollo Scientific Window for various edge conditions. These deviations are predicted with less than one second of arc error. The data contained herein are useful in correcting observations made through the window or for determining which observations can be made with suitable accuracy.

References

1. White, K. C. and Gadeberg, B. L., "Methods for Predicting Spacecraft Window-Induced Line of Sight Deviations," NASA Ames Research Center, NASA TN D-5238, Moffett Field, California, July 1969.

2. Warner, D. N., Jr. and Walsh, T. M., "Effects of Edge Constraints on Optical Qualities of a Spacecraft Window," NASA Ames Research Center, NASA TN D-4845, Moffett Field, California, October 1968.

3. Melosh, R. J., Diether, P. A. and Brennen, M., "Structural Analysis and Matrix Interpretive System (SAMIS) Program Report," Jet Propulsion Laboratory, TM No. 33-307, Pasadena, California, December 1966.

4. Lang, T. E., "Structural Analysis and Matrix Interpretive System (SAMIS) User Report," Jet Propulsion Laboratory, TM No. 33-305, Pasadena, California, March 1967.

5. Melosh, R. J. and Christiansen, H. N., "Structural Analysis and Matrix Interpretive System (SAMIS) Program. Technical Report," Jet Prouplsion Laboratory, TM No. 33-311, Pasadena, California, November 1966.

6. Gadeberg, B. L. and White, K. C., "Theory of the Correction of Celestial Observation Made for Space Navigation or Testing," NASA Ames Research Center, NASA TN D-5239, Moffett Field, California, December 1969.

7. Kelley, D. M. and Diether, P. A., "Computer Program to Predict Spacecraft Window Deformations and Compute Window Induced Angular Deviations of Light Rays," NASA CR73477, Philco-Ford Corporation, Palo Alto, California, September 1970.

8. Timoshenko, S. and Woinowsky-Krieger, S., Theory of Plates and Shells, McGraw-Hill, New York, 1959, 114-116, 197-202.

9. Melosh, R. J., "A Flat Triangular Shell Element Stiffness Matrix," Air Force Flight Dynamics Laboratory, Wright-Patterson AFB, AFFDL-TR-66-80, 1966, 503-509.

10. Utku, S. and Melosh, R. J., "Behavior of Triangular Shell Element Stiffness Matrices Associated with Polyhedral Deflection Distributions," Paper No. 67-114, AIAA 5th Aerospace Sciences Meeting, New York, January 23-26, 1967.

11. Corning Glass Works, "Properties of Selected Commercial Glasses," Corning Glass Works, Corning, New York, 1963, 8-9.

12. Sokolnikoff, I. S., Mathematical Theory of Elasticity, McGraw-Hill, New York, 1956, 89-90.

Appendix A

RECTANGULAR PLATE ANALYSES

This appendix contains equations and numbers for the exact and finite element analyses of a rectangular (square plate). These data include the formulation of the exact equations, the finite element model articulation, and a tabulation of the results of the exact analyses and the various finite element analyses.

SIMPLY SUPPORTED PLATE[1,2]

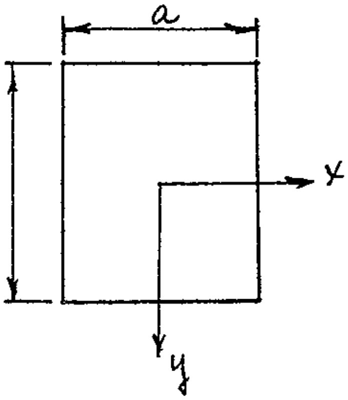

$$\alpha_m = \frac{m\pi b}{2a}$$

$$\beta_m = \frac{m\pi a}{2b}$$

$$w^{s(3)} = \frac{4qa^4}{\pi^5 D} \sum \frac{(-1)^{\frac{m-1}{2}}}{m^5}\left(1 - \left(\frac{2+\alpha_m \tanh\alpha_m}{2\cosh\alpha_m}\right)\cosh\frac{m\pi y}{a} + \frac{m\pi y}{a}\,\frac{\sinh\frac{m\pi y}{a}}{2\cosh\alpha_m}\right)\cos\frac{m\pi x}{a}$$

$$w^s_{,x} = -\frac{4qa^3}{\pi^4 D} \sum \frac{(-1)^{\frac{m-1}{2}}}{m^4}\left(1 - \left(\frac{2+\alpha_m \tanh\alpha_m}{2\cosh\alpha_m}\right)\cosh\frac{m\pi y}{a} + \frac{m\pi y}{a}\,\frac{\sinh\frac{m\pi y}{a}}{2\cosh\alpha_m}\right)\sin\frac{m\pi x}{a}$$

$$w^s_{,y} = \frac{4qa^3}{\pi^4 D} \sum \frac{(-1)^{\frac{m-1}{2}}}{m^4}\left(-\left(\frac{2+\alpha_m \tanh\alpha_m}{2\cosh\alpha_m}\right)\sinh\frac{m\pi y}{a} + \frac{m\pi y}{a}\,\frac{\cosh\frac{m\pi y}{a}}{2\cosh\alpha_m} + \frac{\sinh\frac{m\pi y}{a}}{2\cosh\alpha_m}\right)\cos\frac{m\pi x}{a}$$

$\delta^s_{center} = .0443\,\frac{qa^4}{Et^3} = .00352$ in FOR $q = 1$ psi
$a = 12$ in
$E = 10\ 10^6$ psi, $\nu = .24$
$t = .3$ in

---

1) TIMOSHENKO, S AND WOINOWSKY-KRIEGER, S., THEORY OF PLATES AND SHELLS, McGRAW-HILL, NEW YORK, 1959, pp 114-116, 197-202.

(2) EVANS, T E, "TABLES OF MOMENTS AND DEFLECTIONS FOR A RECTANGULAR PLATE FIXED ON ALL EDGES AND CARRYING A UNIFORMLY DISTRIBUTED LOAD," JOURNAL OF APPLIED MECHANICS, vol 6, 1939, pp 7-10.

3) FOR DEFINITION OF TERMS SEE BELOW.

PLATE WITH CLAMPED EDGES[1,2]

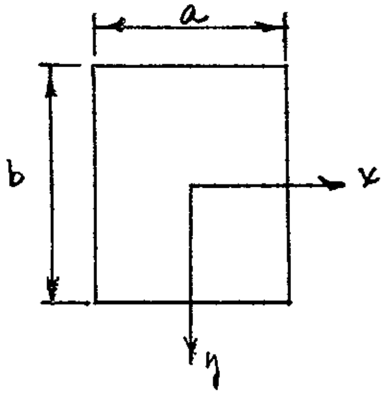

$$\alpha_m = \frac{m\pi b}{2a}$$

$$\beta_m = \frac{m\pi a}{2b}$$

$$w^1 = -\frac{a^2}{2\pi^2 D} \sum \frac{(-1)^{\frac{m-1}{2}}}{m^2} E_m \left(\frac{m\pi y}{a} \frac{\sinh \frac{m\pi y}{a}}{\cosh \alpha_m} - \frac{\alpha_m \tanh \alpha_m}{\cosh \alpha_m} \cosh \frac{m\pi y}{a} \right) \cos \frac{m\pi x}{a}$$

$$w^1_{,x} = \frac{a}{2\pi D} \sum \frac{(-1)^{\frac{m-1}{2}}}{m} E_m \left(\frac{m\pi y}{a} \frac{\sinh \frac{m\pi y}{a}}{\cosh \alpha_m} - \frac{\alpha_m \tanh \alpha_m}{\cosh \alpha_m} \cosh \frac{m\pi y}{a} \right) \sin \frac{m\pi x}{a}$$

$$w^1_{,y} = -\frac{a}{2\pi D} \sum \frac{(-1)^{\frac{m-1}{2}}}{m} E_m \left(\frac{m\pi y}{a} \frac{\cosh \frac{m\pi y}{a}}{\cosh \alpha_m} + \frac{\sinh \frac{m\pi y}{a}}{\cosh \alpha_m} - \frac{\alpha_m \tanh \alpha_m}{\cosh \alpha_m} \sinh \frac{m\pi y}{a} \right) \cos \frac{m\pi x}{a}$$

$$w^2 = -\frac{b^2}{2\pi^2 D} \sum \frac{(-1)^{\frac{m-1}{2}}}{m^2} F_m \left(\frac{m\pi x}{b} \frac{\sinh \frac{m\pi x}{b}}{\cosh \beta_m} - \frac{\beta_m \tanh \beta_m}{\cosh \beta_m} \cosh \frac{m\pi x}{b} \right) \cos \frac{m\pi y}{b}$$

$$w^2_{,x} = -\frac{b}{2\pi D} \sum \frac{(-1)^{\frac{m-1}{2}}}{m} F_m \left(\frac{m\pi x}{b} \frac{\cosh \frac{m\pi x}{b}}{\cosh \beta_m} + \frac{\sinh \frac{m\pi x}{b}}{\cosh \beta_m} - \frac{\beta_m \tanh \beta_m}{\cosh \beta_m} \sinh \frac{m\pi x}{b} \right) \cos \frac{m\pi y}{b}$$

$$w^2_{,y} = \frac{b}{2\pi D} \sum \frac{(-1)^{\frac{m-1}{2}}}{m} F_m \left(\frac{m\pi x}{b} \frac{\sinh \frac{m\pi x}{b}}{\cosh \beta_m} - \frac{\beta_m \tanh \beta_m}{\cosh \beta_m} \cosh \frac{m\pi x}{b} \right) \sin \frac{m\pi y}{b}$$

WHERE E_m AND F_m ARE DEFINED BY.

$$\frac{E_n}{n} \left(\tanh \alpha_n + \frac{\alpha_n}{\cosh^2 \alpha_n} \right) + \frac{8na}{\pi b} \sum \frac{F_m}{m^3 \left(\frac{n^2}{m^2} + \frac{a^2}{b^2} \right)^2} = \frac{4qa^2}{\pi^3 n^4} \left(\frac{\alpha_n}{\cosh^2 \alpha_n} - \tanh \alpha_n \right)$$

$$\frac{F_n}{n} \left(\tanh \beta_n + \frac{\beta_n}{\cosh^2 \beta_n} \right) + \frac{8nb}{\pi a} \sum \frac{E_m}{m^3 \left(\frac{n^2}{m^2} + \frac{b^2}{a^2} \right)^2} = \frac{4qb^2}{\pi^3 n^4} \left(\frac{\beta_n}{\cosh^2 \beta_n} - \tanh \beta_n \right)$$

$w^c = w^s + w^1 + w^2$ $\equiv$ DEFLECTION OF CLAMPED PLATE

$w_{,x}^c = w_{,x}^s + w_{,x}^1 + w_{,x}^2$ $\equiv$ SLOPE ABOUT y-AXIS OF CLAMPED PLATE

$w_{,y}^c = w_{,y}^s + w_{,y}^1 + w_{,y}^2$ $\equiv$ SLOPE ABOUT x-AXIS OF CLAMPED PLATE

$\delta_{center}^c = 0138 \dfrac{qa^4}{Et^3} = 00110$ in FOR $q = 1$ psi
$a = 12$ in
$E = 10 \cdot 10^6$ psi, $\nu = .24$
$t = .3$ in

DEFINITION OF TERMS

w^s $\equiv$ DEFLECTION OF SIMPLY SUPPORTED RECTANGULAR PLATE

$w_{,x}^s = \dfrac{\partial w^s}{\partial x}$ $\equiv$ SLOPE ABOUT y-AXIS OF SIMPLY SUPPORTED RECTANGULAR PLATE

$w_{,y}^s = \dfrac{\partial w^s}{\partial y}$ $\equiv$ SLOPE ABOUT x-AXIS OF SIMPLY SUPPORTED RECTANGULAR PLATE

δ_{center}^s $\equiv$ DEFLECTION AT CENTER OF SIMPLY SUPPORTED RECTANGULAR PLATE EVALUATED FOR PARTICULAR CASE

w^1 $\equiv$ DEFLECTIONS OF RECTANGULAR PLATE SIMPLY SUPPORTED ALONG EDGES OF LENGTH b WITH MOMENTS APPLIED ALONG EDGES OF LENGTH a

$w_{,x}^1 = \dfrac{\partial w^1}{\partial x}$ $\equiv$ SLOPE ABOUT y-AXIS OF RECTANGULAR PLATE UNDER SAME CONDITIONS

$w_{,y}^1 = \dfrac{\partial w^1}{\partial y}$ $\equiv$ SLOPE ABOUT x-AXIS OF RECTANGUAR PLATE UNDER SAME CONDITIONS

w^2 $\equiv$ DEFLECTION OF RECTANGULAR PLATE SIMPLY SUPPORTED ALONG EDGES OF LENGTH a WITH MOMENTS APPLIED ALONG EDGES OF LENGTH b.

$w_{,x}^2 = \dfrac{\partial w^2}{\partial x}$ $\equiv$ SLOPE ABOUT y-AXIS OF RECTANGULAR PLATE UNDER SAME CONDITIONS

$w_{,y}^2 = \dfrac{\partial w^2}{\partial y}$ $\equiv$ SLOPE ABOUT x-AXIS OF RECTANGULAR PLATE UNDER SAME CONDITIONS

δ_{center}^c $\equiv$ DEFLECTION AT CENTER OF CLAMPED RECTANGULAR PLATE EVALUATED FOR PARTICULAR CASE

GRID SYSTEM FOR 12" x 12" PLATE

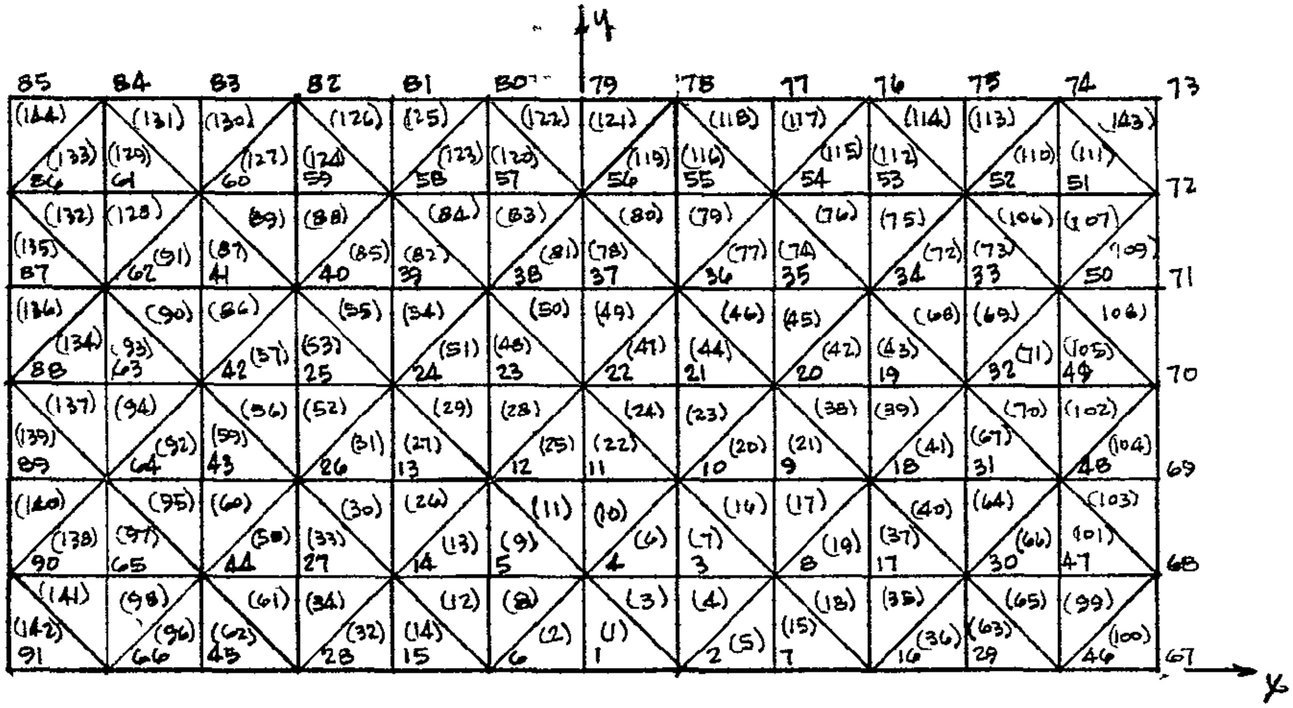

PHYSICAL PROPERTIES

$\nu = .24$[1] $\quad E = 10.0 \cdot 10^6$ psi[1] $\quad t = .030$ in[1]

$$D_{11} = D_{22} = D_{44} = \frac{E(1-\nu)}{(1+\nu)(1-2\nu)} = \frac{(10)(.76)}{(1.24)(.52)} \cdot 10^6 = 1.17866 \cdot 10^7 \text{ psi}$$ [2]

$$D_{21} = D_{41} = D_{42} = \frac{\nu}{1-\nu} D_{11} = \frac{.24}{.76}(1.17866 \cdot 10^7) = 3.72208 \cdot 10^6 \text{ psi}$$ [2]

$$D_{33} = D_{55} = D_{66} = \frac{E}{2(1+\nu)} = \frac{10 \cdot 10^6}{(2)(1.24)} = 4.03226 \cdot 10^6 \text{ psi}$$ [2]

$$D = \frac{Et^3}{12(1-\nu^2)} = \frac{(10)(.3)^3}{12(1-(.24)^2)} \cdot 10^6 = 2.3875 \cdot 10^4 \text{ lb-in}$$ [3]

RESULTS

TABULATED ON FOLLOWING PAGES

(1) *ASSUMED VALUES*

(2) *EQUATIONS TAKEN FROM SAMIS USER'S REPORT (REFERENCE 4)*

(3) *EQUATION TAKEN FROM TIMOSHENKO - WOINOWSKY - KRIEGER*

DEFLECTIONS*- SIMPLE SUPPORT CASE					
x	y	EXACT	1" MESH	1/2" MESH	1/2"-3/1
0	0	.352825-2	.350833-2	353929-2	.349547-2
1	0	.341743-2	.339833-2	.342798-2	.338560-2
2	0	.308831-2	.307000-2	309745-2	305934-2
3	0	.255188-2	253500-2	255886-2	.252766-2
4	0	182971-2	181500-2	.183408-2	.181202-2
5	0	959056-3	949833-3	.960877-3	949509 3
0	1	.341743-2	339833-2	.342806-2	338564-2
1	1	.331023-2	329167-2	.332039-2	.327935-2
2	1	.299182-2	297333-2	300060-2	.296369-2
3	1	.247264-2	245500-2	247934-2	.244912-2
4	1	177336-2	176000-2	177754-2	175616-2
5	1	929760-3	920333-3	931489-3	920463-3
0	2	.308831-2	307000-2	.309766-2	305942-2
1	2	.299182-2	297333-2	300073-2	.296374-2
2	2	270504-2	268667-2	271273-2	267945-2
3	2	.223701-2	222167-2	224283-2	.221555-2
4	2	.160564-2	159167-2	.160923-2	158990-2
5	2	.842509-3	833833-3	.843951-3	833967-3
0	3	255188-2	253500-2	.255912-2	252775-2
1	3	.247264-2	245500-2	247954-2	.244919-2
2	3	.223701-2	222167-2	.224291-2	221558-2
3	3	.185185-2	183667-2	.185627-2	.183381-2
4	3	133101-2	131867-2	133367-2	.132137-2
5	3	.699432-3	691167-3	700420-3	.692146-3
0	4	.182971-2	181500-2	.183432-2	181209-2
1	4	.177336-2	.176000-2	.177772-2	175621-2
2	4	160564-2	159150-2	.160933-2	.158993-2
3	4	.133101-2	.131867-2	133370-2	131771-2
4	4	.958535-3	947833-3	.960071 3	948622-3
5	4	.504846-3	.498167-3	505311-3	.499335-3
0	5	959056-3	.949833-3	.961013-3	.949545-3
1	5	929760-3	920333-3	931596-3	.920492-3
2	5	842509-3	833833-3	.844009-3	833982-3
3	5	699432-3	.691000-3	700443-3	692154-3
4	5	504846-3	.498167-3	505314-3	.499337-3
5	5	.266721-3	261833-3	266736-3	263572-3

* DEFLECTIONS GIVEN IN INCHES

θ_y SLOPES* - SIMPLE SUPPORT CASE					
x	y	EXACT	1" MESH	1/2" MESH	1/2" - 3/1
0	0	0	0	0	0
1	0	0	0	0	0
2	0	0	0	0	0
3	0	0	0	0	0
4	0	0	0	0	0
5	0	0	0	0	0
0	1	- 221096-3	-,219333-3	-,222374-3	-219053-3
1	1	-,213881-3	-215333-3	-215118-3	-,211908-3
2	1	-192555-3	-,190833-3	-,193672-3	-,190783-3
3	1	-,158134-3	-,159050-3	-159040-3	-,156686-3
4	1	-,112487-3	-111183-3	-,113114-3	-,111467-3
5	1	-584895-4	-587500-4	-,588032-4	-,579629-4
0	2	-435358-3	-438167-3	-437986-3	-431330-3
1	2	-421257-3	-417833-3	-,423796-3	-,417353-3
2	2	-379528-3	-381833-3	-,381802-3	-,376007-3
3	2	-,312024-3	-,308833-3	-313864-3	-,309137-3
4	2	-,222228-3	-,223333-3	-,223502-3	-,220181-3
5	2	-115668-3	-114133-3	-,116312-3	-,114610-3
0	3	-634001-3	-628667-3	-,637834-3	-,628053 3
1	3	-613730-3	-617500-3	-617426-3	-,607967-3
2	3	-553632-3	-,548500-3	-556934-3	-,548520-3
3	3	-456053-3	-458500-3	-,458720-3	-,451751-3
4	3	-,325561-3	-321500-3	-,327402-3	-322488-3
5	3	-169789-3	-170500-3	-,170714-3	-168191-3
0	4	-804248-3	-,808333-3	-,808922-3	-,796519-3
1	4	-778995-3	-,771667-3	-783510-3	-771493-3
2	4	-703964-3	-,707500-3	-,708008-3	-,697142-3
3	4	-,581576-3	- 574833 3	-584862-3	-,575884-3
4	4	-,416714-3	-,418500-3	-,419004-3	-,412591-3
5	4	-218101-3	-214500-3	-,219242-3	-,215925-3
0	5	-927196-3	-,917333-3	-,932152-3	-,917848-3
1	5	-898662-3	-,901667-3	-903452-3	-889563-3
2	5	-,813730-3	-,804167-3	-,818072-3	-,805383-3
3	5	-,674614-3	-676833-3	-,678126-3	-667539-3
4	5	-485836-3	-478000-3	-,488326-3	-,480561-3
5	5	-,255793-3	-256667-3	-,257326-3	-252887-3

* SLOPES GIVEN IN RADIANS

θ_y SLOPES* - SIMPLE SUPPORT CASE					
x	y	EXACT	1" MESH	½" MESH	½" - 3/1
0	0	0	0	0	0
1	0	.221096-3	.219333-3	222306-3	219105-3
2	0	435358-3	.438167-3	438084-3	431353-3
3	0	634000-3	628667-3	637846-3	628049-3
4	0	.809196-3	.808333-3	.808856-3	.796495-3
5	0	927160-3	917333-3	.932026-3	.917810-3
0	1	0	0	0	0
1	1	.213881-3	215333-3	.215358-3	.211962-3
2	1	.421257-3	.417833-3	423904-3	417386-3
3	1	613729-3	617333-3	617458-3	.607971-3
4	1	778769-3	771667-3	783458-3	771473-3
5	1	898628-3	.901667-3	903354-3	.889534-3
0	2	0	0	0	0
1	2	192555-3	190833-3	193799-3	.190829-3
2	2	379528-3	381833-3	381920-3	376049-3
3	2	553631-3	548500-3	556988-3	.548437 3
4	2	.703737-3	.707500-3	.707988-3	.697135-3
5	2	813696-3	804167-3	817966-3	805367-3
0	3	0	0	0	0
1	3	158133-3	159050-3	159150-3	156720-3
2	3	.312023-3	.308833-3	313970 3	.309172-3
3	3	456052-3	.458500-3	.458574-3	451773 3
4	3	.581349-3	.574833 3	.584872-3	575889-3
5	3	.674581-3	676833 3	.678110-3	.667537-3
0	4	0	0	0	0
1	4	112486-3	111183-3	113197-3	.111489-3
2	4	.222228-3	.223333-3	223584-3	220207-3
3	4	325560 3	321500-3	.327458-3	.322508-3
4	4	416753-3	418500-3	.419018-3	412596-3
5	4	485802-3	478000-3	488330-3	.480567-3
0	5	0	0	0	0
1	5	584893-4	.587500-4	588528-4	.579752-4
2	5	.115668-3	114133-3	.116358-3	114623-3
3	5	169788-3	.170500 3	.170746-3	.168202-3
4	5	.218139-3	214500-3	219256-3	.215930-3
5	5	.255759-3	.256667-3	257064-3	.252887-3

* SLOPES GIVEN IN RADIANS

DEFLECTIONS* - CLAMPED SUPPORT CASE					
x	y	EXACT	1" MESH	1/2" MESH	1/2" - 3/1
0	0	109896-2	.108983-2	109833-2	.109052-2
1	0	104625-2	103733-2	104542-2	.103811-2
2	0	893444-3	882833-3	892092-3	.886220-3
3	0	658619-3	646833-3	656579-3	652836-3
4	0	.378911-3	.366667-3	376375-3	.374942-3
5	0	.121528-3	.111483-3	119339-3	.119516-3
0	1	104625-2	.103733-2	.104544-2	.103813-2
1	1	.996216-3	986333-3	.995242-3	988390-3
2	1	851114-3	.840667-3	.849663-3	.844165-3
3	1	.627905-3	.616000-3	625837-3	.622343-3
4	1	.361647-3	.349500-3	359152-3	.357830-3
5	1	.116170-3	.107350-3	114045-3	.114232-3
0	2	.893444-3	.882883-3	.892157-3	.886247-3
1	2	.851114-3	.840667-3	.849704-3	.844182-3
2	2	.728156-3	.716833-3	.726416-3	.722007-3
3	2	538440-3	526833-3	536289-3	.533525-3
4	2	.311141-3	299833-3	.308764-3	.307774-3
5	2	.100391-3	.916000-4	.984618-4	.986793-4
0	3	.658619-3	.646833-3	.656656-3	652865-3
1	3	.627905-3	.616000-3	625894-3	622366-3
2	3	.538440-3	526833-3	536312-3	.533536-3
3	3	399657-3	388333-3	397420-3	.395758-3
4	3	.232124-3	.222167-3	229957-3	229481-3
5	3	.753781-4	.687667-4	737775-4	740514-4
0	4	378910-3	366667-3	376432-3	374963-3
1	4	.361647-3	.349500-3	.359197-3	357847-3
2	4	311141-3	.299833-3	308788 3	307784-3
3	4	.232123-3	.222167-3	.229964-3	229485-3
4	4	.135613-3	127550-3	.133812-3	133888-3
5	4	.442349-4	396000-4	431019-4	434377-4
0	5	.121528-3	.111483-3	119360-3	119523-3
1	5	.116170-3	.107350-3	114063-3	.114237-3
2	5	100391-3	.916000-4	.984707-4	.986829-4
3	5	.753778-4	687667-4	.737811-4	740533 4
4	5	.442351-4	.396000-4	.431025-4	.434381-4
5	5	142292-4	.108200-4	136840-4	139806-4

* DEFLECTIONS GIVEN IN INCHES

θ_x SLOPES* CLAMPED SUPPORT CASE					
x	y	EXACT	1" MESH	1/2" MESH	1/2" - 3/1
0	0	0	0	0	0
1	0	0	0	0	0
2	0	0	0	0	0
3	0	0	0	0	0
4	0	0	0	0	0
5	0	0	0	0	0
0	1	-104570-3	-104733-3	-.105326-3	-103849-3
1	1	-992631-4	-101600-3	-999556-4	-985696-4
2	1	-840171-4	-839000-4	-845278-4	-834061-4
3	1	-610055-4	-615833-4	-612366-4	-605281-4
4	1	-.343271-4	-343833-4	-342210-4	-340275-4
5	1	-.106720-4	-859167-5	-.102571-4	-105611-4
0	2	-.198129-3	-203167-3	-.199624-3	-196743-3
1	2	-.188214-3	-.188500-3	-189592-3	-.186880-3
2	2	-.159677-3	-162917-3	-.160707-3	-.158490-3
3	2	-.116425-3	-116067-3	-.116917-3	-115494-3
4	2	-.659418-4	-647833-4	-.657774-4	-653416-4
5	2	-.207033-4	-235667-4	-.199136-4	-.204632-4
0	3	-265512-3	-266500-3	-.267582-3	-263567-3
1	3	-.252536-3	-258667-3	-.254450-3	-250665-3
2	3	-.215052-3	-215167-3	-216504-3	-213399-3
3	3	-.157843-3	-159800-3	-158578-3	-.156531-3
4	3	-.903446-4	-904333-4	-901878-4	-.894691-4
5	3	-.288410-4	-.232000-4	-.277734-4	-.284487-4
0	4	-282974-3	-.290167-3	-285220-3	-280643-3
1	4	-269605-3	-270833-3	-271692-3	-.267366-3
2	4	-.230765 3	-235833-3	-.232382-3	-.228794-3
3	4	-.170831-3	-170667-3	-.171690-3	-169274-3
4	4	-.990404-4	-981333-4	-989340-4	-.979909-4
5	4	-.323008-4	-364667-4	-.311584-4	-.317685-4
0	5	-.213234-3	-215000-3	-214888-3	-210710-3
1	5	-.203625-3	-.207833 3	-205178-3	-201194-3
2	5	-.175452-3	-176500-3	-176698-3	-.173310-3
3	5	-.131193-3	-132917-3	-131902-3	-.129530-3
4	5	-.768637-4	-765167-4	-.768008-4	-758188-4
5	5	-.252570-4	-.216000-4	-243742-4	-.247906-4

* SLOPES GIVEN IN RADIANS

θ_y SLOPES* - CLAMPED SUPPORT CASE					
x	y	EXACT	1" MESH	½" MESH	½" - 3/1
0	0	0	0	0	0
1	0	104569-2	104733-3	,105370-3	103867-3
2	0	198130-3	203167-3	.199653-3	196752-3
3	0	265512-3	266500 3	,267576-3	.263563-3
4	0	282972-3	290167-3	285186-3	.280630-3
5	0	,213239-3	215000-3	214850-3	.210695-3
0	1	0	0	0	0
1	1	.992618-4	101600-3	100001-3	985885-4
2	1	.188216-3	188500-3	189623-3	186892-3
3	1	252536-3	258667-3	254452-3	250666-3
4	1	269603-3	270833-3	,271668-3	.267356-3
5	1	.203630-3	207833-3	.205149-3	.201183-3
0	2	0	0	0	0
1	2	.840159-4	839000-4	845712-4	834222 4
2	2	.159678-3	162917-3	160742-3	158512-3
3	2	.215052-3	215167-3	.216518-3	.213406-3
4	2	.230763-3	235833-3	.232374-3	228790-3
5	2	.175457-3	176500-3	.176684-3	.173305-3
0	3	0	0	0	0
1	3	.610042-4	615833-4	612706-4	605383-4
2	3	.116426-3	116067-3	.116948-3	115507-3
3	3	.157842-3	.159800-3	.158594-3	.156539-3
4	3	.170829-3	.170667-3	171693-3	.169277-3
5	3	131197-3	.132917-3	131899-3	.129531-3
0	4	0	0	0	0
1	4	.343259-4	343833-4	.342410-4	340325-4
2	4	.659433-4	647000-4	.657988-4	.653495-4
3	4	.903443-4	904333-4	.902010-4	894756-4
4	4	.990383-4	981333-4	.989368-4	979923-4
5	4	768685-4	765167-4	.768016-4	.758203-4
0	5	0	0	0	0
1	5	.106707-4	859000 5	.102638-4	105625-4
2	5	.207047-4	235833-4	.199197-4	204651-4
3	5	288408-4	.232000-4	.277774-4	.284504-4
4	5	.322988-4	364667-4	311602-4	.317691-4
5	5	252618-4	216000-4	.243740-4	.247906-4

* SLOPES GIVEN IN RADIANS

Appendix B

FORMULATION OF EXTRAPOLATION CURVES

This appendix contains details of the formulation of the extrapolation curves described in Section 3 of the report. These data include a tabulation of the deformations of the points on a square plate used in the sample, plots of ratios of these deformations, and the resulting extrapolation curves.

The curves were developed in the following manner

1. Ten points were selected at random on the square plate using the one-inch and one-half-inch grid models.
2. The deformations (deflections and rotations) of these points, as determined from the exact, normal facet element and alternate facet element analyses, were tabulated.
3. The ratios of the alternate facet element solutions to the normal facet element solutions and the exact solutions to the normal facet element solutions were then obtained.
4. A plot was made using the ratios of Step 3.
5. Smooth curves were faired through these plotted points. Two such curves were generated, one using the deflection ratios and the other using rotation ratios.

Using these curves and the ratios of the alternate element analysis solutions to the normal element solutions, a determination can be made of the ratio of the "predicted exact" solution to the normal element solution This information leads directly to the amount of error in the normal element solution.

DETERMINATION OF SCALING LAWS GIVEN SQUARE PLATE ANALYSES

- DEFLECTIONS - 12" x 12" SQUARE PLATE - HINGED EDGE

  - 1/2" MESH REFINEMENT

PT[a]	δ_e[b]	$\delta_{1/1}$[b]	$\delta_{3/1}$[b]	$\delta_{3/1}/\delta_{1/1}$	$\delta_e/\delta_{1/1}$	ERROR
1,5	092976^{-2}	093160^{-2}	092049^{-2}	988074	.988025	20%
2,3	223701^{-2}	224291^{-2}	.221558^{-2}	987815	997369	26%
5,4	050485^{-2}	.050531^{-2}	049934^{-2}	988185	999090	.09%
3,5	069943^{-2}	.070044^{-2}	069424^{-2}	991148	998558	14%
1,1	.331023^{-2}	332039^{-2}	.327935^{-2}	987640	.996940	31%
4,2	.160564^{-2}	.160923^{-2}	158990^{-2}	987988	997769	22%
6,3	—	—	—	—	—	—
3,1	247264^{-2}	247934^{-2}	244912^{-2}	987811	997298	27%
0,3	.255188^{-2}	255912^{-2}	252775^{-2}	987742	997171	28%
5,5	026672^{-2}	026674^{-2}	.026357^{-2}	.988115	999925	01%

  - 1" MESH REFINEMENT

PT[a]	δ_e[b]	$\delta_{1/1}$[b]	$\delta_{3/1}$[b]	$\delta_{3/1}/\delta_{1/1}$	$\delta_e/\delta_{1/1}$	ERROR
1,5	.092976^{-2}	092033^{-2}	090817^{-2}	986787	1010246	1 01%
2,3	223701^{-2}	222116^{-2}	218833^{-2}	985219	1007136	.71%
5,4	.050485^{-2}	049817^{-2}	049067^{-2}	.984945	1,013409	1.32%
3,5	.069943^{-2}	.069100^{-2}	068167^{-2}	986498	1.012200	1 21%
1,1	.331023^{-2}	329167^{-2}	324500^{-2}	985822	1005638	56%
4,2	160564^{-2}	159167^{-2}	156983^{-2}	986279	1.008777	87%
6,3	—	—	—	—	—	—
3,1	247264^{-2}	245500^{-2}	242167^{-2}	986424	1.007185	71%
0,3	255188^{-2}	253500^{-2}	249833^{-2}	985535	1.006659	66%
5,5	026672^{-2}	.026183^{-2}	025833^{-2}	.986633	1.018676	1.83%

(a) COORDINATES OF POINTS ON A SQUARE PLATE RANDOMLY CHOSEN

(b) MEASURED IN INCHES

• DEFLECTIONS – 12" x 12" SQUARE PLATE – CLAMPED EDGE

– 1/2" MESH REFINEMENT

PT[a]	δ_e[b]	$\delta_{1/1}$[b]	$\delta_{3/1}$[b]	$\delta_{3/1}/\delta_{1/1}$	$\delta_e/\delta_{1/1}$	ERROR
1,5	$.116170^{-3}$	114863^{-3}	114237^{-3}	994550	1.011379	1 13%
2,3	538440^{-3}	536312^{-3}	533536^{-3}	994824	1 003968	.40%
5,4	$.442349^{-3}$	$.431019^{-3}$	434377^{-3}	1 007791	1 026287	2 56%
3,5	$.075378^{-3}$	073781^{-3}	$.074053^{-3}$	1 003687	1.021645	2 12%
1,1	996216^{-3}	$.995242^{-3}$	$.988390^{-3}$	.993115	1.000979	.10%
4,2	$.311141^{-3}$	$.308764^{-3}$	$.307774^{-3}$	996794	1.007698	76%
6,3	—	—	—	—	—	—
3,1	627905^{-3}	$.625837^{-3}$	$.622343^{-3}$	.994417	1.003304	.33%
0,3	658619^{-3}	$.656656^{-3}$	652865^{-3}	.994227	1.002989	30%
5,5	$.014229^{-3}$	$.013684^{-3}$	013981^{-3}	1.021704	1.039828	3 83%

– 1" MESH REFINEMENT

PT[a]	δ_e[b]	$\delta_{1/1}$[b]	$\delta_{3/1}$[b]	$\delta_{3/1}/\delta_{1/1}$	$\delta_e/\delta_{1/1}$	ERROR
1,5	116170^{-3}	107350^{-3}	107733^{-3}	1.003568	1 082161	7.59%
2,3	538440^{-3}	$.526833^{-3}$	521333^{-3}	.989560	1.022032	2.16%
5,4	442349^{-3}	$.396000^{-3}$	414167^{-3}	1 045876	1.117043	10.48%
3,5	075378^{-3}	068767^{-3}	$.069683^{-3}$	1.013320	1.096136	8.77%
1,1	$.996216^{-3}$	$.986333^{-3}$	$.971000^{-3}$	984455	1.010020	99%
4,2	$.311141^{-3}$	$.299833^{-3}$	299000^{-3}	.997222	1.037714	3 63%
6,3	—	—	—	—	—	—
3,1	627905^{-3}	$.616000^{-3}$	609167^{-3}	988907	1.019326	1 90%
0,3	658619^{-3}	$.646833^{-3}$	$.638833^{-3}$	987632	1.018221	1 79%
5,5	014229^{-3}	010820^{-3}	$.014373^{-3}$	1.328373	1.315065	23 96%

(a) COORDINATES OF POINTS ON A SQUARE PLATE RANDOMLY CHOSEN

(b) MEASURED IN INCHES

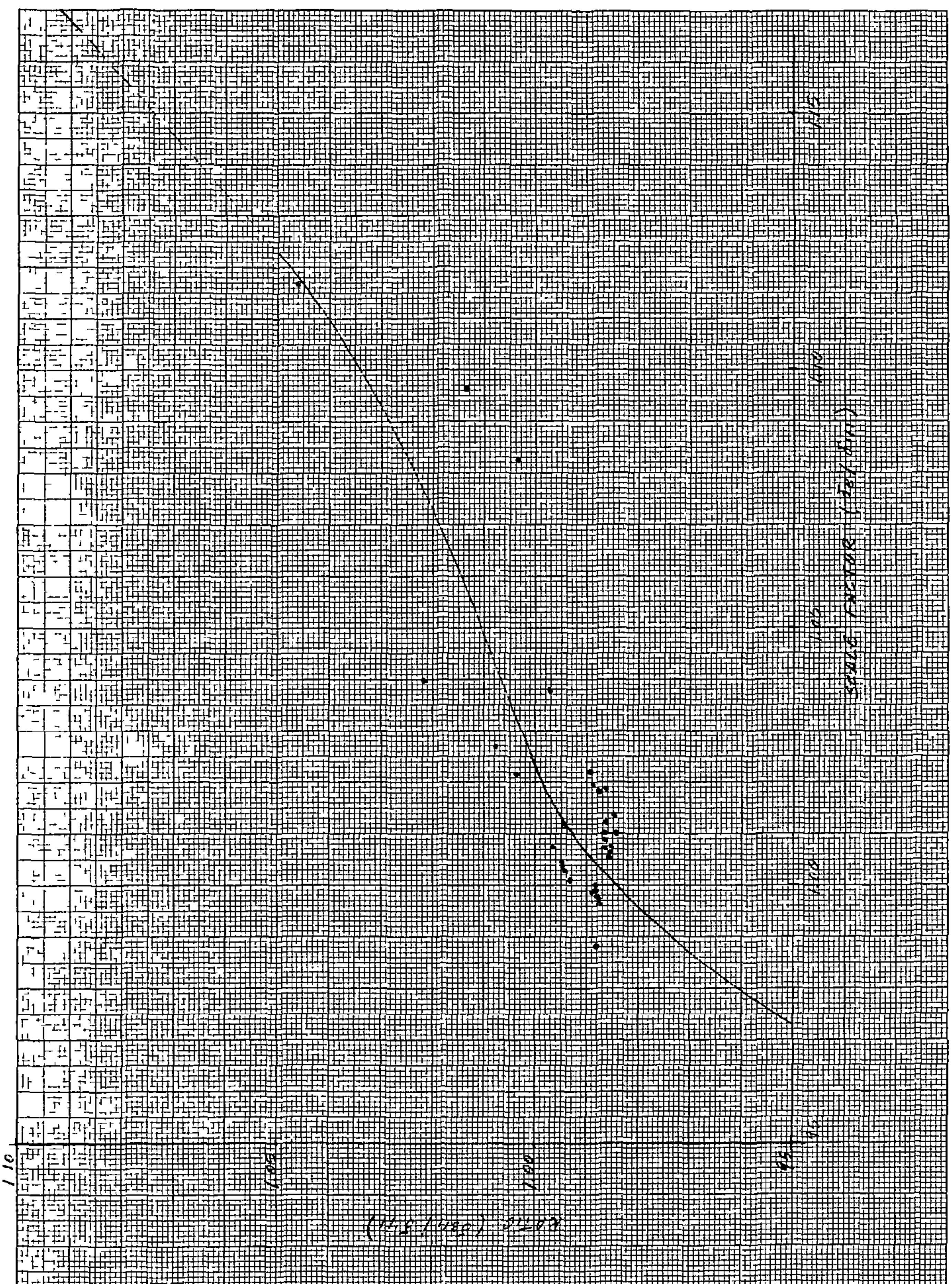
1.10
1.05
1.00
.95
1.15
1.10
1.05
1.00
SCALE FACTOR

• ROTATIONS - 12" X 12" SQUARE PLATE - HINGED EDGE

— 1/8" MESH REFINEMENT

PT[a]	θ_e[b]	$\theta_{1/1}$[b]	$\theta_{3/1}$[b]	$\theta_{3/1}/\theta_{1/1}$	$\theta_e/\theta_{1/1}$	ERROR
1,5	898662^{-3}	903452^{-3}	889563^{-3}	.984627	.994698	.99 sec
2,3	.553632^{-3}	556934^{-3}	.548420^{-3}	.984713	.994071	.68 sec
5,4	.485841^{-3}	488330^{-3}	.480567^{-3}	984103	.994903	.51 sec
3,5	.674614^{-3}	678126^{-3}	.667539^{-3}	984388	.994821	.72 sec
1,1	213881^{-3}	215188^{-3}	211935^{-3}	.984883	.993926	.27 sec
4,2	.703962^{-3}	.707988^{-3}	.697135^{-3}	.984671	994313	.83 sec
6,3	712576^{-3}	.715646^{-3}	704319^{-3}	984172	995710	63 sec
3,1	.613730^{-3}	617458^{-3}	607971^{-3}	984635	.993962	77 sec
0,3	.634001^{-3}	.637834^{-3}	.628054^{-3}	.984667	.993991	.79 sec
5,5	255797^{-3}	.257064^{-3}	.252887^{-3}	983751	995071	.26 sec

— 1" MESH REFINEMENT

PT[a]	θ_e[b]	$\theta_{1/1}$[b]	$\theta_{3/1}$[b]	$\theta_{3/1}/\theta_{1/1}$	$\theta_e/\theta_{1/1}$	ERROR
1,5	898662^{-3}	901667^{-3}	877500^{-3}	.973197	996667	62 sec
2,3	.553632^{-3}	548500^{-3}	.547833^{-3}	.998784	1 009356	1 06 sec
5,4	.485841^{-3}	478000^{-3}	.479167^{-3}	1 002441	1.016404	1 62 sec
3,5	674614^{-3}	676833^{-3}	657500^{-3}	.971436	.996721	.46 sec
1,1	.213881^{-3}	215333^{-3}	210000^{-3}	.975234	.993257	30 sec
4,2	703962^{-3}	.707500^{-3}	.688833^{-3}	.973616	994999	.73 sec
6,3	712576^{-3}	.700500^{-3}	.700833^{-3}	1.000475	1.017239	2.49 sec
3,1	613730^{-3}	617333^{-3}	601833^{-3}	974892	994164	74 sec
0,3	.634001^{-3}	.628667^{-3}	627333^{-3}	.997878	.991587	1 10 sec
5,5	.255797^{-3}	256667^{-3}	.248333^{-3}	.967530	996610	.18 sec

(a) COORDINATES OF POINTS ON A SQUARE PLATE RANDOMLY CHOSEN

(b) MEASURED IN RADIANS

o ROTATIONS - 12" X 12" SQUARE PLATE - CLAMPED EDGE

— 1/2" MESH REFINEMENT

PT[a]	θ_e[b]	θ_{111}[b]	θ_{311}[b]	$\theta_{311}/\theta_{111}$	θ_e/θ_{111}	ERROR
1,5	203625^{-3}	$.205178^{-3}$	201194^{-3}	980583	992431	32 sec
2,3	$.215052^{-3}$	216504^{-3}	213399^{3}	985658	.993293	.30 sec
5,4	076869^{3}	076802^{-3}	$.075820^{-3}$	987214	1 000872	.01 sec
3,5	$.131193^{3}$	131902^{-3}	$.129530^{-3}$	982017	.994625	15 sec
1,1	099262^{-3}	$.100978^{-3}$	098579^{-3}	976242	.983006	35 sec
4,2	$.230763^{-3}$	232374^{-3}	$.228790^{-3}$	.984577	993067	33 sec
6,3	—	—	—	—	—	—
3,1	$.252536^{-3}$	$.254452^{-3}$	250666^{-3}	.985121	.992470	40 sec
0,3	$.265512^{-3}$	$.267582^{-3}$	263567^{-3}	.984995	.992264	.43 sec
5,5	$.025259^{-3}$	024374^{-3}	$.024791^{-3}$	1.017138	1.036309	.18 sec

— 1" MESH REFINEMENT

PT[a]	θ_e[b]	θ_{111}[b]	θ_{311}[b]	$\theta_{311}/\theta_{111}$	θ_e/θ_{111}	ERROR
1,5	203625^{-3}	207833^{-3}	$.196667^{-3}$	.946274	979753	87 sec
2,3	$.215052^{-3}$	215167^{-3}	213000^{-3}	989929	999466	02 sec
5,4	076869^{3}	076517^{-3}	$.077567^{-3}$	1.013722	1 004600	07 sec
3,5	$.131193^{-3}$	132917^{-3}	126383^{-3}	950842	987029	36 sec
1,1	$.099262^{-3}$	101600^{-3}	097183^{-3}	956526	976988	.48 sec
4,2	$.230763^{-3}$	$.235833^{-3}$	$.224000^{-3}$	.949825	978502	1.05 sec
6,3	—	—	—	—	—	—
3,1	252536^{3}	258667^{-3}	246667^{-3}	.953608	976298	1 26 sec
0,3	265512^{-3}	266500^{-3}	$.265500^{3}$	996248	996293	20 sec
5,5	025259^{-3}	$.021600^{-3}$	$.024450^{-3}$	1 131944	1.169398	75 sec

(a) COORDINATES OF POINTS ON A SQUARE PLATE RANDOMLY CHOSEN

(b) MEASURED IN RADIANS

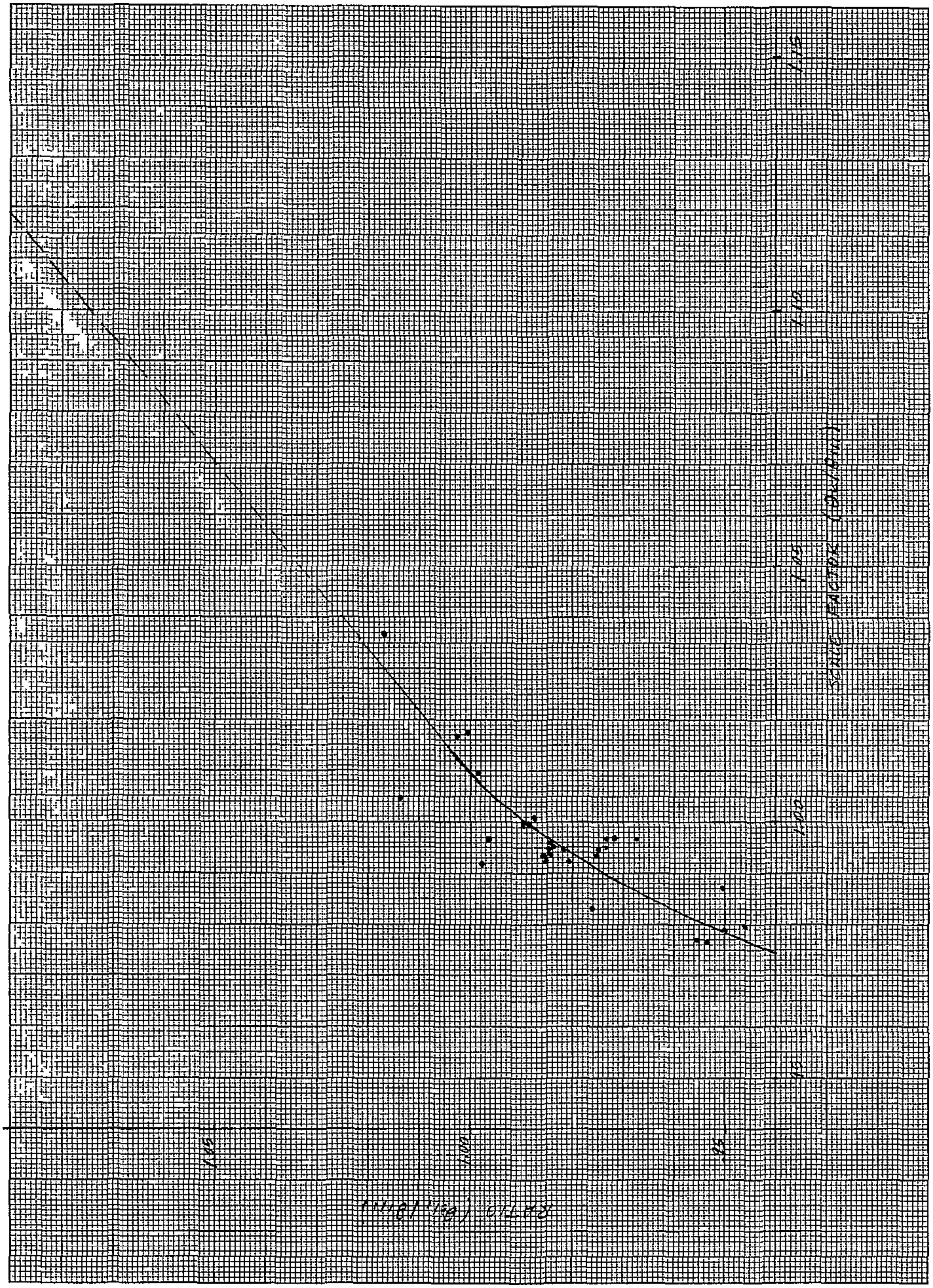
1.15
1.10
1.05
1.00
.95
SCALE FACTOR
1.05
1.00
.95

Appendix C

ISOLATED WINDOW ANALYSES

This appendix defines the model used in the analyses of the isolated Apollo window with idealized edge conditions and presents the results of those analyses. It includes sketches showing the joint numbers and element numbers and a tabulation of the joint coordinates.

Copies of the computer results are available for review at NASA Ames Research Center, Moffett Field, California. These results list, in matrix form, the deformations for each of the two sets of boundary conditions. DFC001 is the matrix of deformations for the simply supported edge condition and DFC002 that for the clamped edge condition. The row codes of the matrices give the joint number and component of the deformations. The component number is the last digit of the row code and is interpreted as follows 1 is displacement in x-direction, 2, displacement in y-direction, 3, displacement in z-direction, 4, rotation about x-axis, 5, rotation about y-axis, and 6, rotation about z-axis. Displacements are given in inches and rotations in radians.

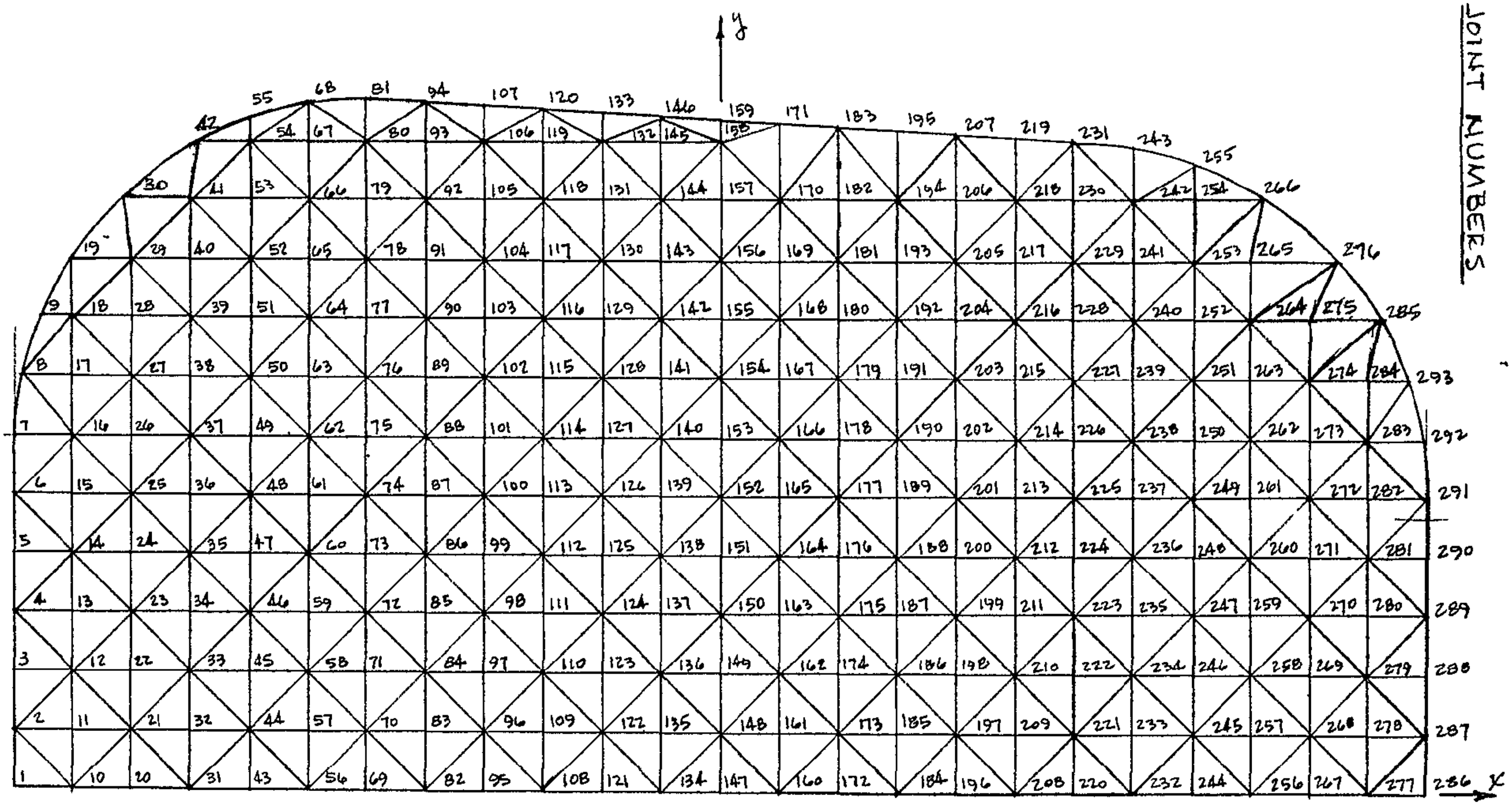

JOINT NUMBERS

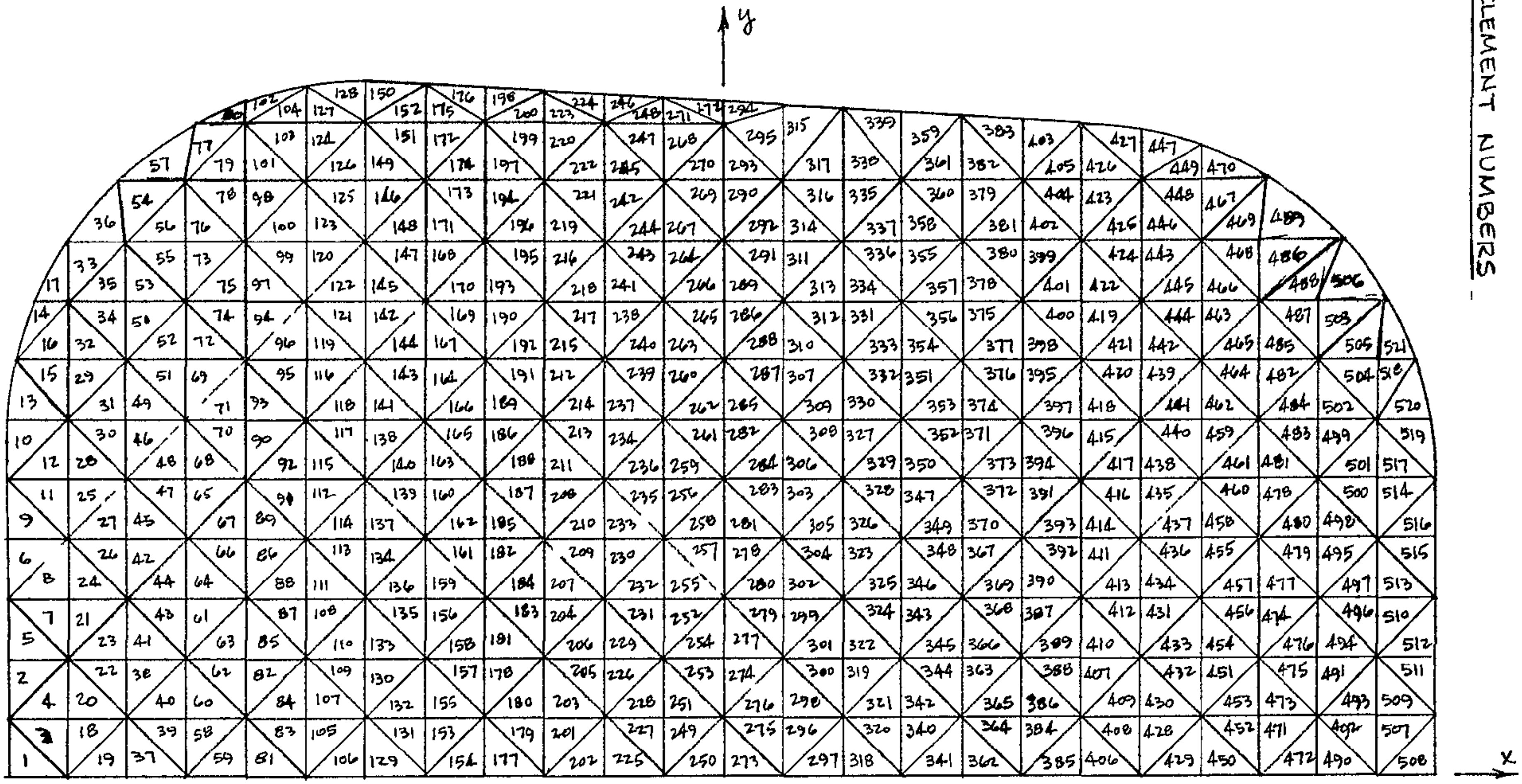

ELEMENT NUMBERS

JOINT COORDINATES

JT	x	y	JT	x	y	JT	x	y	JT	x	y
1	-6.0	0.0	34	-4.5	1.5	67	-3.5	5.5	100	-2.0	2.5
2		0.5	35		2.0	68	-3.5	5.79	101		3.0
3		1.0	36		2.5	69	-3.0	0.0	102		3.5
4		1.5	37		3.0	70		0.5	103		4.0
5		2.0	38		3.5	71		1.0	104		4.5
6		2.5	39		4.0	72		1.5	105		5.0
7	-6.0	3.0	40		4.5	73		2.0	106		5.5
8	-5.92	3.5	41	-4.5	5.0	74		2.5	107	-2.0	5.77
9	-5.77	4.0	42	-4.37	5.5	75		3.0	108	-1.5	0.0
10	-5.5	0.0	43	-4.0	0.0	76		3.5	109		0.5
11		0.5	44		0.5	77		4.0	110		1.0
12		1.0	45		1.0	78		4.5	111		1.5
13		1.5	46		1.5	79		5.0	112		2.0
14		2.0	47		2.0	80		5.5	113		2.5
15		2.5	48		2.5	81	-3.0	5.83	114		3.0
16		3.0	49		3.0	82	-2.5	0.0	115		3.5
17		3.5	50		3.5	83		0.5	116		4.0
18		4.0	51		4.0	84		1.0	117		4.5
19	-5.5	4.5	52		4.5	85		1.5	118		5.0
20	-5.0	0.0	53		5.0	86		2.0	119		5.5
21		0.5	54		5.5	87		2.5	120	-1.5	5.75
22		1.0	55	-4.0	5.66	88		3.0	121	-1.0	0.0
23		1.5	56	-3.5	0.0	89		3.5	122		0.5
24		2.0	57		0.5	90		4.0	123		1.0
25		2.5	58		1.0	91		4.5	124		1.5
26		3.0	59		1.5	92		5.0	125		2.0
27		3.5	60		2.0	93		5.5	126		2.5
28		4.0	61		2.5	94	-2.5	5.8	127		3.0
29	-5.0	4.5	62		3.0	95	-2.0	0.0	128		3.5
30	-5.07	5.0	63		3.5	96		0.5	129		4.0
31	-4.5	0.0	64		4.0	97		1.0	130		4.5
32	-4.5	0.5	65		4.5	98		1.5	131		5.0
33	-4.5	1.0	66	-3.5	5.0	99	-2.0	2.0	132	-1.0	5.5

JT	x	y	JT	x	y	JT	x	y	JT	x	y
133	-1.0	5.72	167	0.5	3.5	201	2.0	2.5	235	3.5	1.5
134	-0.5	0.0	168		4.0	202		3.0	236		2.0
135		0.5	169		4.5	203		3.5	237		2.5
136		1.0	170		5.0	204		4.0	238		3.0
137		1.5	171	0.5	5.63	205		4.5	239		3.5
138		2.0	172	1.0	0.0	206		5.0	240		4.0
139		2.5	173		0.5	207	2.0	5.55	241		4.5
140		3.0	174		1.0	208	2.5	0.0	242		5.0
141		3.5	175		1.5	209		0.5	243	3.5	5.46
142		4.0	176		2.0	210		1.0	244	4.0	0.0
143		4.5	177		2.5	211		1.5	245		0.5
144		5.0	178		3.0	212		2.0	246		1.0
145		5.5	179		3.5	213		2.5	247		1.5
146	-0.5	5.69	180		4.0	214		3.0	248		2.0
147	0.0	0.0	181		4.5	215		3.5	249		2.5
148		0.5	182		5.0	216		4.0	250		3.0
149		1.0	183	1.0	5.6	217		4.5	251		3.5
150		1.5	184	1.5	0.0	218		5.0	252		4.0
151		2.0	185		0.5	219	2.5	5.52	253		4.5
152		2.5	186		1.0	220	3.0	0.0	254		5.0
153		3.0	187		1.5	221		0.5	255	4.0	5.33
154		3.5	188		2.0	222		1.0	256	4.5	0.0
155		4.0	189		2.5	223		1.5	257		0.5
156		4.5	190		3.0	224		2.0	258		1.0
157		5.0	191		3.5	225		2.5	259		1.5
158		5.5	192		4.0	226		3.0	260		2.0
159	0.0	5.66	193		4.5	227		3.5	261		2.5
160	0.5	0.0	194		5.0	228		4.0	262		3.0
161		0.5	195	1.5	5.58	229		4.5	263		3.5
162		1.0	196	2.0	0.0	230		5.0	264		4.0
163		1.5	197		0.5	231	3.0	5.49	265	4.5	4.5
164		2.0	198		1.0	232	3.5	0.0	266	4.66	5.0
165		2.5	199		1.5	233	3.5	0.5	267	5.0	0.0
166	0.5	3.0	200	2.0	2.0	234	3.5	1.0	268	5.0	0.5

JT	x	y	JT	x	y	JT	x	y	JT	x	y
269	5.0	1.0	276	5.24	4.5	283	5.5	3.0	290	6.0	2.0
270		1.5	277	5.5	0.0	284	5.5	3.5	291	6.0	2.5
271		2.0	278		0.5	285	5.6	4.0	292	5 96	3 0
272		2.5	279		1.0	286	6.0	0.0	293	5.83	3.5
273		3.0	280		1.5	287		0.5			
274		3.5	281		2.0	288		1.0			
275	5.0	4 0	282	5.5	2.5	289	6.0	1.5			

Appendix D

APOLLO WINDOW STRUCTURAL ANALYSES

This appendix defines the model used in the coarse analysis of the Apollo window in its structural environment and presents the results of the analysis. It includes a sketch showing the finite element model articulation and joint numbering, tabulations of the model coordinates and constraint conditions, calculations to determine equivalent beam stiffnesses for the fore and aft bulkheads, and calculations to determine beam section properties and equivalent plate properties to model the shell portions of the structure.

Copies of the computer results are available for review at NASA Ames Research Center, Moffett Field, California. These results list, in matrix form, the deformations of the Apollo window for both the normal and alternate element analyses. The row code interpretation is given in Appendix C. The column codes designate the load applied to the structure. 04 denotes uniform cabin pressure and 05 denotes the self-equilibrating load.

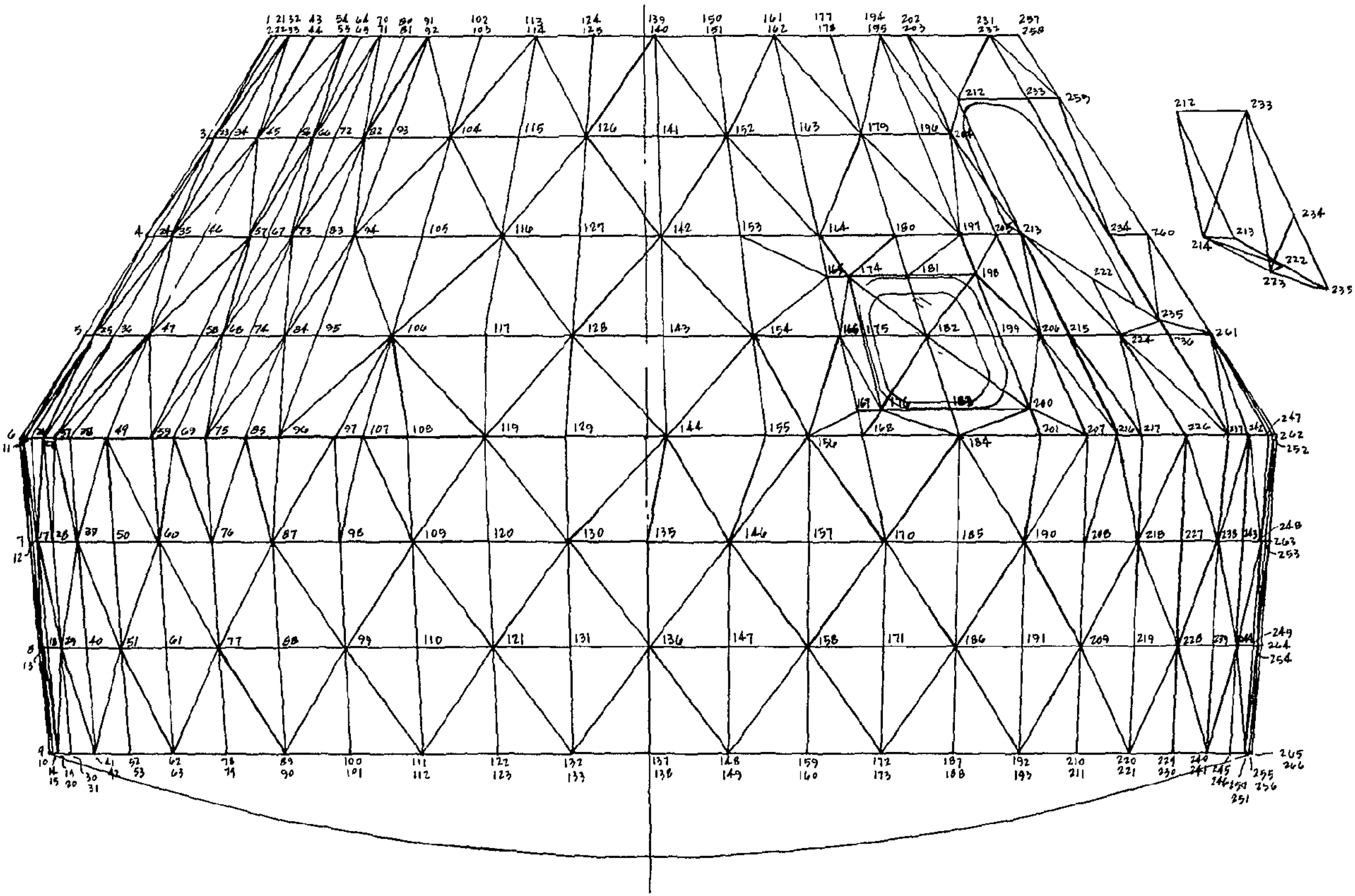

JOINT COORDINATES

JOINT	r	θ	z	JOINT	r	θ	z
1	24.8	0	80	41	57.2	22.5	12
2	34.8	0	80	42	47.2	22.5	12
3	41	0	70.5	43	24.8	27.83	80
4	47.2	0	61	44	34.8	27.83	80
5	53.4	0	51.5	45	41	27.83	70.5
6	59.6	0	42	46	47.2	27.83	61
7	58.8	0	32	47	53.4	27.83	51.5
8	58	0	22	48	59.6	27.83	42
9	57.2	0	12	49	59.6	30	42
10	47.2	0	12	50	58.8	30	32
11	59.6	3.75	42	51	58	30	22
12	58.8	3.75	32	52	57.2	30	12
13	58	3.75	22	53	47.2	30	12
14	57.2	3.75	12	54	24.8	37.5	80
15	47.2	3.75	12	55	34.8	37.5	80
16	59.6	7.5	42	56	41	37.5	70.5
17	58.8	7.5	32	57	47.2	37.5	61
18	58	7.5	22	58	53.4	37.5	51.5
19	57.2	7.5	12	59	59.6	37.5	42
20	47.2	7.5	12	60	58.8	37.5	32
21	24.8	9.33	80	61	58	37.5	22
22	34.8	9.33	80	62	57.2	37.5	12
23	41	9.33	70.5	63	47.2	37.5	12
24	47.2	9.33	61	64	24.8	41	80
25	53.4	9.33	51.5	65	34.8	41	30
26	59.6	9.33	42	66	41	41	70.5
27	59.6	15	42	67	47.2	41	61
28	58.8	15	32	68	53.4	41	51.5
29	58	15	22	69	59.6	41	42
30	57.2	15	12	70	24.8	45	80
31	47.2	15	12	71	34.8	45	80
32	24.8	18.67	80	72	41	45	70.5
33	34.8	18.67	80	73	47.2	45	61
34	41	18.67	70.5	74	53.4	45	51.5
35	47.2	18.67	61	75	59.6	45	42
36	53.4	18.67	51.5	76	58.8	45	32
37	59.6	18.67	42	77	58	45	22
38	59.6	22.5	42	78	57.2	45	12
39	58.8	22.5	32	79	47.2	45	12
40	58	22.5	22	80	24.8	50	80

JOINT	r	θ	z	JOINT	r	θ	z
81	34.8	50	80	121	58	75	22
82	41	50	70.5	122	57.2	75	12
83	47.2	50	61	123	47.2	75	12
84	53.4	50	51.5	124	24.8	82.5	80
85	59.6	50	42	125	34.8	82.5	80
86	59.6	52.5	42	126	41	82.5	70.5
87	58.8	52.5	32	127	47.2	82.5	61
88	58	52.5	22	128	53.4	82.5	51.5
89	57.2	52.5	12	129	59.6	82.5	42
90	47.2	52.5	12	130	58.8	82.5	32
91	24.8	55	80	131	58	82.5	22
92	34.8	55	80	132	57.2	82.5	12
93	41	55	70.5	133	47.2	82.5	12
94	47.2	55	61	134	59.6	90	42
95	53.4	55	51.5	135	58.8	90	32
96	59.6	55	42	136	58	90	22
97	59.6	60	42	137	57.2	90	12
98	58.8	60	32	138	47.2	90	12
99	58	60	22	139	24.8	91.67	80
100	57.2	60	12	140	34.8	91.67	80
101	47.2	60	12	141	41	91.67	70.5
102	24.8	64.17	80	142	47.2	91.67	61
103	34.8	64.17	80	143	53.4	91.67	51.5
104	41	64.17	70.5	144	59.6	91.67	42
105	47.2	64.17	61	145	59.6	97.5	42
106	53.4	64.17	51.5	146	58.8	97.5	32
107	59.6	64.17	42	147	58	97.5	22
108	59.6	67.5	42	148	57.2	97.5	12
109	58.8	67.5	32	149	47.2	97.5	12
110	58	67.5	22	150	24.8	100.83	80
111	57.2	67.5	12	151	34.8	100.83	80
112	47.2	67.5	12	152	41	100.83	70.5
113	24.8	73.33	80	153	47.2	100.83	61
114	34.8	73.33	80	154	53.4	100.83	51.5
115	41	73.33	70.5	155	59.6	100.83	42
116	47.2	73.33	61	156	59.6	105	42
117	53.4	73.33	51.5	157	58.8	105	32
118	59.6	73.33	42	158	58	105	22
119	59.6	75	42	159	57.2	105	12
120	58.8	75	32	160	47.2	105	12

JOINT	r	θ	z	JOINT	r	θ	z
161	24.8	110	80	201	59.6	129	42
162	34.8	110	80	202	24.8	135	80
163	41	110	70.5	203	34.8	135	80
164	47.2	110	61	204	41	135	70.5
165	49	110	58	205	47.2	135	61
166	53.4	110	51.5	206	53.4	135	51.5
167	57.6	110	45	207	59.6	135	42
168	59.6	110	42	208	58.8	135	32
169	59.6	112.5	42	209	58	135	22
170	58.8	112.5	32	210	57.2	135	12
171	58	112.5	22	211	47.2	135	12
172	57.2	112.5	12	212	38.8	138.33	74
173	47.2	112.5	12	213	47.2	138.33	61
174	49.0	115.63	58.0	214	43.1	138.33	61
175	53.4	115.63	51.5	215	53.4	138.33	51.5
176	57.6	115.63	45.0	216	59.6	138.33	42
177	24.8	120	80	217	59.6	142.5	42
178	34.8	120	80	218	58.8	142.5	32
179	41	120	70.5	219	58	142.5	22
180	47.2	120	61	220	57.2	142.5	12
181	49	120	58	221	47.2	142.5	12
182	53.4	120	51.5	222	47.8	147.67	59.9
183	57.6	120	45	223	39.5	147.67	59.9
184	59.6	120	42	224	53.4	147.67	51.5
185	58.8	120	32	225	59.6	147.67	42
186	58	120	22	226	59.6	150	42
187	57.2	120	12	227	58.8	150	32
188	47.2	120	12	228	58	150	22
189	59.6	127.5	42	229	57.2	150	12
190	58.8	127.5	32	230	47.2	150	12
191	58	127.5	22	231	24.8	157.5	80
192	57.2	127.5	12	232	34.8	157.5	80
193	47.2	127.5	12	233	38.8	157.5	74
194	24.8	129	80	234	47.2	157.5	61
195	34.8	129	80	235	51	157.5	55
196	41	129	70.5	236	53.4	157.5	51.5
197	47.2	129	61	237	59.6	157.5	42
198	49	129	58	238	58.8	157.5	32
199	53.4	129	51.5	239	58	157.5	22
200	57.6	129	45	240	57.2	157.5	12

JOINT	r	θ	z
241	47.2	157.5	12
242	59.6	165	42
243	58.8	165	32
244	58	165	22
245	57.2	165	12
246	47.2	165	12
247	59.6	172.5	42
248	58.8	172.5	32
249	58	172.5	22
250	57.2	172.5	12
251	47.2	172.5	12
252	59.6	176.25	42
253	58.8	176.25	32
254	58	176.25	22
255	57.2	176.25	12
256	47.2	176.25	12
257	24.8	180	80
258	34.8	180	80
259	41	180	70.5
260	47.2	180	61
261	53.4	180	51.5
262	59.6	180	42
263	58.8	180	32
264	58	180	22
265	57.2	180	12
266	47.2	180	12

JOINT RESTRAINTS

JOINT	x	y	z	θ_x	θ_y	θ_z
1	1	1	1	1	1	1
2		1		1		1
3		1		1		1
4		1		1		1
5		1		1		1
6		1		1		1
7		1		1		1
8		1		1		1
9		1		1		1
10	1	1	1	1	1	1
15	1	1	1	1	1	1
20	1	1	1	1	1	1
21	1	1	1	1	1	1
31	1	1	1	1	1	1
32	1	1	1	1	1	1
42	1	1	1	1	1	1
43	1	1	1	1	1	1
53	1	1	1	1	1	1
54	1	1	1	1	1	1
63	1	1	1	1	1	1
64	1	1	1	1	1	1
70	1	1	1	1	1	1
79	1	1	1	1	1	1
80	1	1	1	1	1	1
90	1	1	1	1	1	1
91	1	1	1	1	1	1
100			1			
101	1	1	1	1	1	1
102	1	1	1	1	1	1
112	1	1	1	1	1	1
113	1	1	1	1	1	1
123	1	1	1	1	1	1

JOINT	x	y	z	θ_x	θ_y	θ_z
124	1	1	1	1	1	1
133	1	1	1	1	1	1
138	1	1	1	1	1	1
139	1	1	1	1	1	1
149	1	1	1	1	1	1
150	1	1	1	1	1	1
160	1	1	1	1	1	1
161	1	1	1	1	1	1
173	1	1	1	1	1	1
177	1	1	1	1	1	1
188	1	1	1	1	1	1
193	1	1	1	1	1	1
194	1	1	1	1	1	1
202	1	1	1	1	1	1
211	1	1	1	1	1	1
221	1	1	1	1	1	1
230	1	1	1	1	1	1
231	1	1	1	1	1	1
241	1	1	1	1	1	1
246	1	1	1	1	1	1
251	1	1	1	1	1	1
256	1	1	1	1	1	1
257	1	1	1	1	1	1
258		1		1		1
259		1		1		1
260		1		1		1
261		1		1		1
262		1		1		1
263		1		1		1
264		1		1		1
265		1	1	1		1
266	1	1	1	1	1	1

RADIAL STIFFNESS OF AFT BULKHEAD *

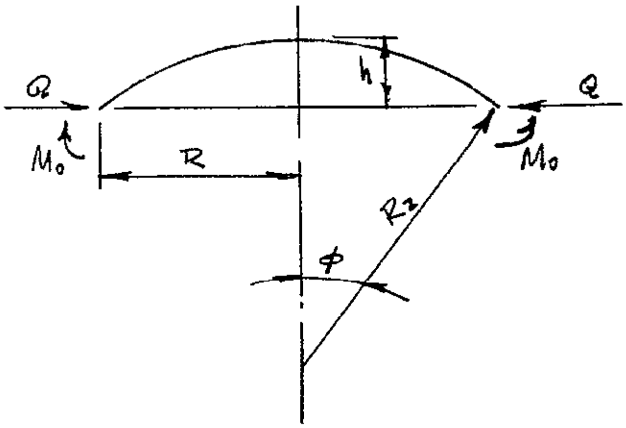

$R = 572$ IN
$h = 112$ IN
$R_2 = 151.7$ IN
$\phi = 22.17°$
$t = 2.53$ IN
$\nu = .325$
$E = 1.29 \times 10^5$ psi

$$\frac{\delta_R^Q}{Q} = \frac{1}{Et}\left(\beta R_2 \sin^2\phi\right)\left(K_2 + \frac{1}{K_1}\right)$$

$$\beta = \sqrt[4]{3(1-\nu^2)\left(\frac{R_2}{t}\right)^2}$$

$$K_1 = 1 - \frac{1-2\nu}{2\beta}\cot\phi$$

$$K_2 = 1 - \frac{1+2\nu}{2\beta}\cot\phi$$

$$\frac{\theta^Q}{Q} = \frac{1}{Et}\left(2\beta^2 \sin\phi\right)\left(\frac{1}{K_1}\right)$$

$$\beta = \sqrt[4]{3(1-(.325)^2)\left(\frac{151.7}{2.53}\right)^2} = 9.9105$$

$$K_1 = 1 - \frac{1-.65}{(2)(}\cot(22.17) = .9567$$

$$K_2 = 1 - \frac{1+.65}{(2)(}\cot(22.17) = .7957$$

* ROARK, R J, <u>FORMULAS FOR STRESS AND STRAIN</u>, McGRAW-HILL, NEW YORK, 1954, p. 272.

$$\frac{\delta_R^Q}{Q} = \frac{10^{-5}}{(1.29)(2.53)} (.99105)(151.7)(.37706)^2 \left(.9567 + \frac{1}{.7957} \right)$$

$$= 1.45 \cdot 10^{-3} \ \text{in/lb/in}$$

$$\frac{\theta^Q}{Q} = \frac{10^{-5}}{(1.29)(2.53)} (2.0)(.99105)^2 (.37706) \left(\frac{1}{.9567} \right)$$

$$= 2.37 \ 10^{-4} \ \text{rad/lb/in}$$

$$\frac{\delta_R^{M_o}}{M_o} = \frac{1}{Et} \left(\frac{2\beta^2 \sin\phi}{K_1} \right) = 2.37 \ 10^{-4} \ \text{in/lb-in/in}$$

$$\frac{\theta^{M_o}}{M_o} = \frac{1}{Et} \left(\frac{4\beta^3}{R_2 K_1} \right) = \frac{10^{-5}}{(1.29)(2.53)} \frac{(4.0)(.99105)^3}{(151.7)(.9567)}$$

$$= 8.22 \ 10^{-6} \ \text{rad/lb in/in}$$

TO DETERMINE BEAM OF EQUIVALENT STIFFNESS

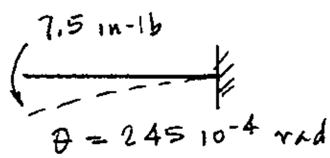

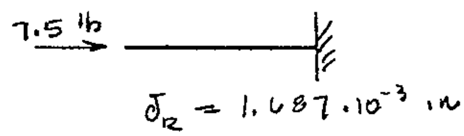

$$I = \frac{M_o L}{E\theta} = \frac{(7.5)(10)}{(12.9)(2.45)}$$

$$I = 2.37 \ \text{in}^4$$

$$A = \frac{PL}{E\delta} = \frac{(7.5)(10)}{(129)(1.687)}$$

$$A = 0.345 \ \text{in}^2$$

RADIAL STIFFNESS OF FORWARD BULKHEAD

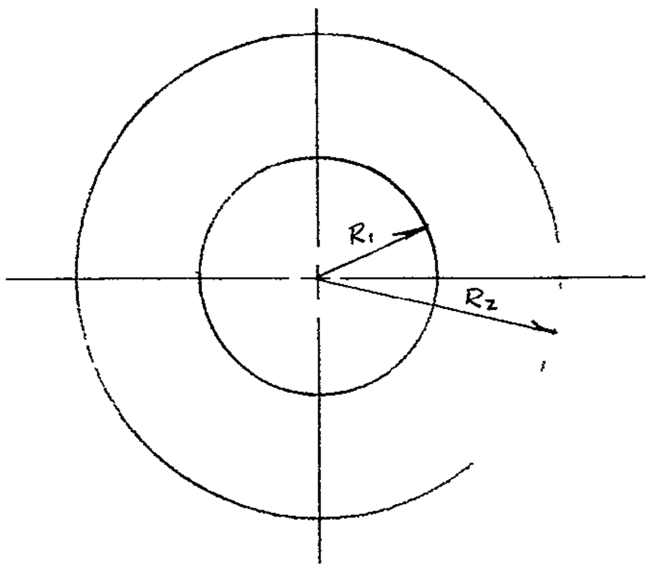

R_1 = 17.4 in

R_2 = 34 8 in

r = 1 42 in

ν = .325

E = $10.6 \cdot 10^6$ psi

t_f = .070 in

CONSIDER INNER EDGE CLAMPED DUE TO RIGIDITY OF 'ESCAPE TOWER'

ASSUME PIE SECTIONS OF PLATE TO DEVELOP EQUIVALENT BEAMS (θ IS INCLUDED ANGLE)

$$A = 2\theta t_f \left(\frac{R_1 + R_2}{2}\right) = 3.654\,\theta$$

$$I = 2\theta t_f \left(\frac{R_1 + R_2}{2}\right)\left(\frac{r}{2}\right)^2 = 1845\,\theta$$

TO DETERMINE THE EFFECT OF ECCENTRIC STIFFNERS CONSIDER THE FOLLOWING TWO CROSS-SECTIONS

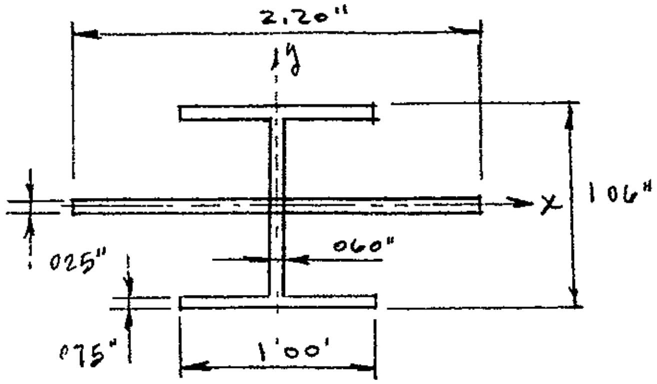

SECTION 1

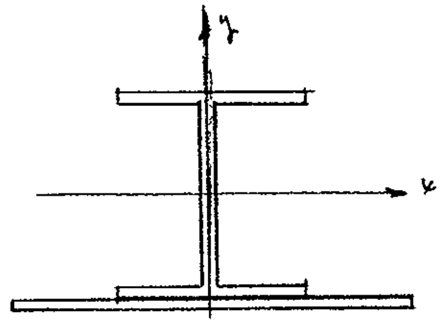

SECTION 2

$A = (.025)(2.2) + (2)(.075)(1.0) + (.060)(.91) = .2596 \text{ in}^2$

FOR SECTION 1

$\bar{y} = 0$

$I_x = \dfrac{(.06)(.91)^3}{12} + (2)(.075)(.493)^2 = .0403 \text{ in}^4$

FOR SECTION 2

$\bar{y} = -\dfrac{(.025)(2.2)(.543)}{.2596} = -.115$

$I_x = .0403 + (.2596)(.115)^2 + (.025)(2.2)(.428)^2 = .0538 \text{ in}^4$

THE CONCLUSION IS THAT THE ECCENTRICITIES HAVE TO BE MODELED. THIS MEANS THAT SUBSTITUTE NODES WILL HAVE TO BE USED IN THE FINITE ELEMENT ANALYSIS.

ACCESS HATCH CHANNEL

MATERIAL 5 ALUM

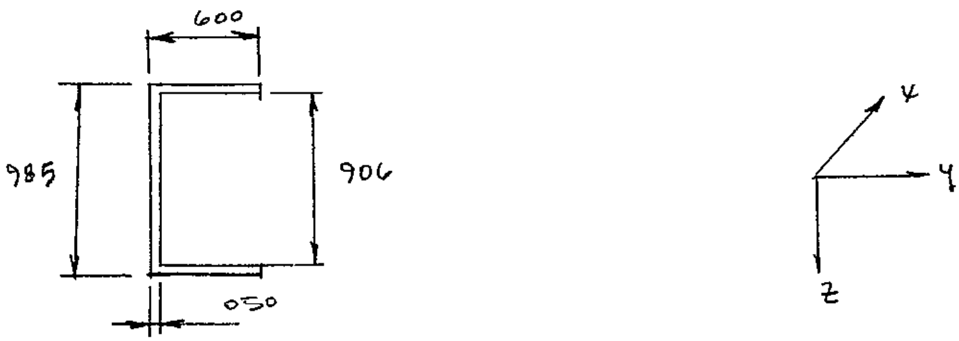

$$A_x = (0.6)(.079) + (.906)(.05) = .0927 \text{ in}^2$$

$$J_x = \Sigma \frac{t^3}{3} d = 2 \frac{(.04)^3}{3}(.6) + (.906)\frac{(.05)^3}{3} = .0000634 \text{ in}^4$$

$$A_y = (0.6)(.079) = .0474 \text{ in}^2$$

$$\bar{y} = \frac{(.079)(.6)(.3) + .906)(.05)(.025)}{.0927} = .1655 \text{ in}$$

$$I_z = \frac{(.079)(.6)^3}{12} + (.079)(.6)(.1345)^2 + (.05)(.906)(.1405)^2$$

$$= .00317 \text{ in}^4$$

$$A_z = (0.985)(.05) = .04925 \text{ in}^2$$

$$I_y = \frac{(.906)^3(.05)}{12} + (2)(.0237)(.473)^2 = .00416 \text{ in}^4$$

WINDOW RECESS MEMBERS

MATERIAL . I ALUM

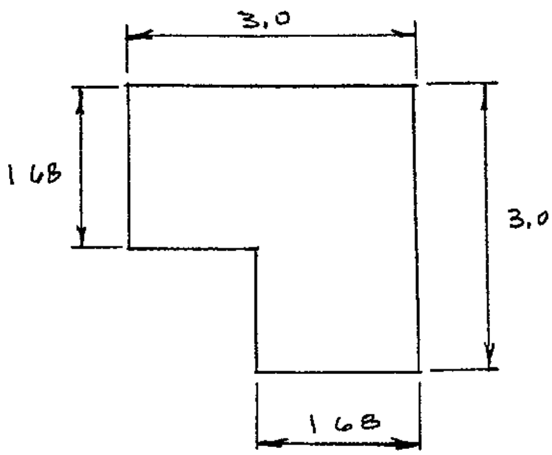

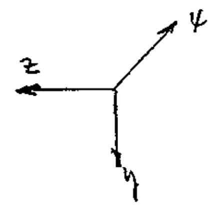

$A_x = (3.0)(3.0) - (1.32)(1.32) = 7.26 \text{ in}^2$

$J_x = I_z + I_y = 15.56 \text{ in}^4$

$A_y = 7.26 \text{ in}^2$

$$\bar{y} = \bar{z} = \frac{(1.68)(3.0)(2.16) + 1.68)(1.32)(.66)}{7.26} = 1.7 \text{ in}$$

$$I_z = \frac{1.68)(3.0)^3}{12} + \frac{(1.32)(1.68)^3}{12} + (1.32)(1.68)(1.04)^2 + 1.68)(3.0)(.46)^2$$

$I_z = 7.78 \text{ in}^4$

$A_z = 7.26 \text{ in}^2$

$I_y = 7.78 \text{ in}^4$

FORWARD SIDE WALL STIFFNER

MATERIAL : 6 ALUM

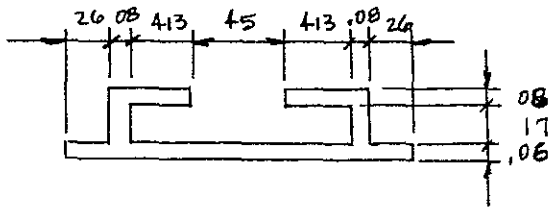

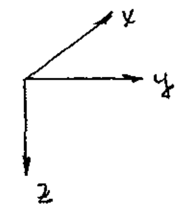

$$A_x = (1956)(.06) + (2)(.17)(.08) + (2)(493)(.08) = 223 \text{ in}^2$$

$$J_x = \Sigma \frac{dt^3}{3} = \frac{(1956)(.06)^3}{3} + \frac{(2)(.17)(.08)^3}{3} + \frac{(2)(493)(08)^3}{3}$$

$$J_x = 000368 \text{ in}^4$$

$$A_y = (2)(493)(08) + 1956)(06) = .196 \text{ in}^2$$

$$\bar{z} = \frac{(1956)(06)(03) + (2)(17)(08)(145) + (2)(.443)(08)(27)}{223}$$

$$\bar{z} = 129$$

$$I_z = \frac{06)(1956)^3}{12} + (2)\frac{(493)^3(.08)}{12} + (2)(493)(.08)(.471)^2 + (2)(.17)(08)(670)^2$$

$$I_z = 0679 \text{ in}^4$$

$$A_z = (2)(31)(.08) = 0497 \text{ in}^2$$

$$I_y = \frac{.08)(.17)^3}{12} + (2)(493)(08)(141)^2 + (1956)(.06)(099)^2$$

$$I_y = .00275 \text{ in}^4$$

AFT SIDE WALL STIFFNER

MATERIAL 6 ALUM

$x_c = 12$ TO $x_c = 32$

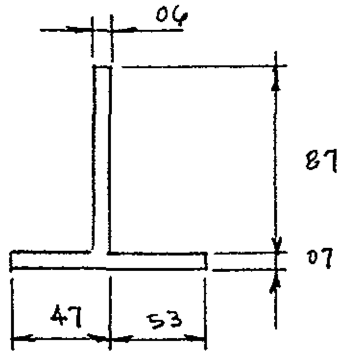

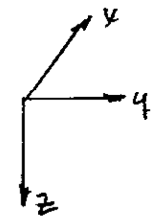

$x_c = 32$ TO $x_c = 42$

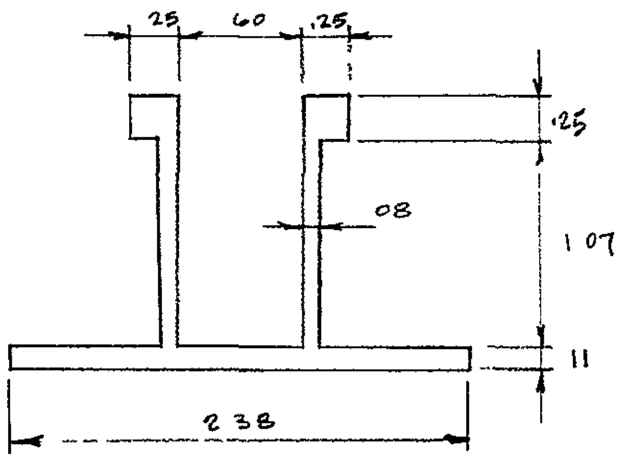

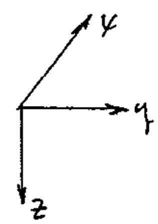

$x_c = 12$ TO $x_c = 32$

$$A_x = (06)(.87) + (1\,0)(07) = 122 \text{ in}^2$$

$$J_x = \Sigma \frac{dt^3}{3} = \frac{1\,0)(.07)^3}{3} + \frac{(87)(06)^3}{3} = .000177 \text{ in}^4$$

$$\bar{y} = \frac{(44)(06)(87) + (5)(07)(1\,0)}{.122} = 475 \text{ in}$$

$$\bar{z} = \frac{(.503)(06)(87) + (035)(07)(1.0)}{122} = .236 \text{ in}$$

$$A_y = 07 \text{ in}^2$$

$$I_z = \frac{(.07)(1\,0)^3}{12} + (07)(1\,0)(.025)^2 + (06)(.87)(035)^2$$

$$I_z = 00594 \text{ in}^4$$

$A_z = .0522 \text{ in}^2$

$I_y = \frac{(.06)(.87)^3}{12} + (.06)(.87)(.269)^2 + (.07)(1.0)(.201)^2$

$I_y = .0099 \text{ in}^4$

$y_c = 32 \text{ To } x_c = 42$

$A_x = (2)(.08)(1.07) + (2)(.25)(.25) + (2.38)(.11) = .558 \text{ in}^2$

$J_x = \Sigma \frac{dt^3}{3} = (2)(.08)^3\frac{(1.32)}{3} + \frac{(2.38)}{3}(.11)^3 = .00151 \text{ in}^4$

$\bar{z} = \frac{(2.38)(.11)(.055) + (2)(.08)(1.07)(.645) + (2)(.25)(.25)(1.305)}{.558}$

$\bar{z} = .517 \text{ in}$

$A_y = (2.38)(.11) + 2(.25)(.25) = .387 \text{ in}^2$

$I_z = \frac{(.11)(2.38)^3}{12} + (2)(.25)(.25)(.425)^2 + (2)(.08)(1.07)(.34)^2$

$I_z = .166 \text{ in}^4$

$A_z = (2)(.08)(1.18) + (2)(.25)(.25) = .314 \text{ in}^2$

$I_y = \frac{(.08)(1.07)^3}{12} + (2)(.08)(1.07)(.128)^2 + (2)(.25)(.25)(.788)^2 + (.11)(2.38)(.462)^2$

$I_y = .145 \text{ in}^4$

LONGERONS

MATERIAL . 6 ALUM

$x_c = 42$ TO $x_c = 51\ 5$

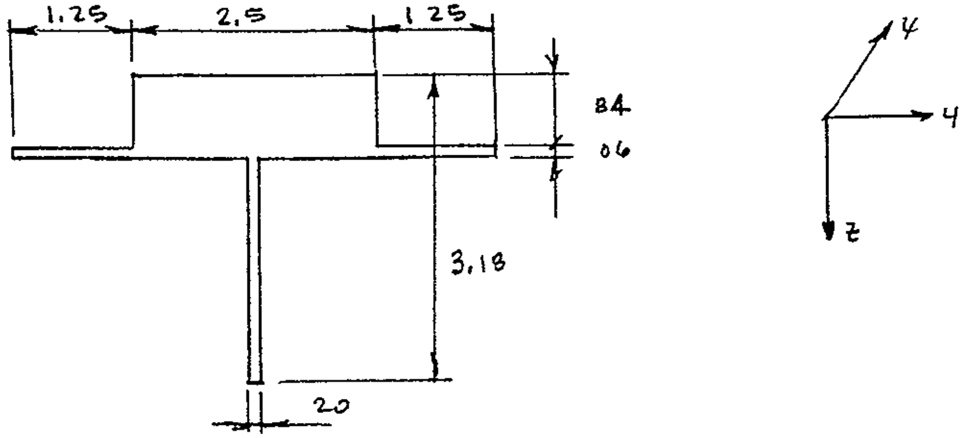

$x_c = 51.5$ TO $x_c = 61.0$

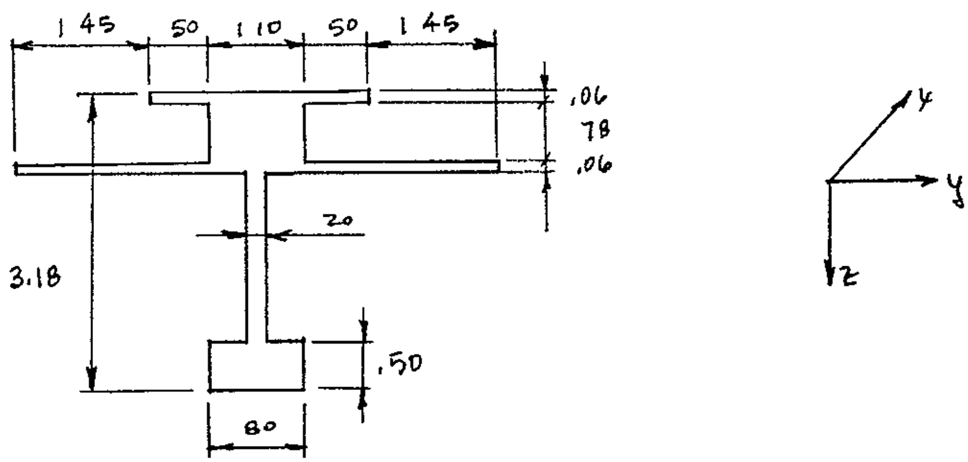

$x_c = 61\ 0$ TO $x_c = 70.5$

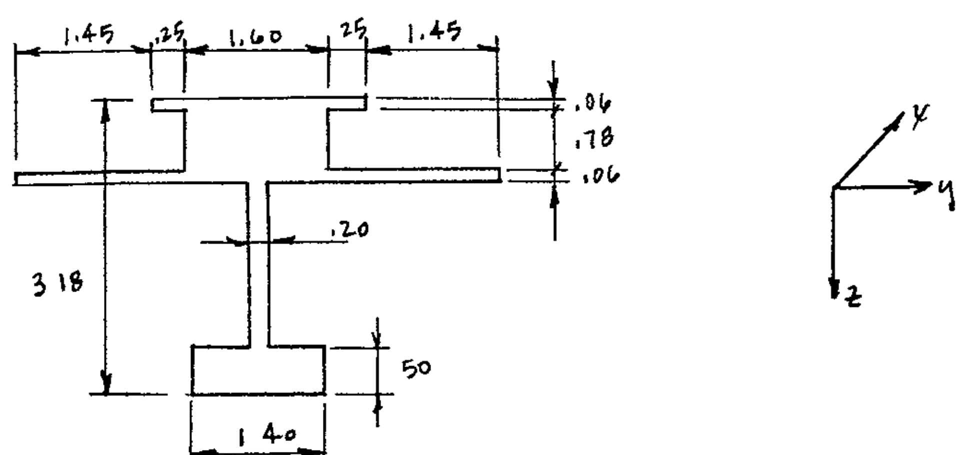

$X_c = 70.5$ TO $X_c = 80$

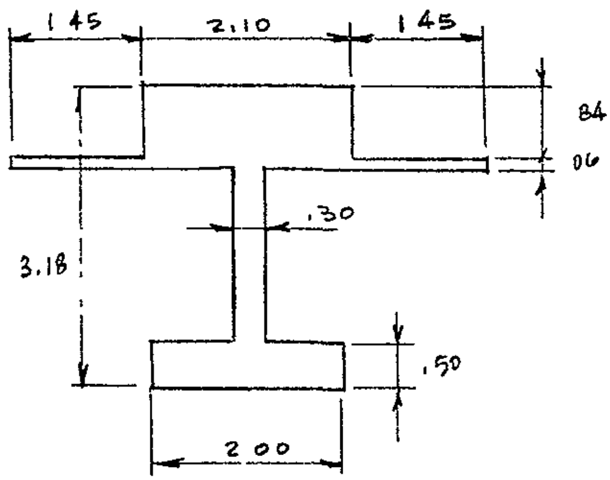

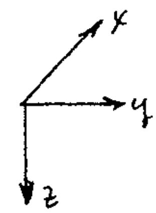

$X_c = 42.0$ TO $X_c = 51.5$

$A_x = (2)(.125)(.06) + (2.28)(.20) + (2.5)(.9) = 2.721 \, in^2$

$J_x = I_y + I_z + (2)(1.25)\frac{(.06)^3}{3} = I_y + I_z + .00018$

$J_x = 2.55 \, in^4$

$\bar{z} = \frac{(.20)(2.28)(1.14) + (2)(1.25)(.06)(2.31) + (2.5)(.9)(2.73)}{2.72} = 2.465 \, in$

$A_y = (2)(1.25)(.06) + (2.5)(.9) = 2.27 \, in^2$

$I_y = \frac{(2.5)(.9)^3}{12} + \frac{(2)(2.28)^3}{12} + (2)(1.25)(.06)(1.55)^2 + (2)(2.28)(1.325)^2 + (2.25)(.24$

$I_y = 1.31 \, in^4$

$A_z = (.2)(2.28) + (2.5)(.9) = 2.71 \, in^2$

$I_z = \frac{(.9)(2.5)^3}{12} + \frac{(2.28)(.2)^3}{12} + (2)(1.25)(.06)(1.875)^2 + \frac{(2)(.06)}{12}(1.25)^3 = 1.25 \, in$

$X_c = 51.5$ TO $X_c = 61.0$

$A_x = (2)(1.95)(.06) + (2)(.50)(.06) + (1.78)(.2) + (.5)(.3) + (1.10)(.9) = 2.04 \, in^2$

$J_x = I_y + I_z + (2)(1.95)\frac{(.06)^3}{3} + (2)(.5)\frac{(.06)^3}{3} = I_y + I_z + .000353$

$J_x = 1.88 \, in^4$

$\bar{z} = \frac{(.4)(.25) + (.356)(1.39) + (2)(1.95)(.06)(2.31) + (2)(.5)(.06)(3.15) + (.99)(2.73)}{2.04}$

$\bar{z} = 1.965 \, in$

$$A_y = (2)(1.95)(.06) + (2)(.5)(.06) + (.8)(.5) + (1.1)(.9) = 1.68 \text{ in}^2$$

$$I_z = \frac{(.9)(1.1)^3}{12} + \frac{(1.78)(.2)^3}{12} + \frac{(.5)(.8)^3}{12} + (2)(.5)(.06)(.8)^2 + (2)(1.95)(.06)(.525)^2$$
$$+ (2)\frac{(.06)(.5)^3}{12} + (2)\frac{(.06)(1.95)^3}{12} = .781 \text{ in}^4$$

$$A_z = (.5)(.8) + (1.1)(.9) + (.2)(1.78) = 1.75 \text{ in}^2$$

$$I_y = \frac{(1.10)(.9)^3}{12} + \frac{(.2)(1.78)^3}{12} + \frac{(.8)(.5)^3}{12} + (2)(.5)(.06)(1.185)^2 + (2)(1.95)(.06)(.345)^2$$
$$+ (.8)(.5)(1.715)^2 + (.2)(1.78)(.575)^2 + (1.1)(.9)(.765)^2 = 1.10 \text{ in}^4$$

$x_c = 610$ TO $x_c = 705$

$$A_x = (2)(1.7)(.06) + (2)(.25)(.06) + (1.78)(.2) + (.5)(1.4) + (1.60)(.9) = 2.73 \text{ in}^2$$

$$J_x = I_x + I_y + (2)(.25)\frac{(.06)^3}{3} + (2)(1.7)\frac{(.06)^3}{3} = I_x + I_y + .000281$$

$$J_x = 4.33 \text{ in}^4$$

$$\bar{z} = \frac{(.7)(.25) + (.356)(1.39) + (2)(1.7)(.06)(2.31) + (2)(.25)(.06)(3.15) + (1.44)(2.73)}{2.73}$$

$$\bar{z} = 1.89 \text{ in}$$

$$A_y = (2)(1.7)(.06) + (2)(.25)(.06) + (1.6)(.9) + (.5)(1.4) = 2.37 \text{ in}^2$$

$$I_z = \frac{(.9)(1.6)^3}{12} + \frac{(1.78)(.2)^3}{12} + \frac{(.5)(1.4)^3}{12} + (2)(.25)(.06)(.925)^2 + (2)(1.7)(.06)(1.65)^2$$
$$+ 2(.06)\frac{(.25)^3}{12} + (2)(.06)\frac{(1.7)^3}{12} = 1.05 \text{ in}^4$$

$$A_z = (.5)(1.4) + (.2)(1.78) + (1.6)(.9) = 2.50 \text{ in}^2$$

$$I_y = \frac{(1.6)(.9)^3}{12} + \frac{(.2)(1.78)^3}{12} + \frac{(1.4)(.5)^3}{12} + (2)(.25)(.06)(1.26)^2 + (2)(1.7)(.06)(.42)^2$$
$$+ (1.4)(.5)(1.64)^2 + (.2)(1.78)(.5)^2 + (1.6)(.9)(.84)^2 = 3.28 \text{ in}^4$$

$x_c = 705$ TO $x_c = 800$

$$A_x = (2)(1.45)(.06) + (1.78)(.3) + (.5)(2.0) + (2.10)(.9) = 3.62 \text{ in}^2$$

$$J_x = I_x + I_y + (2)(1.45)\frac{(.06)^3}{3} = I_x + I_y + .000209$$

$$J_x = 5.57 \text{ in}^4$$

$$\bar{z} = \frac{(1.0)(.25) + (.534)(1.39) + (2)(1.45)(.06)(2.31) + (1.89)(2.73)}{3.62} = 1.82 \text{ in.}$$

$$A_y = (2)(1.45)(.06) + (2.10)(.9) + (.5)(2.0) = 3.06 \text{ in}^2$$

$$I_z = \frac{(.9)(2.1)^3}{12} + \frac{(1.78)(.3)^3}{12} + \frac{(.5)(2.0)^3}{12} + (2)(1.45)(.06)(1.775)^2 + (2)\frac{(.06)(1.45)^3}{12}$$

$$I_z = 1.11 \text{ in}^4$$

$$A_z = (2.1)(.9) + (.3)(1.78) + (.5)(2.0) = 3.42 \text{ in}^2$$

$$I_y = \frac{(2.1)(.9)^3}{12} + \frac{(.3)(1.78)^3}{12} + \frac{(2.0)(.5)^3}{12} + (2)(1.45)(.06)(.49)^2$$
$$+ (2.0)(.5)(1.57)^2 + (.3)(1.78)(.43)^2 + (2.1)(.9)(.91)^2 = 4.46 \text{ in}^4$$

WINDOW FRAMES

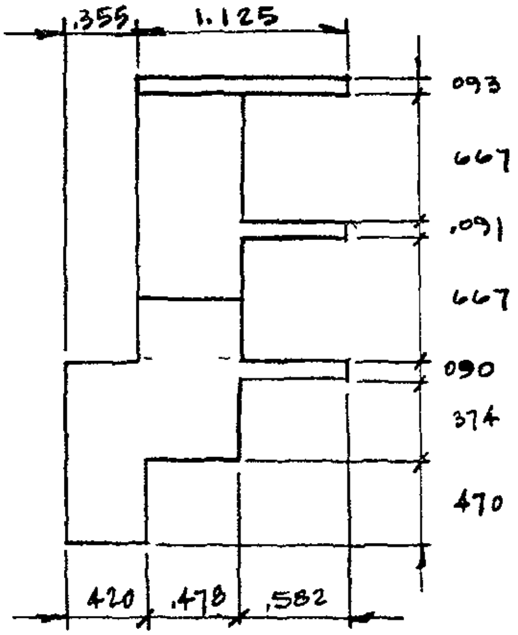

MATERIAL. ALUM

SCIENTIFIC SIDE WINDOW

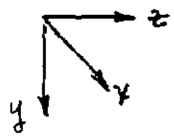

SIDE WINDOW

$$A_x = (.42)(.47) + (.898)(.464) + (.582)(.274) + (1.518)(.543) = 1.60 \text{ in}^2$$

$$J_x = I_x + I_y + \frac{.582}{3}\left((.090)^3 + (.091)^3 + (.093)^3\right) = I_x + I_y + .000444$$

$$J_x = 0.900 \text{ in}^4$$

$$A_x \bar{z} = (.42)(.47)(.235) + (.898)(.464)(.702) + (.543)(1.518)(1.693)$$
$$+ (.09)(.582)(.889) + (.091)(.582)(1.646) + (.093)(.582)(2.405) = 1.996$$

$$\bar{z} = 1.25 \text{ in}$$

$$A_x \bar{y} = (.42)(.47)(.21) + (.898)(.464)(.449) + (.543)(1.518)(.627)$$
$$+ (.274)(.582)(1.189) = .9354$$

$$\bar{y} = .585 \text{ in}$$

$A_y = 1.60 \text{ in}^2$ (A_z FOR SIDE WINDOW)

$$I_z = \frac{(.47)(.42)^3}{12} + \frac{(.464)(.898)^3}{12} + \frac{(1.518)(.543)^3}{12} + \frac{(.274)(.582)^3}{12}$$
$$+ (.47)(.42)(.375)^2 + (.898)(.464)(.136)^2 + (.543)(1.518)(.042)^2$$
$$+ (.274)(.582)(.604)^2 = .151 \text{ in}^4$$ (I_y FOR SIDE WINDOW)

$A_z = 1.44 \text{ in}^2$ (A_y FOR SIDE WINDOW)

$$I_y = \frac{(42)(47)^3}{12} + \frac{(.898)(464)^3}{12} + \frac{(.543)(1\,518)^3}{12} + (47)(42)(1\,015)^2$$
$$+ (898)(.464)(548)^2 + (.543)(1.518)(443)^2 + (.09)(.582)(361)^2$$
$$+ (091)(.582)(396)^2 + (.093)(.582)(1\,155)^2 = 748 \text{ in}^4$$

(I_z FOR SIDE WINDOW)

RING AT R = 34 8 in

MATERIAL 5 ALUM

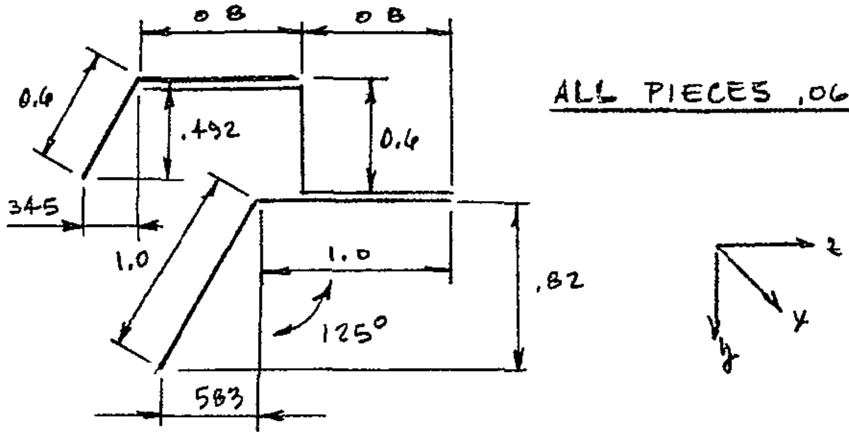

ALL PIECES .060"

$$A_x = .06\,(6 + 1.0 + 1.0 + .8 + .6 + .8 + 8) = .336\ in^2$$

$$J_x = \Sigma\frac{dt^3}{3} = \frac{(.06)^3}{3}(5.6) = .000403\ in^4$$

$$\bar{y} = \frac{(1\ 0)(\ 41) + (1.0)(.82) + (\ 8)(.82) + (.6)(1\ 12) + (1.6)(1\ 42) + (.6)(1\ 174)}{5.6}$$

$$\bar{y} = 99\ in$$

$$\bar{z} = \frac{(1\ 0)(1\ 292) + (1.0)(.5) + (8)(\ 4) + (.6)(.8) + (1.6)(1.2) + (.6)(1.772)}{5.6}$$

$$\bar{z} = 995\ in$$

$$A_y = 06\,(\ 82 + .6 + .492) = .115\ in^2$$

$$I_z = \frac{(\ 06)(.6)^3}{12} + \frac{(06)(.492)^3}{12} + \frac{(.06)(.82)^3}{12} + (.06)(.58)^2 + (.06)(\ 17)^2$$
$$+ (048)(.17)^2 + (.036)(\ 13)^2 + (.096)(.43)^2 + (.036)(.184)^2 = 0428\ in^4$$

$$A_z = .06\,(.583 + 1.0 + .8 + 1.6 + .345) = .260\ in^2$$

$$I_y = \frac{(.06)(\ 583)^3}{12} + \frac{(.06)(1)^3}{12} + \frac{(.06)(.8)^3}{12} + \frac{(12)(.8)^3}{12} + \frac{(.06)(.345)^3}{12}$$
$$+ (.06)(\ 297)^2 + (.06)(\ 495)^2 + (.048)(.595)^2 + (.036)(.195)^2$$
$$+ (.096)(\ 205)^2 + (036)(.777)^2 = .0768\ in^4$$

RING AT R = 57.2 in

MATERIAL . 5 ALUM

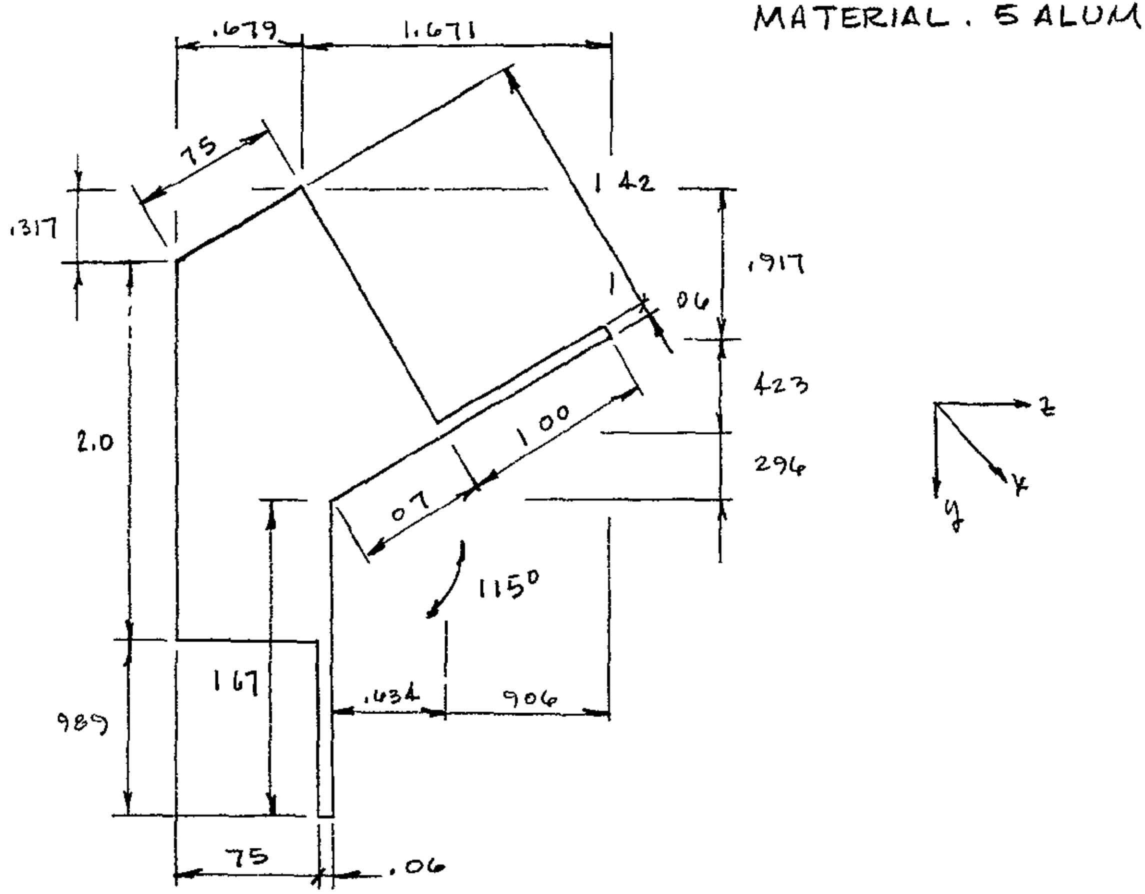

$$A_x = (.06)(1.67) + (.06)(1.0) + (.75)(1.48) + (.75)(.681) + (1.319)(.375) = 2.28\ in^2$$

$$J_x = I_y + I_z + \frac{(1.989)(.06)^3}{3} = I_y + I_z + .000143 = 1.17\ in^4$$

$$A_x\bar{y} = (.06)(1.67)(.83) + (.06)(1.0)(2.178) + (.75)(1.48)(2.483) + (.75)(.681)(1.33)$$
$$+ (1.319)(.375)(2.11) = 4.693$$

$$\bar{y} = 2.06\ in$$

$$A_x\bar{z} = (.06)(1.67)(.78) + (.06)(1.0)(1.897) + (.75)(1.48)(.722) + (.75)(.681)(.375)$$
$$+ (1.319)(.375)(.25) = 1.309$$

$$\bar{z} = .575\ in$$

$$A_y = 2.12 + (.06)(.989) + (.06)(.423) = 2.20\ in^2$$

$$I_z = \frac{(.06)(1.67)^3}{12} + \frac{(.06)(.423)^3}{12} + \frac{(.75)(1.34)^3}{12} + \frac{(.75)(.681)^3}{12} + \frac{(.75)(1.319)^3}{36}$$
$$+ (.06)(1.67)(1.23)^2 + (.06)(1.0)(.118)^2 + (.75)(1.48)(.423)^2$$
$$+ (.75)(.681)(.73)^2 + (1.319)(.375)(.05)^2 = .865\ in^4$$

$$A_z = 2.12 + (.06)(.906) = 2.17 \text{ in}^2$$

$$I_y = \frac{(.06)(.906)^3}{12} + \frac{(.75)(.626)^3}{12} + \frac{(.681)(.75)^3}{12} + \frac{(1.319)(.75)^3}{36}$$
$$+ (.06)(1.67)(.215)^2 + (.06)(1.0)(1.322)^2 + (.75)(1.48)(.147)^2$$
$$+ (.75)(.681)(.2)^2 + (1.319)(.375)(.325)^2 = .306 \text{ in}^4$$

RING AT R = 59.6 in

MATERIAL . 5 ALUM

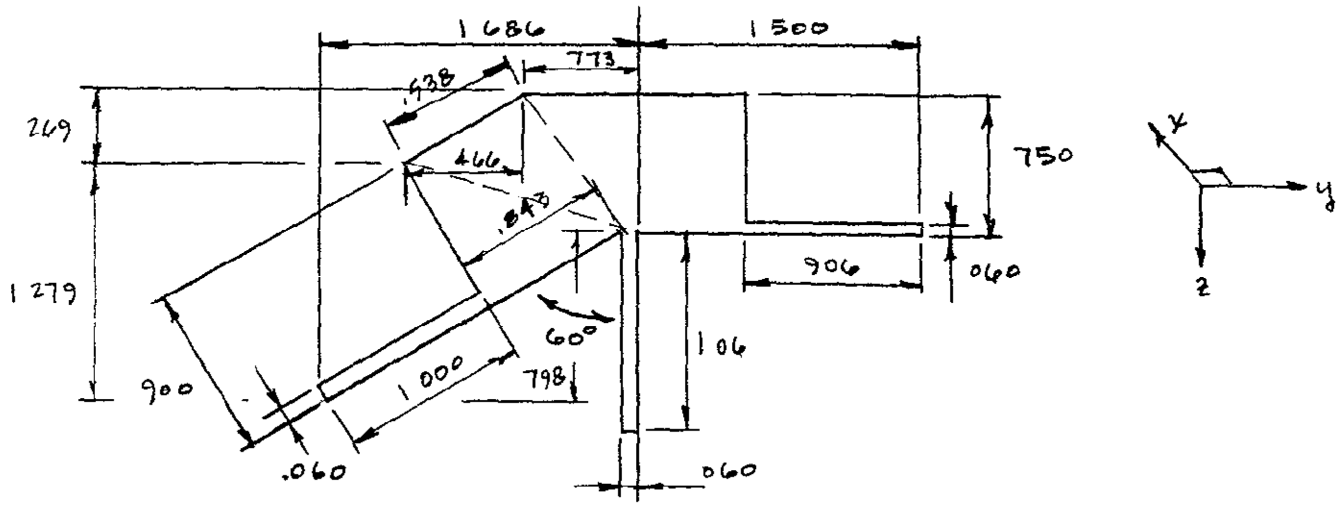

$$A_x = (.06)(1.0) + (.06)(1.06) + (.06)(.906) + (.75)(.594) + (.75)(.417) + (.691)(.90) = 1.56 \text{ in}^2$$

$$J_x = I_y + I_z + \frac{(3.02)(.06)^3}{3} = I_y + I_z + .000218 = .656 \text{ in}^4$$

$$A_x \bar{z} = (.06)(1.0)(.512) + (.06)(1.06)(.53) + (.06)(.906)(1.09) + (.75)(.594)(1.435) + (.843)(.45)(1.144) + (.538)(.45)(1.46) + (.773)(.375)(1.56) = 2.002$$

$$\bar{z} = 1.285 \text{ in}$$

$$A_x \bar{y} = (.06)(1.0)(.462) + (.06)(1.06)(1.656) + (.06)(.906)(2.733) + (.75)(.594)(1.903) + (.843)(.45)(.979) + (.538)(.45)(.908) + (.773)(.375)(1.428) = 2.17$$

$$\bar{y} = 1.39 \text{ in}$$

$$A_y = 1.421 + (.06)(.906) + (.06)(.867) = 1.53 \text{ in}^2$$

$$I_z = \frac{(.06)(.867)^3}{12} + \frac{(.06)(.906)^3}{12} + \frac{(.75)(.594)^3}{12} + \frac{(.75)(.773)^3}{36} + \frac{(.9)(.538)^3}{36} + \frac{(.843)(.9)^3}{36} + (.06)(1.0)(.928)^2 + (.06)(1.06)(.266)^2 + (.06)(.906)(1.343)^2 + (.75)(.594)(.593)^2 + (.843)(.45)(.411)^2 + (.538)(.45)(.482)^2 + (.773)(.375)(.038)^2 = .472 \text{ in}^4$$

$$A_z = 1.421 + (.06)(1.06) + (.06)(.5) = 1.52 \text{ in}^2$$

$$I_y = \frac{(.06)(.5)^3}{12} + \frac{(.06)(1.06)^3}{12} + \frac{(.594)(.75)^3}{12} + \frac{(.773)(.75)^3}{36} + \frac{(.538)(.9)^3}{36} + \frac{(.9)(.843)^3}{36} + (.06)(1.0)(.773)^2 + (.06)(1.06)(.755)^2 + (.06)(.906)(.185)^2 + (.75)(.594)(.15)^2 + (.843)(.45)(.141)^2 + (.538)(.45)(.175)^2 + (.773)(.375)(.275)^2 = .183 \text{ in}^4$$

THE FOLLOWING MATERIAL PROPERTIES FOR THE SCIENTIFIC SIDE WINDOW GASKET WERE DETERMINED FROM THE DATA SUPPLIED BY FRED CLARK OF NORTH AMERICAN AVIATION

SHORE HARDNESS OF 55 (SUPPLIED DATA)
$E = 1200$ psi*
$G = 400$ psi (CALCULATED)
$\nu = 0.50$ (ASSUMED)

THE FOLLOWING DATA ON THE SHELL STRUCTURE WAS SUPPLIED BY JIM GOBLE OF NORTH AMERICA AVIATION

HONEYCOMB - 5052 HEXCELL

FORWARD SIDE WALL	0.94 in
AFT SIDE WALL	0.75 in
AFT BULKHEAD	1.50 in

SKIN - 2014-T6 ALUMINUM

FORWARD SIDE WALL	
NEAR WINDOW	0.030 in
OTHER	0.020 in
AFT SIDE WALL	0.025 in
AFT BULKHEAD	0.016 in

* GOODYEAR TIRE AND RUBBER CO, INC, <u>HANDBOOK OF MOLDED AND EXTRUDED RUBBER</u>, AKRON, OHIO, 1949

EQUIVALENT PLATE ELEMENT FOR HONEYCOMB ELEMENTS *

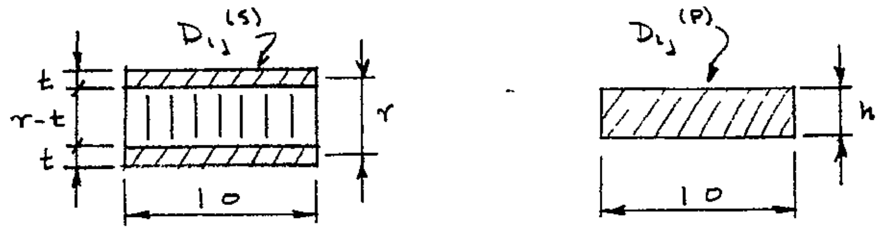

$D_{ij}^{(P)} = \alpha D_{ij}^{(S)}$ $\quad i,j = 1,2,3,4$

$D_{ij}^{(P)} = \beta D_{ij}^{(S)}$ $\quad i,j = 5,6$

$\alpha = \dfrac{2t}{\sqrt{3}\, r}$ $\quad h = \sqrt{3}\, r$

$\beta = \dfrac{1}{\sqrt{3}}$

FORWARD SIDE WALL – NEAR WINDOW

$t = .030$ in $\quad r = .97$ in

$\alpha = \dfrac{(2)(.03)}{(1.732)(.97)} = .0357$ $\quad \beta = .578$

$h = (1.732)(.97) = 1.68$ in

FORWARD SIDE WALL - OTHER

$t = .020$ in $\quad r = .96$ in

$\alpha = \dfrac{(2)(.02)}{(1.732)(.96)} = .0240$ $\quad \beta = .578$

$h = (1.732)(.96) = 1.66$ in

AFT SIDE WALL

$t = .025$ $\quad r = .775$

$\alpha = \dfrac{(2)(.025)}{(1.732)(.775)} = .0372$ $\quad \beta = .578$

$h = (1.732)(.775) = 1.34$ in

* LANG, T. E., "STRUCTURAL ANALYSIS AND MATRIX INTERPRETIVE SYSTEM (SAMIS), USER REPORT", JPL TM 33-305, PASADENA CALIFORNIA, MARCH, 1967

SCIENTIFIC SIDE WINDOW

$t = .563 \text{ in} \qquad r = 813 \text{ in}$

$\alpha = \dfrac{(2)(.563)}{(1732)(.813)} = 799 \qquad \beta = .578$

$h = (1732)(.813) = 141 \text{ in}$

SIDE WINDOW

$t = 191 \text{ in} \qquad r = 467 \text{ in}$

$\alpha = \dfrac{(2)(191)}{(1732)(.467)} = 472 \qquad \beta = .578$

$h = (1732)(.467) = .82 \text{ in}$

AFT BULKHEAD

$t = 016 \text{ in} \qquad r = 1.516 \text{ in}$

$\alpha = \dfrac{(2)(016)}{(1.732)(1.516)} = 0122 \qquad \beta = 578$

$h = (1732)(1.516) = 253 \text{ in.}$

FORWARD BULKHEAD

$t = 070 \text{ in} \qquad r = 0.82$

$\alpha = \dfrac{(2)(070)}{(1732)(0\,82)} = 0984 \qquad \beta = 578$

$h = (1732)(0.82) = 142 \text{ in}$

MATERIAL TABLE CONSTANTS

2014-T6 ALUMINUM

$E = 10.6 \cdot 10^6$ psi

$\nu = .325$

$$D_{11} = \frac{E(1-\nu)}{(1+\nu)(1-2\nu)} = D_{22} = D_{44}$$

$$D_{21} = \frac{\nu E}{(1+\nu)(1-2\nu)} = D_{41} = D_{42}$$

$$D_{55} = \frac{E}{2(1+\nu)} = D_{33} = D_{66}$$

$$D_{31} = D_{32} = D_{43} = D_{65} = 0$$

$$D_{11} = \frac{(10.6)(.675)}{(1.325)(.35)} \cdot 10^6 = 15.4 \cdot 10^6$$

$$D_{21} = \frac{(.325)(10.6)}{(1.325)(.35)} 10^6 = 7.42 \cdot 10^6$$

$$D_{55} = \frac{10.6}{(2)(1.325)} 10^6 = 4.0 \; 10^6$$

GLASS

$E = 10.5 \; 10^6$ psi

$\nu = .16$

$$D_{11} = \frac{(10.5)(.84)}{(1.16)(.68)} \cdot 10^6 = 11.2 \; 10^6$$

$$D_{21} = \frac{(.16)(10.5)}{(1.16)(.68)} 10^6 = 2.13 \cdot 10^6$$

$$D_{55} = \frac{10.5}{2(1.16)} 10^6 = 4.53 \cdot 10^6$$

7075-T6 ALUMINUM

$E = 10.4 \; 10^6$ psi $\quad \nu = .333$

$$D_{11} = \frac{(10.4)(.667)}{(1.333)(.333)} 10^6 = 15.6 \; 10^6$$

$$D_{21} = \frac{(.333)(10.4)}{(1.333)(.333)} \cdot 10^6 = 7.8 \; 10^6$$

$$D_{55} = \frac{10.4}{(2)(1.333)} 10^6 = 3.9 \cdot 10^6$$

FORWARD SIDE WALL - NEAR WINDOW

DESIGNATION: 1ALUM

$D_{11} = (.0357)(15.4\ 10^6) = 5.5\ 10^5 = D_{22} = D_{44}$

$D_{21} = (.0357)(7.42 \cdot 10^6) = 2.65\ 10^5 = D_{41} = D_{42}$

$D_{33} = (\ 0357)(4\ 0\ 10^6) = 1\ 43 \cdot 10^5$

$D_{55} = (.578)(4\ 0\ 10^6) = 2.312 \cdot 10^6 = D_{66}$

$D_{31} = D_{32} = D_{43} = D_{65} = 0$

FORWARD SIDE WALL - OTHER

DESIGNATION 2ALUM

$D_{11} = (.024)(15.4 \cdot 10^6) = 3.7 \cdot 10^5 = D_{22} = D_{44}$

$D_{21} = (\ 024)(7\ 42\ 10^6) = 1\ 78\ 10^5 = D_{41} = D_{42}$

$D_{33} = (.024)(4\ 0\ 10^6) = 9.6 \cdot 10^4$

$D_{55} = (\ 578)(4.0\ 10^6) = 2\ 312 \cdot 10^6 = D_{66}$

$D_{31} = D_{32} = D_{43} = D_{65} = 0$

AFT SIDE WALL

DESIGNATION 3 ALUM

$D_{11} = (.0372)(15.4 \cdot 10^6) = 5.73 \cdot 10^5 = D_{22} = D_{44}$

$D_{21} = (.0372)(7.42 \cdot 10^6) = 2\ 76 \cdot 10^5 = D_{41} = D_{42}$

$D_{33} = (.0372)(4.0\ 10^6) = 1\ 49 \cdot 10^5$

$D_{55} = (.578)(4.0\ 10^6) = 2.312 \cdot 10^6 = D_{66}$

$D_{31} = D_{32} = D_{43} = D_{65} = 0$

SCIENTIFIC SIDE WINDOW

DESIGNATION · 1GLAS

$D_{11} = (.799)(11.2\ 10^6) = 8\ 95 \cdot 10^6 = D_{22} = D_{44}$

$D_{21} = (.799)(2.13 \cdot 10^6) = 1.70 \cdot 10^6 = D_{41} = D_{42}$

$D_{33} = (\ 799)(4\ 53\ 10^6) = 3.63\ 10^6$

$D_{55} = (\ 578)(4.53\ 10^6) = 2.62\ 10^6 = D_{66}$

$D_{31} = D_{32} = D_{43} = D_{65} = 0$

SIDE WINDOW

DESIGNATION 2GLAS

$D_{11} = (.472)(11.2 \cdot 10^6) = 5.29 \cdot 10^6 = D_{22} = D_{44}$

$D_{21} = (.472)(2.13 \cdot 10^6) = 1.01 \cdot 10^6 = D_{41} = D_{42}$

$D_{33} = (\ 472)(4.53\ 10^6) = 2.14 \cdot 10^6$

$D_{55} = (.578)(4.53 \cdot 10^6) = 2\ 62 \cdot 10^6 = D_{66}$

$D_{31} = D_{32} = D_{43} = D_{65} = 0$

AFT BULKHEAD

DESIGNATION · 4ALUM

$D_{11} = (.0122)(15\ 4\ 10^6) = 1\ 88 \cdot 10^5 = D_{22} = D_{44}$

$D_{21} = (.0122)(7\ 42 \cdot 10^6) = 9.05\ 10^4 = D_{41} = D_{42}$

$D_{33} = (.0122)(4.0\ 10^6) = 4.88\ 10^4$

$D_{55} = (\ 578)(4.0\ 10^6) = 2\ 312 \cdot 10^6 = D_{66}$

$D_{31} = D_{32} = D_{43} = D_{65} = 0$

FORWARD BULKHEAD

DESIGNATION · 5ALUM

$D_{11} = (.0984)(15.4 \cdot 10^6) = 1.52 \cdot 10^6 = D_{22} = D_{44}$

$D_{21} = (.0984)(7.42 \cdot 10^6) = 7.31 \cdot 10^5 = D_{41} = D_{42}$

$D_{33} = (.0984)(4.0 \cdot 10^6) = 3.94 \cdot 10^5$

$D_{55} = (0.578)(4.0 \cdot 10^6) = 2.312 \cdot 10^6 = D_{66}$

$D_{31} = D_{32} = D_{43} = D_{65} = 0$

Appendix E

DEFINITION OF APOLLO WINDOW DEFORMATIONS AT THE WINDOW FRAME

This appendix contains the data for the deformation analyses of the Apollo window at the window frame, based on the deformations obtained from the coarse analysis of the Apollo structure. It includes tabulations of the deformations resulting from the analysis of the window in its structural environment and the extrapolation of these deformations using the curves developed in Section 3 of the document, transformation of the deformations to the coordinate system of the isolated window, and interpolation between these deformations to determine the deformations to be imposed at each point on the window frame.

DEFORMATIONS AT WINDOW FRAME RESULTING FROM EXTRAPOLATION OF THE RESULTS OF THE COARSE ANALYSES OF THE APOLLO STRUCTURE USING THE CURVES DEVELOPED IN THE SECTION LABELED DETERMINATION OF SCALING LAWS.

— DEFLECTIONS FOR LOADING OF 4.1 psi

JOINT	δ_{111}	δ_{311}	$\delta_{311}/\delta_{111}$	δ_e/δ_{111} *	δ	ERROR **
1741	-063739^{-1}	-059253^{-1}	929619	.955	-060871^{-1}	4 5
1742	123450^{-1}	116015^{-1}	939773	965	$.119129^{-1}$	3 5
1743	341409^{-1}	343477^{-1}	1 006057	1 040	354895^{-1}	4 0
1751	-054042^{-1}	-051076^{-1}	945117	970	$-.052421^{-1}$	3 0
1752	$.105778^{-1}$	101509^{-1}	959642	.980	103662^{-1}	2 0
1753	327821^{-1}	$.332315^{-1}$	1.013709	1 058	$.346671^{-1}$	5 8
1761	-040907^{-1}	-037401^{-1}	.914293	945	$-.038457^{-1}$	5.5
1762	$.085472^{-1}$	$.080457^{-1}$	.941326	.967	$.082651^{-1}$	3 3
1763	312461^{-1}	$.316428^{-1}$	1.012696	1.055	$.329646^{-1}$	5.5
1811	-060387^{-1}	-056353^{-1}	.933198	960	$-.057972^{-1}$	4.0
1812	$.114315^{-1}$	107805^{-1}	943052	968	110657^{-1}	3 2
1813	$.334386^{-1}$	$.337104^{-1}$	1.008128	1.044	349099^{-1}	4.4
1831	-041571^{-1}	-037558^{-1}	.903466	.935	-038869^{-1}	6 5
1832	085843^{-1}	$.079928^{-1}$	.931095	957	082152^{-1}	4 3
1833	$.311300^{-1}$	$.314438^{-1}$	1.010080	1.049	$.326554^{-1}$	4 9
1981	-054263^{-1}	$-.048560^{-1}$	894901	925	-050193^{-1}	7.5
1982	$.100944^{-1}$	$.092098^{-1}$	912367	.943	095190^{-1}	5.7
1983	324439^{-1}	$.325018^{-1}$	1 001785	1.029	$.333686^{-1}$	2 9
1991	$-.047353^{-1}$	-042804^{-1}	903934	.936	$-.044322^{-1}$	6.4
1992	$.092088^{-1}$	085123^{-1}	924366	.952	087668^{-1}	4.8
1993	316526^{-1}	$.318633^{-1}$	1 006657	1.040	$.329187^{-1}$	4.0
2001	$-.038052^{-1}$	$-.033581^{-1}$	.882503	915	$-.034818^{-1}$	8.5
2002	078956^{-1}	$.072469^{-1}$	.917840	.948	074850^{-1}	5.2
2003	305957^{-1}	308396^{-1}	1.007972	1 044	$.319266^{-1}$	4.4

* TAKEN FROM EXTRAPOLATION CURVE DEVELOPED PREVIOUSLY.

** AMOUNT OF EXTRAPOLATION FROM NOMINAL ELEMENT SOLUTIONS (%).

– ROTATIONS FOR LOADING OF 4.1 psi

ELEMENT	$\theta_{1/1}$	$\theta_{3/1}$	$\theta_{3/1}/\theta_{1/1}$	$\theta_e/\theta_{1/1}$*	θ	ERROR**
1744	-083582^{-3}	$-.066022^{-3}$	.789907	.885	$-.073970^{-3}$	2.0
1745	$-.280496^{-3}$	$-.242762^{-3}$	.865474	.925	-259459^{-3}	4.3
1746	$.302862^{-3}$	257209^{-3}	.849261	920	278633^{-3}	5.0
1754	-327846^{-3}	$-.247327^{-3}$	.754400	870	$-.285226^{-3}$	8.8
1755	-278382^{-3}	-270582^{-3}	.971981	1.000	$-.278382^{-3}$	0
1756	106889^{-3}	141171^{-3}	1 320775	1 390	148576^{-3}	8.6
1764	-294221^{-3}	-351298^{-3}	1 193977	1 235	$-.363363^{-3}$	14.3
1765	-104860^{-3}	-171701^{-3}	1.637431	1.770	$-.185602^{-3}$	16.7
1766	$-.061917^{-3}$	$.006788^{-3}$	−.109631	450	$-.027863^{-3}$	7.0
1814	$-.044957^{-3}$	$-.065119^{-3}$	1.448473	1.545	$-.069459^{-3}$	5.1
1815	$-.213907^{-3}$	$-.226586^{-3}$	1.059273	1.075	$-.229950^{-3}$	3 3
1816	$.209284^{-3}$	216426^{-3}	1.034126	1.050	$.219746^{-3}$	2.2
1834	-186916^{-3}	$-.230624^{-3}$	1 233838	1.285	$-.240187^{-3}$	11.0
1835	$-.175998^{-3}$	-205986^{-3}	1.170400	1.205	$-.212078^{-3}$	7.4
1836	$.057631^{-3}$	043278^{-3}	.750950	870	$.050139^{-3}$	1.5
1984	$.043624^{-3}$	$.031285^{-3}$	.717151	.850	$.037080^{-3}$	1 3
1985	$-.106676^{-3}$	-175636^{-3}	1 646443	1.780	$-.189883^{-3}$	17.2
1986	$.165685^{-3}$	$.230153^{-3}$	1 389486	1.475	244312^{-3}	16.2
1994	$-.189331^{-3}$	$-.103956^{-3}$	.549070	.770	$-.145785^{-3}$	9.0
1995	$-.260618^{-3}$	$-.209677^{-3}$	.804538	895	$-.233253^{-3}$	5.6
1996	$.130287^{-3}$	$.151886^{-3}$	1 165780	1.200	156344^{-3}	5.4
2004	$-.115282^{-3}$	$-.164963^{-3}$	1 430952	1.520	$-.175229^{-3}$	12.4
2005	$-.144931^{-3}$	$-.208746^{-3}$	1 440313	1 535	$-.222469^{-3}$	16.0
2006	$.120137^{-3}$	$.129140^{-3}$	1 074939	1.090	$.130949^{-3}$	2.2

* TAKEN FROM EXTRAPOLATION CURVE DEVELOPED PREVIOUSLY.

** AMOUNT OF EXTRAPOLATION FROM NORMAL ELEMENT SOLUTIONS (sec.)

TRANSFORMATION OF DEFORMATION FROM COORDINATE SYSTEM OF APOLLO STRUCTURE TO COORDINATE SYSTEM OF ISOLATED WINDOW USING THE FOLLOWING OPERATION

$$\{\delta\} = [T]\{\Delta\}$$

WHERE $\{\delta\}$ ARE THE DEFORMATIONS IN THE ISOLATED WINDOW COORDINATE SYSTEM, $[T]$ IS A LINEAR TRANSFORMATION MATRIX DEFINED BELOW, AND $\{\Delta\}$ ARE THE DEFORMATIONS IN THE APOLLO STRUCTURE COORDINATE SYSTEM

$$[T] = \begin{array}{c} \\ w \\ \theta_x \\ \theta_y \end{array} \begin{array}{c} \begin{array}{cccccc} u & v & w & \theta_x & \theta_y & \theta_z \end{array} \\ \left[\begin{array}{c|c|c|c|c|c} -.446976 & .706309 & .548945 & 0 & 0 & 0 \\ 0 & 0 & 0 & .293548 & -.463864 & .835859 \\ 0 & 0 & 0 & .845010 & .534750 & 0 \end{array}\right] \end{array}$$

- TRANSFORMED EXTRAPOLATED DEFORMATIONS FOR 1.0 psi LOAD

JOINT	w	θ_x	θ_y
174	$.746749^{-2}$	808629^{-4}	$-.490856^{-4}$
175	699883^{-2}	413639^{-4}	-950937^{-4}
176	625885^{-2}	$-.106976^{-4}$	-990966^{-4}
181	721234^{-2}	$.658424^{-4}$	$-.443071^{-4}$
183	621117^{-2}	170190^{-4}	$-.771632^{-4}$
198	$.665473^{-2}$	$.739451^{-4}$	-171237^{-4}
199	640090^{-2}	478254^{-4}	$-.604688^{-4}$
200	$.594363^{-2}$	393200^{-4}	$-.651849^{-4}$

DETERMINATION OF DEFORMATIONS AROUND WINDOW FRAME GIVEN THE FOLLOWING EXTRAPOLATED AND TRANSFORMED DEFORMATIONS FROM THE WINDOW SYSTEM ANALYSES

NODE *	x	y	w	θ_x	θ_y
174	6	5.30	$.746749^{-2}$	808629^{-4}	$-.490856^{-4}$
175	0	5.65	699883^{-2}	$.413639^{-4}$	-950937^{-4}
176	-6	6.00	625885^{-2}	$-.106976^{-4}$	$-.990966^{-4}$
181	6	0	$.721234^{-2}$	658424^{-4}	-443071^{-4}
183	-6	0	621117^{-2}	$.170190^{-4}$	$-.771632^{-4}$
198	6	-5.30	$.665473^{-2}$	$.739451^{-4}$	$-.171237^{-4}$
199	0	-5.65	$.640090^{-2}$	478254^{-4}	-604688^{-4}
200	-6	-6.00	594363^{-2}	$.393200^{-4}$	$-.651849^{-4}$

ASSUMING THAT THE DEFORMATIONS ARE A FUNCTION OF POSITION ON THE WINDOW, A MEAN SQUARE SET OF DEFORMATIONS WILL BE FITTED TO THE DATA ABOVE. THIS MEAN SQUARE SET OF DEFORMATIONS WILL THEN BE USED TO INTERPOLATE AROUND THE WINDOW FRAME TO GIVE THE DESIRED DEFORMATIONS WHICH CAN THEN BE APPLIED AS BOUNDARY CONDITIONS ON THE WINDOW. THE DEVIATIONS FROM THE MEAN SQUARE SET OF DEFORMATIONS CAN BE APPLIED AS NOISE TO THE OTHERWISE UNLOADED WINDOW TO DETERMINE IF THIS NOISE DECAYS IN THE INTERIOR.

$$\delta_i = Ax_i + By_i + C$$

$$\begin{aligned}\sigma^2 = {} & (\delta_1 - 6A - 5.3B - C)^2 + (\delta_2 - 5.65B - C)^2 + (\delta_3 + 6A - 6B - C)^2 \\ & + (\delta_4 - 6A - C)^2 + (\delta_5 + 6A - C)^2 + (\delta_6 - 6A + 5.3B - C)^2 \\ & + (\delta_7 + 5.65B - C)^2 + (\delta_8 + 6A + 6B - C)^2\end{aligned}$$

$$\begin{aligned}\sigma^2 = {} & \Sigma\delta_i^2 + 216A^2 + 192.025B^2 + 8C^2 + 12(-\delta_1 + \delta_3 - \delta_4 + \delta_5 - \delta_6 + \delta_8)A \\ & + (-10.6\delta_1 - 11.3\delta_2 - 12.0\delta_3 + 10.6\delta_6 + 11.3\delta_7 + 12.0\delta_8)B \\ & - 2\Sigma\delta_i C + (63.6 - 72.0 - 63.6 + 72.0)AB + 12(1 - 1 + 1 - 1 + 1 - 1)AC \\ & + (10.6 + 11.3 + 12.0 - 10.6 - 11.3 - 12.0)BC\end{aligned}$$

$$\frac{\partial\sigma^2}{\partial A} = 432A + 12(-\delta_1 + \delta_3 - \delta_4 + \delta_5 - \delta_6 + \delta_8) = 0$$

$$A = \frac{12}{432}(\delta_1 - \delta_3 + \delta_4 - \delta_5 + \delta_6 - \delta_8)$$

$$\frac{\partial\sigma^2}{\partial B} = 384.05B + (-10.6\delta_1 - 11.3\delta_2 - 12.0\delta_3 + 10.6\delta_6 + 11.3\delta_7 + 12.0\delta_8)$$

$$B = \frac{1}{384.05}(10.6\delta_1 + 11.3\delta_2 + 12.0\delta_3 - 10.6\delta_6 - 11.3\delta_7 - 12.0\delta_8)$$

$$\frac{\partial\sigma^2}{\partial C} = 16C - 2\Sigma\delta_i$$

$$C = \frac{1}{8}\Sigma\delta_i$$

* NODE NUMBERS CORRESPOND TO THOSE OF THE APOLLO SYSTEM ANALYSIS.

DEFORMATION	A	B	C
w	811364^{-4}	498750^{-4}	664349^{-2}
θ_x	486136^{-5}	-156203^{-5}	$.444351^{-4}$
θ_y	363690^{-5}	$-.296055^{-5}$	-634405^{4}

DEFORMATIONS OF MEAN SQUARE PLANES

JOINT	x	y	w	θ_x	θ_y
174	6	5.30	739465^{-2}	653245^{-4}	$-.573100^{-4}$
175	0	5 65	692528^{-2}	356096^{-4}	$-.801676^{-4}$
176	-6	6 00	$.645592^{-2}$	058948^{-4}	$-.103025^{-3}$
181	6	0	$.713031^{-2}$	736033^{-4}	$-.416191^{-4}$
183	-6	0	$.615667^{-2}$	$.152669^{-4}$	$-.852619^{-4}$
198	6	-5.30	686597^{-2}	$.818820^{-4}$	-259252^{-4}
199	0	-5.65	636170^{-2}	532606^{-4}	-467134^{-4}
200	-6	-6.00	585742^{-2}	$.246391^{-4}$	$-67498[illegible]^{-4}$

DEVIATIONS FROM MEAN SQUARE PLANES

JOINT	x	y	w	θ_x	θ_y
174	6	5.30	007284^{-2}	155384^{-4}	082244^{-4}
175	0	5.65	$.007355^{-2}$	057543^{-4}	-149261^{-4}
176	-6	6.00	-019707^{-2}	-165924^{-4}	039284^{-4}
181	6	0	008203^{-2}	-077609^{-4}	$-.026380^{-4}$
183	-6	0	$.005450^{-2}$	$.017521^{-4}$	080987^{-4}
198	6	-5.30	$-.021124^{-2}$	-079369^{-4}	088045^{-4}
199	0	-5.65	003920^{-2}	-054352^{-4}	$-.137554^{-4}$
200	-6	-6.00	008621^{-2}	146809^{-4}	023137^{-4}

ERROR IN SECONDS ASSOCIATED WITH DEVIATIONS

JOINT	x	y	w	θ_x	θ_y
174	6	5.30	.62	3.21	1.70
175	0	5.65	8.70	1.19	3 08
176	-6	6.00	8 70	3.42	.81
181	6	0	4.96	1 60	55
183	-6	0	8.55	.36	1.67
198	6	-5.30	8 01	1 64	1.82
199	0	-5.65	8.01	1.12	2 84
200	-6	-6.00	1.02	3.03	48

USING THE DEFORMATIONS OF THE EIGHT POINTS GIVEN ABOVE, THE DEFORMATIONS OF TWELVE POINTS ON THE WINDOW FRAME WILL BE DETERMINED USING A LINEAR INTERPOLATION. THIS WILL BE PERFORMED USING THE FOLLOWING OPERATION

$$\{\delta\} = [T_1]\{\Delta\}$$

WHERE $\{\delta\}$ ARE THE DEFORMATIONS AT THE TWELVE POINTS ON THE WINDOW FRAME, $[T_1]$ IS A LINEAR OPERATOR (DEFINED BELOW), AND $\{\Delta\}$ ARE THE DEFORMATIONS GIVEN ABOVE.

$$[T_1] = \begin{array}{r} \\ 11 \\ 41 \\ 71 \\ 342 \\ 393 \\ 678 \\ 729 \\ 994 \\ 1041 \\ 1292 \\ 1317 \\ 1342^{*} \end{array} \begin{array}{c} \begin{array}{cccccccc} 174 & 175 & 176 & 181 & 183 & 198 & 199 & 200 \end{array} \\ \left[\begin{array}{cccccccc} 0 & 0 & 0 & 0 & .5000 & 0 & 0 & 5000 \\ 0 & 0 & 0 & 0 & 1.0000 & 0 & 0 & 0 \\ 0 & 0 & 5000 & 0 & .5000 & 0 & 0 & 0 \\ 0 & 0 & 0 & 0 & 0 & 0 & 5000 & .5000 \\ 0 & 5000 & 5000 & 0 & 0 & 0 & 0 & 0 \\ 0 & 0 & 0 & 0 & 0 & 0 & 1.0000 & 0 \\ 0 & 1.0000 & 0 & 0 & 0 & 0 & 0 & 0 \\ 0 & 0 & 0 & 0 & 0 & 5000 & 5000 & 0 \\ 5000 & 5000 & 0 & 0 & 0 & 0 & 0 & 0 \\ 0 & 0 & 0 & 5283 & 0 & 4717 & 0 & 0 \\ 0 & 0 & 0 & 1.0000 & 0 & 0 & 0 & 0 \\ 4717 & 0 & 0 & 5283 & 0 & 0 & 0 & 0 \end{array}\right] \end{array}$$

KNOWING THE DEFORMATIONS AT THESE TWELVE POINTS ON THE WINDOW FRAME, THE DEFORMATIONS AT THE REST OF THE POINTS ON THE FRAME WILL BE OBTAINED BY THE FOLLOWING OPERATION

$$\{\delta'\} = [T_2]\{\delta\}$$

WHERE $\{\delta'\}$ ARE THE DEFORMATIONS AT THE WINDOW FRAME AND $[T_2]$ IS A LINEAR OPERATOR OBTAINED BY CONSIDERING A LINEAR INTERPOLATION BETWEEN TWO SUCCESSIVE POINTS OF THE TWELVE GIVEN ABOVE. THE FORMATION OF $[T_2]$ IS GIVEN BELOW.

* NODE NUMBERS CORRESPOND TO THOSE OF THE ISOLATED WINDOW ANALYSIS

$(i)^*$ IN δ_i'	DISTANCE FROM PREVIOUS POINT	FACTORS AND (i)s* IN $[T_2]\{\delta_1\}$			
1,3,5	1 08/4 72	.771186	11	228814	342
6,8,10	54/4 72	885593	11	.114407	342
11,13,15	00/3 00	1 000000	11	000000	41
16,18 20	.50/3 00	833333	11	.166667	41
21,23,25	1.00/3 00	666667	11	333333	41
26 28,30	1 50/3.00	500000	11	.500000	41
31,33,35	2 00/3 00	333333	11	666667	41
36,38 40	2 50/3.00	166667	11	.833333	41
41,43,45	3 00/3.00	000000	11	1 000000	41
46 48,50	50/3.00	833333	41	.166667	71
51,53,55	1.00/3.00	.666667	41	333333	71
56,58,60	1.50/3.00	500000	41	.500000	71
61 63,65	2 00/3.00	.333333	41	.666667	71
66,68,70	2.50/3.00	166667	41	833333	71
71,73,75	3 00/3.00	.000000	41	1.000000	71
76,78,80	54/4 72	885593	71	114407	393
81 83,85	1.08/4.72	.771186	71	.228814	393
86,88,90	1.62/4 72	.656780	11	343220	342
125,127,129	1.62/4.72	.656780	71	343220	393
130,132,134	2.32/4 72	508475	11	491525	342
173,175,177	2.32/4.72	.508475	71	.491525	393
178,180,182	3.15/4.72	.332627	11	667373	342
225,227,229	3.15/4.72	.332627	71	.667373	393
230,232,234	3.64/4 72	228814	11	771186	342
281,283,285	3 64/4 72	228814	71	.771186	393
286,288 290	4.18/4.72	.114407	11	885593	342
337,339,341	4.18/4.72	114407	71	.885593	393
342,344,346	4.72/4 72	.000000	11	1.000000	342
393, 395,397	4.72/4 72	.000000	71	1.000000	393
398,400 402	50/3.00	833333	342	.166667	678
449,451,453	.50/3.00	.833333	393	.166667	729
454,456,458	1 00/3.00	.666667	342	333333	678
505,507,509	1.00/3.00	666667	393	.333333	729
510,512,514	1.50/3.00	.500000	342	.500000	678
561, 563,565	1.50/3 00	500000	393	500000	729
566,568,570	2 00/3 00	.333333	342	.666667	678
617,619,621	2.00/3.00	333333	393	.666667	729
622,624,626	2 50/3.00	.166667	342	.833333	678
673,675,677	2 50/3.00	.166667	393	.833333	729

* NODE NUMBERS CORRESPOND TO THOSE OF THE ISOLATED WINDOW ANALYSIS

$(L)^*$ IN δ_i'	DISTANCE FROM PREVIOUS POINT	FACTORS AND (L)'s* IN $[T_2]\{\delta.\}$			
678,680,682	3.00/3.00	000000	342	1.000000	678
729,731,733	3 00/3.00	.000000	393	1.000000	729
734,736,738	.50/3.00	833333	678	.166667	994
781,783,785	50/3.00	.833333	729	.166667	1041
786,788,790	1.00/3.00	666667	678	.333333	994
833,835,837	1.00/3.00	.666667	729	.333333	1041
838,840,842	1.50/3.00	.500000	678	.500000	994
885,887,889	1.50/3.00	.500000	729	500000	1041
890,892,894	2 00/3.00	.333333	678	.666667	994
937,939,941	2 00/3.00	.333333	729	.666667	1041
942,944,946	2.50/3.00	.166667	678	833333	994
989,991,993	2 50/3.00	.166667	729	.833333	1041
994,996,998	3 00/3.00	000000	678	1.000000	994
1041,1043,1045	3 00/3.00	.000000	729	1.000000	1041
1046,1048,1050	.53/4.72	887712	994	.112288	1292
1093,1095,1097	53/4.72	887712	1041	112288	1342
1098,1100,1102	1.06/4.72	.775424	994	224576	1292
1145,1147,1149	1.06/4.72	.775424	1041	.224576	1342
1150,1152,1154	1 70/4.72	.639831	994	360169	1292
1193,1195,1197	1.70/4 72	.639831	1041	360169	1342
1198,1200,1202	2 48/4 72	474576	994	525424	1292
1237,1239,1241	2 48/4.72	.474576	1041	.525424	1342
1242,1244,1246	3.10/4.72	.343220	994	656780	1292
1277,1279,1281	3.10/4.72	.343220	1041	.656780	1342
1282,1284,1286	3.66/4 72	.224576	994	775424	1292
1287,1289,1291	4.19/4.72	.112288	994	887712	1292
1292,1294,1296	4.72/4.72	.000000	994	1.000000	1292
1297,1299,1301	.50/2.50	.800000	1292	.200000	1317
1302,1304,1306	1 00/2.50	.600000	1292	.400000	1317
1307,1309,1311	1.50/2.50	.400000	1292	.600000	1317
1312,1314,1316	2.00/2.50	.200000	1292	.800000	1317
1317,1319,1321	2 50/2.50	.000000	1292	1.000000	1317
1322,1324,1326	.50/2.50	800000	1317	200000	1342
1327,1329,1331	1.00/2.50	600000	1317	.400000	1342
1332,1334,1336	1.50/2.50	400000	1317	.600000	1342
1337,1339,1341	2.00/2.50	.200000	1317	.800000	1342
1342,1344,1346	4.72/4.72	.000000	1041	1.000000	1342
1347,1349,1351	4.19/4.72	.112288	1041	.887712	1342
1352,1354,1356	3.66/4.72	224576	1041	.775424	1342

* NODE NUMBERS CORRESPOND TO THOSE OF THE ISOLATED WINDOW ANALYSIS.

Appendix F

APOLLO WINDOW FINAL DEFORMATION ANALYSES

This appendix contains the definition of the refined model of the Apollo window in its structural environment. Included are sketches showing the joint numbering for both the full- and half-window models, calculations performed in studying the effective stiffness of the window frame, and calculations for defining the model of the window frame to be used in the analyses. It also includes the equations relating the symmetric and asymmetric loading conditions and their resulting deformations Copies of the computer output giving, in matrix form, the deformations for the various load conditions are available for review at NASA Ames Research Center, Moffett Field, California.

Tabulations of results for selected points on the window are also included. These deformations are used in the determination of the reduction of the errors over the interior of the window. The least-square error deflections are ratioed to the actual deflections for loading number one (it is assumed that similar results can be obtained for the other load numbers) for points at the window frame and for selected points on the interior of the window. The results indicated that the error is reduced by 66 percent.

JOINT NUMBERING - WHOLE WINDOW

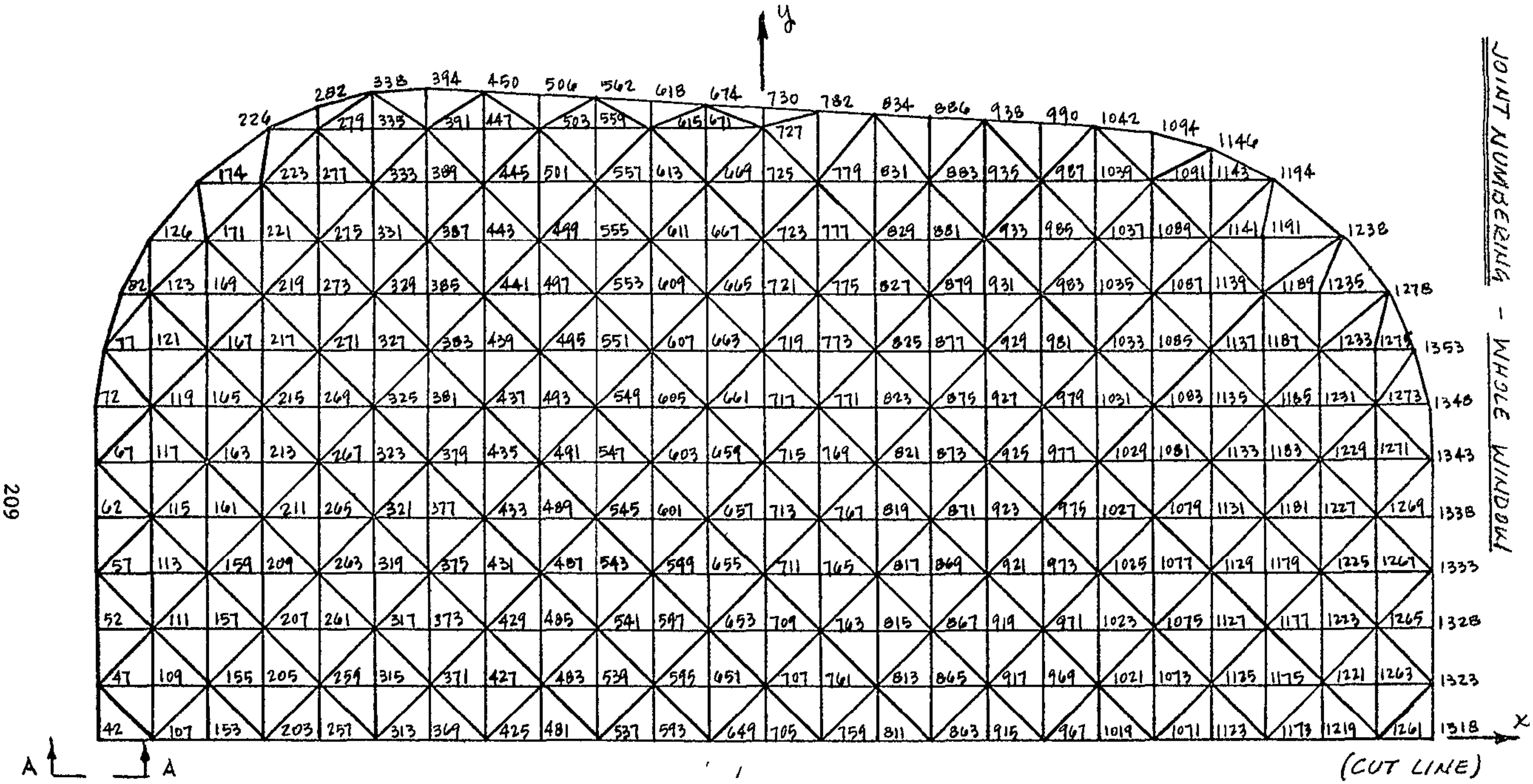

OUTER PANE - LEFT HALF

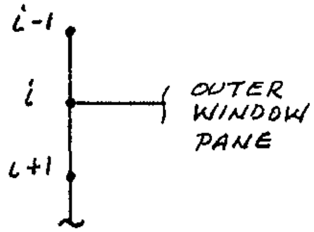

SECTION A-A

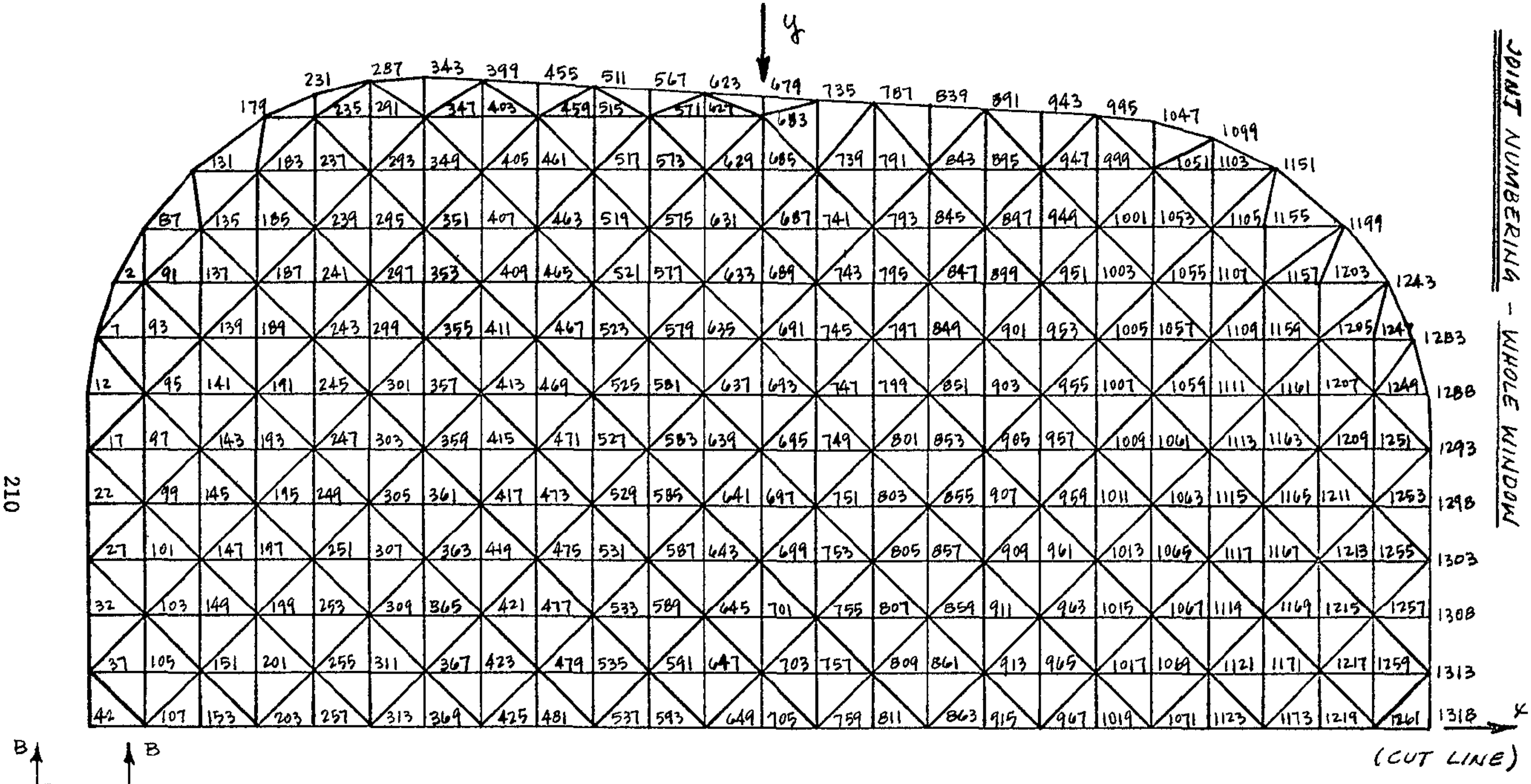

OUTER PANE - RIGHT HALF

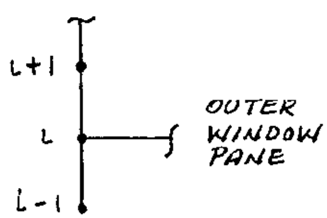

SECTION B-B

JOINT NUMBERING - WHOLE WINDOW

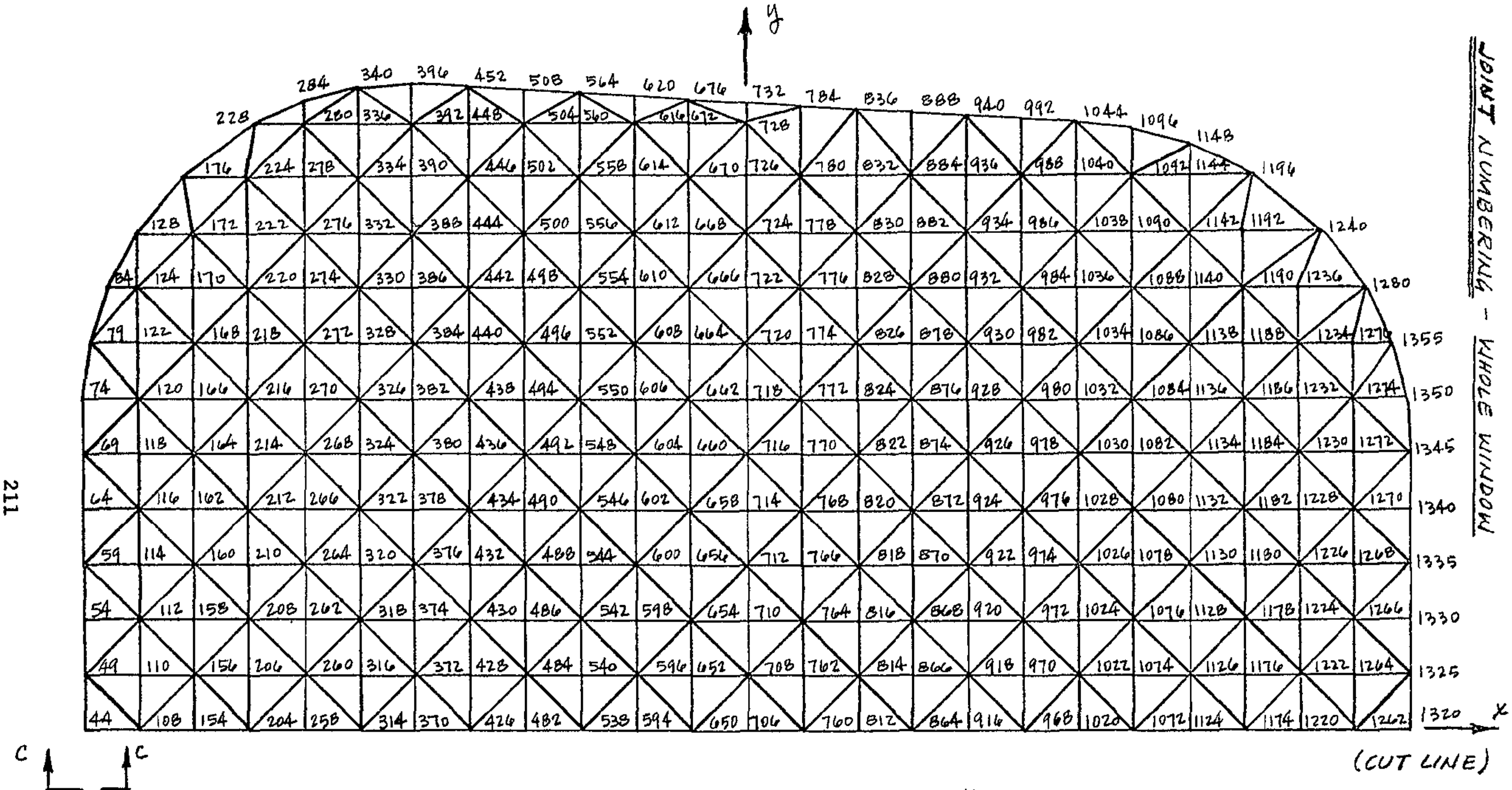

INNER PANE - LEFT HALF

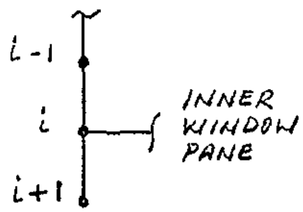

SECTION C-C

JOINT NUMBERING - WHOLE WINDOW

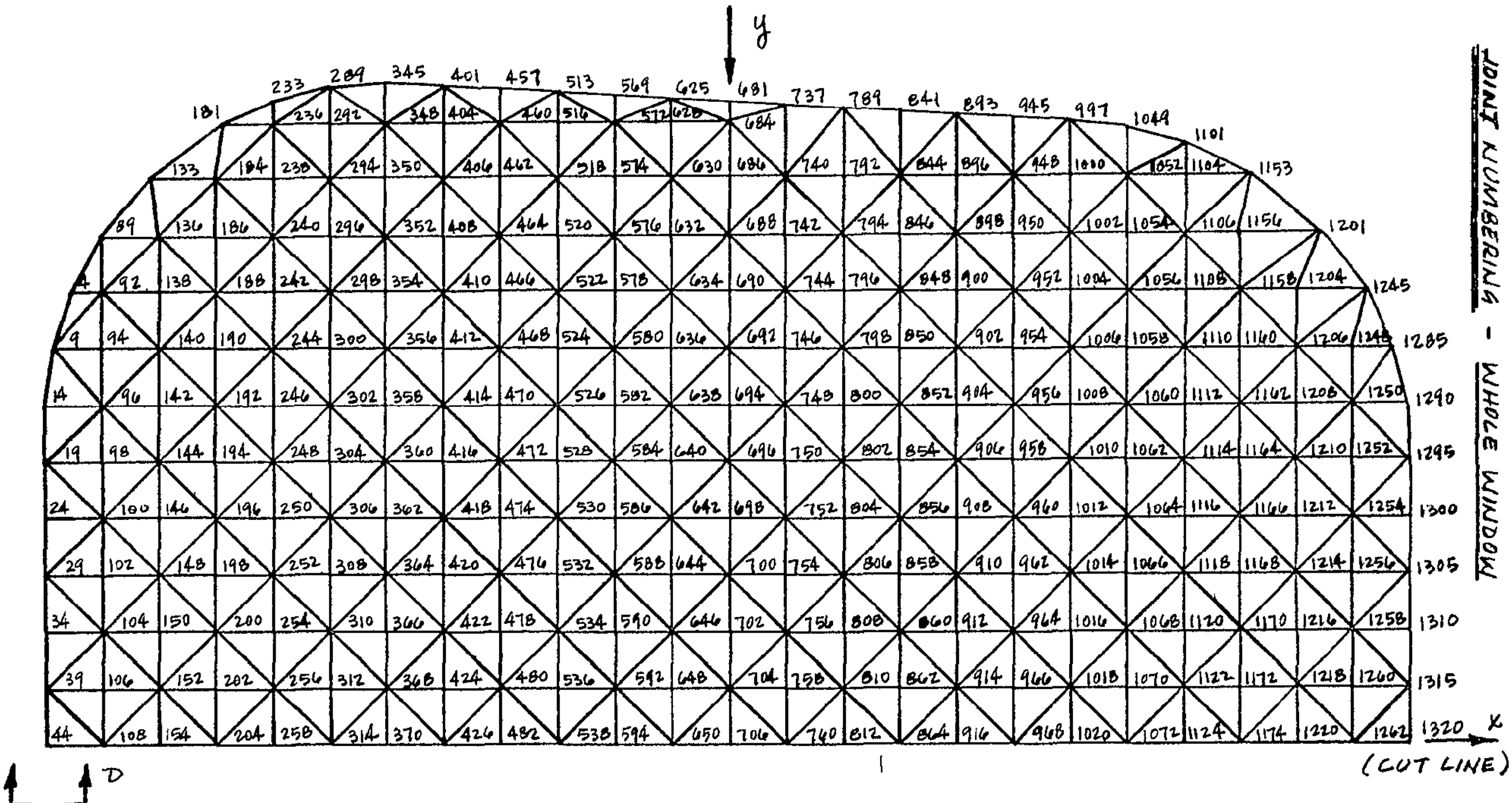

INNER PANE - RIGHT HALF

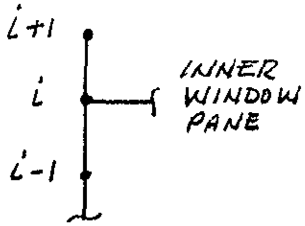

SECTION D-D

JOINT NUMBERING - HALF WINDOW

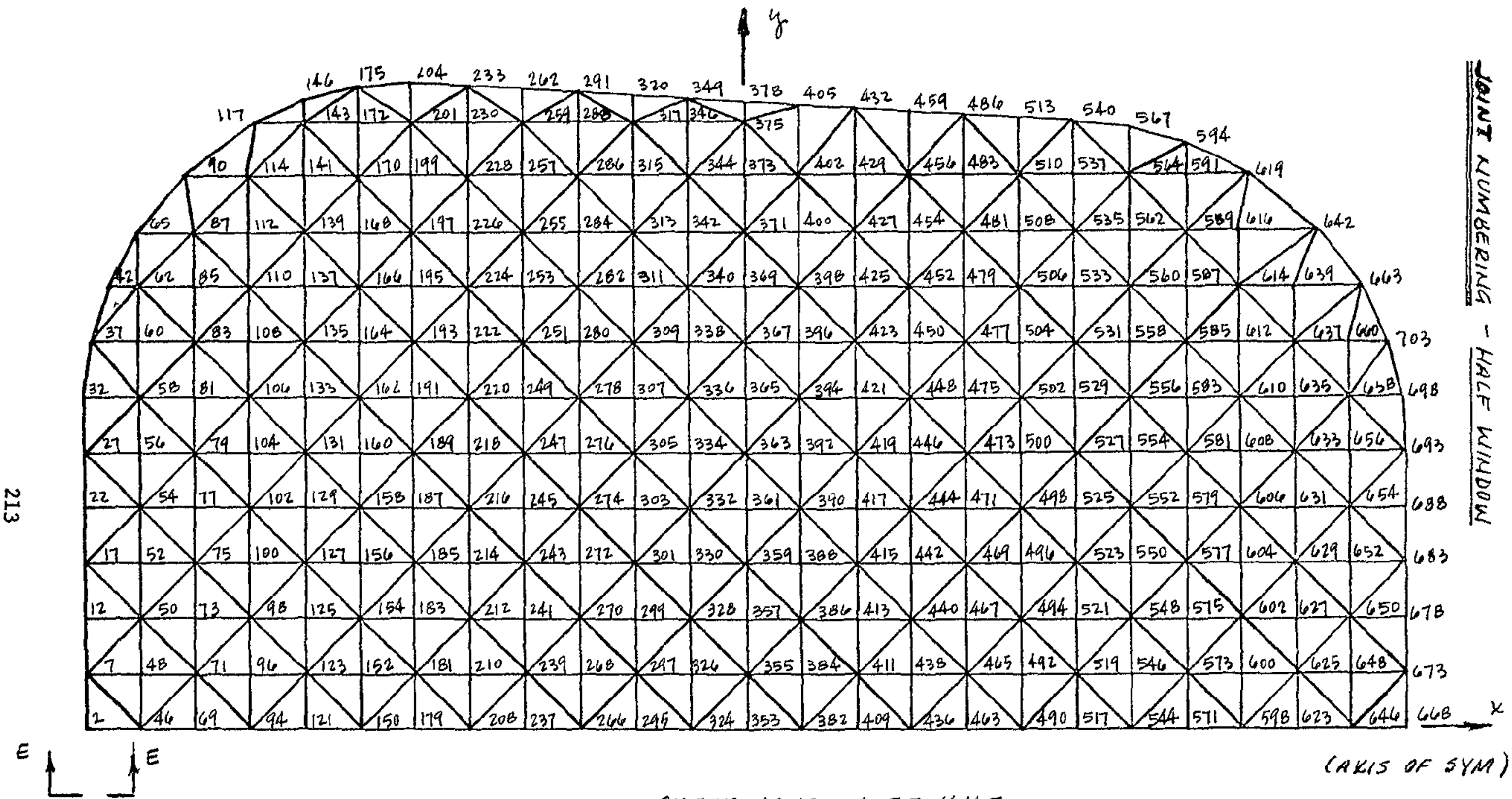

OUTER PANE - LEFT HALF

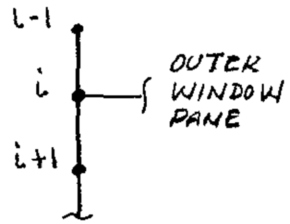

SECTION E-E

JOINT NUMBERING - HALF WINDOW

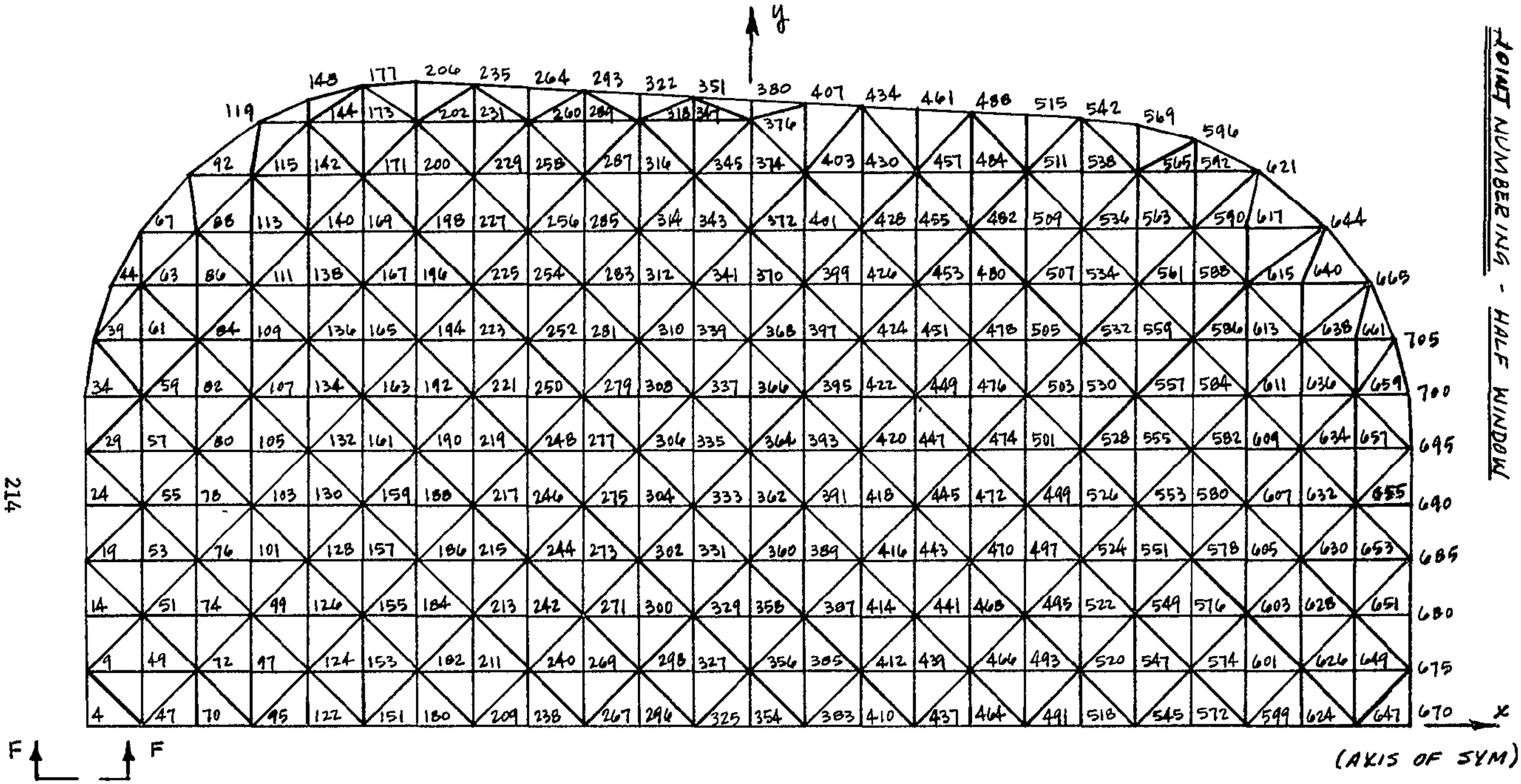

INNER PANE - LEFT HALF

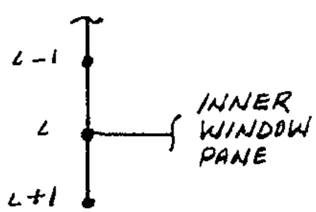

SECTION F-F

SCIENTIFIC SIDE WINDOW FRAME - EFFECTIVE STIFFNESS

LOOKING AT A ONE-HALF INCH LONG SEGMENT OF THE FRAME (IN THE DIRECTION AROUND THE WINDOW) AND ASSUMING THAT THE LOADS TRANSFERRED TO THE FRAME FROM THE WINDOW PANES ARE THOSE WHICH WOULD OCCUR IF THE PANES WERE CLAMPED IN THE FRAME, WE HAVE THE FOLLOWING SITUATION;

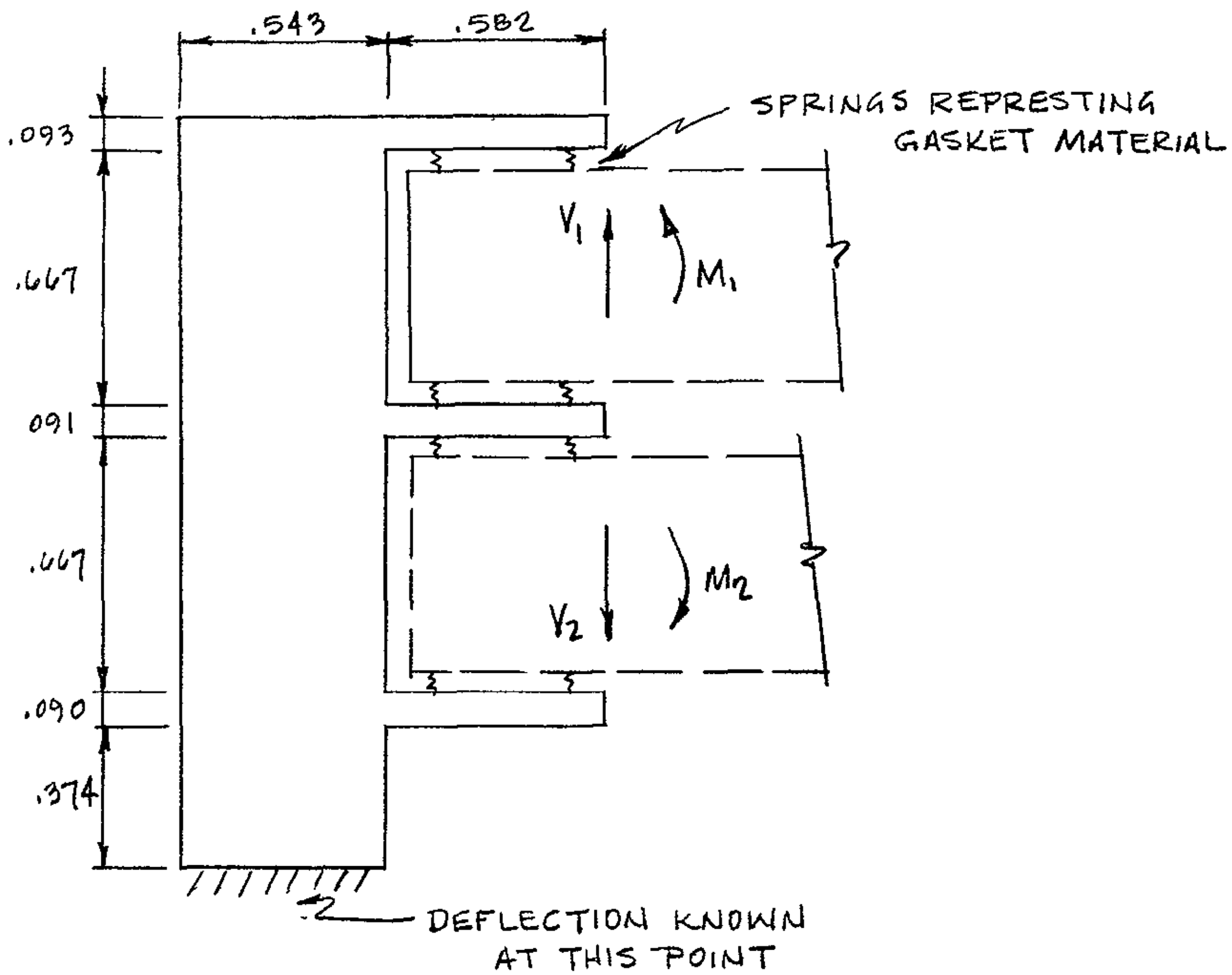

$V_1 = \frac{p'l}{2}$ $\qquad V_2 = \frac{pl}{2}$

$M_1 = \frac{p'l^2}{12}$ $\qquad M_2 = \frac{pl^2}{12}$

$p' = 22\,pli$ $\qquad p = 425\,pli$

$l = 5\text{ in}$

CONSIDER FIRST THE FOLLOWING PORTION OF THE FRAME

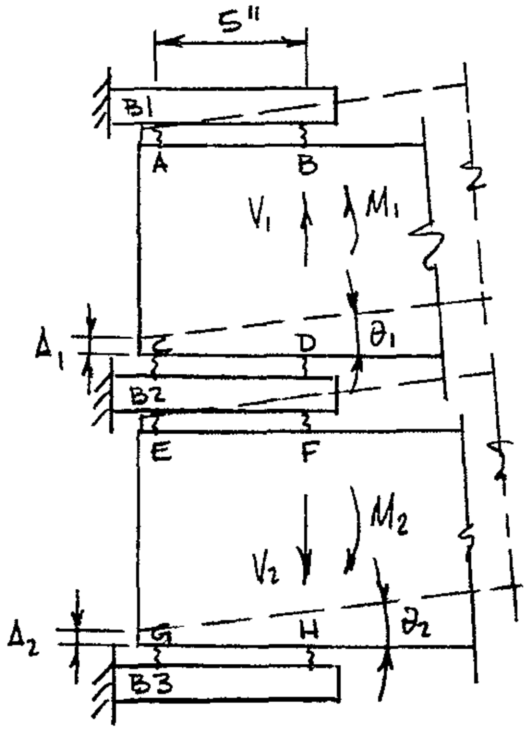

$V_1 = .55$ lb

$V_2 = 1.06$ lb

$M_1 = .046$ lb in

$M_2 = .089$ lb-in

$E = 10\ 10^6$ psi

$I_{B1} = 3.75 \cdot 10^{-7}$ in^4

$\frac{l_1^3}{3EI_1} = 0111$ in/lb

$k_G = 2885$ lb/in

DEFLECTIONS OF SPRINGS

$\delta_A = \Delta_1$ $\qquad\qquad$ $\delta_E = \Delta_2$

$\delta_B = \Delta_1 + 5\theta_1$ $\qquad\qquad$ $\delta_F = \Delta_2 + .5\theta_2$

$\delta_C = \Delta_1$ $\qquad\qquad$ $\delta_G = \Delta_2$

$\delta_D = \Delta_1 + .5\theta_1$ $\qquad\qquad$ $\delta_H = \Delta_2 + .5\theta_2$

DEFLECTIONS OF CANTILEVERS

$$\Delta_{B1} = \frac{F_B(.5)^3}{3EI} = .0111 F_B$$

$$\Delta_{B2} = \frac{(F_D - F_F)(.5)^3}{3EI} = .0111(F_D - F_F)$$

$$\Delta_{B3} = \frac{F_H(.5)^3}{3EI} = 0111 F_H$$

FORCES IN SPRINGS

$F_A = k\delta_A$ $\qquad\qquad$ $F_E = k\delta_E$

$F_B = k(\delta_B - \Delta_{B1})$ $\qquad\qquad$ $F_F = k(\delta_F + \Delta_{B2})$

$F_C = k\delta_C$ $\qquad\qquad$ $F_G = k\delta_G$

$F_D = k(\delta_D - \Delta_{B2})$ $\qquad\qquad$ $F_H = k(\delta_H - \Delta_{B3})$

EQUILIBRIUM EQUATIONS

$$\Sigma F_1 = F_A + F_B + F_C + F_D = V_1 \tag{1}$$

$$\Sigma M_C = 0.5(V_1) + M_1 = (F_B + F_D)(0.5) \tag{2}$$

$$\Sigma F_2 = F_E + F_F + F_G + F_H = -V_2 \tag{3}$$

$$\Sigma M_E = 0.5 V_2 + M_2 = -0.5(F_F + F_H) \tag{4}$$

EVALUATION OF FORCES IN SPRINGS

$$F_A = 2885\,\Delta_1 \quad (C)$$

$$F_B = 2885(\Delta_1 + .5\theta_1 - \Delta_{B1}) \quad (C)$$

$$F_C = 2885\,\Delta_1 \quad (T)$$

$$F_D = 2885(\Delta_1 + .5\theta_1 - \Delta_{B2}) \quad (T)$$

$$F_E = 2885\,\Delta_2 \quad (C)$$

$$F_F = 2885(\Delta_2 + .5\theta_2 + \Delta_{B2}) \quad (C)$$

$$F_G = 2885\,\Delta_2 \quad (T)$$

$$F_H = 2885(\Delta_2 + .5\theta_2 - \Delta_{B3}) \quad (T)$$

$$\frac{F_B}{2885} = \Delta_1 + .5\theta_1 - \Delta_{B1} = \Delta_1 + .5\theta_1 - .0111 F_B$$

$$F_B = 2885(\Delta_1 + 5\theta_1) - 32.0 F_B$$

$$F_B = \frac{2885}{33}(\Delta_1 + .5\theta_1)$$

$$F_H = 2885(\Delta_2 + .5\theta_2) - 2885\,\Delta_{B3}$$

$$F_H = 2885(\Delta_2 + .5\theta_2) - 2885(.0111) F_H$$

$$F_H = \frac{2885}{33}(\Delta_2 + .5\theta_2)$$

$$F_D = 2885(\Delta_1 + .5\theta_1) - 2885(.0111)(F_D - F_F)$$

$$F_F = 2885(\Delta_2 + .5\theta_2) + 2885(.0111)(F_D - F_F)$$

$$F_D = 2885(\Delta_1 + .5\theta_1) - 32 F_D + 32 F_F$$

$$F_D = \frac{2885}{33}(\Delta_1 + .5\theta_1) + \frac{32}{33} F_F$$

$$F_F = 2885(\Delta_2 + .5\theta_2) + 32\left(\frac{2885}{33}(\Delta_1 + .5\theta_1) + \frac{32}{33} F_F - F_F\right)$$

$$F_F = 2885(\Delta_2 + .5\theta_2) + \frac{32}{33} 2885(\Delta_1 + .5\theta_1) + 31 F_F - 32 F_F$$

$$F_F = \frac{2885}{2}(\Delta_2 + .5\theta_2) + \frac{16}{33} 2885(\Delta_1 + .5\theta_1)$$

$$F_D = \frac{2885}{2}(\Delta_1 + .5\theta_1) + \frac{16}{33} 2885(\Delta_2 + .5\theta_2)$$

FROM THE EQUILIBRIUM EQUATIONS WE HAVE

(1) $$\Delta_1 + \frac{\theta_1}{66} + \frac{\Delta_1}{33} + \Delta_1 + \frac{\Delta_1}{2} + \frac{\theta_1}{4} + \frac{16}{33}\Delta_2 + \frac{8}{33}\theta_2 = \frac{V_1}{2885}$$

$$\frac{167}{66}\Delta_1 + \frac{35}{132}\theta_1 + \frac{16}{33}\Delta_2 + \frac{8}{33}\theta_2 = \frac{V_1}{2885}$$

$$334\Delta_1 + 35\theta_1 + 64\Delta_2 + 32\theta_2 = \frac{132}{2885} V_1$$

(2) $$\frac{\Delta_1}{33} + \frac{\theta_1}{66} + \frac{\Delta_1}{2} + \frac{\theta_1}{4} + \frac{16}{33}\Delta_2 + \frac{8}{33}\theta_2 = \frac{V_1 + 2M_1}{2885}$$

$$\frac{35}{66}\Delta_1 + \frac{35}{132}\theta_1 + \frac{16}{33}\Delta_2 + \frac{8}{33}\theta_2 = \frac{V_1 + 2M_1}{2885}$$

$$70\Delta_1 + 35\theta_1 + 64\Delta_2 + 32\theta_2 = \frac{132}{2885}(V_1 + 2M_1)$$

(3) $$\Delta_2 + \frac{\Delta_2}{2} + \frac{\theta_2}{4} + \frac{16}{33}\Delta_1 + \frac{8}{33}\theta_1 + \Delta_2 + \frac{\Delta_2}{33} + \frac{\theta_2}{66} = -\frac{V_2}{2885}$$

$$\frac{167}{66}\Delta_2 + \frac{35}{132}\theta_2 + \frac{16}{33}\Delta_1 + \frac{8}{33}\theta_1 = -\frac{V_2}{2885}$$

$$64\Delta_1 + 32\theta_1 + 334\Delta_2 + 35\theta_2 = -\frac{132}{2885} V_2$$

(4) $$\frac{\Delta_2}{2} + \frac{\theta_2}{4} + \frac{16}{33}\Delta_1 + \frac{8}{33}\theta_1 + \frac{\Delta_2}{33} + \frac{\theta_2}{66} = -\frac{1}{2885}(V_2 + 2M_2)$$

$$\frac{35}{66}\Delta_2 + \frac{35}{132}\theta_2 + \frac{16}{33}\Delta_1 + \frac{8}{33}\theta_1 = -\frac{1}{2885}(V_2 + 2M_2)$$

$$64\Delta_1 + 32\theta_1 + 70\Delta_2 + 35\theta_2 = -\frac{132}{2885}(V_2 + 2M_2)$$

SIMULTANEOUS SOLUTION OF EQUATIONS

$$334\Delta_1 + 35\theta_1 + 64\Delta_2 + 32\theta_2 = \frac{132}{2885} V_1 \qquad (1)$$

$$70\Delta_1 + 35\theta_1 + 64\Delta_2 + 32\theta_2 = \frac{132}{2885}(V_1 + 2M_1) \qquad (2)$$

$$64\Delta_1 + 32\theta_1 + 334\Delta_2 + 35\theta_2 = -\frac{132}{2885} V_2 \qquad (3)$$

$$64\Delta_1 + 32\theta_1 + 70\Delta_2 + 35\theta_2 = -\frac{132}{2885}(V_2 + 2M_2) \qquad (4)$$

SUBTRACTING (2) FROM (1) WE GET

$$264\,\Delta_1 = -\frac{132}{2885}(2M_1)$$

$$\Delta_1 = \frac{-M_1}{2885} = -1.59\cdot 10^{-5} \text{ in.}$$

SUBTRACTING (4) FROM (3)

$$264\,\Delta_2 = +\frac{132}{2885}(2M_2)$$

$$\Delta_2 = \frac{M_2}{2885} = 3.07\cdot 10^{-5} \text{ in}$$

SUBSTITUTING INTO (2)

$$70(-1.59\;10^{-5}) + 35\theta_1 + 64(3.07\cdot 10^{-5}) + 32\theta_2 = \frac{132}{2885}(V_1 + 2M_1)$$

$$-1.11\;10^{-3} + 35\theta_1 + 1.965\;10^{-3} + 32\theta_2 = 2.94\;10^{-2}$$

$$35\theta_1 + 32\theta_2 = .0285 \qquad (5)$$

SUBSTITUTING INTO (4)

$$64(-1.59\;10^{-5}) + 32\theta_1 + 70(3.07\cdot 10^{-5}) + 35\theta_2 = -\frac{132}{2885}(V_2 + 2M_2)$$

$$-1.018\cdot 10^{-3} + 32\theta_1 + 2\,149\;10^{-3} + 35\theta_2 = -5.28\cdot 10^{-2}$$

$$32\theta_1 + 35\theta_2 = -.0529 \qquad (6)$$

SOLVING (5) AND (6) SIMULTANEOUSLY WE GET

$$\theta_1 = .01338 \text{ rad}$$

$$\theta_2 = -.01375 \text{ rad}$$

CALCULATION OF FORCES IN SPRINGS

$$F_A = 2885(-1.59\cdot 10^{-5}) = .0459 \text{ lb } (T)$$

$$F_B = \frac{2885}{33}(-1.59\cdot 10^{-5} + .00669) = .583 \text{ lb } (C)$$

$$F_C = 2885(-1.59\cdot 10^{-5}) = .0459 \text{ lb } (C)$$

$$F_D = \frac{2885}{2}(-1.59\cdot 10^{-5} + .00669) + \frac{16}{33}2885(3.07\;10^{-5} - 006875)$$

$$F_D = .0548 \text{ lb } (T)$$

$$F_E = 2885(3.07\;10^{-5}) = 0886 \text{ lb } (C)$$

$$F_F = \frac{2885}{2}(3.07\;10^{-5} - 006875) + \frac{16}{33}(2885)(-1.59\cdot 10^{-5} + .00669)$$

$$F_F = 540 \text{ lb } (T)$$

$$F_G = 2885(3\,07\;10^{-5}) = .0886 \text{ lb } (T)$$

$$F_H = \frac{2885}{33}(3.07\;10^{-5} - .006875) = .598 \text{ lb } (C)$$

REACTION OF SPRINGS ON FRAME

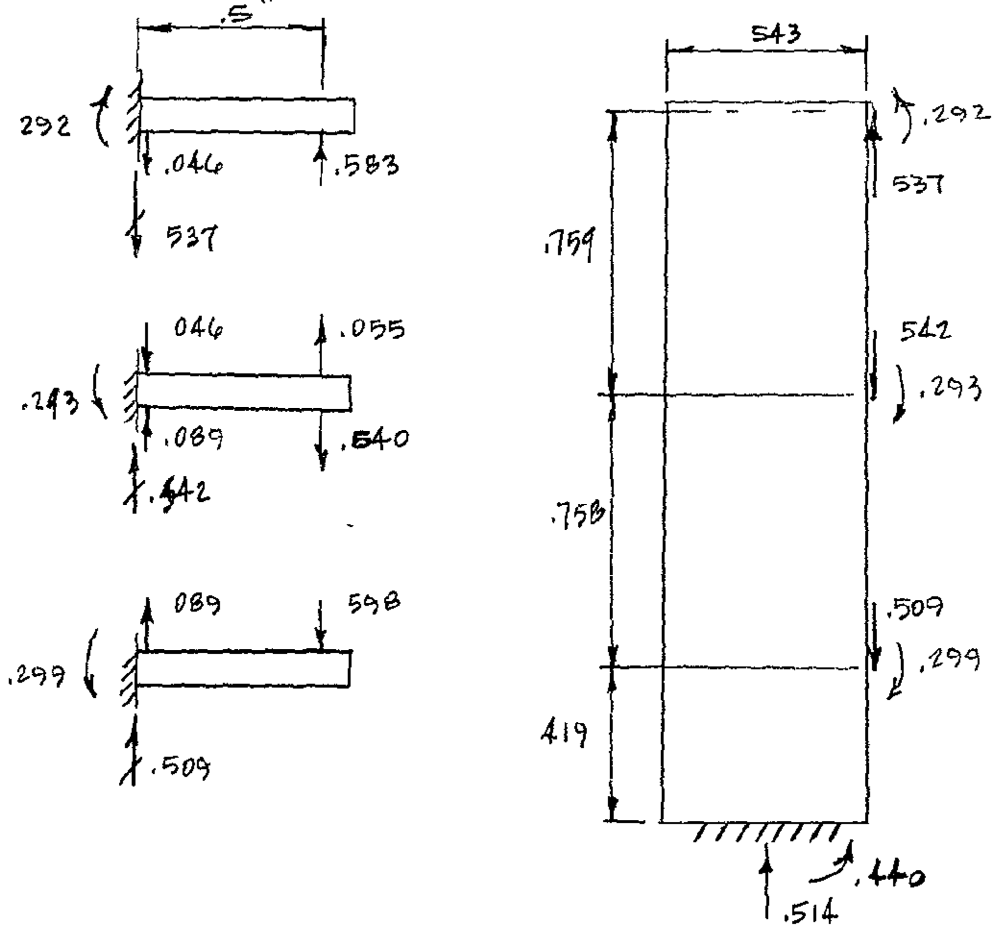

CONSIDER NOW THAT PORTION OF THE FRAME SHOWN ON THE RIGHT ABOVE

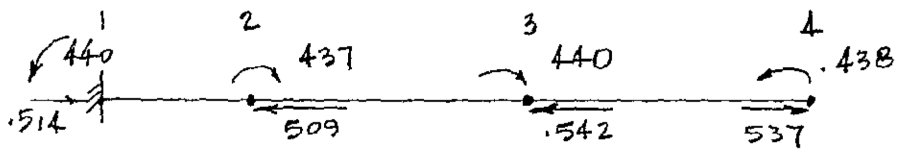

MOMENT DIAGRAM

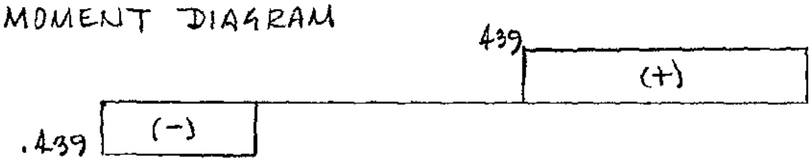

$M = -.439$	$M = 0$	$M = .439$	
$EI\theta = -.439x$	$EI\theta = -.184$	$EI\theta = -.184 + .439x$	$(.333)$
$EIy = -.439\frac{x^2}{2}$	$EIy = -.039 - .184x$	$EIy = -.179 - .184x + .439\frac{x^2}{2}$	$(-.188)$

SECTION PROPERTIES

$E = 1.0 \; 10^7$ psi

$I = \frac{(.5)(.543)^3}{12} = .00667 \text{ in}^4$

$EI = 6.67 \; 10^4$

	1	2	3	4
θ	0	$-2.76 \; 10^{-6}$	$-2.76 \cdot 10^{-6}$	$5.00 \; 10^{-6}$
y	0	$-5.85 \; 10^{-7}$	$-2.69 \cdot 10^{-6}$	$-2.82 \; 10^{-6}$

CONCLUSION

FRAME CAN BE CONSIDERED RIGID UP TO POINTS WHERE CONNECTIONS ARE MADE THAT SUPPORT WINDOW PANES

FRAME MEMBER MODELING SPRING CONSTANTS FOR SCIENTIFIC SIDE WINDOW FRAME

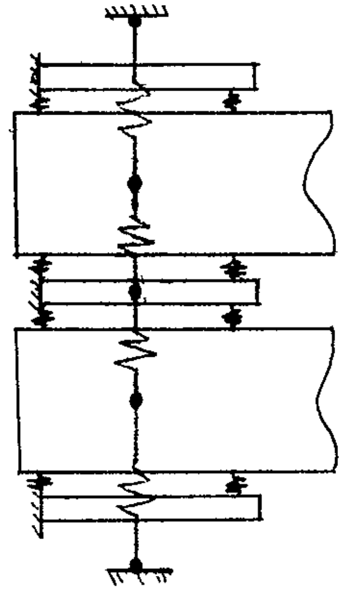

OUTSIDE ELEMENTS

$$K_{SPRINGS} = 2885 \ \text{LB/IN}$$

$$K_{BEAM} = \frac{3EI}{L} = \frac{1}{0111} = 90.090 \ \text{LB/IN}$$

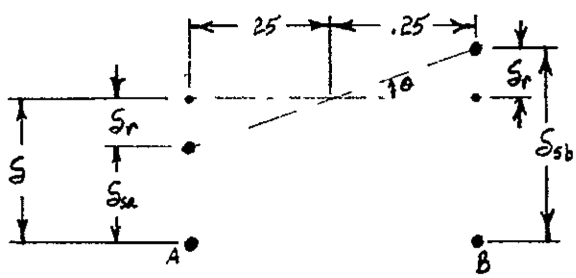

$$\delta_{sa} = \delta - .25\theta$$

$$\delta_{sb} = \delta + 25\theta$$

AT A $\quad \delta = \dfrac{P_a}{2885}$

AT B $\quad \delta = \dfrac{P_{b1}}{2885} + \dfrac{P_{b2}}{90.090}$ $\quad$ WHERE P_{b1} IS LOAD ON SPRING
P_{b2} IS LOAD ON BEAM

$$P_{b1} = P_{b2}$$

$$S = \frac{P_b}{2885} + \frac{P_b}{90\,090} = \frac{P_b}{2885} + \frac{32.0235\,P_b}{2885}$$

$$S = \frac{33.0235\,P_b}{2885}$$

$$\frac{P_a}{2885} = \frac{33.0235\,P_b}{2885}$$

$$P_a = 33\,0235\,P_b$$

LET $P_a + P_b = 1$

$$P_b = 1 - P_a$$

$$P_a = 33\,0235(1 - P_a)$$

$$P_a = 33\,0235 - 33\,0235\,P_a$$

$$34.0235\,P_a = 33\,0235$$

$$P_a = \frac{33.0235}{34.0235} = .970608 \text{ LB}$$

$$P_b = .029392 \text{ LB}$$

P_a MUST BE DECREASED BY ΔP_a AND P_b MUST BE INCREASED BY ΔP_b TO ACCOUNT FOR THE ROTATION.

$$S_{sa} = \frac{P_a - \Delta P_a}{2885} = \frac{.970608}{2885} - \frac{\Delta P_a}{2885} = .0003363 - \frac{\Delta P_a}{2885}$$

$$S_{sb} = \frac{P_b + \Delta P_b}{2885} + \frac{P_b + \Delta P_b}{90\,090}$$

$$= \frac{.029392}{2885} + \frac{.029392}{90{,}090} + \frac{\Delta P_b}{2885} + \frac{\Delta P_b}{90{,}090}$$

$$= \frac{.029392}{2885} + \frac{(32.0235)(.029392)}{2885} + \frac{\Delta P_b}{2885} + \frac{32.0235\,\Delta P_b}{2885}$$

$$S_{sb} = .0003363 + \frac{33.0235\,\Delta P_b}{2885}$$

$$\frac{\Delta P_a}{2885} = \frac{33\ 0235\ \Delta P_b}{2885}$$

$$\Delta P_a = 33\ 0235\ \Delta P_b$$

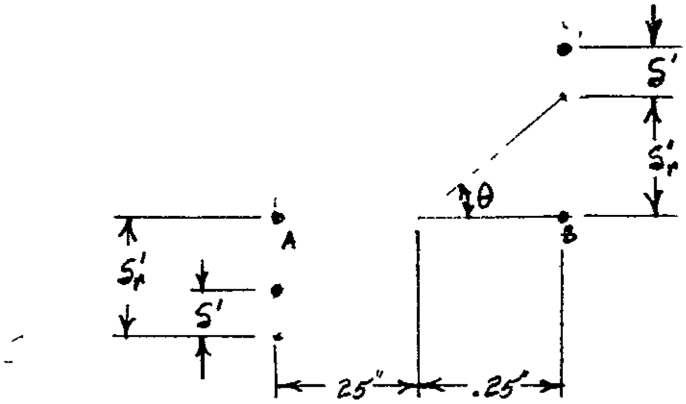

AT A: $$\delta_r' = \frac{P_a'}{2885}$$

AT B: $$\delta_r' = \frac{P_b'}{2885} + \frac{P_b'}{90.090}$$

$$= \frac{P_b'}{2885} + \frac{32\ 0235\ P_b'}{2885}$$

$$\delta_r' = \frac{33.0235\ P_b'}{2885}$$

$$P_a' = 33.0235\ P_b'$$

$$M = 25 P_a' + .25 P_b'$$

$$= .25 (P_a' + P_b')$$

$$= 25 (34\ 0235 P_b')$$

$$M = 8.505875\ P_b'$$

LET $M = 1$

$$P_b' = \frac{1}{8\ 505875} = .117565 \text{ LB.}$$

$$P_a' = 3.882408 \text{ LB.}$$

CALCULATE THE DEFLECTION FROM A UNIT LOAD AND THE ROTATION FROM A UNIT MOMENT.

$$\delta = \frac{970608}{2885} = .0003363 \text{ IN.}$$

$$\delta_r' = \frac{3.882408}{2885} = .001345 \text{ IN}$$

$$\theta = \frac{\delta_r}{.25} = \frac{.001345}{.25} = .005380 \text{ RAD}$$

CALCULATE AE AND EI FOR BEAM ELEMENTS TO GIVE ABOVE DEFLECTIONS AND ROTATIONS.

$$\frac{\cancel{P}^{1}L}{AE} = \delta$$

LET L = 1 IN

$$\frac{1}{AE} = \delta$$

$$AE = \frac{1}{\delta} = \frac{1}{3.363 \times 10^{-4}}$$

$$\underline{\underline{AE = 2974 \text{ LB}}}$$

$$\frac{\cancel{M}^{1}\cancel{L}^{1}}{EI} = \theta$$

$$\frac{1}{EI} = \theta$$

$$EI = \frac{1}{\theta} = \frac{1}{.005380}$$

$$\underline{\underline{EI = 186 \text{ LB-IN}^2}}$$

INSIDE ELEMENTS

$$\frac{1}{K'_{BEQ}} = \frac{2}{K_S} = \frac{2}{2885} = .00069324$$

$$K'_{BEQ} = \frac{1}{.00069324} = 1442.5$$

$$K_{BEQ} = 1442.5 + 90.090 = 1532.59 \text{ LB/IN}$$

$$K_A = 2885 \text{ LB/IN}$$

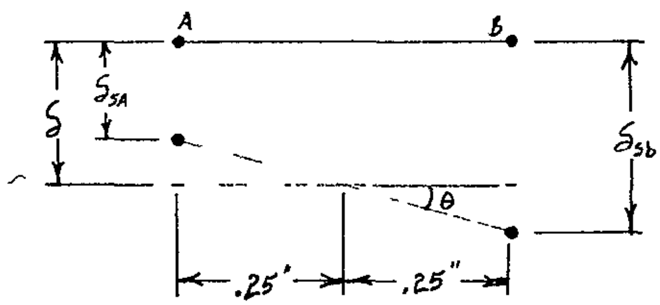

AT A: $\delta = \frac{P_a}{2885}$

AT B $\delta = \frac{P_b}{1532.59}$

$$P_a = \frac{2885\ P_b}{1532.59} = 1.882434\ P_b$$

LET $P_a + P_b = 1$

$$P_b = 1 - P_a$$

$$P_a = 1.882434 - 1.882434\ P_a$$

$$P_a = \frac{1.882434}{2.882434} = .653070 \text{ LB}$$

$$P_b = .346930 \text{ LB}$$

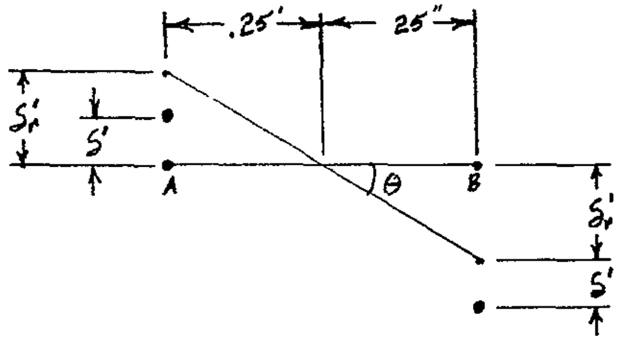

AT A: $\delta_r' = \dfrac{P_a'}{2885}$

AT B: $\delta_r' = \dfrac{P_b'}{1532.59}$

$$P_a' = 1.882434\ P_b'$$

$$M = .25 P_a' + .25 P_b'$$
$$= .25\,(P_a' + P_b')$$
$$= .25\,(2.882434) P_b'$$

$$M = .720608\ P_b'$$

LET $M = 1$

$$P_b' = \frac{1}{.720608} = 1.387717 \text{ LB}$$

$$P_a' = 2.612286 \text{ LB.}$$

CALCULATE THE DEFLECTION FROM A UNIT LOAD AND THE ROTATION FROM A UNIT MOMENT.

$$\delta = \frac{.653070}{2885} = 2.2636 \times 10^{-4} \text{ IN.}$$

$$\delta_r' = \frac{2.612286}{2885} = 9.0547 \times 10^{-4}$$

$$\theta = \frac{\delta_r'}{.25} = \frac{9.0547 \times 10^{-4}}{.25} = 36.2188 \times 10^{-4} \text{ RAD}$$

CALCULATE AE AND EI FOR BEAM ELEMENTS TO GIVE ABOVE DEFLECTIONS AND ROTATIONS.

$$\frac{\cancel{P}^{1} L}{AE} = \delta$$

$$AE = \frac{L}{\delta}$$

$L = .814\ IN$

$$AE = \frac{.814}{2.2636 \times 10^{-4}}$$

$$\underline{\underline{AE = 3596\ LB}}$$

$$\frac{\cancel{M}^{1} L}{EI} = \theta$$

$$EI = \frac{L}{\theta} = \frac{.814}{36.2188 \times 10^{-4}}$$

$$\underline{\underline{EI = 225\ LB\text{-}IN^2}}$$

ASSUME $E = 10 \times 10^6$ PSI

OUTSIDE ELEMENTS

$$A = \frac{2974}{10 \times 10^6} = .0002974$$

$$\underline{\underline{A = 2.974 \times 10^{-4} \text{ IN}^2}}$$

$$I = \frac{186}{10 \times 10^6} = .0000186$$

$$\underline{\underline{I = 1.86 \times 10^{-5} \text{ IN}^4}}$$

INSIDE ELEMENTS

$$A = \frac{3596}{10 \times 10^6} = .0003596$$

$$\underline{\underline{A = 3\,596 \times 10^{-4} \text{ IN}^2}}$$

$$I = \frac{225}{10 \times 10^6} = .0000225$$

$$\underline{\underline{I = 2.25 \times 10^{-5} \text{ IN}^4}}$$

EQUATIONS FOR DEVELOPMENT OF FINAL DEFORMATIONS

TOP PANE OF FULL WINDOW

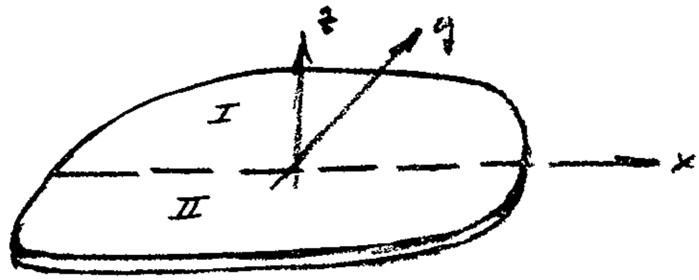

PROBLEM IS TO USE SYMMETRIC AND ASYMMETRIC LOADING CONDITIONS TO DETERMINE THE DEFORMATIONS ON THE ENTIRE WINDOW BUT IN FACT ANALYZING ONLY ONE-HALF.

THE LOADING VECTORS ON EACH HALF (I AND II) CAN BE REPRESENTED AS

$$V_I = \begin{Bmatrix} p_1 \\ \vdots \\ p_n \\ \hline \delta_1 \\ \vdots \\ \delta_n \end{Bmatrix} \qquad V_{II} = \begin{Bmatrix} p_1 \\ \vdots \\ p_n \\ \Delta_1 \\ \vdots \\ \Delta_n \end{Bmatrix}$$

WHERE $\{p_i\}$ ARE THE PRESSURE LOADINGS ON THE INTERIOR POINTS AND $\{\delta_i\}$ AND $\{\Delta_i\}$ ARE THE IMPOSED EDGE DEFORMATIONS FOR I AND II RESPECTIVELY.

BY ADDING AND SUBTRACTING THESE LOADINGS, SETS OF SYMMETRIC AND ASYMMETRIC LOADINGS CAN BE DETERMINED WHICH ALONG WITH THE APPROPRIATE BOUNDARY CONDITIONS ALONG THE X-AXIS CAN BE USED TO FIND A SET OF SYMMETRIC AND ASYMMETRIC DEFORMATIONS

$$V_{sym} = \frac{V_I + V_{II}}{2} = \begin{Bmatrix} p_i \\ \hline \frac{\delta_i + \Delta_i}{2} \end{Bmatrix}$$

$$V_{asym} = \frac{V_I - V_{II}}{2} = \begin{Bmatrix} 0 \\ \hline \frac{\delta_i - \Delta_i}{2} \end{Bmatrix}$$

$$q_I = q_{sym} + q_{asym} = \begin{Bmatrix} q_i^p \\ \hline \delta_i \end{Bmatrix}$$

$$q_{II} = q_{sym} - q_{asym} = \begin{Bmatrix} q_i^p \\ \hline \Delta_i \end{Bmatrix}$$

WHERE $\{q_i\}_{\substack{sym \\ asym}}$ ARE RESULTING DEFORMATIONS

DETERMINATION OF REDUCTION OF ERROR AT WINDOW FRAME

	FRAME			OUTER PANE			INNER PANE		
JOINT	δ (in)	Δ (in)	Δ/δ (%)	δ (in)	Δ (in)	Δ/δ (%)	δ (in)	Δ (in)	Δ/δ (%)
1	2501-1	2813-3	1,12	2699-1	,8812-4	33	2488-1	8812-4	,35
11	2492-1	2885-3	1 16	2689-1	,7275-4	,27	,2475-1	,7275-4	,29
21	2510-1	2668 3	1 06	2688-1	5124-4	19	,2469 1	5124-4	,21
31	,2528-1	2451-3	97	,2686-1	3380-4	,13	2465-1	3380-4	,14
41	2547-1	2234 3	,88	2692-1	,1552-4	06	2470-1	,1552-4	06
51	2550-1	5156-4	,20	2700-1	,6883-5	,03	,2479-1	6883-5	,03
61	2553-1	- 1204-3	47	2707-1	-,1272-4	05	2488-1	-,1272-4	,05
71	2556-1	-,2923 3	1 14	,2711-1	- 4143-4	15	,2497-1	-,4143-4	17
81	,2593-1	-,2833 3	1,09	2725-1	-,7341-4	27	2515-1	-,7341-4	29
130	,2511-1	2730-3	1 09	,2722-1	8565-4	,31	,2513-1	8565-4	34
173	,2636-1	- 2731-3	1,04	2762-1	-,9550-4	35	2553-1	- 9550-4	,37
230	2522-1	2643-3	1,05	2751-1	,7268-4	26	2543-1	7268-4	,29
281	2681-1	-,2622-3	,98	,2812-1	- 9079-4	,32	2605-1	- 9079-4	,35
342	2531-1	2571 3	1 02	2774-1	,6793-4	,24	,2566-1	6793-4	26
393	2718-1	-,2532 3	,93	2851-1	-,6817-4	24	2642-1	- 6817-4	26
454	,2562 1	2250-3	88	2807-1	6359-4	23	2588-1	,6359-4	,25
505	2768-1	- 6831-4	25	2899-1	-,2164-4	07	2680-1	- 2164-4	,08
566	2593-1	,1923 3	74	,2841-1	6203-4	22	,2614-1	6203-4	24
617	,2819-1	1166 3	41	,2945-1	3848-4	13	2713-1	3848-4	,14
678	,2624-1	1607-3	61	,2876-1	6324-4	,22	,2641-1	6324-4	24
729	,2870-1	3016 3	1 05	,2991-1	,1070-3	36	,2756-1	,1070-3	,39
786	2642-1	-,1040-4	04	,2909-1	,7350-4	25	2668-1	7350 4	28
833	,2902-1	3011-3	1 04	3032-1	1661-3	55	,2791-1	1661-3	60
890	2659-1	- 1816-3	68	2938-1	7624 4	26	,2694-1	,7624-4	28
937	2934-1	3006-3	1 02	,3068-1	2081-3	,68	2824-1	2081-3	74
994	,2676 1	-,3527-3	1,32	,2966-1	,6729-4	23	,2721-1	6729-4	25
1041	,2966-1	3001-3	1 01	3098-1	,2344 3	76	,2853-1	,2344-3	82
1098	2715-1	- 3253 3	1,20	2986-1	5671-4	19	2743-1	5671 4	21
1145	2975-1	,3042-3	1,02	3116-1	,2465-3	79	2879-1	2465-3	86
1198	2767-1	- 2837-3	1,04	,3011-1	,5403-4	18	2779-1	,5403-4	,19
1237	,2987-1	3098 3	1,04	3119 1	2388-3	,77	2858-1	2388-3	83
1282	,2810-1	-,2582-3	92	3015-1	,7442-4	25	2810-1	7442-4	,26
1292	,2849-1	- 2309-3	81	3011-1	1048-3	,35	,2776-1	1049-3	,38

	FRAME			OUTER PANE			INNER PANE		
JOINT	δ(in)	Δ(in)	Δ/δ(%)	δ(in)	Δ(in)	Δ/δ(%)	δ(in)	Δ(in)	Δ/δ(%)
1302	2892-1	-.3982-5	.01	3002-1	1419 3	47	.2764-1	.1419-3	51
1312	2935-1	2229-3	76	2993-1	1801-3	60	.2754 1	.1801 3	65
1322	.2967-1	.3328-3	1.12	.3014-1	2005-3	67	.2775-1	.2005 3	74
1332	2987-1	3257-3	1 09	.3046-1	.1956-3	.64	2808-1	.1956-3	70
1342	.3006-1	3185-3	1.06	.3076-1	.2028-3	66	.2842-1	2028-3	.71
1352	.2997-1	.3144 3	1 05	3102-1	2193-3	.71	.2871-1	.2193-3	.76
531	—	—	—	.3148-1	.5765-4	18	.2487-1	5765-4	23
533	—	—	—	3165-1	.5809-4	18	.2484 1	.5809-4	.23
535	—	—	—	3176-1	5834-4	.18	.2483-1	5834 4	23
537	—	—	—	3183-1	5830-4	18	.2485-1	5830-4	.23
539	—	—	—	3184-1	.5786-4	.18	.2490-1	5786-4	23
541	—	—	—	.3179-1	.5691-4	.18	2449 1	.5691-4	.23
543	—	—	—	.3170-1	.5535 4	.17	.2510-1	.5535-4	22
587	—	—	—	.3175-1	.6332-4	20	2497-1	6332-4	.25
599	—	—	—	.3199-1	.6663-4	.21	2520-1	.6663-4	.26
643	—	—	—	.3197-1	6955-4	22	2508-1	.6955-4	28
655	—	—	—	.3222-1	.7846 4	24	2533-1	.7846 4	31
699	—	—	—	.3213-1	.7620-4	.24	.2520-1	.7620-4	.30
711	—	—	—	.3239-1	.9058-4	28	.2546-1	.9058-4	.36
753	—	—	—	.3224 1	8310-4	.26	.2534-1	.8310-4	33
765	—	—	—	3251-1	.1027-3	32	2561-1	.1027-3	.40
805	—	—	—	.3229-1	.9007-4	28	2549-1	.9007-4	.35
817	—	—	—	.3258-1	1146-3	.35	.2578-1	1146-3	44
857	—	—	—	3229-1	9695-4	.30	.2566-1	.9695-4	38
859	—	—	—	.3246-1	.1018-3	31	.2562-1	.1018-3	.40
861	—	—	—	3259-1	.1066-3	33	.2562-1	.1066-3	42
863	—	—	—	3266-1	.1114-3	34	2565-1	.1114 3	.43
865	—	—	—	.3268-1	.1161-3	.36	.2572-1	.1161-3	45
867	—	—	—	3266-1	1209-3	.37	2582-1	1209-3	47
869	—	—	—	.3259-1	.1259 3	.39	.2595-1	.1259-3	.49

δ ≡ DEFLECTIONS DUE TO A CABIN PRESSURE OF 5.1 psia AND AN INTERSTITIAL PRESSURE OF 7.5 psia

Δ ≡ DEFLECTIONS DUE TO APPLICATION OF LEAST SQUARE ERRORS ON FRAME OF UNLOADED WINDOW

FOR WINDOW FRAME

$$\frac{1}{N} \Sigma \left(\frac{\Delta}{\delta}\right)_i = \frac{34.37}{39} = .88$$

FOR WINDOW PANE (AT FRAME)

$$\frac{1}{N} \Sigma \left(\frac{\Delta}{\delta}\right)_i = \frac{28.01}{78} = .36$$

FOR WINDOW PANE (IN INTERIOR)

$$\frac{1}{N} \Sigma \left(\frac{\Delta}{\delta}\right)_i = \frac{14.17}{48} = .30$$